Molybdenum–99 (^{99}Mo): Past, Present, and Future

Guest Editors: Mushtaq Ahmad, George Vandegrift, and Pablo Cristini

Molybdenum-99 (^{99}Mo): Past, Present, and Future

Molybdenum-99 (^{99}Mo): Past, Present, and Future

Guest Editors: Mushtaq Ahmad, George Vandegrift, and Pablo Cristini

Editorial Board

Contents

Editorial

Molybdenum-99 (^{99}Mo): Past, Present, and Future

Mushtaq Ahmad,[1] George Vandegrift,[2] and Pablo Cristini[3]

[1] *Isotope Production Division, Pakistan Institute of Nuclear Science and Technology, Nilore, Islamabad 45650, Pakistan*
[2] *Argonne National Laboratory, 9700 South Cass Avenue, Argonne, IL 60439, USA*
[3] *Ezeiza Atomic Center, National Commission of Atomic Energy, Buenos Aires, Argentina*

Correspondence should be addressed to Mushtaq Ahmad; amushtaq1@hotmail.com

Molybdenum-99 (^{99}Mo, half-life = 66 h) is a parent radionuclide of a diagnostic nuclear isotope. It decays in technetium-99 m (^{99m}Tc, half-life = 6 h), which is used in over 30 million procedures per year around the world. To meet worldwide demand for ^{99m}Tc-radiopharmaceuticals, fresh ^{99}Mo/^{99m}Tc must be delivered regularly to nuclear medical centers, week after week. The risks of global ^{99}Mo supply disruptions increased significantly since 1995 and have been experienced for different reasons. Since the last quarter of 2007, global Mo-99 supplies have been severely disrupted by recurring operational problems at a handful of aging research reactor (NRU Canada, HFR Netherlands, SAFARI-1 South Africa, BR2 Belgium and OSIRIS France) and processing facilities (MDS Nordion in Canada, Mallinckrodt in the Netherlands, IRE in Belgium, and NTP in South Africa). These few facilities are meeting the bulk of the worldwide demand. With the aging of the ^{99}Mo supply network, it is necessary for world Mo-99 market to consider new reliable supply sources. The present and future shortage of ^{99m}Tc or its parent is a worldwide issue. A research reactor is only one piece of the linear supply chain of ^{99}Mo/^{99m}Tc that exists today. In April 2010, the United States and 46 other countries signed an agreement to phase out HEU for civilian uses to reduce proliferation concerns. Now scientists and engineers involved in ^{99}Mo production are working to determine how to continue to make ^{99}Mo with (1) low-enriched uranium (LEU, <20% ^{235}U) or (2) other alternatives that do not require fissioning of ^{235}U. To overcome the shortage of various routes of its production by accelerators and reactors generating high

and low specific activity ^{99}Mo or ^{99m}Tc directly is being researched.

Investigators were invited to contribute original research articles as well as review articles to stimulate the continuing efforts to understand the issues related to production of ^{99}Mo that is acceptable to end users and environmentalists. The article selected for this special issue represent the rich and many-faceted technical know-how that we have the pleasure of sharing with our readers. We would like to thank the authors for their excellent contributions and patience in assisting us. Finally, the fundamental work of all reviewers on these papers is also highly appreciated.

This special issue contains nine papers, where four papers deal with the production of ^{99}Mo using LEU targets in a reactor. Two papers are on ^{99m}Tc generators development and its utilization. One paper deals with the production of ^{99}Mo and ^{99m}Tc using a cyclotron. An article on immobilization of higher activity wastes from reactor production of ^{99}Mo is also included in this issue. One paper deals with research and development of chemical process, hot-cell infrastructure, and commercial production of ^{99}Mo.

In the paper entitled "^{99m}Tc *Generator Development: Up-to-date* ^{99m}Tc *recovery technologies for increasing the effectiveness of* ^{99}Mo *utilization*" by V. S. Le (Australia) presents a review on the ^{99}Mo sources available today and on the ^{99m}Tc generators developed up to now for increasing the effectiveness of ^{99}Mo utilization. The latest results of the endeavors in this field are also surveyed in regard to the technical solution for overcoming the shortage of ^{99}Mo

supply. The technical topics are grouped and discussed to reflect the similarity in the technological process of each group. The following topics are included in this review.

(i) High specific activity ^{99}Mo (the issues for current production, efforts for more effectiveutilization, the ^{99m}Tc generator based on high-specific activity ^{99}Mo, and ^{99m}Tc concentration units)

(ii) Low specific activity ^{99}Mo (^{99}Mo production based on neutron capture and accelerators' direct production of ^{99m}Tc and the methods of increasing the specific activity of ^{99}Mo using the Szilard-Chalmersreaction and a high power isotope separator.)

The entitled articles "*Immobilisation of higher activity wastes from nuclear reactor production of ^{99}Mo*" by M. Stewart et al. (Australia) discusses progress in waste-form development and processing to treat ANSTO's intermediate-level waste (ILW) streams arising from ^{99}Mo production. The various waste forms and the reason for the process option chosen are reviewed. The options considered were cement-based, glass, glass-ceramic, and ceramic waste forms.

The entitled paper "*Evaluation of ^{99}Mo and ^{99m}Tc productions based on a high-performance cyclotron*" by J. Esposito et al. (Italy) describes possibilities to replace the current reactor-based method with the accelerator ones. A feasibility study was started in 2011 based on the new, high-beam-current, high-energy cyclotron scheduled to be available in the next coming years at Legnaro Laboratories (LNL). A molybdenum metallic target, enriched to 99.05% ^{100}Mo, has been assumed, as it is currently available on the isotopes market. A series of in-target quality parameters has thus been calculated for both radionuclides at the End of Bombardment (EOB), based on the maximum (i.e., 500 μA) proton-beam output current. TENDL 2012 theoretical excitation functions, extended up to (p,6n) (p,p5n) and (p,2p4n) levels, were used to get a detailed map of the radionuclides expected. Results point out that accelerator-^{99}Mo is of limited interest for a possible massive production, mainly because of in-target specific activities, which are a factor of 10^4 lower than reactor ^{99}Mo.

The article entitled "*History and actual state of non-HEU fission-based Mo-99 production with low-performance research reactors*" by S. Dittrich (Germany) discusses that 50 years ago, one of the worldwide first industrial production processes able to produce fission-Mo-99 for medical use had started at ZfK Rossendorf (now HZDR, Germany). On the occasion of this anniversary, it is worth mentioning that this original process (called LITEMOL now) together with its target concept used at that time can be applied still. LITEMOL can be adapted very easily to various research reactors and applied at each site, which maybe still of interest for very small-scale producers. Besides this original process, two further and actually proven processes are suitable as well and recommended for small-scale LEU fission Mo-99 production also.

The article entitled "*Influence of the generator in-growth time on the final radiochemical purity and stability of ^{99m}Tc*

radiopharmaceuticals" by L. Uccelli et al. (Italy) describes both theoretical investigations and preliminary irradiations tests on ^{100}Mo-enriched samples. The authors argue that both the ^{99g}Tc/^{99m}Tc ratio and the ^{99m}Tc specific activity will be different in accelerator-produced Tc than that milked from generator, and this might affect radiopharmaceutical procedures. The aim of this work was the evaluation of possible impacts of different ^{99g}Tc/^{99m}Tc isomeric ratios on the preparation of different Tc-labeled pharmaceutical kits. A set of measurements with ^{99m}Tc, eluted from a standard ^{99}Mo/^{99m}Tc generator, was performed and results on both radiochemical purity and stability studies (following the standard Quality Control procedures) are reported for a set of widely used pharmaceuticals (i.e., ^{99m}Tc-Sestamibi, ^{99m}Tc-ECD, ^{99m}Tc-MAG$_3$, ^{99m}Tc-DTPA, ^{99m}Tc-MDP, ^{99m}Tc-HMDP, ^{99m}Tc-nanocolloids, and ^{99m}Tc-DMSA).

The entitled articles, the work of S. G. Govindarajan et al. (USA), "*Assembly and irradiation modeling of residual stresses in low-enriched uranium foil-based annular targets for molybdenum-99 production*" considers a composite cylindrical structure, with low-enriched uranium (LEU) foil enclosed between two aluminum 6061-T6 cylinders. A recess is cut all around the outer circumference of the inner tube to accommodate the LEU foil of open cross-section. To obtain perfect contact at the interfaces of the foil and the tubes, an internal pressure is applied to the inner tube, thereby plastically and elastically deforming it. The residual stresses resulting from the assembly process are used along with a thermal-stress model to predict the stress margins in the cladding during irradiation. The whole process was simulated as a steady-state 2-dimensional problem using the commercial finite element code Abaqus FEA. The irradiation behavior of the annular target has been presented and the effect of the assembly residual stresses has been discussed.

The article entitled "*The fission-based ^{99}Mo production process ROMOL-99 and its application to PINSTECH Islamabad*" by R. Muenze et al. (Germany and Pakistan) presents an innovative process for fission based ^{99}Mo production developed under Isotope Technologies Dresden (ITD) GmbH (former Hans Wälischmiller GmbH (HWM), Branch Office Dresden), and its functionality has been tested and proved at the Pakistan Institute of Nuclear Science and Technology (PINSTECH), Islamabad. Targets made from uranium-aluminum alloy clad with aluminum were irradiated in the core of Pakistan Research Reactor-1 (PARR-1). More than 50 batches of fission ^{99}Mo have been produced that meet the international purity/pharmacopoeia specifications using this ROMOL-99 process. The process is based on alkaline dissolution of the neutron-irradiated targets in the presence of NaNO$_3$, chemically extracting the ^{99}Mo from various fission products and purifying the product by column chromatography.

In the article entitled "*A solution-based approach for Mo-99 production: Considerations for nitrate versus sulfate media*" A. J. Youker et al. (USA) describe how Argonne National Laboratory is assisting two potential domestic suppliers of

Mo-99 by examining the effects of a uranyl-nitrate versus a uranyl-sulfate fuel or target solution compositions on Mo-99 production. Uranyl-nitrate solutions are easier to prepare and do not generate detectable amounts of peroxide upon irradiation, but the effect of a high radiation field (radiolysis of nitrate ion) can lead to a large increase in solution pH, which can lead to the precipitation of fission products and uranyl hydroxides. Uranyl-sulfate solutions are more difficult to prepare, and enough peroxide is generated during irradiation to cause precipitation of uranyl peroxide, but this can be prevented by adding a catalyst to the solution. A titania sorbent can be used to recover Mo-99 from a highly concentrated uranyl nitrate or sulfate solution; however, different approaches must be taken to prevent precipitation of uranium and other fission products during Mo-99 production.

In the article entitled "*Production cycle for large scale fission Mo-99 separation by the processing of irradiated LEU uranium silicide fuel element targets,*" A.-H. A. Sameh (Germany) describes experiments and related high-activity demonstrations that highlight the advantage of uranium silicide fuels as a target material for the production of fission Mo-99. Silicide targets combine features predestinating them as feed materials for a large-scale production of fission nuclides when starting from LEU.

Mushtaq Ahmad
George Vandegrift
Pablo Cristini

Review Article

^{99m}Tc Generator Development: Up-to-Date ^{99m}Tc Recovery Technologies for Increasing the Effectiveness of ^{99}Mo Utilisation

Van So Le

MEDISOTEC and CYCLOPHARM Ltd., 14(1) Dwyer Street, Gymea, NSW 2227, Australia

Correspondence should be addressed to Van So Le; vansole01@gmail.com

A review on the ^{99}Mo sources available today and on the ^{99m}Tc generators developed up to date for increasing the effectiveness of ^{99}Mo utilisation is performed in the format of detailed description of the features and technical performance of the technological groups of the ^{99}Mo production and ^{99m}Tc recovery. The latest results of the endeavour in this field are also surveyed in regard of the technical solution for overcoming the shortage of ^{99}Mo supply. The technological topics are grouped and discussed in a way to reflect the similarity in the technological process of each group. The following groups are included in this review which are high specific activity ^{99}Mo: the current issues of production, the efforts of more effective utilisation, and the high specific activity ^{99}Mo-based ^{99m}Tc generator and ^{99m}Tc concentration units; low specific activity ^{99}Mo: the ^{99}Mo production based on neutron capture and accelerators and the direct production of ^{99m}Tc and the methods of increasing the specific activity of ^{99}Mo using Szilard-Chalmers reaction and high electric power isotopic separator; up-to-date technologies of ^{99m}Tc recovery from low specific activity ^{99}Mo: the solvent extraction-based ^{99m}Tc generator, the sublimation methods for ^{99}Mo/^{99m}Tc separation, the electrochemical method for ^{99m}Tc recovery, and the column chromatographic methods for ^{99m}Tc recovery. Besides the traditional ^{99m}Tc-generator systems, the integrated ^{99m}Tc generator systems (^{99m}Tc generator column combined with postelution purification/concentration unit) are discussed with the format of process diagram and picture of real generator systems. These systems are the technetium selective sorbent column-based generators, the high Mo-loading capacity column-based integrated ^{99m}Tc generator systems which include the saline-eluted generator systems, and the nonsaline aqueous and organic solvent eluent-eluted generator systems using high Mo-loading capacity molybdategel and recently developed sorbent columns. ^{99m}Tc concentration methods used in the ^{99m}Tc recovery from low specific activity ^{99}Mo are also discussed with detailed process diagrams which are surveyed in two groups for ^{99m}Tc concentration from the saline and nonsaline ^{99m}Tc-eluates. The evaluation methods for the performance of ^{99m}Tc-recovery/concentration process and for the ^{99m}Tc-elution capability versus Mo-loading capacity of generator column produced using low specific activity ^{99}Mo source are briefly reported. Together with the theoretical aspects of ^{99m}Tc/^{99}Mo and sorbent chemistry, these evaluation/assessment processes will be useful for any further development in the field of the ^{99m}Tc recovery and ^{99}Mo/^{99m}Tc generator production.

1. Introduction

The development of the original ^{99m}Tc generator was carried out by Walter Tucker and Margaret Greens as part of the isotope development program at Brookhaven National Laboratory in 1958 [1]. ^{99m}Tc is currently used in 80–85% of diagnostic imaging procedures in nuclear medicine worldwide every year. This radioisotope is produced mainly from the ^{99m}Tc generators via β-particle decay of its parent nuclide ^{99}Mo. ^{99}Mo nuclide decays to ^{99m}Tc with an efficiency of

about 88.6% and the remaining 11.4% decays directly to ^{99}Tc. A ^{99m}Tc generator, or colloquially a "technetium cow," is a device used to extract the ^{99m}Tc-pertechnetate generated from the radioactive decay of ^{99}Mo ($T_{1/2} = 66.7$ h). As such, it can be easily transported over long distances to radiopharmacies where its decay product ^{99m}Tc ($T_{1/2} = 6$ h) is extracted for daily use. ^{99}Mo sources used in different ^{99m}Tc generators are of variable specific activity (SA) depending on the production methods applied. Based on the nuclear reaction data

TABLE 1: Current application of ^{99m}Tc for clinical SPECT imaging and activity dose requirement; (*) The injection activity dose (mCi ^{99m}Tc) normally delivered in 1 mL solution of the ^{99m}Tc-based radiopharmaceutical [167].

Organ	^{99m}Tc radiopharmaceutical	Injection activity dose (*)	Organ	^{99m}Tc radiopharmaceutical	Injection activity dose (*)
Brain	^{99m}Tc-ECD	10–20 mCi		^{99m}Tc-MAG3	5–15 mCi
	^{99m}Tc-ceretec (HmPAO)	10–2 mCi		^{99m}Tc-DTPA	5–15 mCi
Lung	^{99m}Tc-MAA	2–4 mCi	Kidney	^{99m}Tc-Gluceptate	5–15 mCi
	^{99m}Tc-DTPA aerosol	30 mCi/3 mL (10 mCi/mL)		^{99m}Tc-DMSA	2–5 mCi
	^{99m}Tc-Technegas	100–250 mCi/mL	Skeleton	^{99m}Tc-MDP	10–20 mCi
Thyroid	^{99m}Tc-pertechnetate	5–10 mCi		^{99m}Tc-HDP	10–20 mCi
Liver	^{99m}Tc-IDA	5–10 mCi	Heart	^{99m}Tc-Sestamibi	10–30 mCi
	^{99m}Tc-sulfur/albumine colloid	5–15 mCi		^{99m}Tc-PYP	10–15 mCi
Spleen	^{99m}Tc-sulfur/albumine colloid	2-3 mCi		^{99m}Tc-Tetrofosmin	5–25 mCi
	^{99m}Tc-red blood cells	2-3 mCi	Tumour	^{99m}Tc-Sestamibi	15–20 mCi

available today, two types of ^{99}Mo sources of significantly different SA values (low and high SA) can be achieved using different ^{99}Mo production ways. Accordingly, ^{99m}Tc generators using low or high SA ^{99}Mo should be produced by suitable technologies to make them acceptable for nuclear medicine uses. The safe utilisation of the ^{99m}Tc generators is definitely controlled by the quality factors required by the health authorities. However, the acceptability of the ^{99m}Tc generator to be used in nuclear diagnostic procedures, the effective utilisation of ^{99m}Tc generator, and the quality of ^{99m}Tc-based SPECT imaging diagnosis are controlled by the generator operation/elution management, which is determined by the ^{99m}Tc concentration of the ^{99m}Tc eluate/solution. This also means that the efficacy of the ^{99m}Tc generator used in nuclear medicine depends on the ^{99m}Tc concentration of the solution eluted from the generator, because the volume of a given injection dose of ^{99m}Tc-based radiopharmaceutical is limited. The current clinical applications of ^{99m}Tc are shown in Table 1. As shown, the injection dose activity of ^{99m}Tc-based radiopharmaceutical delivered in 1 mL solution is an important factor in determining the efficacy of the ^{99m}Tc solution produced from the generators. So it is clear that the ^{99m}Tc concentration of the solution eluted from the generator is the utmost important concern in the process of the generator development, irrespectively using either fission-based high specific activity ^{99}Mo or any ^{99}Mo source of low specific activity. It is realised that a complete review on the ^{99}Mo and ^{99m}Tc production/development may contribute and stimulate the continuing efforts to understand the technological issues and find out the ways to produce a medically acceptable ^{99}Mo/^{99m}Tc generator and to overcome the shortage/crisis of ^{99}Mo/^{99m}Tc supply. So this review is to give a complete survey on the technological issues related to the production and development of high and low specific activity ^{99}Mo and to the up-to-day ^{99m}Tc recovery technologies, which are carried out in many laboratories, for increasing the effectiveness of ^{99}Mo

utilisation. The evaluation methods for the performance of the ^{99m}Tc-recovery/concentration process and for the ^{99m}Tc-elution capability versus Mo-loading capacity of the generator column produced using (n, γ) ^{99}Mo (or any low specific activity ^{99}Mo source) are briefly reported. Together with the theoretical aspects of ^{99m}Tc/^{99}Mo and sorbent chemistry, these evaluation/assessment processes could be useful for any further development in the field of the ^{99m}Tc recovery and ^{99}Mo/^{99m}Tc generator production. The achievements gathered worldwide are extracted as the demonstrative examples of today progress in the field of common interest as well.

2. High Specific Activity ^{99}Mo: Current Issues of Production and Efforts of More Effective Utilisation

2.1. Production of High Specific Activity ^{99}Mo. High SA ^{99}Mo is currently produced from the uranium fission. The fission cross-section for thermal fission of ^{235}U is of approximately 600 barns. 37 barns of this amount result in the probability of a ^{99}Mo atom being created per each fission event. In essence, each one hundred fission events yields about six atoms of ^{99}Mo (6.1% fission yield). Presently, global demand for ^{99m}Tc is met primarily by producing high specific activity (SA) ^{99}Mo from nuclear fission of ^{235}U and using mainly five government-owned and funded research reactors (NRU, Canada; HFR, the Netherland; BR2, Belgium; Osiris, France; Safari, South Africa). After neutron bombardment of solid uranium targets in a *heterogeneous research reactor*, the target is dissolved in a suitable solution and the high SA ^{99}Mo is extracted, purified and packed in four industrial facilities (MDS Nordion, Canada; Covidien, the Netherland; IRE, Belgium; NTP, South Africa), and supplied to manufacturers of ^{99m}Tc generators around the world [2–12]. CNEA/INVAP (Argentina), ANSTO (Australia), Russia, and

BATAN (Indonesia) also produce fission ^{99}Mo and total supply capacity of these facilities is about 5% of the global demand of ^{99}Mo [3]. The weekly demand of ^{99}Mo is reported to be approximately 12000 Ci at the time of reference (6-day Ci). This is equivalent to 69300 Ci at the end of bombardment (EOB). All five of the major production reactors use highly enriched uranium (HEU) targets with the isotope ^{235}U enriched to as much as 93% to produce ^{99}Mo (except Safari 1 in South Africa which uses 45% HEU). As mandated by the US Congress, non-HEU technologies for ^{99}Mo and ^{99m}Tc production should be used as a Global Initiative to Combat Nuclear Terrorism (GICNT) [13, 14]. The ^{99}Mo production plans for conversion of HEU to low enriched uranium (LEU) based technology, using heterogeneous research reactors, achieved a major milestone in years 2002–2010 and currently the production of high SA ^{99}Mo from LEU targets is routinely performed in Argentina (from 2002), in Australia (from 2009), and in South Africa (from 2010). CNEA/NVAP (Argentina) is a pioneer in the conversion of HEU to LEU by starting LEU-based ^{99}Mo production in 2002 after decommissioning of HEU technology which has been operated 17 years ago [15, 16]. INVAP also demonstrated the maturity of LEU technology via technology transfer to ANSTO for a modest industrial scale manufacture of a capacity of 300–500 6-day curies per batch. With an announcement last year on a great expansion of production capacity of LEU-based facility being started in 2016 in Australia [17], ANSTO and CNEA/INVAP will become the first organisations confirming the sustained commercial large-scale production of ^{99}Mo based on LEU technology. High SA ^{99}Mo is of approximately 50,000 Ci ^{99}Mo/g of total Mo at EOB (The OPAL reactor, Australia, thermal neutron flux: 9.10^{13} n/cm^{-2} sec^{-1}), irrespectively using either HEU or LEU-based fission technologies. With the effort in maintaining the supply of high SA ^{99}Mo, several alternative non-HEU technologies are being developed. Fission of ^{235}U to produce ^{99}Mo is also performed using *homogeneous (solution) nuclear reactor* and ^{99}Mo recovery system, so-called Medical Isotope Production System (MIPS) [18]. The reactor fuel solution in the form of an LEU-based nitrate or sulphate salt dissolved in water and acid is also the target material for ^{99}Mo production. In essence, the reactor would be operated for the time required for the buildup of ^{99}Mo in the fuel solution. At the end of reactor operation, the fuel solution pumped through the ^{99}Mo-recovery columns, such as Termoxid 52, Termoxid 5M, titana, PZC sorbent, and alumina, which preferentially sorbs molybdenum [19, 20]. The ^{99}Mo is then recovered by eluting the recovery column and subsequently purified by one or more purification steps. It is estimated that a 200 kW MIPS is capable of producing about 10,000 Ci of ^{99}Mo at the end of bombardment (five-day irradiation) [2, 18, 21]. The possibility of using the *high power linear accelerator-driven proton* (150–500 MeV proton with up to 2 mA of beam current, ~10^{16} particles/s) to generate high intensities of thermal-energy neutrons for the fission of ^{235}U in metallic LEU foil targets has been proposed [2, 22]. This accelerator can produce an order of magnitude more secondary neutrons inside the target from fission. The *low energy accelerator* (300 keV deuteron with 50 mA of beam current)-based neutron production via the D,T reaction for the fission of ^{235}U in LEU solution targets has been reported [2]. The fission of ^{235}U for the ^{99}Mo production can be performed with neutrons generated from the *>2.224 MeV photon-induced breakup of D_2O* in a subcritical LEU solution target. *Accelerator-driven photon-fission ^{238}U(γ,f)* ^{99}Mo is also proposed as an approach to produce high SA ^{99}Mo using natural uranium target [2, 23–25].

Under the consultation for the fission ^{99}Mo plant in ANSTO, the author of this review paper has proposed a project of *"Automated modular process for LEU-based production of fission ^{99}Mo"* [26]. The consent of the Chief Executive Officer of ANSTO is a positive signal that might get scientists ahead of the game with next generation (cheaper, better, and faster) Mo-99 plant design. The aim of this project is to provide the integrated facility, composed of automated compact high technology modules, to establish medium-scale production capability in different nuclear centres running small reactors around the world. In essence, this project is to decentralize the ^{99}Mo production/supply and the radioactive waste treatment burden in the large facilities and to bring ^{99}Mo production closer to users (^{99m}Tc generator manufacturers) to minimize the decay ^{99}Mo loss. The modular technology-based production is standardized for the secure operation sustainable with the supply of replaceable standardized modules/components for both ^{99}Mo processing and radioactive waste treatment. The above-mentioned objectives are in combination to solve basically the ^{99}Mo undersupply problem or crisis by increasing the numbers of smaller ^{99}Mo processing facilities in hundreds of nuclear centres owning ^{99}Mo production-capable reactors in the world and to reduce the cost of ^{99}Mo for patient use. The brief of the modular ^{99}Mo technology is the following. Currently, three main medical radioisotopes ^{99}Mo, ^{131}I, and ^{133}Xe are routinely produced from uranium fission. So, it is conceivable to say that the fission uranium based medical isotope production facility is composed of 6 main technological modules: target digestion module, ^{99}Mo separation module, ^{131}I separation module, ^{133}Xe separation module, uranium recovery module, and waste treatment modules (gas, solid, and liquid waste modules). For ^{99}Mo production alone, the numbers of main modules can be reduced to 4, comprising main module for uranium target digestion; main module for ^{99}Mo separation; main module for uranium recovery; main module for waste treatment (gas, solid, and liquid waste modules).

Each main module in this description is composed of several different functional modules. As an example, the main module for ^{99}Mo separation incorporates 7 functional modules, such as five ion exchange resin/sorption functional modules and two solution delivery functional modules (radioactive and nonradioactive).

A pictorial description of the structure of one main module which is capable of incorporating five functional modules (below illustrated with two functional modules as examples) is shown in Figure 1.
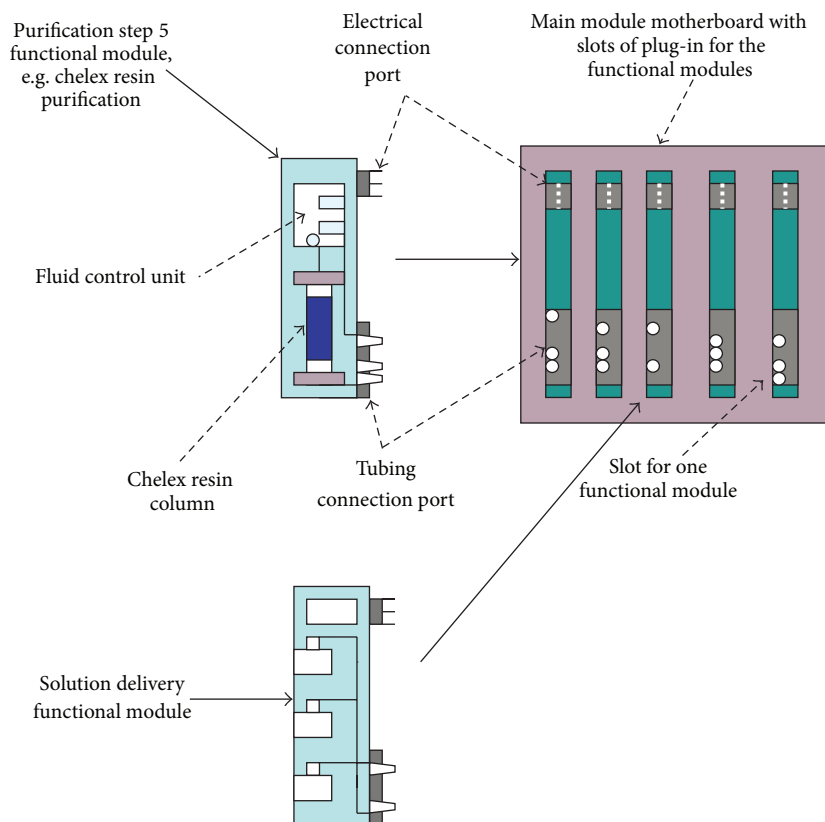
FIGURE 1: Conceptual diagram of the modular technology of fission-^{99}Mo recovery [26].

The operation of this main module is automated and computerized. The integrated fluid flow and radioactivity monitoring system using photo and/or radiation diode sensors provides the feedback information for safe and reliable process control. The in-cell maintenance based on the replacement of failed functional module is completed quickly ensuring continuous production run. Advantages of this facility setup are the following: compact system with controllable and reliable process; less space required that minimizes the cost of the facility (one double-compartment hot cell for whole process); minimal maintenance work required that due to highly standardized modular integration; high automation capability; low cost production of ^{99}Mo making this modular technology feasible for small nuclear research centres in many countries of the world; centralizing the module supply and maintenance giving high security and sustainability of production to small producers with few resources; high capability of the network-based ^{99}Mo production/supply to overcome any global ^{99}Mo crisis.

The W impurity in massive LEU targets is still challenging the quality of ^{99}Mo obtained from different ^{99}Mo recovery processes, because the WO_4^{2-} ions and radioactive impurity (^{188}Re) generated from neutron-activated W cause serious problems in the ^{99m}Tc generator manufacture and in the use of ^{99m}Tc-pertechnetate solution, respectively. The effort to remove W impurity from the ^{99}Mo solution produced from LEU target is being performed as shown in Figure 2 [27].

2.2. High Specific Activity Fission ^{99}Mo-Based ^{99m}Tc Generators and Concentrators. The isolation of ^{99}Mo from uranium fission typically generates ^{99}Mo with a specific activity greater than >10,000 Ci/g at the six-day-Ci reference time (specific activity of carrier-free ^{99}Mo is 474,464.0 Ci/g [28]). This SA value permits extraction of the ^{99m}Tc daughter nuclide using chromatographic alumina column [1, 29–35]. Today, most commercial ^{99m}Tc generators are designed by taking advantage of much stronger retaining of the MoO_4^{2-} anions compared with the TcO_4^{-} anions on acidic alumina sorbent. Although the adsorption capacity of the alumina for MoO_4^{2-} anions is low (<10 mg Mo/g), the very low content of Mo in the high SA ^{99}Mo solution (0.1 mg Mo per Ci ^{99}Mo), which is loaded on a typical column containing 2-3 g of alumina for a 4 Ci activity generator, ensures a minimal ^{99}Mo breakthrough in the medically useful ^{99m}Tc-pertechnetate solution extracted from the generator system. When the ^{99}Mo decays it forms pertechnetate (^{99m}TcO$_4^{-}$) which is easily eluted with saline solution from the alumina column resulting an injectable saline solution containing the ^{99m}Tc in the form of sodium-pertechnetate. The most stable form of the radionuclide ^{99m}Tc in aqueous solution is the tetraoxopertechnetate
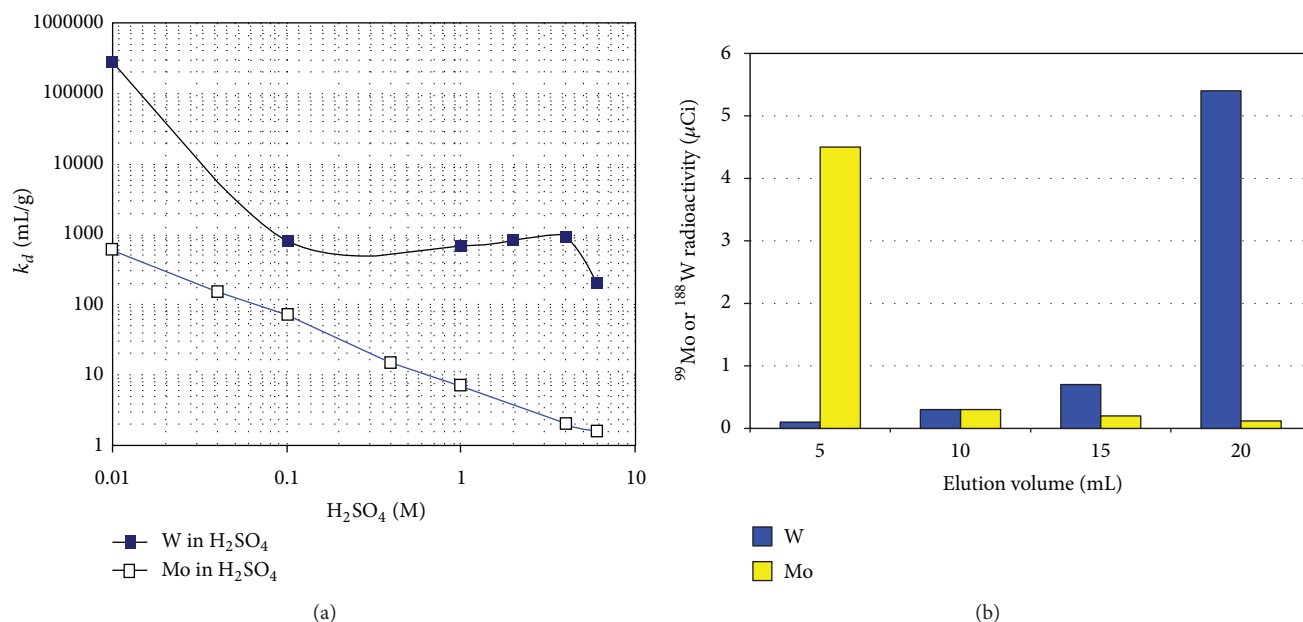
FIGURE 2: W/Mo adsorption and separation using alumina column: (a) weight distribution coefficients of WO_4^{2-} and MoO_4^{2-} ions on alumina versus acidity of H_2SO_4 solution; (b) elution profile of WO_4^{2-} and MoO_4^{2-} ions (column: 1 g alumina; eluent: 6 M H_2SO_4 for MoO_4^{2-} elution and 1 M NH_4OH for WO_4^{2-} stripping; loading solution: 8 mg Mo + 10 mg W) [27].

anion. The most important requirement for the design of an alumina column-based ^{99m}Tc recovery system is that it must exhibit both a high elution efficiency (typically >85%) and minimal [99]Mo breakthrough (<0.015%) [36, 37]. The generators are sold on the world market with different sizes from 200 mCi to 4000 mCi and the elution of ^{99m}Tc is performed with 5–10 mL normal saline. Fission [99]Mo-based [99]Mo/^{99m}Tc generators commercially available in the US are of the activity range between 0.2 Ci and 4.0 Ci at the six-day curies reference time and in ANSTO (Australia) between 0.45 Ci to 3.2 Ci. The cost-effective utilisation of a [99]Mo/^{99m}Tc generator and the quality of ^{99m}Tc based single photon emission computed tomography (SPECT) imaging diagnoses is controlled by the generator operation/elution management. The primary factor pertaining to the nuclear medicine diagnostic scans' quality is the concentration of ^{99m}Tc obtained from the [99]Mo/^{99m}Tc generator elution, which is expressed as activity per mL. The injection dose activity of ^{99m}Tc-based radiopharmaceuticals delivered in 1 mL solution (^{99m}Tc-concentration, mCi/mL) is an important factor in determining the useful life time of the ^{99m}Tc generators and the quality of ^{99m}Tc based SPECT imaging diagnosis as well. Generally, a ^{99m}Tc eluate is produced from the [99]Mo/^{99m}Tc generator in fixed volume and the concentration of the ^{99m}Tc in the eluted solution decreases with the life time of the [99]Mo/^{99m}Tc generator due to the radioactive decay of the parent nuclide [99]Mo. Consequently, the useful life time of the generator is also a function of available ^{99m}Tc concentration of the eluate. If we consider that the value 10–20 mCi of ^{99m}Tc per mL is used as a limit of the medically useful ^{99m}Tc solution, the assessment of the ^{99m}Tc generator utilisation effectiveness shows the following:

wasted residual activity of a used generator of 2 Ci activity eluted with 10 mL saline is 5–10% of its total activity, while smaller generators of 500 mCi activity waste up to 20–40%. In case of the concentrator used to increase the ^{99m}Tc concentration of the eluate eluted from these generators, all the activity of the generator will efficiently be exploited. So, the radioisotope concentrator device should be developed to increase the concentration and quality of injectable ^{99m}Tc eluates and consequently the generator life time or the effectiveness of the generator utilisation. Some concentration methods have been developed for increasing ^{99m}Tc concentration of the saline eluate for extension of the life time of the fission-[99]Mo-based ^{99m}Tc generators [38–44]. All these methods used a chloride-removing column containing Ag+ ions, which couple with a pertechnetate-concentrating sorbent column such as alumina, Bonelut-SAX, QMA, and multifunctional sorbent. Alternative concentration methods have also been developed. The alternatives are based on the elution of the alumina column of the generator with a nonchloride aqueous eluent (such as ammonium-acetate solution and less-chloride acetic acid solution) or with a nonchloride organic eluent (such as tributylammonium-bromide and acetone solvent). ^{99m}Tc-pertechnetate of this eluate is concentrated using a sorbent column (concentration column) or an organic solvent evaporator, respectively. Then ^{99m}Tc-pertechnetate is recovered in a small volume of normal saline for medical use [45–60]. These methods have significantly increased the life time of the generators. The use of nonchloride eluent in replacement of saline normally used in a commercial generator may not be preferable due to legal issues of the amended registration requirement. Unfortunately, no concentrator device prototypes developed based

(a)

(b)

(c)

(d)
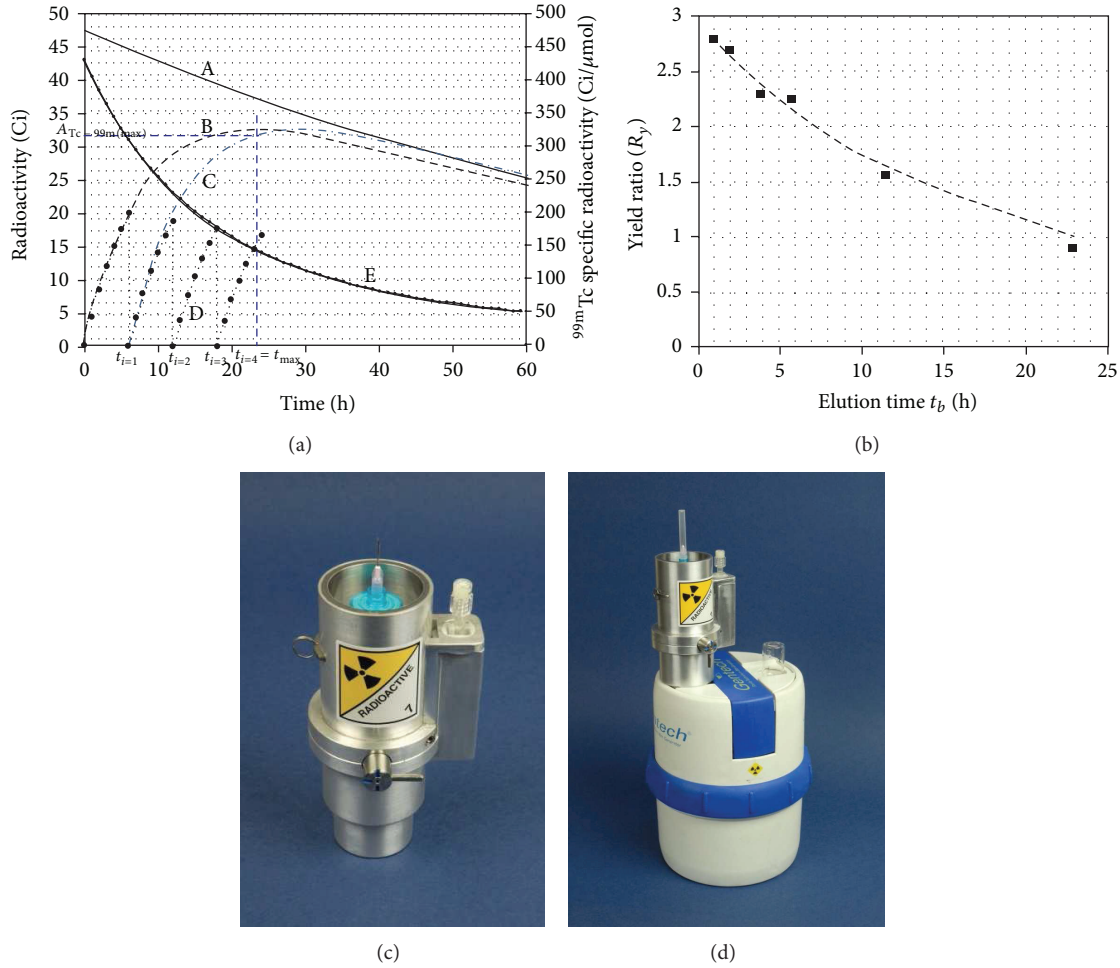
FIGURE 3: Radioisotope concentrator ULTRALUTE (patent-pending) and Effectiveness of ^{99m}Tc/^{99}Mo utilisation: (a) kinetics of radioactive decay/^{99m}Tc-activity buildup in the generator eluted with an early elution regime (A: ^{99}Mo-activity; B: ^{99m}Tc-activity buildup from beginning; C: ^{99m}Tc-activity growth after first elution; D: ^{99m}Tc-activity growth/eluted at 6-hour elutions; E: ^{99m}Tc-SA in the system of ^{99m}Tc-radioactivity buildup from beginning) [58]; (b) effectiveness of "early" elution regime for increasing ^{99m}Tc-elution yield of the generator compared with that normally eluted at the time point of maximal ^{99m}Tc-buildup (square is experimental and dashed line is theoretical calculation result) [58]; (c) ULTRALUTE concentrator device [41, 61]; (d) ULTRALUTE concentrator device inline-coupled with a ^{99m}Tc generator.

on the developed methods are commercially available up to date. Recently, Cyclopharm Ltd. (Australia) in cooperation with Medisotec (Australia) has developed a ^{99m}Tc /^{188}Re concentrator device ULTRALUTE [40–42] using a new sorbent as a concentrator column coupled with the saline-eluted commercial generator. This device (Figures 3(c) and 3(d)) is a sterile multielution cartridge which is operated/eluted by evacuated-vial through disposable sterile filters to increase the ^{99m}Tc concentration of the saline eluate of aged commercial ^{99m}Tc generators. The increase in ^{99m}Tc concentration in the eluate enhances the utilisation of ^{99m}Tc in Technegas generator-based lung perfusion (100–250 mCi/mL) and other SPECT (20–30 mCi/mL) imaging studies. The ^{99m}Tc-pertechnetate of the generator eluate was concentrated more than 10-fold with a ^{99m}Tc recovery yield of >85% using this radioisotope concentrator device. Five repeated elutions were successfully performed with each cartridge. So, each

cartridge can be effectively used for one week in daily hospital environment for radiopharmaceutical formulation. The useful lifetime of the ^{99m}Tc generator was significantly extended depending on the activity of the generator as shown in Table 2. The ^{99}Mo impurity detectable in the ^{99m}Tc solution directly eluted from Gentech generator was totally eliminated by this radioisotope concentrator device and ultrapure, concentrated ^{99m}Tc-pertechnetate solution was achieved. The concentrated ^{99m}Tc solution is well suited to labeling in vivo kits and to loading the crucibles of Technegas aerosol generator for V/Q SPECT imaging. The useful life time of the ^{99m}Tc generator (Table 2) was significantly extended from 10 to 20 days for the generators of 300–3000 mCi activity, respectively. This means that about 20% of the generator activity is saved by extending the life time of the generator. Besides that about 20% of the generator ^{99m}Tc-activity can be saved as a result of the extension of ^{99m}Tc-generator life time,

the use of radioisotope concentrator for the optimization of generator elution to increasing the ^{99m}Tc-activity yield and the effectiveness of ^{99}Mo utilization was reported by Le (2013) [58, 61]. This fact is shown as follows. ^{99m}Tc continuously decays to ^{99}Tc during his buildup from the decay of ^{99}Mo. This process not only reduces the ^{99m}Tc-activity production yield of the generator (i.e. a large quantity of ^{99m}Tc activity wasted during ^{99m}Tc activity buildup results in a lower ^{99m}Tc-activity production yield of the generator, so it is noneconomically exploited), but also makes the specific activity (SA) of ^{99m}Tc continuously decreased. The low SA may cause the labelling quality of ^{99m}Tc eluate degraded. This means that the elutions of the generator at a shorter build-up time of daughter nuclide will result in a higher accumulative daughter-activity production yield (more effectiveness of ^{99m}Tc/^{99}Mo activity utilisation) and a better labelling quality of the generator eluate. Accumulative production yield is the sum of all the yields achieved in each early elution performed before the maximal build-up time. However, each early ^{99m}Tc-elution at shorter build-up time ("early" elution) will result in a lower ^{99m}Tc-elution yield and thus yields an eluate of lower ^{99m}Tc-concentration because ^{99m}Tc is eluted from the generator in fixed eluent volume. These facts show that a high labelling quality solution of clinically sufficient ^{99m}Tc concentration could be achieved if the generator eluate obtained at an "early" elution is further concentrated by a certified radioisotope concentrator device.

A general method described in previous work of V. S. Le and M. K. Le [58] was applied for evaluation of the effectiveness of "early" elution regime in comparison with a single elution performed at maximal build-up time point of the radionuclide generators. For this evaluation, the daughter nuclide-yield ratio (R_y) is set up and calculated based on quotient of the total of daughter nuclide-elution yields ($\sum_{i=1}^{i=n} A_{d(E_i)}$) eluted in all i elutions (E_i is the index for the ith elution) divided by the maximal daughter nuclide-yield or daughter nuclide-activity ($A_{d(\text{Max})}$) which could be eluted from the generator at maximal build-up time t_{Max}: $R_y = \sum_{i=1}^{i=n} A_{d(E_i)}/A_{d(\text{Max})}$.

Starting from the basic equation of radioactivity buildup/yield (A_d) of a daughter nuclide and the maximal build-up time (t_{Max}) for attaining the maximal activity buildup of daughter nuclide radioactivity growth-in in a given radionuclide generator system, the equation for calculation of daughter nuclide-yield ratio (R_y) was derived as follows [58]:

$$R_y = \frac{\sum_{i=1}^{i=n} A_{d(E_i)}}{A_{d(\text{Max})}} = \frac{\sum_{x=0}^{x=i-1}\left[e^{-\lambda_p \cdot x \cdot t_b} \times \left(e^{-\lambda_p \cdot t_b} - e^{-\lambda_d \cdot t_b}\right)\right]}{\left(e^{-\lambda_p \cdot t_{\text{Max}}} - e^{-\lambda_d \cdot t_{\text{Max}}}\right)}.$$

(1)

(The subscripts p and d in the above equations denote the parent and daughter radionuclides, resp.).

As an example, the details of the case of ^{99m}Tc/^{99}Mo generator system are briefly described as follows:

numbers of radioactive ^{99}Mo nuclides:

$$N_{\text{Mo}} = N_{0,\text{Mo}} \times e^{-\lambda_{\text{Mo}} \cdot t}.$$

(2)

Radioactivity of ^{99m}Tc nuclides in the generator:

$$A_{\text{Tc-99m}} = \lambda_{\text{Tc-99m}} \times N_{0,\text{Mo}} \times b$$
$$\times \left(\frac{\lambda_{\text{Mo}}}{\lambda_{\text{Tc-99m}} - \lambda_{\text{Mo}}}\right) \times \left(e^{-\lambda_{\text{Mo}} \cdot t} - e^{-\lambda_{\text{Tc-99m}} \cdot t}\right),$$

(3)

the maximal build-up time (at which the maximal ^{99m}Tc-activity buildup/yield in ^{99}Mo/^{99m}Tc generator system is available):

$$t_{\text{Max}} = \frac{\left[\ln\left(\lambda_{\text{Tc-99m}}/\lambda_{\text{Mo-99}}\right)\right]}{\left(\lambda_{\text{Tc-99m}} - \lambda_{\text{Mo-99}}\right)}.$$

(4)

Numbers of Tc atoms at build-up time:

$$N_{\text{Tc}} = N_{\text{Tc-99}} + N_{\text{Tc-99m}}$$
$$= N_{0,\text{Mo}} - N_{\text{Mo}} = N_{0,\text{Mo}} \times \left(1 - e^{-\lambda_{\text{Mo}} \cdot t}\right).$$

(5)

Specific activity of carrier-included ^{99m}Tc in the ^{99m}Tc generator system or ^{99m}Tc-eluate is calculated using (3) and (5) as follows:

$$SA_{\text{Tc-99m}}$$
$$= \frac{A_{\text{Tc-99m}}}{N_{\text{Tc}}}$$
$$= \frac{\lambda_{\text{Tc-99m}} \cdot b \cdot \left(e^{-\lambda_{\text{Mo}} \cdot t} - e^{-\lambda_{\text{Tc-99m}} \cdot t}\right)}{0.6144 \times 10^{-7} \times \left(\left(\lambda_{\text{Tc-99m}}/\lambda_{\text{Mo}}\right) - 1\right) \times \left(1 - e^{-\lambda_{\text{Mo}} \cdot t}\right)}$$
$$(\text{Ci/mol}).$$

(6)

^{99m}Tc-Yield Ratio (R_y) Calculation for Multiple "Early" Elution Regime. The R_y value is calculated based on quotient of the total ^{99m}Tc-elution yields eluted (or ^{99m}Tc-activity produced/used for scans) in all i elution numbers (E_i is the index for the ith elution) divided by the maximal ^{99m}Tc-activity ($A_{\text{Tc-99m(Max)}}$) which would be eluted from the generator at maximal build-up time t_{Max}.

The total ^{99m}Tc-elution yields eluted in all i elutions are the sum of ^{99m}Tc-radioactivities at a different elution number i ($A_{\text{Tc-99m}(Ei)}$). This amount is described as follows:

$$\sum_{i=1}^{i=n} A_{\text{Tc-99m}(E_i)} = \lambda_{\text{Tc-99m}} \times \sum_{i=1}^{i=n} N_{\text{Tc-99m}(E_i)}$$
$$= \lambda_{\text{Tc-99m}} \sum_{x=0}^{x=i-1}\left[N_{0,\text{Mo}} \times e^{-\lambda_{\text{Mo}} \cdot x \cdot t_b} \times b \right.$$
$$\times \left(\frac{\lambda_{\text{Mo}}}{\lambda_{\text{Tc-99m}} - \lambda_{\text{Mo}}}\right)$$
$$\left. \times \left(e^{-\lambda_{\text{Mo}} \cdot t_b} - e^{-\lambda_{\text{Tc-99m}} \cdot t_b}\right)\right].$$

(7)

TABLE 2: Performance of ^{99m}Tc radioisotope concentrator device ULTRALUTE (effect of concentrator on generator useful life) [41, 61].

Generator activity, mCi (GBq)	Generator useful life for SPECT imaging, days		Generator useful life for lung imaging with Technegas, days	
	Without concentrator	Postelution concentrator	Without concentrator	Postelution concentrator
100 (3.7)	1	6	0	1
300 (11.1)	4	10	0	4
500 (18.5)	6	12	0	6
1000 (37.0)	9	15	1	9
3000 (111.0)	14	20	4	14

The maximal ^{99m}Tc-activity buildup/yield in ^{99}Mo/^{99m}Tc generator system is described using (3) and (4) as follows:

$$A_{\text{Tc-99m(Max)}} = \lambda_{\text{Tc-99m}} \times N_{0,\text{Mo}} \times b \times \left(\frac{\lambda_{\text{Mo}}}{\lambda_{\text{Tc-99m}} - \lambda_{\text{Mo}}} \right) \\ \times \left(e^{-\lambda_{\text{Mo}} \cdot t_{\text{Max}}} - e^{-\lambda_{\text{Tc-99m}} \cdot t_{\text{Max}}} \right). \quad (8)$$

^{99m}Tc-yield ratio (R_y) is derived from (7) and (8) as follows:

$$R_y = \frac{\sum_{i=1}^{i=n} A_{\text{Tc-99m}(E_i)}}{A_{\text{Tc-99m(Max)}}} \\ = \frac{\sum_{x=0}^{x=i-1} \left[e^{-\lambda_{\text{Mo}} \cdot x \cdot t_b} \times \left(e^{-\lambda_{\text{Mo}} \cdot t_b} - e^{-\lambda_{\text{Tc-99m}} \cdot t_b} \right) \right]}{\left(e^{-\lambda_{\text{Mo}} \cdot t_{\text{Max}}} - e^{-\lambda_{\text{Tc-99m}} \cdot t_{\text{Max}}} \right)}, \quad (9)$$

where b is the ^{99m}Tc-branch decay factor of ^{99}Mo($b = 0.875$); i is the number of the early elutions needed for a practical schedule of SPECT scans. The build-up time (t_b) for each elution is determined as $t_b = (t_{\text{Max}}/i)$; x is the number of the elutions which have been performed before starting a ^{99m}Tc-build-up process for each consecutive elution. At this starting time point no residual Tc atoms left in the generator from a preceding elution are assumed (i.e., ^{99m}Tc-elution yield of the preceding elution is assumed 100%).

The results of the evaluation (Figures 3(a) and 3(b)) based on (3), (6), and (9) show that the ^{99m}Tc-activity production yield of the generator eluted with an early elution regime of build-up/elution time <6 hours increases by a factor >2 and the ^{99m}Tc specific activity values of the eluates are remained higher than 160 Ci/μmol.

Obviously, the radioisotope concentrator not only may have positive impact on the extension of useful life time of the generators, but also is capable to increase both the ^{99m}Tc-activity production yield of the generator/effectiveness of ^{99m}Tc/^{99}Mo utilisation and the specific activity by performing the early elutions of the generator at any time before maximal buildup of ^{99m}Tc.

With the utilization of ^{99m}Tc concentrator device which gives a final ^{99m}Tc-solution of 1.0 mL volume, the experimental results obtained from a 525 mCi generator, as an example, confirmed that the concentration and the yield of ^{99m}Tc solution eluted with a 6-hour elution regime is much better than that obtained from the elution regime performed at the maximal build-up time (22.86 hours). Within first 6 days of elution, ^{99m}Tc-concentration of the generator eluates is in the range 200–44 mCi/mL and total ^{99m}Tc-activity eluted is 1715.7 mCi for a 6-hour elution regime (including the zero day elution) while the concentration of 83–18.2 mCi/mL and the total activity of 1015.1 mCi are for the elution regime performed at the maximal build-up time, respectively [58, 61]. The effectiveness of this early elution mode was also confirmed experimentally in the prior-of-art of ^{68}Ga/^{68}Ge generator [62–64].

3. Low Specific Activity ^{99}Mo: Current Issues of Production and Prospects

^{99}Mo/^{99m}Tc generators can be produced using low specific activity ^{99}Mo. Some technologies for producing low SA ^{99}Mo have been established. Unfortunately, several alternatives are not yet commercially proven or still require further development. Presently, no nuclear reaction-based nonfission method creates a ^{99}Mo source of reasonably high or moderate specific activity. The reason is that the cross-section of all these types of nuclear reactions, which are performed by both the nuclear reactor and accelerator facility, is low ranging from several hundreds of millibarns to <11.6 barns, compared with ^{99}Mo-effective fission cross-section (37 barns) of ^{235}U-fission used in the production of high SA ^{99}Mo as mentioned above. As shown below, SA of nonfission ^{99}Mo produced from nuclear reactor and accelerator facilities is in a range of 1–10 Ci/g Mo. To produce the ^{99m}Tc generators of the same activity size (1–4 Ci) as in case of high SA ^{99}Mo mentioned above, the ^{99m}Tc recovery system capable for processing Mo-target of several grams weight should be available, even though the enriched ^{98}Mo and/or ^{100}Mo targets are used instead of natural Mo target [2].

3.1. ^{99}Mo Production Based on Reactor Neutron Capture. Neutron capture-based ^{99}Mo production is a viable and proven technology established in the years 1960s. There are thirty-five isotopes of molybdenum known today. Of seven naturally occurring isotopes with atomic masses of 92, 94, 95, 96, 97, 98, and 100, six isotopes are stable with atomic masses from 92 to 98. ^{100}Mo is the only naturally occurring radioactive isotope with a half-life of approximately 8.0E18 years, which decays double beta into ^{100}Ru. All radioactive isotopes of molybdenum decay into isotopes of Nb, Tc, and Ru. ^{98}Mo, ^{94}Mo, and ^{100}Mo (with natural abundance 24.1%, 9.25%, and 9.6%, resp.) are the most common isotopes used in

the targetry for production of two important medical isotopes ^{99m}Tc and ^{94}Tc.

High SA ^{99}Mo cannot be produced via (n, γ) reaction using Mo targets because the thermal neutron cross-section for the (n, γ) reaction of ^{98}Mo is relatively small at about 0.13 barn, a factor of almost 300 times less than that of the ^{235}U fission cross-section. In this respect, irradiation of Mo targets in an epithermal neutron flux could be economically advantageous with respect to producing higher SA ^{99}Mo. The epithermal neutron capture cross-section of ^{98}Mo is about 11.6 barn. The assessment of reaction yield and SA of the Mo targets irradiated with reactor neutrons [28, 65] shows that the irradiation time needed to reach a maximum yield and maximum SA in Mo targets is too long, while the improvement in reaction yield/SA is insignificant due to the low cross-section of ^{98}Mo$(n, \gamma)^{99}$Mo reactions. Neutron capture-based ^{99}Mo production with an 8-day irradiation in a reactor of $1.0E14\,\text{n} \cdot \text{cm}^{-2} \cdot \text{sec}^{-1}$ thermal neutron flux gives a ^{99}Mo product of low SA as evaluated at EOB as follows: ~1.6 Ci ^{99}Mo/g of natural isotopic abundance molybdenum and/or 6 Ci ^{99}Mo/g of 98%-enriched ^{98}Mo target. These values show a factor of 10^4 times less than that of fission-produced high SA ^{99}Mo as mentioned above. The loose-packed MoO$_3$ powder (density of $> 2.5\,\text{g/cm}^3$), pressed/sintered Mo metal powder (density of $< 9.75\,\text{g/cm}^3$), and granulated Mo metal can be used as a target material. High-density pressed/sintered ^{98}Mo metal targets are also commercially available for the targetry. MoO$_3$ powder can be easily dissolved in sodium hydroxide. Molybdenum metallic targets can be dissolved in alkaline hydrogen peroxide or electrochemically. The metal form takes more time to dissolve than the MoO$_3$ powder form. However, the advantage of using Mo metal target is that larger weight of Mo can be irradiated in its designated irradiation position in both the research and power nuclear reactors [66, 67]. The neutron flux depression in the MoO$_3$ target may cause decreasing in ^{99}Mo production yield when a large target is used [68–70]. The production capacities of 230 6-day Ci/week and 1000 6-day Ci/week are estimated for the irradiation with JMTR research reactor in Oarai and with a power reactor BWR of Hitachi-GE Nuclear Energy, Ltd., in Japan, respectively [66, 71]. The use of enriched ^{98}Mo target material of 95% isotopic enrichment offers the ^{99}Mo product of higher SA. The W impurity in the natural Mo target material should be <10 ppm and that is not detectable in the enriched ^{98}Mo targets. Due to high cost of highly enriched ^{98}Mo, the economical use of this target material requires a well-established recycling of irradiated target material [2, 24, 25, 66, 67, 72–74].

3.2. Accelerator Based ^{99}Mo/^{99m}Tc Production.
All of the accelerator-based nonfission approaches rely on highly enriched ^{100}Mo target. While the 99% enrichment ^{100}Mo is sufficient for all accelerator-based ^{99}Mo productions, the direct production of ^{99m}Tc may require enrichments exceeding >99.5% due to the possible side reactions which generate long-lived technetium and molybdenum isotopes because these impure radionuclides would cause an unnecessary radiation dose burden to the patient and the waste disposal issues as well. The SA of ^{99}Mo produced from the accelerators is too low for use in existing commercial ^{99m}Tc generator systems that use alumina columns. New ^{99m}Tc recovery technology that is suitable for processing the accelerator targets of low specific activity ^{99}Mo and allowing effective recycling of ^{100}Mo should be developed [2].

While the specific activity of ^{99}Mo produced using accelerators (ranging up to 10 Ci/g at EOB) is not significantly higher than that of ^{99}Mo produced by neutron capture using nuclear reactor, the ^{99}Mo production using accelerator is presently focused in many research centres with regards to its safer and less costing operation compared with nuclear reactor operation. It is important to be addressed that all of the accelerator-based nonfission-^{99}Mo production routes need a well-established technology for recycling of the ^{100}Mo target material. This will be somewhat complicated since the ^{100}Mo target material is contaminated with the ^{99}Mo left from the used ^{99m}Tc generator systems. Handling this material presents some complicated logistics in that the target material will have to be stored until the level of ^{99}Mo is sufficiently low so as to not present radiation handling problems. Moreover, the purification of the used ^{100}Mo target must be addressed to ensure completely removing all impurities which are brought from the chemicals and equipment used in the production processes.

3.2.1. Photon-Neutron Process ^{100}Mo$(\gamma, n)^{99}$Mo.
High energy photons known as Bremsstrahlung radiation are produced by the electron beam (50 MeV electron energy with 20–100 mA current) as it interacts and loses energy in a high-Z converter target such as liquid mercury or water-cooled tungsten. The photon-neutron process is performed by directing the produced Bremsstrahlung radiation to another target material placed just behind the convertor, in this case ^{100}Mo, to produce ^{99}Mo via the ^{100}Mo$(\gamma, n)^{99}$Mo reaction (maximal cross-section around 170 millibarns at 14.5 MeV photon energy [25]). Although the higher SA ^{99}Mo (360 Ci/g) can be achieved with a smaller weight target (~300 mg ^{100}Mo), the ^{99}Mo produced based on a routine production base has a much lower SA, approximately 10 Ci/g [75].

3.2.2. Proton-Neutron Process ^{100}Mo$(p, pn)^{99}$Mo.
30 MeV cyclotron can be used for ^{99}Mo production based on ^{100}Mo$(p, pn)^{99}$Mo reaction (maximal cross-section around 170 millibarns at 24 MeV proton energy). ^{99}Mo production yield of <50 Ci can be achieved with a bombardment current 500 mA for 24 hours [76–79].

3.2.3. Neutron-Neutron Process ^{100}Mo$(n, nn)^{99}$Mo.
^{99}Mo production based on ^{100}Mo$(n, 2n)^{99}$Mo reaction (maximal cross-section around 1000 millibarns at 14 MeV neutron energy) using fast neutron yielded from the $D(T, n)$ reaction. The established targetry, sufficient flux of neutrons, and improvement in ^{99m}Tc separation are issues to be addressed for further development [80].

3.2.4. Direct Production of ^{99m}Tc. The first report on the feasibility of producing ^{99m}Tc by proton irradiation of ^{100}Mo stated that a theoretical yield of 15 Ci ^{99m}Tc per hour can be achieved with 22 MeV proton bombardment at 455 μA [81]. More recently, Takács et al. found a peak cross-section of 211 ± 33 mb at 15.7 MeV [79]. Scholten and colleagues suggested that the use of a >17 MeV cyclotron could be considered for regional production of ^{99m}Tc with a production yield of 102.8 mCi/μA at saturation [78]. Estimated yield of ^{99m}Tc production based on a routine production basis is 13 Ci ^{99m}Tc (at EOB), using 18 MeV proton beam of 0.2 mA current for a 6-hour irradiation. A irradiation of highly enriched ^{100}Mo target (pressed/sintered metallic ^{100}Mo powder) using GE PET Trace cyclotron (16.5 MeV proton beam, 0.04 mA current, and 6-hour bombardment) at Cyclopet (Cyclopharm Ltd., Australia) can achieve >2.0 Ci ^{99m}Tc at EOB as reported by Medisotec (Australia). Using >99.5% enriched ^{100}Mo target produces very pure ^{99m}Tc. The ^{99m}Tc product of >99.6% radionuclide purity can be achieved. The major contaminants include ^{99g}Tc, ^{95}Tc, and ^{96}Tc. Trace amounts of ^{95}Nb are produced from the ^{98}Mo$(p, \alpha)^{95}$Nb reaction [75–83].

3.3. Methods of Increasing the Specific Activity of ^{99}Mo

3.3.1. Szilard-Chalmers Recoiled ^{99}Mo. A method to increase the specific activity of neutron activated ^{99}Mo in the natural and/or enriched Mo targets using Szilard-Chalmers recoiled atom chemistry was recently reported by the scientists at the Delft University of Technology in the Netherland. The targets used in this process are ^{98}Mo containing compounds such as molybdenum(0)hexacarbonyl [Mo(CO)$_6$] and molybdenum(VI)dioxodioxinate [C$_4$H$_3$(O)–NC$_5$H$_3$)]$_2$–MoO$_2$, molybdenum nanoparticles (~100 nm), and other molybdenum tricarbonyl compounds. The neutron irradiated targets are first dissolved in an organic solvent such as dichloromethane (C$_2$H$_2$Cl$_2$), chloroform (CH$_3$Cl), benzene (C$_6$H$_6$), and toluene (CH$_3$–C$_6$H$_5$). Then the ^{99}Mo is extracted from this target solution using an aqueous buffer solution of pH 2–12. The target material is to be recycled. This process is currently in the stage of being scaled up towards demonstration of commercial production feasibility. The specific activity of ^{99}Mo increased by a factor of more than 1000 was achieved, making the specific activity of neutron capture-based ^{99}Mo comparable to that of the high SA ^{99}Mo produced from the ^{235}U fission. So the ^{99}Mo produced by this way can be used in existing commercial ^{99m}Tc generator systems that use alumina columns [84, 85].

3.3.2. High Electric Power Off-Line Isotopic Separator for Increasing the Specific Activity of ^{99}Mo. A high power ion source coupled to a high resolution dipole magnet would be used to generate beams of Mo ions and separate the respective isotopes with the aim of producing ^{99}Mo with specific activity of greater than 1000 Ci/gram. The construction of a high power off-line isotope separator to extract high specific activity ^{99}Mo that had been produced via ^{98}Mo(n, γ) and/or ^{100}Mo(γ, n) routes would allow for rapid introduction of the ^{99}Mo into existing supply chain. The feedstock for the separator system will be low specific activity ^{99}Mo generated from the thermal neutron capture of ^{98}Mo or the photon induced neutron emission on ^{100}Mo. The proposed system would have the advantage that the ^{99}Mo produced will fit directly into the existing commercial generator system, eliminating the use of HEU and LEU targets, and can be used to generate the required target material (^{98}Mo/^{100}Mo) during the separation process. In addition, it can be used in conjunction with a neutron or photon sources to create a distributed low cost delivery system [2, 86].

4. Up-to-Date Technologies of ^{99m}Tc Recovery from Low Specific Activity ^{99}Mo: ^{99}Mo/^{99m}Tc Separation Methods, ^{99m}Tc Purification/Concentration, and ^{99m}Tc Generator Systems

Unfortunately, the low SA ^{99}Mo produced using the methods mentioned above contains the overwhelming excess of nonradioactive molybdenum so as the alumina columns used in existing commercial ^{99m}Tc generator systems would be sufficiently loaded to produce the medically useful ^{99m}Tc doses because the ^{99m}Tc recovery from this ^{99}Mo source of low SA requires significantly more alumina resulting in a large elution volumes. Consequently, a solution of low ^{99m}Tc-concentration is obtained from these generator systems. To make a low SA ^{99}Mo source useful for nuclear medicine application, some ^{99m}Tc recovery technologies for producing medically applicable ^{99m}Tc solution have been established. Unfortunately, several alternatives are not yet commercially proven or still require further development. The primary factor pertaining to the nuclear medicine scans' quality is the concentration of ^{99m}Tc in the solution produced from the ^{99}Mo/^{99m}Tc generator, which is expressed as ^{99m}Tc activity per mL. The injection dose activity of ^{99m}Tc-based radiopharmaceuticals delivered in 1 mL solution is an important factor in determining the efficacy of the ^{99m}Tc generators and the quality of ^{99m}Tc-based SPECT imaging diagnosis as well. So, the ^{99m}Tc recovery technologies should be developed so as a sterile injectable ^{99m}Tc solution of high activity concentration and low radionuclidic and radiochemical/chemical impurity is obtained.

Up-to-date ^{99m}Tc recovery technologies fall into four general categories: solvent extraction, sublimation, electrolysis, and column chromatography.

4.1. Solvent Extraction for ^{99}Mo/^{99m}Tc Separation and Solvent Extraction-Based ^{99m}Tc Generator Systems. Solvent extraction is the most common method for separating ^{99m}Tc from low specific activity ^{99}Mo dated back to the years 1980s. The solvent extraction method can produce ^{99m}Tc of high purity comparable to that obtained from alumina column-based ^{99m}Tc generator loaded with fission-^{99}Mo of high specific activity. Several extraction systems (extractant-solvent/back-extraction solution) using different extractant agents (such as
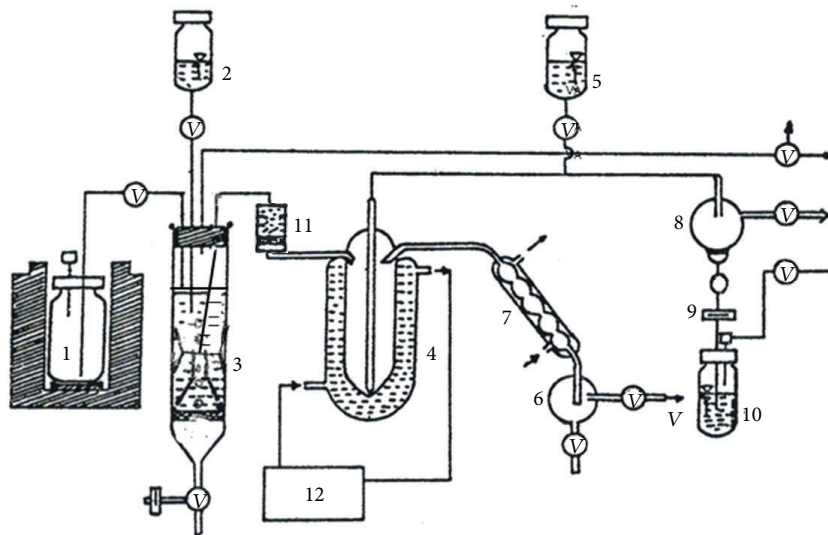
FIGURE 4: Diagram of MEK extraction-based ^{99}Mo/^{99m}Tc generator [60]. 1: alkaline ^{99}Mo-molybdate solution; 2: MEK solvent; 3: extractor; 4: MEK evaporator; 5: saline; 6: MEK receiver; 7: condenser; 8: ^{99m}Tc solution receiver; 9: Millipore filter; 10: final ^{99m}Tc solution vial; 11: acidic alumina column; 12: 70°C water circulator; v: valve; V: vacuum line.

ketones, crow ethers, trioctylamine, tricapryl methyl ammonium chloride (Aliquat-336), liquid ion-exchangers, and ionic liquids) were investigated [35, 60, 87–91]. Among the extractant compounds investigated, methyl ethyl ketone (MEK) is the best for the extraction of ^{99m}Tc-pertechnetate in terms of high extraction yield, high radiation stability, and low boiling temperature. Generators based on MEK extraction of ^{99m}Tc-pertechnetate from alkaline aqueous molybdate solutions have been widely used for the production of ^{99m}Tc. The extraction cycle consists of adding a mixture of MEK solvent containing 1% aqueous hydrogen peroxide to the 5 M NaOH solution of ^{99}Mo target and mechanically stirring the mixture to selectively extract the ^{99m}Tc from the aqueous phase into the MEK phase. The hydrogen peroxide is added to keep the ^{99}Mo and ^{99m}Tc in the appropriate oxidation state. After standing of the mixture to allow the phase separation, the supernatant MEK/^{99m}Tc solution/organic phase containing the extracted ^{99m}Tc is removed by sucking effected by a negative pressure and then it is passed through an acidic alumina to remove any ^{99}Mo that may be coextracted with ^{99m}Tc into the MEK solution. In the following, the MEK/^{99m}Tc solution is transferred to an evaporation vessel (evaporator). The evaporator is heated to ~70°C under a slight negative pressure to hasten the evaporation of the MEK. After the MEK has been completely removed, sterile saline is added to the evaporator to recover the ^{99m}Tc in the form of sodium-(^{99m}Tc) pertechnetate dissolved in the saline. This ^{99m}Tc saline solution is then sterilized by passing through a Millipore filter and transferred into a sterile vial for further processing at quality control and for formulating the radiopharmaceuticals.

The centralized solvent extraction-based ^{99m}Tc generator systems have been successfully performed for more than decade in Australia [92] and Czechoslovakia [6, 35, 93, 94].

Some other systems are routinely used in Russia, Peru, and in Asian countries where the fission ^{99}Mo-based chromatographic ^{99m}Tc generators do not enter the competition [60, 87, 95–97]. As an example, a centralized extraction-based ^{99m}Tc generator used for many years in a hospital in Vietnam is shown in Figure 4 [60].

The shortage in the fission ^{99}Mo supply today, however, has encouraged the ^{99m}Tc users over the world to use more effectively the solvent extraction-based ^{99m}Tc as well. So the less competitive solvent extraction-based ^{99m}Tc-generator systems developed several decades before should be upgraded to be used as a user-friendly prototype for a daily use in hospital environments. The update solvent extraction-based ^{99m}Tc generator systems under development are designed for an automated or semiautomated operation based either on the established extraction process [95, 98–100] as mentioned above or on the improved extraction technologies. The improvement in the removing of MEK from the extracted ^{99m}Tc-MEK organic phase to obtain ^{99m}Tc-pertechnetate is essential in the update MEK extraction technologies, because this will make the extraction being performed with ^{99m}Tc recovery into a aqueous solution without the complicated step of MEK evaporation, thus facilitating the process automation. This improved technology is based on the nonevaporation removing of MEK by passing the extracted ^{99m}Tc-MEK organic phase through a cation-exchange resin or basic alumina column coupled with an acidic alumina column, followed by a water wash to completely remove both ^{99}Mo contaminant and MEK. Then the ^{99m}Tc pertechnetate retained on the acidic alumina column will be eluted with a small volume of saline solution to achieve an injectable ^{99m}Tc pertechnetate solution. This approach has been developed in Japan in 1971 [71, 101, 102] and recently resurrected in India and Russia [95, 99, 100]. The process is pictorially described

in Figure 5. A computerized compact module for ^{99m}Tc separation based MEK extraction coupled with the MEK removing unit, which composes of a tandem of basic/acidic alumina columns, is developing in BRIT [100].

4.2. Sublimation Methods for ^{99}Mo/^{99m}Tc Separation and Sublimation-Based ^{99m}Tc Generator Systems.

Three sublimation methods for ^{99}Mo/^{99m}Tc separation have been developed and commercially used in past decades [6, 35, 66, 70, 71, 92, 94, 112, 113]. The first is the high temperature sublimation method developed at the end of the sixties and used for many years in Australia, which is based on the heating a neutron-activated MoO$_3$ target on >800°C in a furnace with oxygen stream passed through. The sublimed ^{99m}Tc in the form of Tc$_2$O$_7$ is condensed in the cold finger at the end of the furnace and ^{99m}TcO$_4^-$ is isolated by rinsing the cold finger with a hot 0.1 mM NaOH solution followed by purification on alumina. Some modified versions of this method were performed to achieve higher ^{99m}Tc recovery yield. The highest yield obtained was around 80% with a sublimation time of 20–30 minutes. The second method is the medium temperature sublimation. This method relies on heating a eutectic mixture of ^{99}Mo-molybdenum oxide and metal oxides on temperature between 500 and 750°C in an air flow and ~90% of ^{99m}Tc is recovered in the same way as applied in the first method. The third method is the low temperature sublimation. This method is based on the heating the solid powders of ^{99}Mo-molybdate of tetravalent metals such as titanium and zirconium molybdate on 380–450°C in a water vapour flow and 40–65% of ^{99m}Tc is recovered in the saline in form of ready-to-use. Based on this method, the portable sublimation ^{99m}Tc generators were commercially produced in the nineteen eighties and used for years in several hospitals in Hungary [92, 94, 114, 115]. The thermochromatographic separation at an oven temperature of 1090°C has also been successfully utilized for the recovery of ^{94m}Tc from ^{94}MoO$_3$ in the years 1990s [116]. This approach is expected to be used for the ^{99m}Tc separation from ^{99}Mo targets. From that time until now, no update version of the sublimation-based ^{99m}Tc recovery technology is found in the literature.

4.3. Electrochemical Methods for ^{99m}Tc Recovery.

In the past the electrochemical separation of ^{99m}Tc from ^{99}Mo was performed for a radioanalytical purpose. Recently, Chakravarty et al. have further developed this method for seeking a ^{99m}Tc production capability using a low specific activity ^{99}Mo. The ^{99m}Tc electrodeposit and the followed pertechnetate recovery were performed at the voltage 5 V (current 500 mA and current density 300 mA/cm^2) and 10 V (reversed polarity), respectively. Postelectrolysis purification of ^{99m}Tc solution was also completed with an alumina column [117, 118].

4.4. Column Chromatographic Methods for ^{99m}Tc Recovery and Integrated ^{99m}Tc Generator Systems (Column Chromatography-Based ^{99m}Tc Generator Coupled with Postelution Purification/Concentration Process).

The ^{99m}Tc recovery technologies used in the separation of ^{99m}Tc from low specific activity ^{99}Mo, which are based on the column chromatographic method, are recognized as the best ways to bring the low SA ^{99}Mo-based ^{99m}Tc generators to the hospital users with minimal fission/nonfission Mo discrimination. Conventional chromatographic generators using alumina columns are not compatible with the loading with low SA ^{99}Mo due to its overwhelming excess of nonradioactive molybdenum. By rule of thumb, 1-2% of adsorption capacity of the alumina column loaded with molybdenum is tolerated to avoid a harmful ^{99}Mo breakthrough in the final ^{99m}Tc saline eluate. To produce a generator of acceptable activity using low SA ^{99}Mo a significantly large alumina column is required to be capable to adsorb 1-2 g of Mo target, because the capacity of alumina for Mo adsorption is limited (~20 mg Mo/g of alumina). A large alumina column requires large volume of the eluent to elute patient-dose quantities of ^{99m}Tc. As a consequence, large eluent volumes cause the radioactive concentration of the ^{99m}Tc-pertechnetate to become unacceptably low for use in most radiopharmaceutical diagnostic procedures. So, the postelution concentration process is required to increase the ^{99m}Tc-activity concentration. Although the recovery of ^{99m}Tc from enriched molybdenum target material has been applied in Uzbekistan and POLATOM, the ^{99m}Tc concentration of the eluate eluted from an enriched ^{98}Mo target-based generator is moderately improved with the use of high neutron flux reactor irradiation [2].

In principle, there is no impediment for simple in-line concentration of the ^{99m}Tc solution obtained from large alumina column generators using simple postelution concentration technologies. As examples, the large alumina column-based ^{99m}Tc generators using low specific activity ^{99}Mo, eluted with chloride (saline) or nonchloride (acetone) eluent and combined with a ^{99m}Tc concentration unit, were tested. The first low SA (7–15 GBq/g) ^{99}Mo-based ^{99m}Tc generator system using up to 80-gram alumina column (jumbo alumina column generator) was developed in India [52, 53]. 70 mL saline is used for ^{99m}Tc elution from this system and a concentration process with three consecutive processing steps (^{99m}Tc loading onto Dowex-1×8 resin column; ^{99m}Tc elution from the resin column with 0.2 M NaI solution; removing of I$^-$ ions from the effluent downstream with AgCl column) was applied. The second generator system was developed in Pakistan using a large alumina (16 g) column and acetone eluent (nonchloride organic eluent) [51]. ^{99m}Tc recovery in a small volume of saline was followed after removing acetone from the ^{99m}Tc /acetone eluate.

Despite the high recovery yield and good labelling quality of the highly concentrated ^{99m}Tc solution achieved, the time consumption for a large volume elution and the complexity in processing at concentration stage make large alumina column-based generator systems as described above inconvincible for a commercial scale production and for the convenient utilization in the hospital environment. So, the recovery of ^{99m}Tc from the low SA ^{99}Mo still requires further development to make it useful for nuclear medicine application. As a result of the development performed in many laboratories

(a)

(b)

(c)
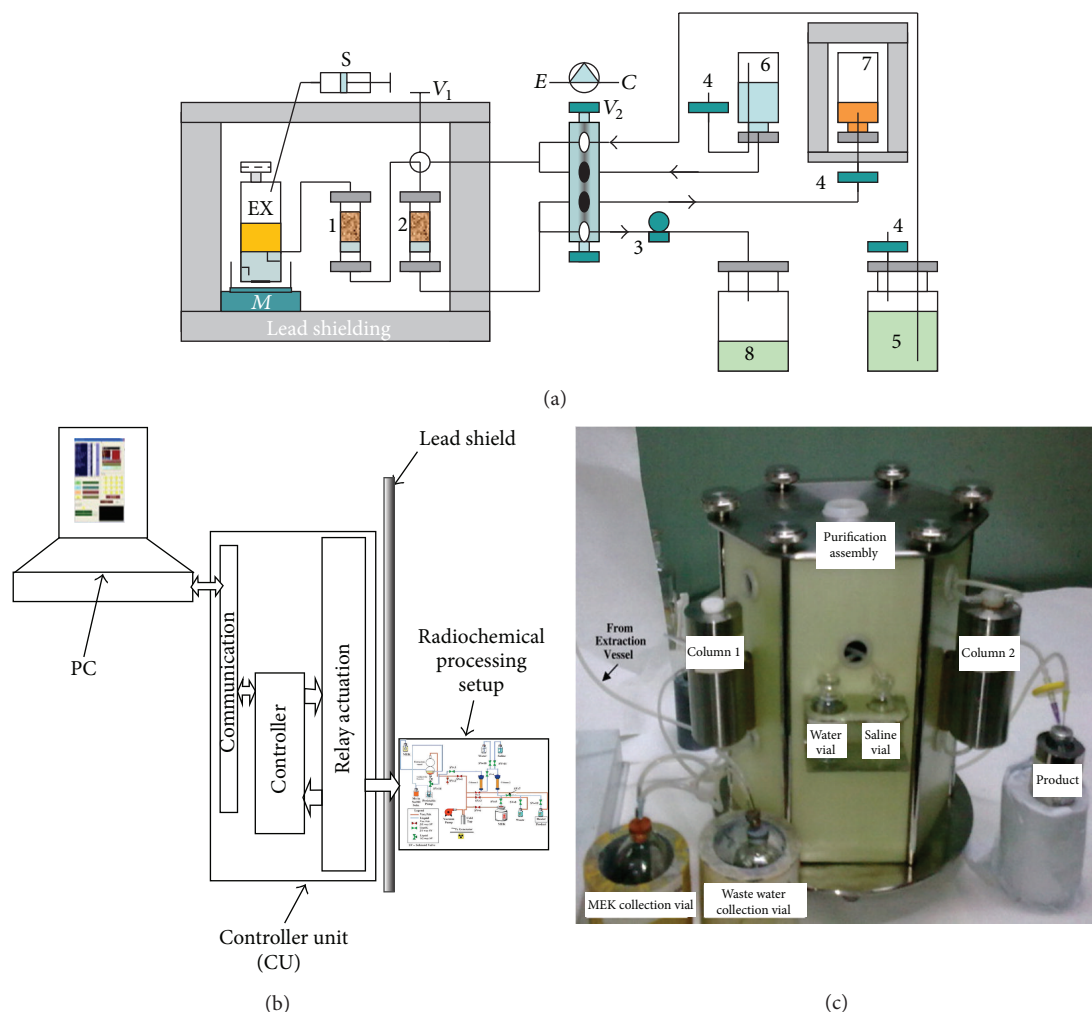
FIGURE 5: MEK extraction of ^{99m}Tc using a tandem sorbent column system for nonevaporation removing of MEK from the extracted ^{99m}Tc-MEK phase: (a) conceptual process diagram of ^{99m}Tc recovery by MEK extraction using a tandem cation-exchange resin/acidic alumina column system for nonevaporation removing of MEK (1: cation-exchange resin column; 2: alumina column; 3: peristaltic pump; 4: Milipore filter; 5: redistilled water; 6: saline; 7: final sterile ^{99m}Tc-pertechnetate solution; 8: waste container; V_1 and V_2: solenoid valves; S: syringe for MEK addition; EX: extractor containing ^{99}Mo; M: magnetic stirrer). The generator design is performed by author of this paper based on the processes reported in the literature [98, 102]. (b) Process diagram and (c) computerized module developed in BRIT for ^{99m}Tc separation based on the MEK extraction coupled with MEK-removing using a tandem basic/acidic alumina column system [99, 100].

around the world, some useful ^{99m}Tc recovery technologies developed up to date are described in the following.

It is the fact that the solution of high ^{99m}Tc concentration cannot directly be produced from the low specific activity ^{99}Mo source, except the ^{99m}Tc production based on the solvent extraction, sublimation, and electrochemical methods mentioned above. So, the technetium recovery technology based on the coupling a chromatographic ^{99m}Tc-generator column of high Mo-loading capacity with a postelution purification/concentration process/unit should be considered as an important solution. This technical solution is performed by an integrated system, so-called RADIGIS (radioisotope generator integrated system) to produce a medically useful ^{99m}Tc-pertechnetate solution of sufficiently

high ^{99m}Tc-concentration. In the following, different versions of RADIGIS developed to date are described.

4.4.1. Technetium Selective Sorbent Column-Based ^{99m}Tc Recovery and Relevant Integrated ^{99m}Tc Generator System. Several sorbents have been developed for selective adsorption of pertechnetate ions from aqueous solutions. Some of them, such as TEVA Spec resin (Aliquat-336 or tricapryl methyl ammonium chloride extractant impregnated in an inert substrate) and activated charcoal, adsorb TcO_4^- ions strongly in dilute nitric acid solutions. However, the strong acidic solution (8 M HNO_3) required for recovery of TcO_4^- ions is not preferred for practical application on the basis of daily use in nuclear medicine [119–123]. Some sorbents, such as

ABEC (aqueous biphasic extraction chromatographic) resin and strong anion-exchange (Dowex-1×8) resin, adsorb TcO_4^- ions from alkaline or neutral aqueous solutions. These resins are suitable for use in the production of ^{99m}Tc-generator by virtue of the fact that TcO_4^- ions can be easily desorbed from these sorbents by contacting with water or suitable organic solvent [124, 125].

(1) Aqueous Biphasic System-Based ^{99m}Tc-Pertechnetate Recovery Method [124, 126–131]. A ^{99m}Tc selective sorbent (ABEC-2000) column is recently developed to separate ^{99m}Tc from the alkaline solution of low specific activity ^{99}Mo. A new generator system developed by NorthStar Medical Radioisotopes (USA) using low specific activity ^{99}Mo is based on the ABEC-2000 resin column coupled with an alumina guard column. This system is shown in Figure 6.

The separation process is performed as follows. An alkaline ^{99}Mo solution in 5 M NaOH obtained from dissolution of molybdenum targets is fed onto the ABEC-2000 resin column which is specifically designed to adsorb pertechnetate. Once the column is loaded, it is first washed with 5 M NaOH solution to remove any molybdate that also may have been adsorbed on the column and then by a buffer solution of pH 8. Following the wash, the technetium is stripped from the column with a normal saline solution which is then passed through an alumina guard column to remove the residual ^{99}Mo impurities. The eluate is then passed through dual 0.22 micron sterility filters to achieve an injectable ^{99m}Tc-pertechnetate solution. The process can be repeated once a day as the ^{99m}Tc builds up in the ^{99}Mo solution. The ^{99m}Tc separation efficiencies for several consecutive days of operation were >90% with no detectable ^{99}Mo breakthrough. To date, the inherent disadvantage of this generator system reflected from the comment of user is that the elution process of this system takes a long time (about 40 minutes) and requires a 15-minute procedure for cleaning of column and tubing before the next elution is available. There is also some process to replace some components of the generator system that must be done after 5 elutions. Although the automated operation of this system facilitates the cumbersome elution-cleaning-replacing process, its being accepted as a user-friendly device may be challenged by the hospital user's community who is quite familiar to the simple operation of the current fission ^{99}Mo-based ^{99m}Tc generators.

The specific volume of ^{99m}Tc solution produced by this ^{99m}Tc recovery system is comparable to that of an alumina column generator loaded with the high SA fission. This new generator system is currently in the process of being validated for nuclear pharmacy use through a NDA on file with the US Food and Drug Administration [2, 130, 131].

(2) Organic Solvent-Eluted Ion-Exchange Resin Column-Based ^{99m}Tc-Pertechnetate Recovery Method. The chromatographic system of Dowex-1×8 resin column combined with tetrabutyl-ammonium-bromide (TBAB) eluent has been developed for separation of pertechnetate ions from aqueous ^{99}Mo-molybdate solution. Using commercially available anion-exchange resin Dowex-1×8 (25 mg) to selectively trap

and separate ^{99m}TcO$_4^-$ from a low specific activity ^{99}Mo solution and then recovering ^{99m}TcO$_4^-$ ions from the Dowex-1×8 column by elution with TBAB in CH_2Cl_2 were reported. After being purified by passing through a neutral alumina column and washing the resin column with water, the alumina column will be flushed with saline to strip Na^{99m}TcO$_4$. Subsequent quality control revealed no significant levels of trace metal contaminants or organic components. ^{99m}Tc recovery yields of greater than 90% were demonstrated, while radiochemical purity was consistently over 99% [125].

4.4.2. High Mo-Loading Capacity Column-Based ^{99m}Tc Recovery and Relevant Integrated ^{99m}Tc Generator Systems. The assessment on the capable utilisation of the high Mo-loading columns loaded with low specific activity $(n, \gamma)^{99}$Mo for production of ^{99m}Tc-generator is performed based on the ^{98}Mo $(n, \gamma)^{99}$Mo reaction yield (A_{Mo-99}) and Mo-loading capacity of column packing material (K). The relationship between the neutron flux Φ of the reactor used for the ^{99}Mo production and the Mo-loading capacity (K) of the column packing material is derived [69, 70, 103, 132].

Based on the activation equation for the neutron capture reaction ^{98}Mo$(n, \gamma)^{99}$Mo $\rightarrow$ ^{99m}Tc, the ^{99}Mo activity/yield (A_{Mo-99}) and the relationship between A_{Mo-99} and K are calculated as follows:

$$A_{Mo-99} = 1.628 \times 10^{-13} \left(\frac{\Theta \times G \times \sigma_{act} \times \Phi}{a} \right)$$
$$\times \left(1 - e^{-0.693(t/T)} \right),$$
$$A_{Mo-99} = 2.055 \times 10^{-14} \times G \times \Phi \times \left(1 - e^{-0.0104 \times t} \right) \quad (10)$$
$$G = \frac{A_{Mo-99}}{2.055 \times 10^{-14} \times \Phi \times \left(1 - e^{-0.0104 \times t} \right)},$$
$$K = \frac{G}{m} = \frac{A_{Mo-99}}{2.055 \times 10^{-14} \times m \times \Phi \times \left(1 - e^{-0.0104 \times t} \right)}.$$

$K = G/m$ is the Mo-loading capacity of the packing material loaded in one generator column. $G(g)$ is the weight of molybdenum element target, which will be used for the production of one generator. $m(g)$ is the weight of column packing material packed in one generator column. A_{Mo-99}(Ci) is the given ^{99}Mo radioactivity of the generator, which is planned to be produced. t is the activation time, hour. $\Theta = 23.75\%$ is the natural abundance of ^{98}Mo. $a = 95.94$ is the molecular weight of molybdenum. $T = 66.7$ hours is the halt-life of ^{99}Mo. $\sigma_{Act} = 0.51$ barn is the normalised thermal and epithermal neutron activation cross-section of ^{98}Mo nuclide.

It is assumed that a generator column of the best performance for pertechnetate elution can be eluted with an eluent of volume V(mL) $= 2m$, where m (g) is the weight of the column packing material. The relationship between the ^{99m}Tc concentration in the eluate (C_{Tc}), the neutron flux, and K is also set up. This relationship shown in Figure 7 is for a given case of the following conditions. The weight of the column packing material is 5 g and corresponding elution volume is 10 mL. The activation time of natural Mo target is l00 hours.
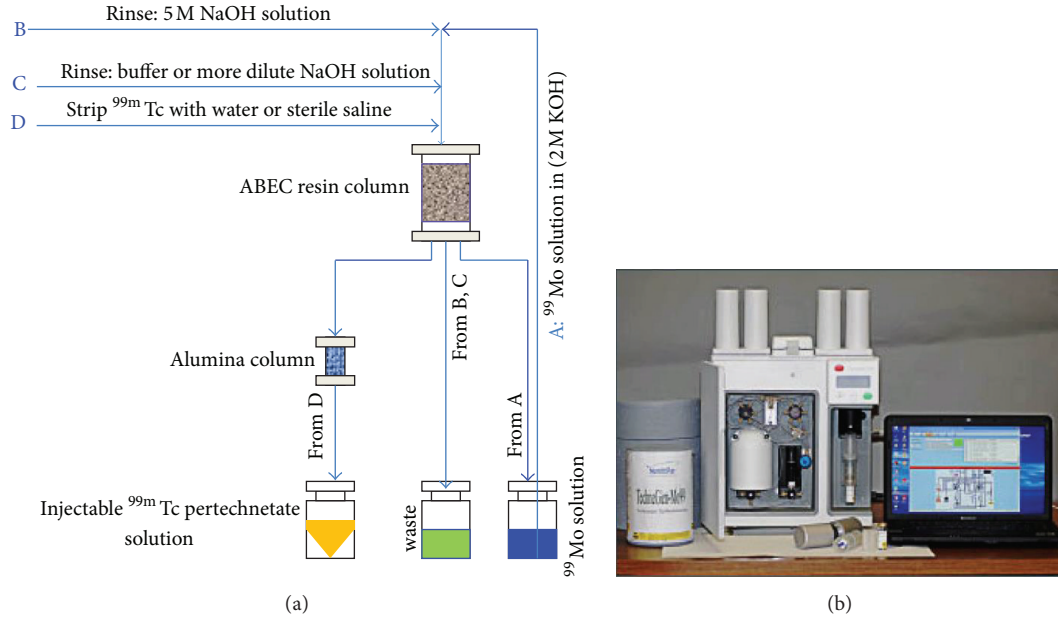
FIGURE 6: ^{99m}Tc recovery using ABEC resin column: (a) process diagram; (b) automated radionuclide separator ARSII developed by NorthStar Medical Radioisotopes (USA) using ABEC resin column [2].
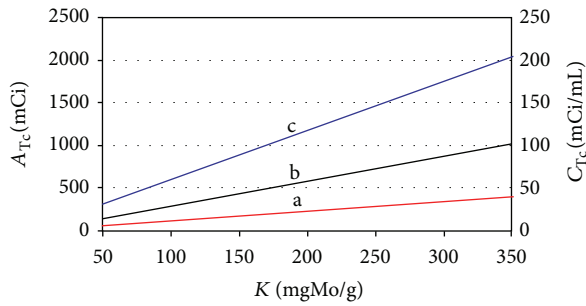
FIGURE 7: Assessment on the ^{99m}Tc-radioactivity (A_{Tc}) and ^{99m}Tc-concentration (C_{Tc}) of the eluate eluted from the generators of 5-gram weight column-packing materials of variable Mo-loading capacity K (low specific activity ^{99}Mo solutions used are produced in the nuclear reactors: (a) thermal neutron flux $\Phi = 2.1013$ n·cm^{-2}·sec^{-1}; (b) $\Phi = 5.1013$ n·cm^{-2}·sec^{-1}; (c) $\Phi = 1014$ n·cm^{-2}·sec^{-1}. The saline eluate volume is 10 mL).

With these conditions, the above mentioned K-equation is derived as follows:

$$K_{(5,100)} = \frac{1.72 \times 10^{13}}{\Phi} \times A_{Tc}. \qquad (11)$$

$K_{(5,100)} = G/5$ is the Mo-loading capacity of the packing material used in the generator. A_{Tc}(mCi) = $(0.875 \times A_{Mo\text{-}99})$ is the radioactivity of ^{99m}Tc in this generator. C_{Tc} (mCi/mL) is the radioactive concentration of ^{99m}Tc in the eluate eluted from the generator.

This relationship shows a general assessment on the potential use of the column packing material of given Mo-loading capacity for the ^{99m}Tc-generator production using $(n, \gamma)^{99}$Mo produced ex-natural molybdenum. As an example, the result assessed by above equations indicates that the column packing material of molybdenum loading capacity $K \geq 172$ mg Mo/g could be used to produce a ^{99m}Tc generator of approximately 300 mCi at the generator calibration using a ^{99}Mo source of 500 mCi activity (at EOB) produced in a reactor of $\Phi = 5.1013$ n·cm^{-2}·sec^{-1} and thus a ^{99m}Tc-pertechnetate solution of concentration <30 mCi ^{99m}Tc /mL could be achieved. This ^{99m}Tc solution could be used for limited numbers of organ imaging procedures due to its low ^{99m}Tc concentration as shown in Table 1. With the thermal neutron flux $\Phi > 5.1013$ n·cm^{-2}·sec^{-1} available in the majority of the research reactors around the world, it is justified that the column packing material of $K \geq 172$ mg Mo/g should be developed for the effective use in the process of ^{99m}Tc-generator production. Several sorbents, such as acidic/basic alumina, hydrous zirconium oxide, hydrous titanium oxide, manganese dioxide, silica gel, hydrotalcites, inorganic ion-exchange materials (zirconium-salt form of zirconium-phosphate ion exchanger), hydroxyapatite, mixed oxide of tetravalent metals, and diatomaceous earth, have been developed/investigated over the years [20, 133–141]. These sorbents are only used for the production of fission-^{99}Mo-based ^{99m}Tc-generators but they are unsuitable for ^{99m}Tc-generators loaded with ^{99}Mo of low specific activity due to their low Mo-adsorption capacity (<100 mg Mo/g).

Presently, there are the limitations in the available specific activity of ^{99}Mo produced from nuclear facilities: 1–6 Ci/g Mo (1–4 Ci/g at generator calibration day) of ^{99}Mo produced in the reactors of high neutron flux (> 1014 n·cm^{-2}·s^{-1}) using both the natural molybdenum and enriched ^{98}Mo targets and ~10 Ci/g Mo of ^{99}Mo produced from the accelerators as mentioned above. The use of these ^{99}Mo sources and

the recently developed column packing materials of high Mo-loading capacity in the process of the ^{99m}Tc generator production, however, remain to be addressed. In order to reduce the ^{99m}Tc solution volume eluted from a column chromatographic generator using low SA ^{99}Mo to facilitate the postelution ^{99m}Tc-purification/concentration process, the columns of as high as possible Mo-loading capacity must be used. Although the Mo-loading capacity >0.25 g Mo per gram of column-packing material is achieved to date, the loading of this material with 1-2% of its capacity (similar to the loading regime of the alumina column in the fission ^{99}Mo-based generators) using a low specific ^{99}Mo available today will result in a generator of unacceptably low activity, because the $(n, \gamma)^{99}$Mo produced in the majority of high neutron flux nuclear reactors and in the accelerators has a specific activity of 10000 times lower than that of the fission-based ^{99}Mo. So, the *fully Mo-loaded generator columns* should be used [57, 59, 60, 69, 70, 103–109, 112, 113, 132, 142–154]. As an example, the ^{99m}Tc generated in a 4-gram weight column of high Mo-loading capacity (250 mg Mo/g), which is fully loaded with 1.0 g Mo of low specific ^{99}Mo-activity to produce a generator of 1–4 Ci ^{99}Mo on generator calibration day, can be exhaustively eluted in 10 mL saline. This ^{99m}Tc eluate contains a higher ^{99}Mo breakthrough than that required for an injectable ^{99m}Tc solution due to the feature of the fully Mo-loaded generator column as mentioned above. This eluate needs to be purified to remove ^{99}Mo breakthrough contaminant by passing through a sorbent column such as alumina column of ~2-gram weight. Finally, an additional volume of the saline must be used to recover all ^{99m}Tc activity from the system. As a consequence, a low concentration ^{99m}Tc solution of approximately 20 mL volume is produced. This value means a double of saline volume used in a fission ^{99}Mo-based ^{99m}Tc generator column of 4 Ci activity loaded with 2 g alumina.

In case of the fully Mo-loaded generator columns used, the Mo affinity to the sorbent should be high enough to ensure a minimal Mo-breakthrough into the ^{99m}Tc eluate eluted from the generator, because the Mo breakthrough is directly proportional with the Mo amount loaded on the column and reversely with its affinity to the sorbent (known as distribution coefficient K_d). To achieve a maximal affinity for the adsorption process, the chemosorption with covalent bonding between molybdate ions and functional groups of the sorbent should be expected in the process of sorbent design.

Asif and Mushtaq [155] have tested to highly load alumina column with $(n, \gamma)^{99}$Mo to produce a medically acceptable pertechnetate solution of higher ^{99m}Tc concentration. However, the high ^{99}Mo breakthrough in the ^{99m}Tc eluate and the moderate Mo-loading capacity of this fully Mo-loaded alumina column (150 mg/g) remain inconvincible for a practical application of this technique for the generator production.

The efforts of using a fully Mo-loaded column of high Mo-loading capacity and high adsorption affinity, however, are not the all to be done in this endeavour in the process

development of ^{99m}Tc-generator production, because the solution volume and ^{99}Mo breakthrough of the ^{99m}Tc eluate eluted from fully Mo-loaded generator columns loaded with low specific activity ^{99}Mo are still unacceptably higher compared with those obtained from the fission ^{99}Mo/alumina-based generators. All these issues suggest that the high Mo-loading capacity column-based ^{99m}Tc recovery should be combined with a postelution purification/concentration process to produce a ^{99m}Tc-pertechnetate solution of medically useful radioactive concentration for use in most radiopharmaceutical diagnostic procedures.

With regard to the development of ^{99m}Tc generator using low SA ^{99}Mo, the column packing materials of high Mo-loading capacity developed in several laboratories are classified into two following groups. The first group includes the chemically formed solid powder materials containing molybdenum in the form of a chemical compounds such as polymolybdate compounds of tetravalent metals (in the form of solid gels) such as Zr-, Ti-, Sn-molybdates, and so forth [57, 59, 60, 69, 70, 103–106, 112, 113, 132, 142–147]. The second group composes of the sorbents of high Mo-adsorption capacity such as the functionalized alumina [156], the polymeric compounds of zirconium (PZC), titanium (PTC), and so forth [107, 108, 148–154, 157], the nanocrystalline mixed oxides of tetravalent metals [62–64, 109–111, 118, 158], the nanocrystalline zirconium/titanium-oxide and alumina [159–161], and recently multifunctional sorbents [40–42, 58]. Such materials, as discussed below, are shown to be suitable for ^{99m}Tc generator production. All these column-packing materials have a significantly higher Mo-loading capacity (>250 mg Mo per gram) than that of the alumina ('10–20 mg Mo per gram). The ^{99m}Tc can be separated from these column packings by elution with a small volume of nonsaline or saline eluents. The choice of the eluent is subject to the postelution ^{99m}Tc-purification/concentration process preferred for the optimal design of an integrated system RADIGIS to produce the medically useful pertechnetate solution of sufficiently high ^{99m}Tc concentration.

The chemistry of molybdate ion sorption on hydrous metal oxides is a good guide in the process of sorbent development. It is established that there are 4 adsorption sites/groups on the alumina surface: basic OH group (=Al–OH), neutral OH group (–Al–OH–Al–), acidic OH group (–Al–OH[–Al–]$_2$), and coordinatively unsaturated site (–Al^{3+}–). All these sites adsorb the molybdate ions to different extents depending on the pH of the solution and type of alumina sorbent used. Molybdate reacts irreversibly in a reaction (chemosorption) with the basic OH groups (at pH 8.5–6). However, as soon as these are protonated, molybdate also starts to be reversibly adsorbed by electrostatic interaction. The neutral OH groups, when protonated, also reversibly adsorb the molybdate ions. Molybdate is strongly adsorbed by the coordinatively unsaturated sites and by acidic OH groups via a physisorption/electrostatic interaction at pH <5. For this reason, acidic alumina is used for the ^{99}Mo/^{99m}Tc generator production. Among tetravalent metal oxides, titania and zircona are usually used in many studies for the ^{99m}Tc
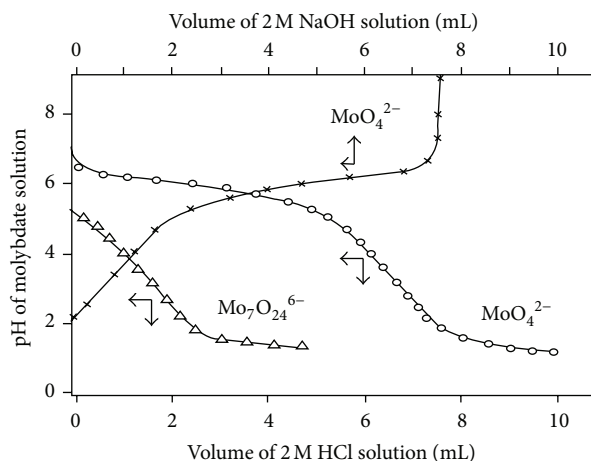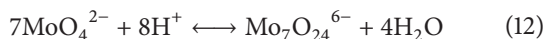
FIGURE 8: pH titration curves of molybdate solutions [57].

FIGURE 9: pH titration curves of molybdate gel sorbents [57, 59, 60, 69].

recovery from ^{99}Mo. Titania and possibly nanocrystalline tetragonal zircona (calcined at 600°C, IEP at the pH 4.5 [62, 156, 161]) contain mainly coordinatively unsaturated sites, so these sorbents may adsorb molybdate ions via a physisorption/electrostatic interaction at pH <5. However, hydrous titanium oxide and zirconium oxide sorbents contain many acidic and basic OH groups, respectively. Consequently molybdate ions are adsorbed on the hydrous titanium oxide surface by a physisorption mechanism at pH <4 with a less adsorption affinity compared with that of hydrous zirconium oxide which adsorbs molybdate by an irreversible chemical reaction/chemosorption. Molybdate ions adsorb on the metal oxides in different forms depending on the pH of the solution because the molybdate polymerizes in weakly acidic solution as follows:

$$7MoO_4^{2-} + 8H^+ \longleftrightarrow Mo_7O_{24}^{6-} + 4H_2O \qquad (12)$$

On the polymerization, the polymerized molybdate molecules have variable molecular weights depending on the pH. This property can be experienced from the results of the potentiometric titration of molybdate solutions shown in Figure 8. As shown the molybdate is in the form of polymolybdate $Mo_7O_{24}^{6-}$ at pH <5 [57].

When the titanium- and zirconium-molybdate gels are used as column packing materials in the ^{99}Mo/^{99m}Tc generator preparation, the molybdate covalently bonds with Ti^{4+} and/or Zr^{4+} ions in the way of nonstoichiometry. So the residual charges of the polymolybdate ions will be neutralized by the positive charge of the protons and the gels will behave as a cation exchanger. Le (1987–1994) has found the polyfunctional cation-exchange property of the titanium-and zirconium-molybdate gels [59, 69, 104]. He has taken this advantage of the molybdate gels to design the water- and organic solvent (acetone)-eluted gel-type ^{99m}Tc generators as shown in Figures 14, 17, and 18 [57, 59, 60, 69, 103–106, 146]. The molybdate gels have two functional groups in their structure and the total ion-exchange capacity of approximately 10 meq/g was found as shown in Figure 9. The ^{99m}TcO$_4^-$ anions, as the counter ions of the cation-exchange
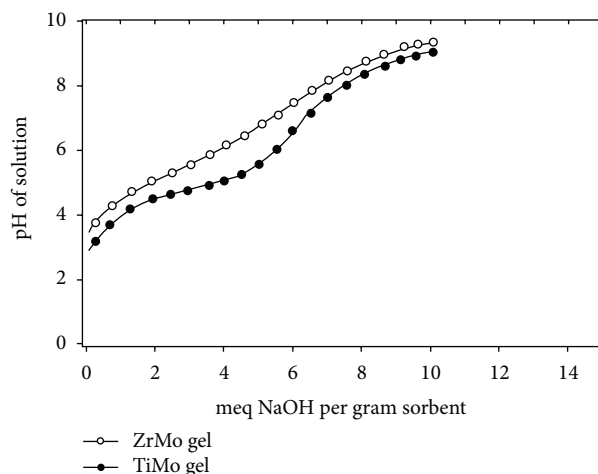
gel matrix, can be easily eluted with the water and water-soluble organic solvent from the column of gel-type ^{99m}Tc generator. Sarkar et al. (2004) also developed a water-eluted zirconium-molybdate gel-based ^{99m}Tc generator [49].

The cation exchange property can be found in all the sorbents which are fully loaded with molybdate ions. So the elution of ^{99m}Tc with water or with acetone (as nonsaline eluents) from the generator column fully loaded with ^{99}Mo will provide the advantages for a consecutive postelution purification/concentration process. Le (2011) has developed an automated system of the radioisotope generator coupled with purification/concentration process using PTC/PZC sorbent columns and an eluent composed of water containing small amount of NaCl (0.005%). This system called RADIGIS-^{99m}Tc is shown in Figure 16 [62–64, 109, 109–111, 158].

The ^{99m}TcO$_4^-$ anions are hardly eluted from a partly Mo-loaded sorbent column with nonsaline eluents due to its strong adsorption on the unoccupied residual OH groups of the sorbent. However, this elution can be achieved if the column is wetted with a sufficient amount of residual saline. This phenomenon has been experienced in the case of the ^{99m}Tc elution with acetone from an alumina column [51]. In this case the water in the aqueous saline phase existing on the sorbent surface plays a role of an ion transporter for ^{99m}TcO$_4^-$ and Cl$^-$ ions.

(1) Saline-Eluted Generator Systems Using High Mo-Loading Capacity Columns and Integrated Generator Systems

(i) Saline-Eluted Molybdate-Gel Column-Based ^{99m}Tc-Generator Systems. A zirconium-molybdate (ZrMo) and titanium-molybdate (TiMo) gels are the generator column packing materials used exclusively with low specific activity ^{99}Mo for ^{99m}Tc recovery. The molybdate gel column is considered as a fully Mo-loaded sorbent column as well. These materials were first developed by Evans et al. [143] and Evans and Mattews [162] and then further improved by several research groups around the world in the 1980s

[49, 57, 59, 60, 69, 70, 103–106, 132, 146, 147]. A comprehensive description of molybdate gel-based ^{99m}Tc generator systems using low specific activity ^{99}Mo is presented in IAEA-TECDOC-852 [70]. ZrMo and TiMo gels are prepared in the form of water insoluble solid powders containing molybdenum under a strictly controlled synthesis condition to ensure the best performance when used as a column packing material in chromatographic ^{99m}Tc generators. The conditions under which a molybdate (zirconium or titanium) is prepared will influence the nanostructure of the gels and thus the ^{99m}Tc generator's performance. Different ^{99m}Tc elution performances were found with the gels of amorphous or crystalline/semicrystalline structure [57, 59, 69, 132]. As a rule of thumb, the ^{99}Mo breakthrough from the generator column and the ^{99m}Tc elution yield are higher with the amorphous gels, while the performance of the crystalline structure gels reverses. The porosity of the solid gel particles is also an important factor influencing the out-diffusion of the pertechnetate ions and thus the ^{99m}Tc elution profile and ^{99m}Tc-elution yield of the generator column. So the gel synthesis conditions such as the molar ratios of zirconium (or titanium) to molybdenum, the solution concentrations, the order of reactive agent addition, the reaction temperature, the gel aging conditions (time and temperature), the acidity of reaction mixture, the drying conditions of the gel product (time, temperature, and atmosphere), and so forth must be properly controlled in order to consistently reproduce the properties of the gel.

The ^{99m}Tc-elution performance of the gels is assessed based on the following important factors: the ^{99m}Tc elution efficiency, the ^{99}Mo breakthrough in the ^{99m}Tc eluate, mechanical stability, and the uniformity/size of the gel particles, and the capability of thermal (steam) autoclaving.

The dried gel contains about 25% by weight of molybdenum (0.25 g Mo per gram of gel) and has the characteristics of a cation exchanger as discussed above. The passage of an aqueous eluent (typically either water or normal saline) through a molybdate-gel column releases the ^{99m}Tc. However, an additional small column of alumina is required to remove ^{99}Mo-impurities from the ^{99m}Tc eluate.

As in the case of the alumina-based ^{99m}Tc generator system, the radiochemical purity of the ^{99m}Tc eluted from a molybdate gel-type generator can be impacted by the effects of radiation, changes in temperature or pH, and the presence of reducing/oxidizing agents. Finished product quality control testing clearly demonstrates that the radiochemical purity is equivalent to that of the traditional alumina column/fission ^{99}Mo-based ^{99m}Tc generator.

TiMo and ZrMo gels are prepared in two different forms: the post-irradiation synthesized ^{99}Mo-containing molybdate gel and the preformed nonradioactive Mo-containing molybdate gel. In contrast to postirradiation gels which is chemically synthesized from the ^{99}Mo solution of neutron-activated Mo target, the preformed gel target is synthesized under nonradioactive conditions and the gel powders are loaded into the generator column after being activated with neutron in the reactor to perform ^{98}Mo$(n, \gamma)^{99}$Mo reaction. However,

the disadvantage of the preformed gel is that this gel powder material requires a thoughtful neutron irradiation condition to avoid any adverse effects on the change of gel structure and chemical properties, which is caused by high temperature and extremely high radiation dose during reactor irradiation. In consequence the ^{99m}Tc elution performance of the neutron-activated gels will be degraded. So, a special design of the irradiation container and specific radical scavenger have been used to save the original properties of the pre-formed gel during its long time irradiation in the reactor [69, 70, 104, 132]. A great care should be taken during the synthesis of TiMo gel to avoid any contaminants which may generate the radionuclidic impurities during neutron activation of the TiMo gel targets [163].

Originally, the molybdate gel-column-based generators (Figure 10) are specifically designed to use low specific activity ^{99}Mo to provide the ^{99m}Tc solution for diagnostic imaging the limited numbers of the organs due to low activity concentration of ^{99m}Tc solution eluted from these generators. Typical elution profiles of the molybdate-gel column-based ^{99m}Tc-generator are presented in Figure 11. The technical maturity of this chromatographic gel-based ^{99m}Tc recovery system has advanced significantly in the last decades.

(ii) Saline-Eluted High Mo-Loading Capacity Sorbent Column-Based ^{99m}Tc Generator Systems

(a) Polymeric Zirconium Compound and Polymeric Titanium Compound Sorbents. Polymeric zirconium-oxychloride or polymeric zirconium compound (PZC) and polymeric titanium-oxychloride or polymeric titanium compound (PTC) sorbent materials were first developed for use in $(n, \gamma)^{99}$Mo-based ^{99m}Tc generators. These titanium/zirconium-based inorganic polymers exhibit both excellent ^{99}Mo-adsorption capacity and ^{99m}Tc-elution. The main constituents of this sorbent material are zirconium, oxygen, and chorine. The adsorption capacity of PZC and PTC for ^{99}Mo was reported to be much higher than that of the conventional alumina. Many research activities were performed in JAEA (Japan), in NRI (Vietnam), and in other countries in Asia on the use of PTC and/or PZC materials as high Mo-loading capacity sorbent materials for packing of various radionuclide-generator columns [62–64, 107–111, 148–154, 158]. The PTC/PZC sorbent of high Mo-adsorption capacity serves as a ^{99}Mo-loaded column from which the ^{99m}Tc can be eluted in patient-dose quantities. In contrast to a traditional alumina of low Mo-adsorption capacity currently used in a commercial chromatographic generator system loaded with high specific activity ^{99}Mo solution, the high adsorption capacity of PTC and PZC sorbent for ^{99}Mo (270–275 mg Mo/g) is useful in reducing the size of the generator column and thus the daughter nuclide eluate volume, when these columns are used for low specific radioactivity ^{99}Mo-based generator production.

PZC and PTC sorbents were synthesized from isopropyl alcohol (iPrOH) and the relevant anhydrous metallic chloride under strictly controlled reaction conditions. A given amount

(a) (b)
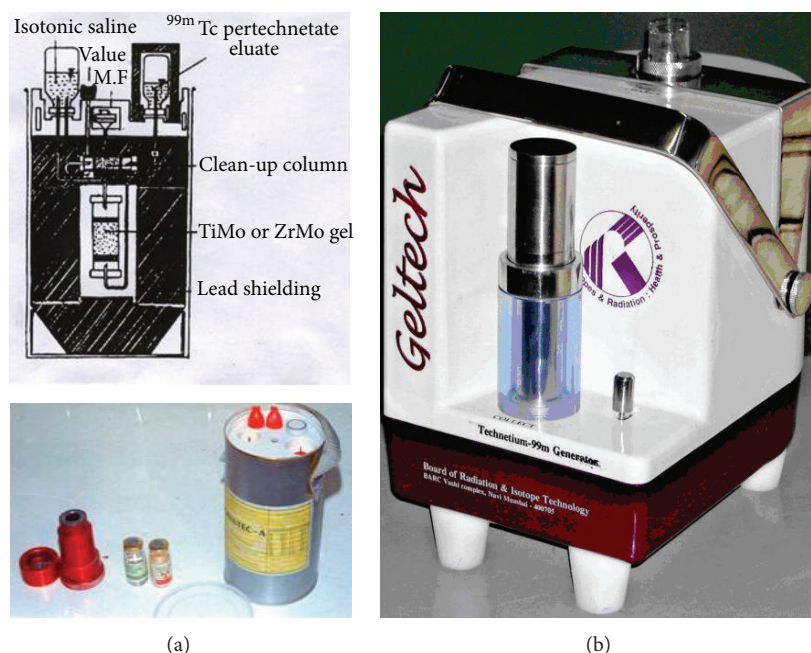
FIGURE 10: Typical chromatographic gel-type ^{99m}Tc generators (dual column systems compose of a ZrMo (^{99}Mo) gel column coupled with a purification acidic-alumina column): (a) Gelutec-A ^{99m}Tc-generator manufactured by NRI (Vietnam); (b) Geltech ^{99m}Tc-generator by BRIT (India). (Note: no ^{99m}Tc-concentration is available in these generator systems. In Gelutec-A system, two alumina columns are installed in parallel and a selector/valve is inserted between them to direct the ^{99m}Tc eluate from the gel column being passed over each column for 5 consecutive purification/elutions) [2, 57, 59, 60, 103].
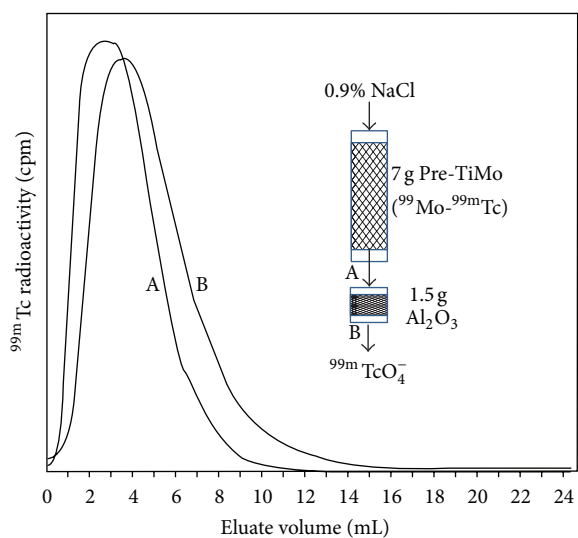
FIGURE 11: ^{99m}Tc elution profiles of Gelutec-A generator. A: the generator column without coupling with alumina purification column; B: the generator column coupled with alumina purification column [57, 59, 60, 103–106].

of relevant anhydrous metallic chloride (ZrCl$_4$ for PZC or TiCl$_4$ for PTC) was carefully added to different amounts of iPrOH. The temperature of the reaction mixture immediately reached 96–98°C for the iPrOH-ZrCl$_4$ mixture and 92–94°C for iPrOH-TiCl$_4$. The temperature of solution was maintained at these values and stirred gently by magnetic stirrer in open air until the solution became viscous. As the reaction temperature increased, a water-soluble PZC or PTC gel (the intermediate precursors) was formed at 129–131°C for PZC and at 111–113°C for PTC sorbent. The water-insoluble, solid PZC or PTC materials of particle size of 0.10 mm to 0.01 mm were split out by keeping the reaction temperature at 141-142°C (30 minutes) for PZC and at 124–126°C (45 minutes) for PTC. These were the finished products of PZC and PTC sorbents. The characterizations of the PZC and PTC materials synthesized and their preparation conditions are summarised in the literature [62, 107–109, 149–154].

The molecular formula of PZC sorbent was also estimated. The actual molecular weight (organic residue included) was determined to be $M = 5901.3$, where X is the organic molecules in one PZC molecule which was equivalent to 9.63% of PZC molecular weight as seen at thermal analysis. Because the organic substance in this formula was attributed to a residual organic by-product of chemical synthesis reaction and was completely being released from polymer matrix in aqueous solution, the segment unit of real polymer compound is of the following formula: $Zr_{15}(OH)_{30}Cl_{30}(ZrO_2)\cdot126H_2O$. The steric arrangement of atoms in this molecule is shown as Scheme 1.

The molecular weight of PZC sorbent is 5333.02. Chlorine content is 5.63 millimol Cl per gram PZC sorbent. Ion exchange capacity is 5.63 meq per gram PZC sorbent. The ion exchange capacity derived from the above chemical formula offers an adsorption capacity of 270.0 mg Mo/g PZC or

SCHEME 1

Ti atom: 1   2   3   4   5   6   7   8   9   10   (11→17) 18   19
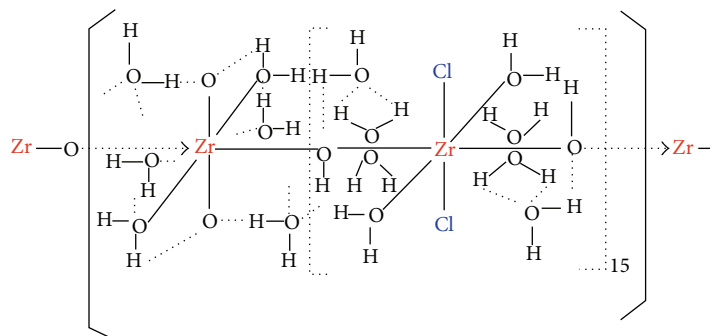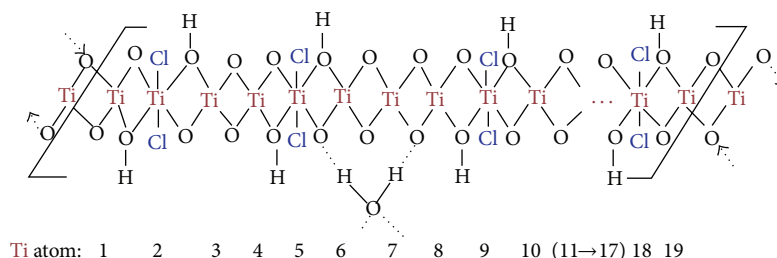
SCHEME 2

517.1 mg W/g PZC by assuming molybdate or tungstate ions adsorbed on PZC in the form of MoO_4^{2-} or WO_4^{2-}, respectively. In addition it is assumed that one molarity of MoO_4^{2-} or WO_4^{2-} ion consumes 2 equivalents of ion-exchange capacity of PZC and PTC sorbents (one equivalent of MoO_4^{2-} ion is 48 g molybdenum and one equivalent of WO_4^{2-} ion is 91.925 g). This type of strong adsorption suggests a covalent bond between molybdate or tungstate ions and zirconium metal atom.

The segment unit of real polymer compound is of the following formula $Ti_{40} Cl_{80} (OH)_{80} (TiO_2)_{97} \cdot 60H_2O$. The steric arrangement of atoms in this molecule is shown as Scheme 2.

The molecular weight of PTC sorbent is 14939.56. The chlorine content of PTC sorbent is 5.35 millimol/gram PTC sorbent (18.965% of chlorine element in one gram PTC). This is equivalent to the ion exchange capacity of 5.35 meq/g PTC sorbent and consequently offers very high adsorption capacities of 257.0 mg Mo/g PTC or 491.8 mg W/g PTC by assuming molybdate or tungstate ions adsorbed on PTC in the form of MoO_4^{2-} or WO_4^{2-}, respectively, and one molarity of MoO_4^{2-} or WO_4^{2-} ion consuming 2 equivalents of ion-exchange capacity of PTC sorbent. This type of strong adsorption gives a covalent bond between molybdate or tungstate ions and titanium metal atom. The theoretical values of adsorption capacity calculated from the molecular formula of PZC and PTC compounds detailed above are in good agreement with the practical values achieved at the potential titration and at the Mo and/or W adsorption experiments. The adsorption capacity of both sorbents was variable depending on the temperature, reaction time, and gel aging process before forming the solid PZC and PTC polymers. The actual molybdenum adsorption of PZC and

PTC sorbents, which is to some extent higher than the above mentioned values, accounted for the noncovalently adsorbed molybdate ions and/or for adsorption of small amounts of poly-molybdate ions. These polyanions could form at the beginning stage of adsorption in the strongly acidic solution which resulted from the hydrolysis of –Zr–Cl (or–Ti–Cl) groups of the back-bone of PZC or PTC molecules.

The PZC sorbents in its original forms, which are developed in Japan and Vietnam, contain so much HCl content in their structure and are subject to hydrolysis in an aqueous solution resulting a strong acidity. So the "in-pot" adsorption process should be applied to load ^{99}Mo-molybdate onto the sorbent before packing it into the generator column. This process is performed automatically using a smart machine (Figure 12(a)) developed by Japan Atomic Energy Agency (JAEA) and Kaken Co. Ltd. (Japan).

The PZC/PTC sorbents modified by further physico-chemical treatments performed in ANSTO and NRI, which are used for different radionuclide generator developments, are used for packing the generator column, so-called the prepacked column. This prepacked PZC/PTC column is then loaded with ^{99}Mo-molybdate solution to produce the ^{99}Mo/^{99m}Tc generators in the same manner as that used for the production of the traditional alumina-based ^{99m}Tc generators (Figure 12(b)). Although the ^{99}Mo-adsorption capacity of the modified/prepacked PZC/PTC sorbent column is to some extent lower than that of original form of PZC sorbent, the former is preferred due to an easy-to-load property of the nonradioactive column loading procedure [108].

The saline-eluted high Mo-adsorption capacity PZC/PTC column (fully Mo-loaded column)-based ^{99m}Tc generator systems have been developed and the pertechnetate eluates of

(a)

(b)

FIGURE 12: Loading of ^{99}Mo solution on the PZC/PTC sorbents for ^{99m}Tc-generator production: (a) automatic machine developed by Kaken Co. Ltd. (Japan) for the in-pot ^{99}Mo-adsorption on PZC sorbent followed by packing of ^{99}Mo-loaded PZC into the generator column in the process of PZC sorbent-based ^{99m}Tc-generator production [107]; (b) the ^{99m}Tc-generators installed with prepacked PZC/PTC sorbent columns are in-line loaded with low specific activity ^{99}Mo solution in the process of PZC/PTC-based ^{99m}Tc-generator production at NRI [108].

^{99m}Tc concentration suitable for a limited numbers of SPECT imaging procedures were obtained. The design of this type of the generator is similar to the molybdate gel-type generator described in Figure 10.

(b) Nanocrystalline Sorbents. Le (2009) has recently developed a group of nanocrystalline tetravalent metal oxide and mixed oxide sorbents for the radionuclide generator technology and radiochemical separation development [62–64, 109–111]. The tetravalent metal is each selected from the group consisting of Zr, Ti, Sn, and Ge. The chemical composition of the sorbents are described as $Zr_xM_yO_z(OH)_{(2x+2y-z)}$, where x and y value pairs (x, y) are $(1.0, 0.0)$, $(0.75, 0.25)$, $(0.5, 0.5)$, and $(0.0, 1.0)$ and the value z is variable depending on heating of the powder so as to form the sorbent at the last step of synthesis process. Each M is, independently, Ti, Sn, or Ge. The process for making the sorbent comprises several steps: reacting a metal halide or a mixture of metal halides and an alcohol to form a gel and heating the gel to activate the condensation and/or polymerisation reaction for the formation of a particulate material. This solid polymer gel material in powder form with particle sizes from 0.10 to 0.01 mm is then left to cool at room temperature overnight before starting further chemical treatment. The solid polymer gel powder is treated in an alkali solution which contains oxidizing agent NaOCl: about 10 mL 0.5 M NaOH solution containing 1%

by weight NaOCl is used per gram of solid polymer gel powder. The solid powder/oxidant solution mixture is gently shaken using a mechanical shaker for at least 4 h so as to convert the gel structure solid powder into a macroporous solid powder and to convert any lower-valence metallic ions to their original 4^+ valence. The volume of solution required per gram of solid gel powder is determined so that the pH of solution at the process end is between 2 and 5. The solid matter is then separated by filtering through a sintered glass filter, washed several times with double-distilled water to remove all dissolved sodium and chloride ions, and dried at 80°C for 3 h to dryness to obtain a white solid powder. The resulting white solid powder is calcined at a temperature in the range from 500°C to 700°C for a time of about 3 h (the actual temperature depending on the particular sorbent being prepared) (the actual temperature depending on the particular sorbent being prepared). The calcinations are to complete the crystallization/recrystalization of the nanoparticles so as to form the sorbent. At the end of this heating process, the resulting powder is sieved. In particular, the fraction of particle size between about 50 and about 100 μm may be collected to be used as a sorbent for chromatographic column packing applied to chemical separation processes. The initially formed solid is commonly in the form of white solid powder particles composed of different clusters of greater than about 100 nm in size. The clusters are aggregates of amorphous and semicrystalline nanoparticles (less than about 5 nm). The clusters appear to be held together by weak hydrogen bonds and van der Waals bonds. Consequently, the aggregate particles are macroporous and soft. During high-temperature calcining the amorphous and semicrystalline nanoparticles (less than about 5 nm) crystallize to form crystalline nanoparticles inside clusters. Simultaneously, these crystalline nanoparticles partially melt and combine with other nanoparticles inside the same cluster with interfacial coordinatively bond/ordered structure to form larger porous crystalline particles. Because there is longer distance between the clusters than that between nanoparticles within a single cluster, the nanoparticles belonging to different clusters do not combine with each other to form a single mass. Adjacent nanoparticles on the surface of clusters fuse into a limited area of the cluster surface to form a bridge to crosslink the clusters (at this stage, the clusters have already become larger crystalline particles) to form sorbent particles. In this way, meso/macroporosity formed between the former clusters may be maintained. The partial fusion and surface coordinative connection are thought to cross-link the particles to create a hard porous matrix of solid material. The high chemical and mechanical stability of the product is thought to result at least in part from the formation of stable crystalline monophase in the solid material. The crystalline structure of the product is stable when exposed to high radiation doses from radioactive materials. The powders obtained using the above process have high stability and high porosity (average pore size ~120 Å) and may be used as a state-of-the-art sorbent for different chemical separation processes, for example, for the separation of highly radioactive materials. The doping by different amounts of metal ions (e.g., Ti, Sn, or Ge) added to zirconium chloride solution in the synthesis is thought to

(a)

(b)

(c)

(d)

(e)

(f)
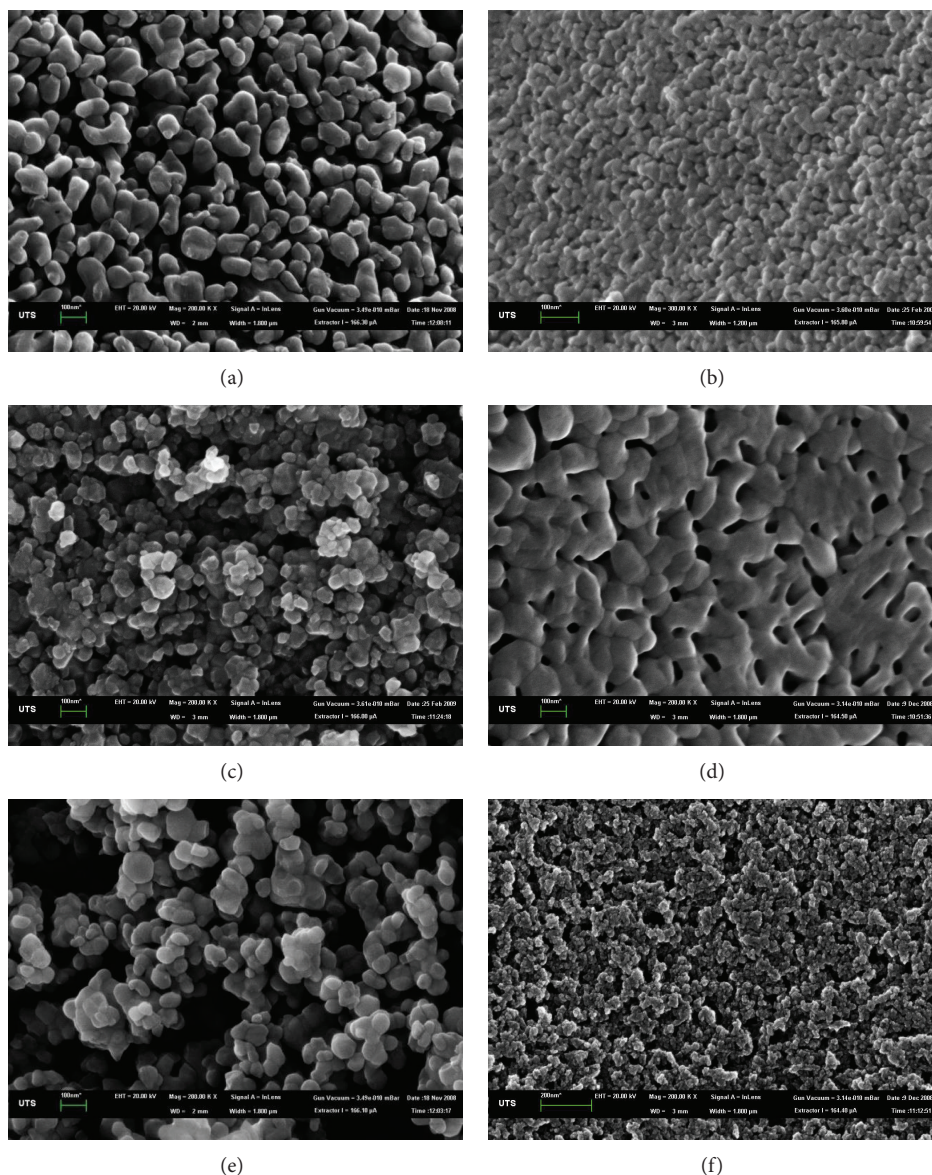
FIGURE 13: SEM picture of the nanocrystalline sorbents used for packing radionuclide generator columns. Sorbents: (a) ZiSorb, (b) TiSorb, (c) SnSorb, (d) ZT-11, (e) ZT-31, and (f) organic-polymer resin OASIS-HLB (Waters) of average pore diameter 80 Å (for a comparison purpose) [62].

be responsible for a stabilized crystalline phase which makes the product chemically and mechanically stable. The doping of smaller ions, Ge^{4+} (radius 0.53 Å), Ti^{4+} (radius 0.605 Å), and Sn^{4+} (radius 0.69 Å), onto the matrix of larger ions Zr^{4+} (radius 0.80 Å) facilitates isomorphism-based adsorption of the parent nuclides such as $^{68}Ge^{4+}$, $^{113}Sn^{4+}$, and $^{44}Ti^{4+}$ ions from its acidic solution for the preparation of the $^{68}Ge/^{68}Ga$, $^{113}Sn/^{113m}In$, $^{110}Sn/^{110m}In$, and $^{44}Ti/^{44}Sc$ generators, respectively. Moreover, the doping process is also to increase the numbers of covalently unsaturated sites ($= M^{-+}$) and to reduce the isoelectric point (IEP) of zircona (at pH ~8) to a value (at pH ~4–6), which are suitable to the adsorption of parent nuclide ions and to the elution of daughter isotope in the process of $^{99}Mo/^{99m}Tc$

and $^{188}W/^{188}Re$ generator production. The Mo-adsorption capacity of these sorbents is in the range 200–240 mg Mo/g and saline-eluted ^{99m}Tc-pertechnetate recovery is satisfied with medical use requirement. Scanning electron microscopy (SEM) images showing the micro- and mesoporosity of the sorbent materials synthesized above are presented in Figure 13. X-ray diffraction patterns of these sorbents showed a monophase of the nanocrystalline structure [62, 64].

The nanocrystalline zircona (tetragonal phase, t-ZrO_2), nanocrystalline titania, and nanocrystalline alumina sorbents of high Mo-adsorption capacity were also developed in Bhabha Atomic Reasearch Center, Mumbai (India), for use in the ^{99m}Tc generator production [160, 161, 164, 165]. The sorbents were synthesized by controlled hydrolysis of 0.17 M

zirconium chloride solution in a well stirred 2.5 M ammonia solution at pH 9–11. The formed hydrogel was washed with deionized water until free of chloride ions. Subsequently the hydrogel was then refluxed at 96°C for 24 h in an ammonia solution of pH 12 and then filtered, washed with water, dried at 100°C overnight, calcined at 600°C for 5 h, and ground and sieved to get particles of 50–100 mesh for chromatographic column packing. The specific area of these materials (100–340 m^2/g) is in the range of that reported for alumina (150 m^2/g). These sorbents have high Mo-adsorption capacity and good ^{99m}Tc elution properties. The static ^{99}Mo-adsorption capacity >250 mg Mo per gram sorbent was reported. The breakthrough capacity was 100 mg/g. The column loaded with 25% of its total static Mo-adsorption capacity was investigated on the ^{99m}Tc elution performance. The ^{99m}Tc elution yield of >90% was achieved with saline eluent. The ^{99m}Tc elution performance of fully Mo-loaded nanocrystalline sorbent columns was not tested. The long time of 50 min is needed to attain the adsorption equilibrium of molybdate and tungstate ions in the static adsorption process. The kinetics of ^{99}Mo-adsorption process is rather slow using these materials, probably; because their pore size is smaller than the size of the molybdate/tungstate ions (pore size of ~0.4 nm for the sorbent compared with the ion size of 0.646 nm for MoO_4^{2-} and 0.648 nm for WO_4^{2-}). This fact may reduce the practical application of this sorbent due to high potential of particle cracking when it is highly loaded with Mo/W. The utilisation of these sorbents for loading of low specific activity ^{99}Mo in the process of the production of ^{99m}Tc/^{188}Re generators needs more experimental investigations for improvement in the porosity and dynamic loading capacity. Continuing the developments of nanomaterial-based sorbents for ^{99m}Tc and ^{188}Re-generator production, the above mentioned scientist group also reported the capability of mesoporous nanocrystalline alumina in the production of ^{99m}Tc/^{188}Re generators [164, 165]. Although the Mo-adsorption capacity (230 mg/g) is in the similar range as that achieved by the above-mentioned sorbents (PZC/PTC sorbents and nanocrystalline zirconia), the effort was made to use this new alumina in a tandem system of double columns for ^{99m}Tc-generator preparation. Despite the use of double columns for increasing the Mo-loading capacity of the generator, this configuration requires the $(n, \gamma)^{99}$Mo of improved specific activity produced in a high neutron flux (10^{14}-10^{15} n·cm^2·s^{-1}) to produce a clinical scale ^{99}Mo/^{99m}Tc generator.

(c) Functionalized Sorbents. Functional alumina sorbents (sulfated alumina and alumina sulphated zircona) developed in Korea [156] have a ^{99}Mo-adsorption capacity >200 mg Mo per gram of sorbent. The sorbents were synthesized by the reaction of aluminium-tri-sec butoxide, zirconium-prop-oxide, and anhydrous H_2SO_4 in mixture of HCl and alkyl alcohol. The obtained precipitate was dried at 100°C to get the final sorbent product. This sorbent material was used for the ^{99m}Tc generator production. The ^{99m}Tc-pertechnetate was eluted by saline with 60–85% elution yield.

The multifunctional sorbents were also developed by MED-ISOTEC (Australia) for the ^{99m}Tc generator production and for several radiochemical separations including the uses in ^{99}Mo/^{99m}Tc and ^{188}W/^{188}Re generator production [58]. These sorbent materials may comprise porous silica having a plurality of groups of formula -O$_{4-z}$(M)A$_i$X$_{z-i-k}$R$_k''$ on the surface thereof, wherein each M is, independently, Ti, Zr, Hf, Sn, Th, Pb, Si, or Ge; each A is, independently, either OH or R (where R is an alkyl group C$_n$H$_{2n+1}$ and n is from 1 to 18); each R$''$ is an aminoalkyl group [(CH$_2$)$_m$-(Amino group1)], where m is from 1 to 6; each X is a [M$'$(oxo-hydroxyl-alkyl-aminoalkyl)M$''$(oxo-hydroxyl-alkyl-aminoalkyl)] group of formula [(OM$'$)$_j${(OH)$_a$(C$_b$H$_{2b+1}$)$_c$[(CH$_2$)$_d$-(Aminogroup2)]$_e$} {(OM$''$)$_f$(OH)$_g$(C$_h$H$_{2h+1}$)$_p$[(CH$_2$)$_q$-(Amino group3)]$_v$}], where each M$'$ is, independently, Si, Ti, Zr, or Hf and each M$''$ is, independently, Si, Ti, Zr, or Hf; z is from 1 to 3; i is from 0 to 3; $(i + k)$ is from 0 to 3; j is 0 or 1; a is from 0 to 3; b is from 1 to 6; c is from 0 to 3; d is from 1 to 6; e is from 0 to 3; $(a + c + e)$ is 3; f is 0 or 1; g is from 0 to 3; h is from 1 to 6; p is from 0 to 3; q is from 1 to 6; v is from 0 to 3; and $(g + p + v)$ is 3. The ^{99}Mo-adsorption capacity of these materials (>600 mg Mo/g) is significantly higher than that of the sorbents developed up to date. The kinetics of ^{99}Mo-adsorption process is fast with these materials due to their high porosity (pore size 2–10 nm) and high surface area (>700 m^2/g). The excellent ^{99m}Tc elution properties of these sorbents are well confirmed when used with saline eluent. The functional sorbent generator columns can be sterilized by a normal steam process in the autoclave. A commercial production of the ^{99m}Tc generators using these sorbents for loading of low specific activity ^{99}Mo is well promising.

(2) Nonsaline Eluent-Eluted Generator Systems Using High Mo-Loading Capacity Columns and Integrated Generator Systems. In contrast to the saline-eluted generator systems using high Mo-loading capacity columns which are used for a limited number of SPECT imaging procedures due to a rather low ^{99m}Tc concentration of ^{99m}Tc eluate obtained, the nonsaline aqueous solution-eluted ^{99m}Tc generators or ^{99m}Tc recovery processes are mainly developed to couple with the ^{99m}Tc-purification/concentration process to set up the ^{99}Mo/^{99m}Tc generator systems which are suitable for a routine production of ^{99m}Tc solution of medically useful radioactivity concentration effectively used in all the diagnostic SPECT imaging procedures.

(i) Nonsaline Aqueous Solution-Eluted ^{99m}Tc Generator Systems Using Molybdate-Gel Columns. Recent advances in radiopharmaceutical diagnostic applications using the ^{99m}Tc-pertechnetate of moderate to high activity concentration (as shown in Table 1) require the development of the integrated generator system RADIGIS which composes of a molybdate-gel column-based ^{99m}Tc generator coupled with a postelution ^{99m}Tc concentrator to produce a medically useful pertechnetate solution of sufficiently high ^{99m}Tc concentration.

A version of RADIGIS developed in the 1980s is presented in Figure 14. The operation of this system is semiautomated.

(a)

(b)
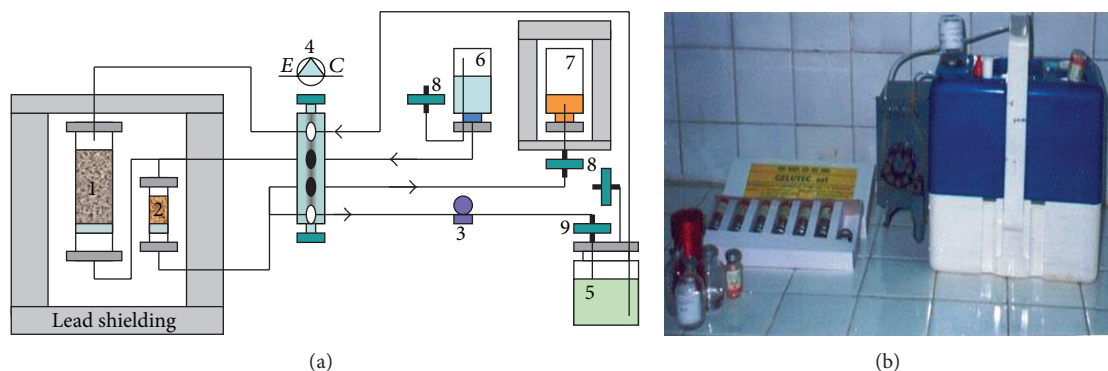
FIGURE 14: Integrated ^{99m}Tc-generator system (RADIGIS): (a) process diagram and design; (b) photo of GELUTEC-C system used for years in Vietnam which composes of a ZrMo (^{99}Mo) gel column coupled with a zircona/alumina column-based purification/concentration unit: 1: gel column; 2: zircona/alumina column; 3: peristaltic pump; 4: selector valve; 5: circulating eluent container (water containing 0.005% NaCl); 6: saline vial; 7: final ^{99m}Tc solution; 8: Milipore filter; 9: coarse filter. (Specifications: Semi-automated operation based on the circulating elution with an eluent of redistilled water containing 0.005% NaCl; Processing time 20 min; Final ^{99m}Tc solution of 100–200 mCi/mL concentration depending on the activity of ^{99}Mo-loading) [57, 103].

(a)

(b)
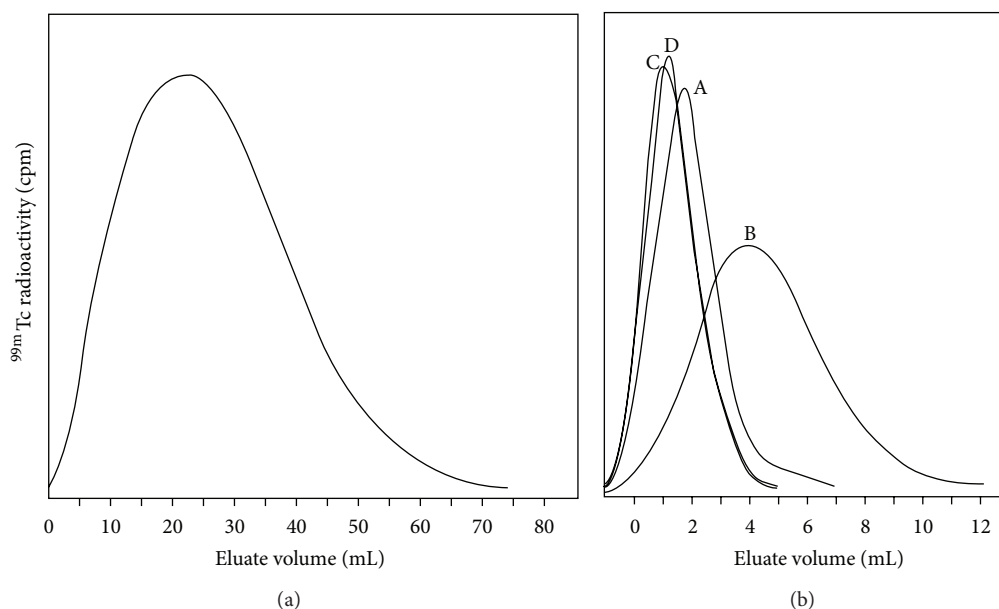
FIGURE 15: ^{99m}Tc elution profiles of the system GELUTEC-C (ZrMo(^{99}Mo) gel column coupled with a metal-oxide sorbent column-based purification/concentration unit): (a) the elution profile of the generator column of 50 g weight of titanium-molybdate gel eluted with redistilled water; (b) the elution profiles of the concentration columns of 1.5 g weight eluted with saline: A: alumina; B: zisorb; C: titania; D: MnO$_2$ [57].

This integrated generator system has been used for years in the hospitals in Vietnam [57, 59, 60, 103]. The low-cost automation of the generator elution using a simple electronic time-sequence-based control unit provides the convenience in operation and preference for use in a daily hospital environment. The ^{99m}Tc elution profile of the molybdate gel-column-based generator is shown in Figure 15. TiMo and ZrMo gel columns are prepared as described in the previous section "Saline-eluted molybdate-gel column. Both the post-irradiation synthesized gel and preformed gel columns are equally used for the preparation of nonsaline aqueous solution-eluted ^{99m}Tc generator systems. Redistilled water is

used as eluent for both TiMo and ZrMo gel columns, while the water containing 0.005% NaCl is more effectively used for ZrMo gel column [57, 59, 60, 69, 70, 103–106, 132, 146]. Similarly, the zirconium-molybdate gel-based ^{99m}Tc generator which is eluted with water is developed in India [49].

(ii) Nonsaline Aqueous Solution-Eluted ^{99m}Tc Generator Systems Using High Mo-Loading Capacity Sorbent Columns

(a) PZC/PTC Sorbent Column-Based Generators. Research is in progress at MEDISOTEC (Australia) on the use of the high Mo-adsorption capacity PTC/PZC sorbent materials for the
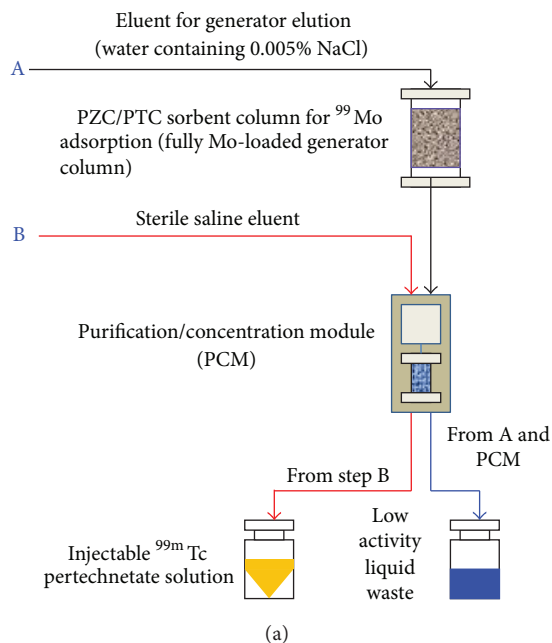
FIGURE 16: Integrated radioisotope generator system (radionuclide generator column coupled with an automated purification/concentration unit of the programmable time sequence control): (a) process diagram; (b) photo of the system recently developed at MEDISOTEC and ANSTO [58, 62–64, 109–111].

production of a nonsaline aqueous solution-eluted ^{99m}Tc generator system. These sorbents are prepared as described in the previous section "Saline-eluted high Mo-adsorption capacity sorbent columns". The PTC and PZC sorbent columns are loaded with a low specific activity ^{99}Mo solution and the ^{99m}Tc-pertechnetate eluted with redistilled water containing 0.005% NaCl is consecutively concentrated using a small alumina concentration column.

The automated purification/concentration unit coupled with ^{99m}Tc generator column is shown in Figure 16. This device is a versatile radionuclide generator system which can be used for the production of different daughter nuclide solutions (such as ^{99m}Tc, ^{188}Re, ^{90}Y, and ^{68}Ga) of high activity concentration using low specific radioactivity parent nuclides [63]. The chemical process applied in this system is based on the selective adsorption of ^{99m}Tc, which is eluted from a large ^{99}Mo-PZC/PTC column, onto a significantly smaller concentration column. In the following step the technetium is stripped from the column with a small volume of injectable saline solution. Optionally, this small sorbent column is washed to remove any parent nuclide ions and metallic impurities that also may have been adsorbed on the column. Following the wash, the daughter nuclide is stripped from the column with a small volume of solution suitable for injection or for investigational purposes.

The process of the daughter radionuclide elution from the generator followed by the postelution purification/concentration process was performed using a low-cost automated bench-top system [62–64]. This system was designed based on the timing sequence of several processing steps without feedback control. The variable flow rate of eluents

used for elution/purification in this system also ensures the optimisation of operating times with respect to different adsorption/desorption kinetics of daughter radionuclide ion species, which is controlled by the sorbents used in the generator and the purification columns.

(b) Alumina Column-Based Generator Systems. Several research groups reported on using different nonsaline aqueous eluents for elution of ^{99m}Tc from alumina-based generator systems which couple with a concentration unit for increasing the pertechnetate concentration of the ^{99m}Tc solution. The eluents used are the following: the mixture of 0.7 M acetic acid and 0.0225 M NaCl solution [50], the solution of the salt of weak acids such as ammonium acetate, citrate, titrate, and so forth, and the mixture of acetic acid and ammonium acetate solution [43–48]. Although the elution performance of these eluents is excellent and suitable for the concentration processes using an anion exchange materials such as QMA Sep-Pak Cartridge, NH_2 Amberlite, BondElut SAX, Dowex-1, DEAE Cellulose, and so forth, the large volume of the eluents used for the ^{99m}Tc elution from large alumina column-based generators is the main issue for the routine use of all these methods. The details of ^{99m}Tc concentration techniques will be reviewed in the next sections.

(c) New Sorbent-Based Generator Systems. No work on using nonsaline aqueous eluents for the elution of ^{99m}Tc from recently developed high Mo-adsorption capacity sorbent materials (such as nanocrystalline zircona (tetragonal phase, t-ZrO_2), nanocrystalline titania, nanocrystalline alumina,
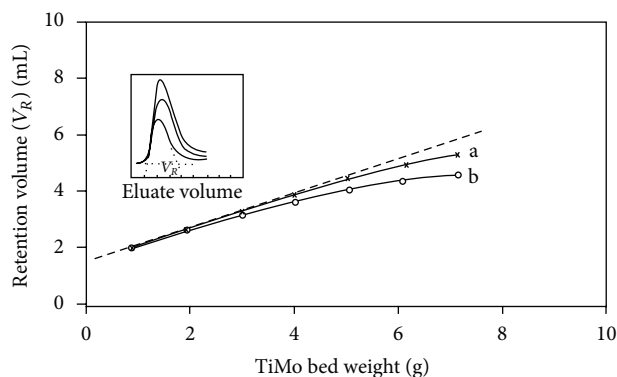
FIGURE 17: Retention volume V_R versus TiMo-column-bed weight (TiMo particle size 100–200 mesh; column size 10 mm i.d.). a: acetone as eluent; b: 0.9% NaCl solution as eluent [59, 106].

FIGURE 18: Process diagram of the solid-liquid extraction-based ^{99m}Tc-generator system GELUTEC-B developed in NRI. 1: ^{99}Mo-loaded molybdate-gel column; 2: acetone evaporator; 3: air pump; 4: acetone reservoir/condenser; 5: saline for recovery of ^{99m}Tc-pertechnetate; 6: ^{99m}Tc-pertechnetate injectable solution; V_{1-3}: valves; G: alumina guard column; MF: Millipore filter [57, 59, 60, 103, 105, 106].

and functional alumina sorbents (sulfated alumina and alumina sulphated zircona)) was performed until now. The integrated ^{99m}Tc-generator systems (integration of elution, purification, concentration, and column-generation) using a column containing multifunctional sorbent materials of high Mo-adsorption capacity and an acetate solution as circulating eluent are recently developed by MEDISOTEC [58].

(iii) Nonsaline Organic Solvent-Eluted ^{99m}Tc Generator Systems Using Molybdate-Gel Columns and Acetone Eluent (Solid-Liquid Extraction ^{99m}Tc Generator). ^{99m}Tc can be eluted from a zirconium/titanium-molybdate gel-type generator column and from ^{99}Mo-loaded diatomaceous earth sorbent using organic solvents (so-called "solid-solvent" extraction) [57, 59, 60, 103–106, 141, 146]. The results of investigations on the elution of ^{99m}Tc from TiMo and ZrMo-gel columns using organic solvents such as methyl ethyl ketone (MEK), acetone, ethyl ether, chloroform, and so forth showed that the separation yield of ^{99m}Tc was around 80% for acetone eluent and <40% for the others. The ^{99m}Tc elution profile of the acetone elution is very similar to that of saline eluent (Figure 17). So the acetone can be used as a useful eluent for a solid-solvent extraction-based generator using zirconium/titanium-molybdate- gel columns of high Mo-loading capacity.

The solid-liquid extraction-based ^{99m}Tc generator system using acetone as eluent operates as follows. First the ^{99}Mo-molybdate gel (TiMo or ZrMo) columns are prepared as described in the previous section "Saline-eluted molybdate gel columns". Then the ^{99m}Tc is eluted with acetone eluent. In the following steps the ^{99m}Tc-acetone eluate is evaporated to dryness and the recovery of ^{99m}Tc pertechnetate into a small volume of saline is followed. The ^{99m}Tc pertechnetate is then passed through a small alumina and Millipore filter giving a sterile pertechnetate solution of high ^{99m}Tc concentration. The generator flowchart is shown in Figure 18.

Acetone is a less toxic volatile solvent. Low boiling temperature and low risk of polymerization of the acetone offers the advantages of economical low temperature evaporation

of ^{99m}Tc /acetone eluate of small volume, which is performed faster using a less elaborated apparatus as compared with MEK extraction-based ^{99m}Tc generator system described above. Thus the generator system based on solid-solvent extraction using acetone as eluent is found to meet the requirements of an effective method of ^{99m}Tc recovery from low specific activity ^{99}Mo. The quality of pertechnetate solution obtained from this generator system was found to meet all the requirements of ^{99m}Tc pertechnetate injection as specified in various pharmacopeia [36, 37].

^{99m}Tc elution from an alumina column-based generator using acetone eluent was also tested and reported with a positive result [51].

(iv) Nonsaline Organic Solvent-Eluted ^{99m}Tc Generator Systems Using High Mo-Loading Capacity Sorbent Columns. No work on using organic eluent for ^{99m}Tc elution from the recently developed sorbent materials of high Mo-adsorption capacity (such as nanocrystalline zircona t-ZrO$_2$, nanocrystalline titania, nanocrystalline alumina, and functional alumina sorbents (sulfated alumina and alumina sulphated zircona), polyfunctional sorbents) was performed until now.

4.4.3. ^{99m}Tc Concentration Methods Used in the ^{99m}Tc Recovery from Low Specific Activity ^{99}Mo

(1) Characterization and Performance Assessment of Chromatographic Column Concentration Process. Le (2003) has developed a method for assessment of concentration factor

values which are achievable in different concentrating processes. This method rely on the basic parameters currently used in the chromatographic processes such as the retention time/volume and the distribution coefficient of the solute [103]. This evaluation is an important guide for designing of the concentrator with optimal operation conditions. In his further development, as being reported in this review, a standardization method of concentration factor evaluation is developed using a standard elution, which is performed with normal saline solution (0.9% NaCl), as a reference. In this case, the normal saline may play both the role of a generator eluate containing solute (^{99m}Tc), which is fed/loaded onto the concentration column to be concentrated, and the role of the eluate of final concentrated ^{99m}Tc-product which is stripped from the concentration column. This approach is useful for the researchers in the process of concentration method development to evaluate the effectiveness of one concentration system (sorbent-eluent system) in comparison with others which could or would be performed under the similar (normalized) conditions of the experiments.

In general, the performance of the concentration process is characterized with the concentration factor n:

$$n = \frac{c_2}{c_1}. \tag{13}$$

For a concentration process of solute recovery yield (k), the following mass balance is established:

$$V_2 \times c_2 = k \times c_1 \times V_1. \tag{14}$$

Relating the above equations, the following is derived:

$$n = \frac{c_2}{c_1} = k \times \frac{V_1}{V_2}, \tag{15}$$

where V_1 and V_2 are the solution volumes before and after concentration, respectively. c_1 is the solute concentration in the solution before the concentration and c_2 is the solute concentration in the solution after the concentration using a given concentration process.

In individual case of ^{99m}Tc concentration, c_1 is the ^{99m}Tc radioactivity concentration in the eluate eluted from the ^{99m}Tc generator and c_2 is the ^{99m}Tc radioactivity concentration in the ^{99m}Tc solution concentrated using a given concentration process.

Except being concentrated by the evaporation of solvent or by the electrolysis, all the chromatographic column concentration processes are described by the following basic equations.

For a sorbent (e.g., ion-exchange resin) characterized with a volume of solid substrate used in the concentration column,

$$V_1 = V_m + K_V \times V_S. \tag{16}$$

For a sorbent (e.g., alumina) characterized with a specific surface area of solid substrate used in the concentration column,

$$V_1 = V_m + K_S \times S, \tag{17}$$

where

$$S = m_c \times \overline{S}$$

$$V_S = m_c \times \overline{V}_S = m_c \times \frac{1}{\rho_{Re}}, \tag{18}$$

$$K_V = \rho_{Re} \times K_W$$

(more details about these equations for refer to [166]).

The following is received by relating (16) and (17):

$$K_V \times V_S = K_S \times S. \tag{19}$$

K_S value is calculated by putting the value of K_V, V_S, and S into this equation:

$$K_S = \frac{K_W}{\overline{S}}, \tag{20}$$

where K_S (mL/m^2), K_V (mL/mL), K_W (mL/g) are the area, volume, and weight distribution coefficient of the solute (^{99m}TcO$_4^-$) in a given sorbent-solution system, respectively; S is the surface area of the sorbent (m^2); V_s is the volume of the dry resin (mL); m_c is the weight of the dry resin/sorbent loaded in the column (g); $\overline{S}$ is the specific surface area of the sorbent (m^2/g); $\overline{V}_S$ is the specific volume of the resin (mL/g); ρ_{Re} is the weight density of the resin (g/mL).

Based on the above equations (assuming the dead volume of the concentration column $V_m \ll V_2$), the concentration factor (n) is assessed for the designing of the concentrator column as follows.

For the ion-exchange resin column,

$$n = k \times \frac{V_1}{V_2} = k \times \left[\frac{V_m}{V_2} + K_V \times \left(\frac{V_s}{V_2} \right) \right] = k \times K_V \times \left(\frac{V_s}{V_2} \right). \tag{21}$$

For the sorbent column,

$$n = k \times \frac{V_1}{V_2} = k \times \left[\frac{V_m}{V_2} + K_S \times \left(\frac{S}{V_2} \right) \right] = k \times K_S \times \left(\frac{S}{V_2} \right). \tag{22}$$

If V_2 is given as a designed value, the concentration factor (n) only depends on the value of k, K_S, and S (or K_V and V_S).

As an example, the design of the generator systems, which are composed of the molybdate gel (Figure 14) or PZC/PTC nanocrystalline sorbent (Figure 16) generator column coupled with a alumina concentrator column described above, was based on the following parameters calculated using the above equations: $K_S = 2.0$, $V_2 = 5.0$ mL, and $k = 0.95$; the available concentration factor for a bolus elution (with $V_1 = 460$ mL for a generator TiMo (or PZC/PTC)-column of 375–380 g weight, $V_2 = 7.5$ mL and $k = 1$) is $n = 55.7$; the elution-by-elution (with $V_1 = 65$ mL for each elution from a 53 g weight-sorbent column, Mo-breakthrough of <40 μg/mL, $V_2 = 5.0$ mL and $k = 0.95$) concentration factor is $n = 11.2$. The design is also performed with a conservation of the influence of MoO$_4^{2-}$ breakthrough in the primary solution eluted

from the generator column. The above-described calculation method was also successfully applied for the evaluation and designing of a compact concentrator ULTRALUTE using a more effective new sorbent concentration-column as shown in Figure 3.

Due to the diversity of the eluents of variable volume used for the elution of ^{99m}Tc-generators, the evaluation of concentration factor of the integrated generator systems (integrated elution-concentration processes) should be harmonized using a common language for communication/justification on the elution/concentration performance of the given systems. When a nonsaline solvent-eluted process is applied for the ^{99m}Tc generator elution and consecutively the eluate of this elution is concentrated using a chromatographic column concentration method, we need a tool to assess/justify the effectiveness of each elution-concentration process in comparison with others. So we need a reference to be used for the comparison. The saline-eluted process of the ^{99m}Tc generator is considered as a gold standard/reference elution due to its suitability for clinical use. The reference is set up as follows.

V_{Eqv} (equivalent volume) is the volume of nonsaline eluent used for the elution of ^{99m}Tc from a generator (with a nonspecified activity) giving a ^{99m}Tc elution yield f_E which is equal to the yield achieved by an elution performed with the volume V_{S1} of saline.

V_E is the volume of nonsaline eluent (containing ^{99m}Tc) actually passed through the concentration column of the weight m, in which the ^{99m}Tc will be retained with adsorption yield (x) from its total amount present in the volume V_E.

At the stage of the elution of the concentration column with a small volume of saline, V_{S2} is the volume of the saline used to recover the ^{99m}Tc from the concentration column to achieve a concentrated ^{99m}Tc solution and the elution yield of this concentration column is y. The yield of the overall concentration process k is composed of the adsorption yield x and recovery elution yield y, as follows:

$$k = x \times y. \qquad (23)$$

The normalized concentration factor will be set up as follows:

$$n = k \times \frac{V_{S1}}{V_{Eqv}} \times \frac{V_E}{V_{S2}}. \qquad (24)$$

With introduction of the weight of the sorbent (m) used in the concentration column, the further analysis of the above equation is shown as follows:

$$\overline{V} \times m = V_{S2}, \qquad (25)$$

$$n = \frac{V_{S1}}{V_{Eqv}} \times \frac{x}{\overline{V}} \times \frac{y \times V_E}{m}, \qquad (26)$$

where $\overline{V}$ (mL/g) is the specific elution volume of the concentration column eluted with saline to get a concentrated ^{99m}Tc solution of volume V_{2S}.

Equation (26) composes four components characterizing the system involved.

The term (V_{S1}/V_{Eqv}) characterizes the relation of the saline elution versus alternative nonsaline elution of a given generator column.

The term ($1/\overline{V}$) characterizes the saline elution of the concentrator column.

(V_E/m) and K characterize the adsorption/elution capability of the sorbent for the pertechnetate ions with an alternative nonsaline eluent.

The equations described above can be used for both the theoretical and practical evaluations of the normalized concentration factor:

$$n_T = k_T \times \frac{V_{S1}}{V_{Eqv}} \times \frac{V_{E-T}}{V_{S2-T}}. \qquad (27)$$

Equation (27) is used for theoretical assessment of the normalized concentration factor, where $k_T = 1$; V_{E-T} and V_{S2-T} are obtained from the practical determination of retention time/retention volume using an established standard chromatographic procedure performed with the same column or are calculated from the distribution coefficient K as described above. K_W is determined as described in the literature [166]. n_T value is used for the evaluation of the effectiveness of the concentration system (sorbent-eluent)/method of interest, while n_P value is to evaluate the performance of a practical procedure/concentrator device designed using this concentration system/method. n_P value is calculated as follows:

$$n_P = k_P \times \frac{V_{S1}}{V_{Eqv}} \times \frac{V_{E-P}}{V_{S2-P}}, \qquad (28)$$

where V_{E-P} and V_{S2-P} are the volume of nonsaline eluent and saline actually used in the concentration procedure/device, respectively.

Note that the overall ^{99m}Tc recovery yield of the integrated generator-concentration system will be

$$Y = f_E \times k, \qquad (29)$$

where f_E is the elution yield of the generator column and k is the purification/concentration yield.

Table 3 shows the majority of the concentration methods developed up to date and the normalized concentration factor values assessed by the approach described above using the process performance parameters extracted from the literatures. It may be interesting to note that in many cases the optimal design of a practical procedure/concentrator device was not performed to match the inherent effectiveness of the method developed.

(2) Chemistry and Methods of ^{99m}Tc Concentration. The chemistry of pertechnetate ions should be reviewed herein in regard to the development of the ^{99m}Tc concentration methods. Except for the materials containing cyclic compounds of π-electrons, almost all the anion-exchange materials reversibly adsorb the pertechnetate ions in aqueous solutions. Unfortunately the chloride ions compete strongly with pertechnetate ions in the adsorption on these sorbents. This fact makes the concentration of ^{99m}Tc-pertechnetate from a saline solution very hard. The following parameters are useful to justify a proper selection of the sorbent and suitable eluent to develop an effective process for ^{99m}Tc concentration.

TABLE 3: Assessment of normalized concentration factor of the concentration methods (electrolysis- and solvent-evaporation-based concentration methods are not included herein.).

Method and concentration column (CC)/(generator column)	Generator elution volumes		Adsorption: Retention volume of nonsaline eluent passed over CC		Elution: volume of saline eluted from concentration column		Values calculated using K_W or retention volume (V_{E-T})		Values calculated based on experiment parameters (exp. result)		Reference
	V_{Eqv}	V_{S1}	V_{E-T}	V_{E-P}	V_{S2-T}	V_{S2-P}	k_T	n_T	k_P	n_P	
0.3 M NH$_4$OAc + 0.01 M NH$_4$NO$_3$ QMA-SepPak (130 mg)/(alumina)	20**	10**	—	20	—	0.5	1.0	—	0.69	13.8 (40)	Knapp et al. (1998) [43–45]
0.7 M AcOH + 0.132% (0.025 M) NaCl QMA-SepPak (130 mg)/(alumina)	10	10	10	10	1.5	2.0	1.0	6.6	0.9	4.5 (4.5)	Mushtaq (2004) [50]
0.5 M AcOH + 0.025% NaCl QMA-SepPak (130 mg)/(alumina)	25	10	13	13	1.5	1.5	1.0	3.5	0.9	3.2 (3.1)	Le (2013) (for this report)
0.7 M AcOH + 0.025 M NH$_4$OAc DEAE-cellulose (300 mg)/(alumina)	40	45	40	40	6.0	6.0	1.0	7.5	0.8	6.0 (5-7)	Sarkar et al. (2001) [47, 48]
0.1 M AcOH + 0.05% NaCl DEAE-cellulose (0.25 mL)/(alumina)	40	10	120	120	6.0	6.0	1.0	5.0	0.95	4.75 (4.5)	Le (2013) (for this report)
0.3 M AcOH + 0.05% NaCl DEAE-cellulose (0.25 mL)/(alumina)	27	10	108	108	6.0	6.0	1.0	6.7	0.95	6.3 (6.0)	Le (2013) (for this report)
0.3 M AcOH + 0.05% NaCl DEAE-cellulose (0.25 mL)/(alumina)	27	10	108	108	4.0*	3.5*	1.0	10.0	0.85	9.7 (9.4)	Le (2013) (for this report)
0.5 M AcOH + 0.1% NaCl DEAE-sephadex (0.125 mL)/(alumina)	15	10	20	20	4.0	4.0	1.0	3.3	0.9	3.0 (3.0)	Le (2013) (for this report)
0.5 M AcOH + 0.05% NaCl Isosorb-MOX-01 (100 mg)/(alumina)	20	10	18	16	1.5	1.5	1.0	6.0	0.95	5.0 (4.5)	Le and Le (2013) [58]
0.1 M AcOH + 0.05% NaCl Isosorb-FS-01 (100 mg)/(alumina)	40	10	40	35	1.5	1.5	1.0	6.6	0.90	5.25 (5.0)	Le and Le (2013) [58]
H$_2$O alumina (2.0 g)/(ZrMo molybdate gel)	16	16	—	20	—	3.0	1.0	—	0.9	6.0 (4.0)	Sarkar et al. (2004) [49]

Table 3: Continued.

Method and concentration column (CC)/(generator column)	Generator elution volumes		Adsorption: Retention volume of nonsaline eluent passed over CC		Elution: volume of saline eluted from concentration column		Values calculated using K_W or retention volume (V_{E-T})		Values calculated based on experiment parameters (exp. result)		Reference
	V_{Eqv}	V_{S1}	V_{E-T}	V_{E-P}	V_{S2-T}	V_{S2-P}	k_T	n_T	k_P	n_P	
H_2O alumina (1.5 g)/ (TiMo/ZrMo molybdate gel)	11	10	460	65***	7.5	5.0	1.0	55.7	0.95	11.2 (10.5)	Le (1990) [57]
H_2O $MnO_2 \cdot xH_2O$ (1.5 g)/ (TiMo/ZrMo molybdate gel)	11	10	440	62***	7.0	5.0	1.0	62.8	0.95	11.8 (10.4)	Le (1990) [57]
H_2O $TiO_2 \cdot xH_2O$ (1.5 g)/ (TiMo/ZrMo molybdate gel)	11	10	400	55***	6.5	5.0	1.0	61.5	0.95	10.5 (10.1)	Le (1990) [57]
H_2O $ZrO_2 \cdot xH_2O$ (1.5 g)/ (TiMo/ZrMo molybdate gel)	11	10	660	95***	12.0	10.0	1.0	55.0	0.8	7.6 (7.0)	Le (1990) [57]
Saline → H_2O Ag-resin-alumina (0.25 mL; ~260 mg)/ (alumina)	10	10	—	20	3.0	—	1.0	—	0.98	6.53 (6.57)	Ruddock (1978) [38]
Saline → H_2O Ag-resin-alumina (0.5 g)/ (alumina)	10	10	150	150	2.5	2.5	1.0	60	0.90	54.0 (50.0)	Le et al. (2013) [40]
Saline → H_2O Ag-resin-MnO_2 (0.5 g)/ (alumina)	10	10	145	145	2.2	2.2	1.0	65.9	0.90	59.3 (53.0)	Le and Le (2013) [58]
Saline → H_2O Ag-resin-TiO_2 (0.5 g)/ (alumina)	10	10	140	140	2.0	2.0	1.0	70	0.90	63.0 (57.0)	Le and Le (2013) [58]
Saline → H_2O Ag-resin-microcrystalline ZT-11 sorbent (0.5 g)/ (alumina)	10	10	155	155	2.75	2.5	1.0	56.3	0.90	55.8 (53)	Le (2010-2013) [63, 64]
Saline → H_2O Ag-resin-microcrystalline ZT-31 sorbent (0.5 g)/ (alumina)	10	10	200	200	5.0	5.0	1.0	40.0	0.8	32.0 (31.0)	Le (2010-2013) [63, 64]
Saline → H_2O Ag-resin-isosorb-FS-01 (0.5 g)/ (alumina)	10	10	275	275	5.0	5.0	1.0	55.0	0.95	52.2 (50)	Le and Le (2013) [58]
Saline → H_2O Ag-resin-QMA SepPak (130 mg)/ (alumina)	10	10	—	10	—	1.0	1.0	—	0.82	8.2	Knapp et al. (1998) [43, 44]

TABLE 3: Continued.

Method and concentration column (CC)/(generator column)	Generator elution volumes		Adsorption: Retention volume of nonsaline eluent passed over CC		Elution: volume of saline eluted from concentration column		Values calculated using K_W or retention volume (V_{E-T})		Values calculated based on experiment parameters (exp. result)		Reference
	V_{Eqv}	V_{S1}	V_{E-T}	V_{E-P}	V_{S2-T}	V_{S2-P}	k_T	n_T	k_P	n_P	
Saline $\rightarrow$ H$_2$O Ag-resin-BondElut-SAX (100 mg)/ (alumina)	10	10	25	10	2.0	2.0	1.0	12.5	0.95	4.75 (4.7)	Blower (1993) [39]
Saline $\rightarrow$ 0.2 M NaI Dowex 1 $\times$ 8-resin (10 mg) $\rightarrow$ AgCl, 1.0 g/ (alumina)	10	10	66	70	5.5	7.5	1.0	12.0	0.8	7.5 (7.7)	Chattopadhyay et al. (2002) [53]
0.02 M Na$_2$SO$_4$ $\rightarrow$ H$_2$O Pb-resin-alumina (300 mg)/ (alumina)	45	60	45	45	1.5	1.0	1.0	40	0.9	54 (38)	Bokhari et al. (2007) [54]

* Concentrator column is eluted with 0.15 M NaOH and followed by passing over a cation-exchange resin column.
** Value is assumed based on different data sources.
*** Values are designed for a useful life (14 elution cycles) of the generator without replacement of the concentrator column.

TABLE 4: Details of the methods of ^{99m}Tc-pertechnetate concentration from the saline eluate of ^{99m}Tc-pertechnetate (dual column concentration methods).

Scheme	Concentration process			^{99m}Tc-generator column	References
	Elution	Interfering ions remover	^{99m}Tc concentrator		
1A	Step A: saline Step B: saline	Cation exchange resin (Ag form)	Alumina, zircona, and MnO$_2$ columns	Alumina	Ruddock (1978) [38]
1A	Step A: saline Step B: saline	Cation exchange resin (Ag form) OnGuard-AG	BondElut-SAX column	Alumina	Blower (1993) [39]
1A	Step A: saline Step B: saline	Cation exchange resin (Ag form) OnGuard-AG	QMA-SepPak column	Alumina	Knapp et al. (1998) [43, 44]
1A	Step A: saline Step B: saline	Cation exchange resin (Ag form)	Functional sorbent (isosorb-FS-01) columns	Alumina	Le and Le (2013) [58]
1A	Step A: saline Step B: saline	Cation exchange resin (Ag form)	MnO$_2$, TiO$_2$, ZrO$_2$, ZT-11, ZT-31 sorbent columns	Alumina	Le et al. (2013) [40]
2A	Step A: saline Step B: NaI solution	AgCl powder column	Anion exchange resin (Dowex-1 × 8) column	Large alumina	Chattopadhyay et al. (2002) [53]
3A	Step A: saline Step B: Tetrabutylammonium bromide in methylene chloride	Not needed	Anion exchange resin (Dowex-1 × 8) column combined with solvent evaporator	Large alumina	Chattopadhyay and Das (2008) [52]
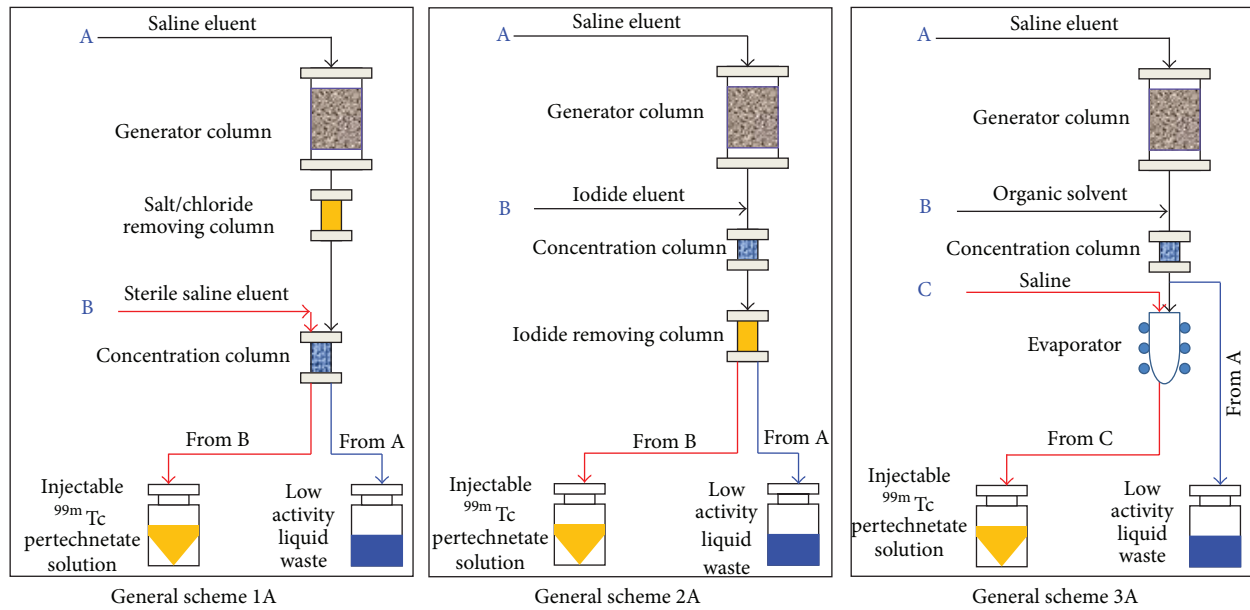
FIGURE 19: Group 1 of concentration methods: ^{99m}Tc-pertechnetate concentration from the saline eluate of the ^{99m}Tc generator.

Technetium has an electron configuration with presence of d-orbital electrons, (K L M 4s^2 4p^6 4d^5 5s^2), while that of chlorine is (K L 3s^2 3p^5) and oxygen K 2s^2 2p^4. The energy of outer electrons of these atoms is in the range of 2p$_{oxygen}$ ~ 3p$_{chlorine}$ ~ 4d$_{technetium}$ < 5s$_{technetium}$. The ion radius of TcO$_4^-$ is 3.2 Å, while that of Cl$^-$ ion is 1.81 Å. This big difference in the ion radius justifies a strong competition of

chloride in the adsorption with pertechnetate ions when the anion exchange resin is applied for TcO$_4^-$/Cl$^-$ separation.

In the aqueous solutions, pertehnic acid (HTcO$_4$) has an ionization constant $pK_a = 0.3$. So the weak acid of $pK_a > 0.3$ should be used as eluent in the process of ^{99m}Tc pertechnetate elution from the generator/concentration system. The weak acid used must also have a pK_a value below that of the sorbent

FIGURE 20: Group 2 of concentration methods: ^{99m}Tc-pertechnetate concentration from nonsaline eluate of the ^{99m}Tc generator.

Table 5: Details of methods of ^{99m}Tc-pertechnetate concentration from the nonsaline eluate of ^{99m}Tc-pertechnetate (single and dual column concentration methods).

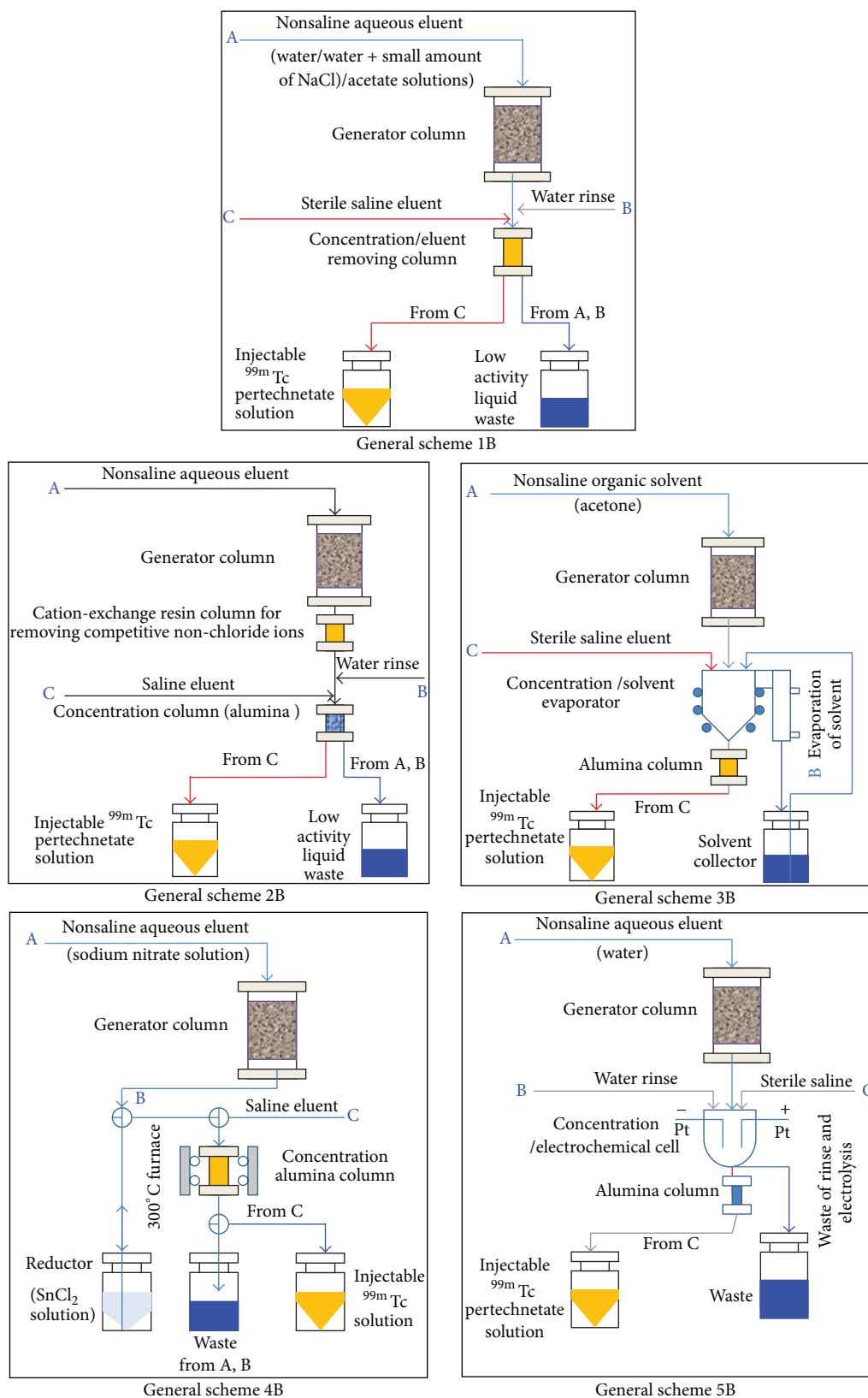| Scheme	Concentration process		Generator column	References
	Elution	^{99m}Tc concentrator		
1B	A: H_2O B: saline	Alumina and/or TiO_2, MnO_2, zircona	TiMo/ZrM molybdate gel	Le (1990) [57]
1B	A: H_2O B: saline	Alumina	ZrMo molybdate gel	Sarkar et al. (2004) [49]
1B	A: $NH_4OAc + NH_4NO_3$ B: water C: saline	QMA SepPak	Alumina	Knapp et al. (1998) [43–45]
1B	A: acetic acid + NaCl B: water C: saline	QMA SepPak	Alumina	Mushtaq (2004) [50] Le (2013) (for this review)
1B	A: acetic acid + ammonium-acetate B: water C: saline	DEAE-cellulose	Alumina	Sarkar et al. (2001) [47, 48]
1B	A: acetic acid + NaCl B: water C: saline	DEAE-cellulose	Alumina	Le (2013) (for this review)
1B	A: acetic acid + NaCl B: water C: saline	DEAE-sephadex	Alumina	Le (2013) (for this review)
1B	A: acetic acid + NaCl B: water C: saline	Isosorb-FS-01	Alumina	Le and Le (2013) [58]
2B	A: Na_2SO_4 B: H_2O C: saline	Pb-resin-alumina	Alumina	Bokhari et al.(2007) [54]
3B	Step A: acetone Step C: saline	Evaporator	TiMo/ZrMo gel	Le (1987–1994) [57, 59, 60, 104]
3B	Step A: acetone Step C: saline	Evaporator	Alumina	Mushtaq (2003) [51]
4B	A: $NaNO_3$ B: $NaNO_3 + SnCl_2$ C: saline	Redox agent + alumina	Alumina	Seifert et al. (1994) [55]
5B	A: H_2O B: H_2O C: saline	Electrochemical cell with Pt electrodes	ZrMo molybdate gel	Chakravarty et al. (2012) [56]

used in a consequent pertechnetate-concentration process to ensure the reversible adsorption of TcO_4^- ions in a sorbent column of reasonably small volume.

The conflict exists between the conventional/convenient use of saline in the elution of medical isotope generator and the challenge of chloride ions in the process of ^{99m}Tc concentration. So, the ^{99m}Tc concentration methods developed up to date in different laboratories are dedicated to the ^{99m}Tc concentration from the saline eluate or from nonsaline eluate of the generators. Accordingly, they are classified in two following groups and described as follows.

(i) Group 1: ^{99m}Tc-Pertechnetate Concentration from the Saline Eluate of the ^{99m}Tc Generato r. In the first group of concentration methods are briefly described in Table 4.

The general process diagrams are shown in Figure 19. The main characteristic of this group is the increase of *^{99m}Tc-pertechnetate concentration from a saline elutate of the ^{99m}Tc generator.* As an example, in one of the dual column purification/concentration processes (Scheme 1 in Figure 19), the saline eluate of the generator is first passed through a small silver ions loaded sorbent (or an ion exchange resin in Ag^+ form) column which traps the chloride anions allowing subsequent in-tandem passage through a sorbent cartridge (concentration column) with specific trapping of the TcO_4^- ions. The pertechnetate anion is subsequently easily removed with a small volume of normal saline ready for "kit" radiolabeling. The concentration factors can be as high as 10–60, with the silver ion stoichiometry based on the volume of the saline eluant. Among concentrator prototypes developed using this

postelution concentration concept the commercially available concentrator device ULTRALUTE is shown in Figure 3 [40–42].

(ii) Group 2: ^{99m}Tc-Pertechnetate Concentration from the Nonsaline Elution of the ^{99m}Tc Generator. In the second group of concentration methods are briefly described in Table 5. The general process diagrams are shown in Figure 20. The main characteristic of this group is the increase of ^{99m}Tc-pertechnetate concentration from a nonsaline elutate of the ^{99m}Tc generator. These methods are generally known as the single column concentration methods developed in years 1980s for the purification/concentration of the dilute solution of ^{99m}Tc, which is eluted from the low specific activity $(n, \gamma)^{99}$Mo column generator [57, 59, 60]. Recently, many alternatives have been further developed and improved with an automated operation, as shown in Figures 5, 14, and 16. This process is based on the selective adsorption of ^{99m}Tc eluted from the ^{99}Mo column onto a significantly smaller sorbent column (concentration column). In the following step, the technetium is stripped from the column with a small volume of injectable saline solution. Optionally, this small sorbent column can be washed to remove any parent nuclide ions and metallic impurities that may also have been adsorbed onto the column. Following the wash, the daughter nuclide is stripped from the column with a small volume of solution suitable for injection or for other investigational purposes. The automated purification/concentration unit coupled radionuclide generator shown in Figure 16 is a versatile system which can be used for production of different daughter nuclides (such as ^{99m}Tc, ^{188}Re, ^{90}Y and ^{68}Ga) giving solutions of high radioactive concentration from low specific radioactivity parent nuclides.

5. Summary

^{99m}Tc plays an important role in diagnostic nuclear medicine imaging. Demographic and medical trends suggested that in the near future, the global demand for ^{99m}Tc will grow at an average rate between 3% and 8% per year as new markets. So, there is a need for diversity in all aspects of the ^{99m}Tc production using different specific activity ^{99}Mo sources to provide important supplements for increasing reliability of ^{99}Mo /^{99m}Tc generator supply. Accordingly, ^{99m}Tc recovery should be performed by suitable technologies to make them acceptable for nuclear medicine uses. Several alternative/supplementary technologies for producing high and low specific activity ^{99}Mo solutions and for ^{99m}Tc recovery therefrom have been developed and proposed. Some of them are not yet commercially proven or still require further development. To provide the researchers/producers a look into up-to-date ^{99}Mo/^{99m}Tc technologies, a review on the ^{99}Mo sources available today and on the ^{99m}Tc generators developed up to date for increasing the effectiveness of ^{99}Mo utilization is performed in the format of detailed description of the features and technical performance of the technological groups of the

^{99}Mo production and ^{99m}Tc recovery. Presently, the technologies of ^{99m}Tc recovery from low specific activity ^{99}Mo are playing an increasing role in ensuring the security of supplies of ^{99m}Tc to users worldwide. Various ^{99m}Tc recovery processes using low specific activity ^{99}Mo have been reported. Besides the low specific volume of ^{99m}Tc eluate obtained, the problem of complexity in operation of ^{99m}Tc-generator and of the high cost for automation/computerization of ^{99m}Tc-recovery process remain to be solved regarding cheaper, better, safer, and faster supply of ^{99m}Tc solution for SPECT imaging use in a daily hospital environment. Definitely, each technology developed may have some limitation. However the indispensable criteria of ^{99m}Tc production technology, which reflect the acceptance of the hospital users, are the reliability/reproducibility, the simplicity and safety in operation, and the proven capability to provide the ^{99m}Tc-pertechnetate solution which is safe for human use and effective for a wide range of the ^{99m}Tc-labeled radiopharmaceutical preparations. In terms of compliance with the requirements of human use, the technologies developed should not contain any materials of high toxicity for human use, which will make the registration process complicated and thus the delay in the technological product delivery.

Conflict of Interests

The author declares no conflict of interests.

Acknowledgments

References

[1] P. Richards, W. D. Tucker, and S. C. Srivastava, "Technetium-99m: an historical perspective," *International Journal of Applied Radiation and Isotopes*, vol. 33, no. 10, pp. 793–799, 1982.

[2] *Non-HEU Production Technologies for Molybdenum-99 and Technetium-99m*, IAEA Nuclear Energy Series no. NF-T-5.4, International Atomic Energy Agency, Vienna, Austria, 2013.

[3] Expert Review Panel on Medical Isotope Production, *Report of the Expert Review Panel on Medical Isotope Production*, Ministry of Natural Resources of Canada, Ottawa, Canada, 2009.

[4] National Research Council of the National Academies, *Medical Isotope Production without Highly Enriched Uranium*, The National Academies Press, 2009.

[5] OECD Nuclear Energy Agency, *The Supply of Medical Radioisotopes: Review of Potential Molybdenum-99/Technetium-99m Production Technologies*, OECD, Paris, France, 2010.

[6] IAEA-TECDOC-1065, *Production Technologies for Molybdenum-99 and Technetium-99m*, International Atomic Energy Agency, Vienna, Austria, 1999.

[7] IAEA TECDOC-515, "Fission molybdenum for medical use," in *Proceedings of the Technical Committee Meeting*, International Atomic Energy Agency, Karlsruhe, Germany, October 1987.

[8] A. A. Sameh and H. J. Ache, "Production techniques of fission molybdenum-99," *Radiochimica Acta*, vol. 41, pp. 65–72, 1987.

[9] H. Arino, H. H. Kramer, J. J. McGovern, and A. K. Thornton, "Production of high purity fission product molybdenum-99," U.S. patent no. 3799883, March 1974.

[10] D. Novotny and G. Wagner, "Procedure of small scale production of Mo-99 on the basis of irradiated natural uranium target," in *Proceedings of the IAEA Consultancy Meeting on Small Scale Production of Fission Mo-99 for Use in Tc-99m Generators*, Vienna, Austria, July 2003.

[11] A. A. Sameh and A. Bertram-Berg, "HEU and LEU as target materials for the production of fission molybdenum," in *Proceedings of the International Meeting on Reduced Enrichment for Research and Test Reactors*, pp. 313–333, RERTR, Roskilde, Denmark, 1992, TM19, Conf-9209266.

[12] T. N. van der Walt and P. P. Coetzee, "The isolation of ^{99}Mo from fission material for use in the ^{99}Mo/^{99m}Tc generator for medical use," *Radiochimica Acta*, vol. 92, no. 4–6, pp. 251–257, 2004.

[13] A. Perkins, A. Hilson, and J. Hall, "Global shortage of medical isotopes threatens nuclear medicine services," *The British Medical Journal*, vol. 337, article a1577, 2008.

[14] N. Ramamoorthy, "Commentary: supplies of molybdenum-99—need for sustainable strategies and enhanced international cooperation," *Nuclear Medicine Communications*, vol. 30, no. 12, pp. 899–905, 2009.

[15] R. O. Marque's, P. R. Cristini, H. Fernandez, and D. Marziale, "Operation of the installation for fission Mo-99 production in Argentina," IAEA-TECDOC 515, 1989.

[16] P. R. Cristini, H. J. Cols, R. Bavaro, M. Bronca, R. Centurio'n, and D. Cestan, "Production of molybdenum-99 from low enriched uranium targets," in *Proceedings of the International Meeting on Reduced Enrichment for Research and Test Reactor*, Bariloche, Argentina, November 2002.

[17] ANSTO Media Releases, "ANSTO to help supply the world with nuclear medicine," http://www.ansto.gov.au/AboutANSTO/News/ACSTEST_039937.

[18] IAEA TECDOC-1601, *Homogeneous Aqueous Solution Nuclear Reactors for the Production of Mo-99 and Other Short Lived Radioisotopes*, International Atomic Energy Agency, Vienna, Austria, 2008.

[19] A. J. Ziegler, D. C. Stepinski, J. F. Krebs, S. D. Chemerisov, A. J. Bakel, and G. F. Vandegrift, "Mo-99 recovery from aqueous-homogeneous-reactor fuel- behavior of termoxid sorbents," in *Proceedings of the International RERTR Meeting*, Washington, DC, USA, October 2008.

[20] D. C. Stepinski, A. V. Gelis, P. Gentner, A. J. Bakel, and G. V. Vandegrift, "Evaluation of radisorb, isosorb (Thermoxid) and PZC as potential sorbents for separation of ^{99}Mo from a homogenous-reactor fuel solution," IAEA-TECDOC-1601, September 2009.

[21] S. Khamyanov and S. Voloshin, "A proposed international project of low-enriched uranium salt solution reactor for medical isotope production," in *Proceedings of the International Meeting on Reduced Enrichment for Research and Test Reactors*, Lisbon, Portugal, October 2010.

[22] F. Stichelbaut and Y. Jongen, "^{99}Mo production by proton-induced fission with LEU," in *Proceedings of the CNS Workshop on the Production of Medical Radionuclides*, Ottawa, Canada, 2009.

[23] F. Y. Tsang, "Techniques for on-demand production of medical isotopes such as Mo-99/Tc-99m and radioactive iodine isotopes including I-131," World Intellectual Property Organization, WO, 2011/093938 A2, August 2011.

[24] S. Lapi, T. Ruth, and J. D'Auria, "The MoRe Project: an alternative route to the production of high specific activity ^{99}Mo," in *Proceedings of the International Symposium on Technetium and Other Radiometals in Chemistry and Medicine*, Brixen, Italy, 2010.

[25] A. Fong, T. I. Meyer, and K. Zala, *Making Medical Isotopes: Final Report of the Task Force on Alternatives for Medical-Isotope Production*, TRIUMF, Vancouver, Canada, 2008.

[26] V. S. Le, "Automated modular fission Mo-99 production process," Project Proposal, ANSTO Life Sciences, Australian Nuclear Science and Technology Organisation, 2010.

[27] V. S. Le and C. D. Nguyen, "Separation of Tungsten from LEU fission-produced ^{99}Mo solution to improve technological performance in both the processes of ^{99}Mo and ^{99m}Tc generator production," in *Proceedings of the 5th Asia-Pacific Symposium on Radiochemistry*, p. 197, Kanazawa, Japan, September 2013.

[28] V. S. Le, "Specific radioactivity of neutron induced radioisotopes: assessment methods and application for medically useful ^{177}Lu production as a case," *Molecules*, vol. 16, no. 1, pp. 818–846, 2011.

[29] W. C. Eckelman, "Unparalleled contribution of technetium-99m to medicine over 5 decades," *JACC: Cardiovascular Imaging*, vol. 2, no. 3, pp. 364–368, 2009.

[30] P. Gould, "Medical isotopes: time to secure supplies?" *The Lancet Oncology*, vol. 9, no. 11, p. 1027, 2008.

[31] *Technetium-99m Radiopharmaceuticals: Manufacture of Kits*, IAEA Technical Report Series no. 466, International Atomic Energy Agency, Vienna, Austria, 2008.

[32] W. C. Eckelman and B. M. Coursey, "Technetium-99 m generators, chemistry and preparation of radio-pharmaceuticals," *The International Journal of Applied Radiation and Isotopes*, vol. 33, pp. 793–950, 1982.

[33] J. J. M. de Goeij, "Routes for supply of technetium-99m for diagnostic nuclear medicine," *Transactions of the American Nuclear Society*, vol. 77, p. 519, 1997.

[34] K. Bremer, "Large-scale production and distribution of Tc-99 m generators for medical use," *Radiochimica Acta*, vol. 41, pp. 73–81, 1987.

[35] V. J. Molinski, "A review of ^{99m}Tc generator technology," *International Journal of Applied Radiation and Isotopes*, vol. 33, no. 10, pp. 811–819, 1982.

[36] United States Pharmacopeial Convention, *Official Monographs: USP 28, Sodium Pertechnetate Tc^{99m} Injection*, United States Pharmacopiea (USP) 28- National Formulary (NF) 23, 2005.

[37] British Pharmacopoeia Commission, *British Pharmacopoeia*, The Stationery Office, Norwich, UK, 2008, http://www.pharmacopoeia.org.uk/.

[38] C. F. Ruddock, "Purification of Technetium-99m pertechnetate solution," U.S. patent no. 4123497, October 1978.

[39] P. J. Blower, "Extending the life of a ^{99m}Tc generator: a simple and convenient method for concentrating generator eluate for clinical use," *Nuclear Medicine Communications*, vol. 14, no. 11, pp. 995–997, 1993.

[40] V. S. Le, J. McBrayer, and N. Morcos, "A radioisotope concentrator device for use with a radioisotope source, a system, and a process for capturing at least one radioisotope from a radioisotope solution obtained from a radioisotope source," Australia patent application, AU2012904683, October 2012.

[41] V. S. Le, N. Morcos, J. McBrayer, Z. Bogulski, C. Buttigieg, and G. Phillips, "Disposable cartridge-based radioisotope concentrator device for increasing ^{99m}Tc and ^{188}Re concentration of commercial radionuclide generator eluates," *Journal of Labelled Compounds and Radiopharmaceuticals*, vol. 56, supplement 1, p. S190, 2013.

[42] V. S. Le and N. Morcos, "An in-line, cartridge-based radioisotope concentrator device for use with multiple elutions from ^{99m}Tc and ^{188}Re generators," *Journal of Nuclear Medicine*, vol. 54, supplement 2, p. 609, 2013.

[43] F. F. Knapp Jr., A. L. Beets, S. Mirzadeh, and S. Gluhlke, "Use of a new tandem cation/anion exchange system with clinical-scale generators provides high specific volume solutions of technetium-99m and rhenium-188," IAEA-TECDOC-1029, 1998.

[44] F. F. Knapp, "The development and use of radionuclide generators in nuclear medicine: recent advances and future perspectives," in *Modern Trends in Radiopharmaceuticals for Diagnosis and Therapy*, IAEA-TECDOC-1029, pp. 485–495, International Atomic Energy Agency, Vienna, Austria, 1998.

[45] F. F. Knapp Jr., A. L. Beets, S. Mirzadeh, and S. Guhlke, "Concentration of perrhenate and pertechnetate solutions," U.S. patent no. 5729821, March 1998.

[46] S. Mirzadeh, F. F. Knapp Jr., and E. D. Collins, "A tandem radioisotope generator system for preparation of highly concentrated solutions of Tc-99m from low specific activity Mo-99," U.S. patent no. 5774782, June 1998.

[47] S. K. Sarkar, G. Arjun, P. Saraswathy, and N. Ramamoorthy, "Post-elution concentration of ^{99m}TcO$_4^-$ by a single anion exchanger column I: feasibility of extending the useful life of column chromatographic ^{99m}Tc generator," *Applied Radiation and Isotopes*, vol. 55, no. 4, pp. 561–567, 2001.

[48] S. K. Sarkar, G. Arjun, P. Saraswathy, and N. Ramamoorthy, "Post-elution concentration of (TcO$_4^-$)-^{99m}Tc by a single anion exchanger column: II. Preparation and evaluation of jumbo alumina column chromatographic generator for ^{99m}Tc," *Nuclear Medicine Communications*, vol. 22, pp. 389–397, 2001.

[49] S. K. Sarkar, P. Saraswathy, G. Arjun, and N. Ramamoorthy, "High radioactive concentration of ^{99m}Tc from a zirconium [^{99}Mo]molybdate gel generator using an acidic alumina column for purification and concentration," *Nuclear Medicine Communications*, vol. 25, no. 6, pp. 609–614, 2004.

[50] A. Mushtaq, "Concentration of ^{99m}TcO$_4^-$/ ^{188}ReO$_4^-$ by a single, compact, anion exchange cartridge," *Nuclear Medicine Communications*, vol. 25, no. 9, pp. 957–962, 2004.

[51] A. Mushtaq, "Preparation of high specific-volume solutions of technetium-99m and rhenium-188," *Applied Radiation and Isotopes*, vol. 58, no. 3, pp. 309–314, 2003.

[52] S. Chattopadhyay and M. K. Das, "A novel technique for the effective concentration of ^{99m}Tc from a large alumina column loaded with low specific-activity (n,γ)-produced ^{99}Mo," *Applied Radiation and Isotopes*, vol. 66, no. 10, pp. 1295–1299, 2008.

[53] S. Chattopadhyay, M. K. Das, S. K. Sarkar, P. Saraswathy, and N. Ramamoorthy, "A novel ^{99m}Tc delivery system using (n,γ)^{99}Mo adsorbed on a large alumina column in tandem with Dowex-1 and AgCl columns," *Applied Radiation and Isotopes*, vol. 57, no. 1, pp. 7–16, 2002.

[54] T. H. Bokhari, A. Mushtaq, and I. U. Khan, "Lead (Pb) column for concentration of ^{99m}Tc-pertechnetate," *Radiochimica Acta*, vol. 95, no. 11, pp. 663–667, 2007.

[55] S. Seifert, G. Wagner, and A. Eckardt, "Highly concentrated [^{99m}Tc]pertechnetate solutions from (n,γ)^{99}Mo/ ^{99m}Tc generators for nuclear medical use," *Applied Radiation and Isotopes*, vol. 45, no. 5, pp. 577–579, 1994.

[56] R. Chakravarty, S. K. Sarkar, M. Venkatesh, and A. Dash, "An electrochemical procedure to concentrate ^{99m}Tc availed from a zirconium [^{99}Mo] molybdate gel generator," *Applied Radiation and Isotopes*, vol. 70, no. 2, pp. 375–379, 2012.

[57] V. S. Le, "Preparation of gel type chromatographic ^{99m}Tc generators using Titanium and Zirconium Molybdate columns containing (n,γ)Mo-99," in *Proceedings of the IAEA Research Coordination Meeting*, Bombay, India, March 1990.

[58] V. S. Le and M. K. Le, "Multifunctional sorbent materials and uses thereof," Australia patent application, AU2013903629, September 2013.

[59] V. S. Le, "Production of ^{99m}Tc isotope from chromatographic generator using zirconium-molybdate and titanium-molybdate targets as column packing materials," in *Proceedings of the IAEA Research Coordination Meeting*, Bandung, Indonesia, October 1987.

[60] V. S. Le, "The radioisotope and radiopharmaceutical production in Vietnam," in *Proceedings of the 2nd Asian Symposium on Research Reactors (ASRR '89)*, vol. 2, pp. 1–19, Jakarta, Indonesia, May 1989.

[61] V. S. Le, N. Morcos, J. McBrayer et al., "Development of the in-line, multiple elution cartridge -based radioisotope concentrator device for increasing ^{99m}Tc and ^{188}Re concentration of commercial radionuclide generator eluates and effectiveness of ^{99}Mo utilisation," in *Proceedings of the 5th Asia-Pacific Symposium on Radiochemistry (APSORC '13)*, Kanazawa, Japan, September 2013, abstract ID 23-RPP-01.

[62] V. S. Le, "Sorbent material," U.S. patent application publication, US, 2013/0048568 A1, February 2013, World Intellectual Property Organization, WO, 2011/106847 A1, September 2011, Australia patent application, AU2010900902, March 2010.

[63] V. S. Le, "Gallium-68 purification," U.S. patent application publication, US, 2013/0055855 A1, March 2013, World Intellectual Property Organization, WO, 2011/106846 A1, September 2011, Australia patent application, AU2010900900, March 2010.

[64] V. S. Le, "Gallium-68 generator integrated system: elution-purification-concentration integration," in *Theranostics, Gallium-68, and Other Radionuclides, Recent Results in Cancer Research 194*, R. P. Baum and F. Rösch, Eds., pp. 43–75, Springer, Berlin, Germany, 2013.

[65] V. S. Le, "Identifying optimal conditions for the production of next generation radiopharmaceutiucals," in *Research Selections*, pp. 71–73, ANSTO, 2011, http://apo.ansto.gov.au/dspace/handle/10238/3886.

[66] T. Genka, "Needs and current status of Mo-99/Tc-99m production in Japan," in *Proceedings of the Meeting on Mo-99 Production by (n,γ) Method*, Tokyo, Japan, March 2012.

[67] A. Mushtaq, "Producing radioisotopes in power reactor," *Journal of Radioanalytical and Nuclear Chemistry*, vol. 292, pp. 793–802, 2012.

[68] V. S. Le, "Utilisation of nuclear research reactor in Vietnam," in *Proceedings of the IAEA Advisory Group Meeting on Optimisation of Research Reactor Utilisation for Production of Radioisotopes*, JAERI, Tokai-Mura, Japan, October 1995.

[69] V. S. Le, "Development of alternative technologies for a gel-type chromatographic ^{99m}Tc generator," in *Proceedings of the IAEA Research Coordination Meeting*, Vienna, Austria, May 1994.

[70] IAEA-TECDOC-852, *Alternative Technologies for* ^{99m}*Tc Generators*, International Atomic Energy Agency, Vienna, Austria, 1995.

[71] K. Tsuchiya, "Atatus of ^{99}Mo-^{99m}Tc production development by (n,γ) reaction in Japan," in *Proceedings of the Specialist Meeting on Mo-99 Production by (n,γ) Method*, Tokyo, Japan, March 2012.

[72] E. Ishitsuka and K. Tatenuma, "Process for producingradioactive molybdenum," World Intellectual Property Organization, WO, 2008/047946, April 2008.

[73] B. J. Jun, M. Tanimotor, A. Kimura, N. Hori, H. Izumo, and K. Tsuchiya, "Feasibility study on mass production of (n,γ) ^{99}Mo," JAEA-Research Report 2010-046, Japan Atomic Energy Agency, 2011.

[74] Y. Inaba, K. Iimura, J. Hosokawa, H. Izumo, N. Hori, and E. Ishitsuka, "Status of development on ^{99}Mo production technologies in JMTR," *IEEE Transactions on Nuclear Science*, vol. 58, no. 3, pp. 1151–1158, 2011.

[75] C. Ross, R. Galea, P. Small et al., "Using the ^{100}Mo photonuclear reaction to meet Canada's requirement for ^{99m}Tc," *Physics in Canada*, vol. 66, pp. 19–24, 2010.

[76] M. C. Lagunas-Solar, P. M. Kiefer, O. F. Carvacho, C. A. Lagunas, and Y. P. Cha, "Cyclotron production of NCA ^{99m}Tc and ^{99}Mo. An alternative non-reactor supply source of instant ^{99m}Tc and ^{99}Mo $\rightarrow$ ^{99m}Tc generators," *Applied Radiation and Isotopes*, vol. 42, no. 7, pp. 643–657, 1991.

[77] M. C. Lagunas-Solar, "Accelerator production of ^{99m}Tc with proton beams and enriched ^{100}Mo targets," in *IAEA-TECDOC-1065, Production Technologies for Molybdenum-99 and Technetium-99m*, International Atomic Energy Agency, Vienna, Austria, 1999.

[78] B. Scholten, R. M. Lambrecht, M. Cogneau, H. V. Ruiz, and S. M. Qaim, "Excitation functions for the cyclotron production of ^{99m}Tc and ^{99}Mo," *Applied Radiation and Isotopes*, vol. 51, no. 1, pp. 69–80, 1999.

[79] S. Takács, Z. Szücs, F. Tárkányi, A. Hermanne, and M. Sonckz, "Evaluation of proton induced reactions on ^{100}Mo: new cross sections for production of ^{99m}Tc and ^{99}Mo," *Journal of Radioanalytical and Nuclear Chemistry*, vol. 257, no. 1, pp. 195–201, 2003.

[80] Y. Nagai and Y. Hatsukawa, "Production of ^{99}Mo for nuclear medicine by ^{100}Mo(n, 2n)^{99}Mo," *Journal of the Physical Society of Japan*, vol. 78, no. 3, Article ID 033201, 2009.

[81] J. E. Beaver and H. B. Hupf, "Production of ^{99m}Tc on a medical cyclotron: a feasibility study," *Journal of Nuclear Medicine*, vol. 12, no. 11, pp. 739–741, 1971.

[82] M. B. Challan, M. N. H. Comsan, and M. A. Abou-Zeid, "Thin target yields and Empire: II. predictions on the accelerator production of technetium-99m," *Journal of Nuclear and Radiation Physics*, vol. 2, no. 1, pp. 1–12, 2007.

[83] K. Gagnon, F. Bénard, M. Kovacs et al., "Cyclotron production of ^{99m}Tc: experimental measurement of the ^{100}Mo(p,x)^{99}Mo, ^{99m}Tc and ^{99g}Tc excitation functions from 8 to 18 MeV," *Nuclear Medicine and Biology*, vol. 38, no. 6, pp. 907–916, 2011.

[84] H. T. Wolterbeek and P. Bode, "A process for the production of no-carrier added ^{99}Mo," European Patents EP, 2131369 (A1), December 2009, Worldwide Patent 2009148306, December 2009, EP, 2301041 (A1), March 2011, U.S. patent US, 2011118491 (A1), May 2011.

[85] B. S. Tomar, O. M. Steinebach, B. E. Terpstra, P. Bode, and H. T. Wolterbeek, "Studies on production of high specific activity ^{99}Mo and ^{90}Y by Szilard Chalmers reaction," *Radiochimica Acta*, vol. 98, no. 8, pp. 499–506, 2010.

[86] T. J. Ruth, "Two routes to solving the Mo/Tc isotope crisis: direct production of ^{99m}Tc and isotope separation," in *Proceedings of the CNS Workshop on the Production of Medical Radionuclides*, Ottawa, Canada, 2009.

[87] E. P. Belkas and D. C. Perricos, "Technetium-99m production based on the extraction with methyl-ethyl ketone," *Radiochimica Acta*, vol. 11, p. 56, 1969.

[88] G. D. Robinson, "A simple manual system for the efficient, routine production of ^{99m}Tc by methyl-ethyl-ketone extraction," *Journal of Nuclear Medicine*, vol. 12, p. 459, 1971.

[89] M. P. Zykov, V. N. Romanovskii, D. W. Wester et al., "Use of extraction generator for preparing a ^{99m}Tc radiopharmaceutical," *Radiochemistry*, vol. 43, no. 3, pp. 297–300, 2001.

[90] T. le Minh and T. Lengyel, "On the separation of molybdenum and technetium crown ether as extraction agent," *Journal of Radioanalytical and Nuclear Chemistry Letters*, vol. 135, no. 6, pp. 403–407, 1989.

[91] M. Maiti and S. Lahiri, "Separation of ^{99}Mo and ^{99m}Tc by liquid-liquid extraction using trioctylamine as extractant," *Journal of Radioanalytical and Nuclear Chemistry*, vol. 283, no. 3, pp. 661–663, 2010.

[92] R. E. Boyd, "Technetium-99m generators—the available options," *International Journal of Applied Radiation and Isotopes*, vol. 33, no. 10, pp. 801–809, 1982.

[93] K. Svoboda, "Survey of solvent extraction ^{99m}Tc-generator technologies," *Radiochimica Acta*, vol. 41, pp. 83–89, 1987.

[94] "Radionuclide generator technology," *Radiochimica Acta*, vol. 41, no. 2-3, 1987.

[95] A. A. Kuznetsov, A. A. Kudrin, and G. E. Kodina, "Semi-automatic ^{99m}Tc solvent extraction system," in *Proceedings of the 7th International Symposium on Technetium and Rhenium-Science and Utilization*, Moscow, Russia, July 2011, abstract book 4.P13.

[96] E. Taskaev, M. Taskaeva, and P. Nikolov, "Extraction generator for [^{99m}Tc]sodium pertechnetate production," *Applied Radiation and Isotopes*, vol. 46, no. 1, pp. 13–16, 1995.

[97] O. P. D. Noronha, "Solvent extraction technology of ^{99}Mo-^{99m}Tc generator system," in *Proceedings of the Conference on Radiopharmaceuticals and Labelled Compounds*, Tokyo, Japan, 1984.

[98] Y. N. Reshetnik, A. N. Bykov, G. E. Kodina, and A. O. Malysheva, "Sorption removal of Na ^{99m}TcO$_4$ from extracts of extraction generator ^{99}Mo/^{99m}Tc," in *Proceedings of the 7th International Symposium on Technetium and Rhenium-Science and Utilization*, Moscow, Russia, July 2011, abstract book 4.P12.

[99] S. Chattopadhyay, S. S. Das, and L. Barua, "A simple and rapid technique for recovery of ^{99m}Tc from low specific activity (n,γ)^{99}Mo based on solvent extraction and column chromatography," *Applied Radiation and Isotopes*, vol. 68, no. 1, pp. 1–4, 2010.

[100] S. Chattopadhyay, L. Barua, A. De et al., "A computerized compact module for separation of ^{99m}Tc-radionuclide from molybdenum," *Applied Radiation and Isotopes*, vol. 70, no. 11, pp. 2631–2637, 2012.

[101] M. Tanase, A. Kimura, Y. Morikawa et al., "R&D in on extraction and concentration of ^{99m}Tc: a preliminary study using Re instead of ^{99m}Tc," in *Proceedings of the Specialist Meeting on Mo-99 Production by (n,γ) Method*, Tokyo, Japan, March 2012.

[102] S. Tachimori, H. Amano, and H. Nakamura, "Preparation of Tc-99m by direct adsorption from organic solution," *Journal of Nuclear Science and Technology*, vol. 8, pp. 357–362, 1971.

[103] V. S. Le, "^{99m}Tc generator preparation using (n,γ)^{99}Mo produced ex-natural molybdenum," in *Proceedings of the FNCA Workshop on the Utilization of Research Reactors*, pp. 216–223, Japan Atomic Energy Research Institute, 2003, JAERI-Conf 2003-004.

[104] V. S. Le and R. M. Lambrecht, "Development of alternative technologies for a gel-type chromatographic ^{99m}Tc generator," *Journal of Labelled Compounds and Radiopharmaceuticals*, vol. 35, pp. 270–272, 1994.

[105] V. S. Le, "Recent progress in radioisotope production in Vietnam," in *Proceedings of the Workshop on the Utilization of Research Reactors*, pp. 308–314, Japan Atomic Energy Research Institute, 1998, JAERI-conf 98-015.

[106] V. S. Le, "Preparation of chromatographic and solid-solvent extraction ^{99m}Tc generator using gel-type targets," in *Proceedings of the Workshop on the Utilization of Research Reactors*, pp. 187–192, Japan Atomic Energy Research Institute, 2000, JAERI-conf 2000-017.

[107] T. Genka, "Development of PZC-based Tc-99m Generator," Forum for Nuclear Cooperation in Asia (FNCA), no. 2, March 2007.

[108] V. S. Le, "Procedures for the production of poly-zirconium-compound (PZC) based chromatographic ^{99m}Tc generator to be available for clinical application," in *Proceedings of the FNCA Workshop on the Utilization of Research Reactors*, pp. 229–256, Japan Atomic Energy Agency, 2006, JAEA-Conf 2006-001.

[109] V. S. Le, C. D. Nguyen, P. Pellegrini, and V. C. Bui, "Polymeric titanium oxychloride sorbent for ^{188}W/^{188}Re nuclide pair separation," *Separation Science and Technology*, vol. 44, no. 5, pp. 1074–1098, 2009.

[110] V. S. Le, "Medical radioisotope development, radionuclide development group, project no. RRI-0168," Report at ANSTO's Board Review Panel, ANSTO, 2009.

[111] V. S. Le, "^{68}Ga PET-radionuclide generator development," in *Proceedings of the Seminar on Radiopharmaceutical Development*, Radiopharmaceutical Research Institute, ANSTO, June 2009.

[112] R. E. Boyd, "^{99}Mo/^{99m}Tc generator," *Radiochimica Acta*, vol. 30, no. 3, pp. 123–146, 1982.

[113] R. E. Boyd, "Technetium generators—status and prospects," *Radiochimica Acta*, vol. 41, no. 2-3, pp. 59–63, 1987.

[114] J. Gerse, J. Kern, J. Imre, and L. Zsinka, "Examination of a portable ^{99}Mo/^{99m}Tc isotope generator /SUBLITECH(R)/," *Journal of Radioanalytical and Nuclear Chemistry*, vol. 128, no. 1, pp. 71–80, 1988.

[115] L. Zsinka, "^{99m}Tc sublimation generators," *Radiochimica Acta*, vol. 41, pp. 91–96, 1987.

[116] F. Rösch, A. F. Novgorodov, and S. M. Qaim, "Thermochromatographic separation of ^{94m}Tc from enriched molybdenum targets and its large scale production for nuclear medical application," *Radiochimica Acta*, vol. 64, pp. 113–120, 1994.

[117] R. Chakravarty, M. Venkatesh, and A. Dash, "A novel electrochemical ^{99}Mo/^{99m}Tc generator," *Journal of Radioanalytical and Nuclear Chemistry*, vol. 290, no. 1, pp. 45–51, 2011.

[118] R. Chakravarty, A. Dash, and M. Venkatesh, "A novel electrochemical technique for the production of clinical grade ^{99m}Tc using (n,γ)^{99}Mo," *Nuclear Medicine and Biology*, vol. 37, no. 1, pp. 21–28, 2010.

[119] K. Tagami and S. Uchida, "Elution behavior of Tc and Re through a Tc-selective chromatographic resin column," *Journal of Radioanalytical and Nuclear Chemistry*, vol. 239, p. 643, 1999.

[120] X. Hou, M. Jensen, and S. Nielsen, "Use of ^{99m}Tc from a commercial ^{99}Mo/^{99m}Tc generator as yield tracer for the determination of ^{99}Tc at low levels," *Applied Radiation and Isotopes*, vol. 65, no. 5, pp. 610–618, 2007.

[121] M. Fikrle, J. Kučera, and F. Šebesta, "Preparation of ^{95m}Tc radiotracer," *Journal of Radioanalytical and Nuclear Chemistry*, vol. 286, no. 3, pp. 661–663, 2010.

[122] A. Bartosova, P. Rajec, and M. Reich, "Preparation and characterization of an extraction chromatography column for technetium separation based on Aliquat-336 and silica gel support," *Journal of Radioanalytical and Nuclear Chemistry*, vol. 261, no. 1, pp. 119–124, 2004.

[123] E. Akatsu, R. Ono, K. Tsukuechi, and H. Uchiyama, "Radiochemical study of adsorption behavior of inorganic ions on zirconium-phosphate, silica gel and charcoal," *Journal of Nuclear Science and Technology*, vol. 2, pp. 141–148, 1965.

[124] R. Rogers, P. E. Horwitz, and A. H. Bond, "Process for recovering pertechnetate ions from an aqueous solution also containing other ions," U.S. patent no. 5603834, February 1997.

[125] S. Chattopadhyay, S. S. Das, M. K. Das, and N. C. Goomer, "Recovery of ^{99m}Tc from Na_2[^{99}Mo]MoO_4 solution obtained from reactor-produced (n,γ) ^{99}Mo using a tiny Dowex-1 column in tandem with a small alumina column," *Applied Radiation and Isotopes*, vol. 66, no. 12, pp. 1814–1817, 2008.

[126] R. D. Rogers, A. H. Bond, J. Zhang, and E. Philip Horwitz, "New technetium-99m generator technologies utilizing polyethylene glycol-based aqueous biphasic systems," *Separation Science and Technology*, vol. 32, no. 1–4, pp. 867–882, 1997.

[127] S. K. Spear, S. T. Griffin, J. G. Huddleston, and R. D. Rogers, "Radiopharmaceutical and hydrometallurgical separations of perrhenate using aqueous biphasic systems and the analogous aqueous biphasic extraction chromatographic resins," *Industrial and Engineering Chemistry Research*, vol. 39, no. 9, pp. 3173–3180, 2000.

[128] J. E. Young and J. J. Hines, "Compact automated radionuclide separator," U.S. patent no. 6770195, August 2004.

[129] H. Bond, J. J. Hines, J. E. Young, and E. P. Horwitz, "Automated radionuclide separation system and method," U.S. patent no. 67870427, September 2004.

[130] E. P. Horwitz and A. H. Bond, "Multicolumn selectivity inversion generator for production of ultrapure radionuclides," U.S. patent no. 6998052, February 2006.

[131] D. R. McAlister and E. P. Horwitz, "Automated two column generator systems for medical radionuclides," *Applied Radiation and Isotopes*, vol. 67, no. 11, pp. 1985–1991, 2009.

[132] V. S. Le, "Development of alternative technologies for a gel-type chromatographic ^{99m}Tc generator," IAEA-TECDOC 852, December 1995.

[133] J. J. Pinajian, "A technetium-99m generator using hydrous zirconium oxide," *The International Journal of Applied Radiation and Isotopes*, vol. 17, no. 11-12, pp. 664–670, 1966.

[134] Q. M. Qazi and A. Mushtaq, "Preparation and evaluation of hydrous titanium oxide as a high affinity adsorbent for molybdenum (^{99}Mo) and its potential for use in ^{99m}Tc generators," *Radiochimica Acta*, vol. 99, no. 4, pp. 231–235, 2011.

[135] S. Meloni and A. Brandone, "A new technetium-99m generator using manganese dioxide," *The International Journal of Applied Radiation and Isotopes*, vol. 19, no. 2, pp. 164–166, 1968.

[136] J. Serrano Gómez and F. Granados Correa, "^{99m}Tc generator with hydrated MnO$_2$ as adsorbent of ^{99}Mo," *Journal of Radio-analytical and Nuclear Chemistry*, vol. 254, no. 3, pp. 625–628, 2002.

[137] Y. Maki and Y. Murakami, "^{99m}Tc generator by use of silica gel as adsorbent," *Nipon Kagaku Zasshi*, vol. 92, pp. 1211–1212, 1971.

[138] J. Serrano, H. González, H. López, N. Aranda, F. Granados, and S. Bulbulian, "Sorption of ^{99}MoO$_4{}^{2-}$ ions on commercial hydrotalcites," *Radiochimica Acta*, vol. 93, no. 9-10, pp. 605–609, 2005.

[139] V. S. Le, *Investigation on inorganic ion exchangers supported on silica matrix [Ph.D. thesis]*, Isotope Institute, Hungarian Academy of Sciences, 1985.

[140] F. Monroy-Guzman, V. E. Badillo Almaraz, J. A. Flores de la Torre, J. Cosgrove, and F. F. Knapp Jr., "Hydroxyapatite-based ^{99}Mo/^{99m}Tc and ^{188}W/^{188}Re generator systems," in *Trends in Radiopharmaceutical (ISTR-2005)*, vol. 1, IAEA, Vienna, Austria, 2007.

[141] T. Braun, H. Imura, and N. Suzuki, "Separation of ^{99m}Tc from parent ^{99}Mo by solid-phase column extraction as a simple option for a new ^{99m}Tc generator concept," *Journal of Radioanalytical and Nuclear Chemistry Letters*, vol. 119, no. 4, pp. 315–325, 1987.

[142] V. S. Le, "Study on the titanium- and zirconium-molybdate gel-type ^{99m}Tc generators," Annual Report, Vietnam Atomic Energy Committee, 1984.

[143] J. V. Evans, P. W. Moore, M. E. Shying, and J. M. Sodeau, "Zirconium molybdate gel as a generator for technetium-99m—I. The concept and its evaluation," *International Journal of Radiation Applications and Instrumentation A*, vol. 38, no. 1, pp. 19–23, 1987.

[144] P. W. Moore, M. E. Shying, J. M. Sodeau, J. V. Evans, D. J. Maddalena, and K. H. Farrington, "Zirconium molybdate gel as a generator for technetium-99m—II. High activity generators," *International Journal of Radiation Applications and Instrumentation A*, vol. 38, no. 1, pp. 25–29, 1987.

[145] R. E. Boyd, "The gel generator: a viable alternative source of ^{99m}Tc for nuclear medicine," *Applied Radiation and Isotopes*, vol. 48, no. 8, pp. 1027–1033, 1997.

[146] V. S. Le, "Development of alternative technologies for a gel-type chromatographic ^{99m}Tc generator," in *Proceedings of the IAEA Research Coordination Meeting*, Budapest, Hungary, February 1993.

[147] J. A. Osso Junior, A. L. V. P. Lima, N. C. da Silva, R. C. Nieto, and A. C. de Velosa, "Preparation of a gel of zirconium molybdate for use in the generators of ^{99}Mo—^{99m}Tc prepared with ^{99}Mo produced by the ^{98}Mo(n,γ)^{99}Mo reaction," in *Proceedings of the International Meeting on Reduced Enrichment for Research and Test Reactors*, San Paulo, Brazil, October 1998.

[148] V. S. Le, "Investigation on the performance of polymer zirconium compound (PZC) for chromatographic ^{99m}Tc generator preparation," in *Proceedings of the FNCA Workshop on the Utilization of Research Reactors*, pp. 90–104, Japan Atomic Energy Research Institute, 2004, JAERI-Conf 2004-010.

[149] Y. Hasegawa, M. Nishino, T. Takeuch et al., "Mo adsorbent for ^{99}Mo-^{99m}Tc generators and manufacturing thereof," US patent no. 5681974, October 1997.

[150] M. Tanase, K. Tatenuma, K. Ishikawa, K. Kurosawa, M. Nishino, and Y. Hasegawa, "A ^{99m}Tc generator using a new inorganic polymer adsorbent for (n,γ) ^{99}Mo," *Applied Radiation and Isotopes*, vol. 48, no. 5, pp. 607–611, 1997.

[151] V. S. Le, "Preparation of PZC based ^{99m}Tc generator to be available for clinical application," in *Proceedings of the IAEA Research Coordination Meeting on Development of Generator Technologies for Therapeutic Radionuclides*, ANSTO, Vienna, Austria, October 2004, http://apo.ansto.gov.au/dspace/handle/10238/3713.

[152] V. S. Le, "Chemical synthesis and application of zirconium and titanium polymer compounds for the preparation of Tc-99m and Re-188 chromatographic generators," in *Proceedings of the 2nd Research Coordination Meeting on Development of Generator Technologies for Therapeutic Radionuclides*, ANSTO, Milan, Italy, April 2006, http://apo.ansto.gov.au/dspace/handle/10238/3714.

[153] V. S. Le, C. D. Nguyen, V. C. Bui, and C. H. Vo, "Synthesis, characterization and application of PTC and PZC sorbents for preparation of chromatographic ^{99m}Tc and ^{188}Re generators," in *Proceedings of the IAEA Research Coordination Meeting on Development of Generator Technologies for Therapeutic Radionuclides*, ANSTO, Daejeon, Republic of Korea, October 2007, http://apo.ansto.gov.au/dspace/handle/10238/3715.

[154] V. S. Le, C. D. Nguyen, V. C. Bui, and C. H. Vo, "Preparation of inorganic polymer sorbents and their application in radionuclide generator technology," in *Therapeutic Radionuclide Generators: ^{90}Sr/^{90}Y and ^{188}W/^{188}Re Generators*, IAEA Technical Report Series no. 470, chapter 20, International Atomic Energy Agency, Vienna, Austria, 2009.

[155] M. Asif and A. Mushtaq, "Evaluation of highly loaded low specific activity ^{99}Mo on alumina column as ^{99m}Tc generator," *Journal of Radioanalytical and Nuclear Chemistry*, vol. 284, no. 2, pp. 439–442, 2010.

[156] J. S. Lee, H. S. Han, U. J. Park et al., "Adsorbents for radioisotopes, preparation method thereof, and radioisotope generators using the same," U.S. patent application publication, US, 2009/0277828 A1, November 2009.

[157] A. Mushtaq, "Inorganic ion-exchangers: their role in chromatographic radionuclide generators for the decade 1993–2002," *Journal of Radioanalytical and Nuclear Chemistry*, vol. 262, no. 3, pp. 797–810, 2004.

[158] V. S. Le, M. Izard, P. Pellegrini, and M. Zaw, "Development of ^{68}Ga generator at ANSTO," in *Proceedings of the 1st World Congress on Ga-68 and Peptide Receptor Radionuclide Therapy (THERANOSTICS '11)*, ANSTO, Bad Berka, Germany, June 2011, World Journal of Nuclear Medicine, vol. 10, no. 1, pp. 73–89, P-023, http://apo.ansto.gov.au/dspace/handle/10238/3701.

[159] R. Chakravarty, R. Shukla, S. Gandhi et al., "Polymer embedded nanocrystalline titania sorbent for ^{99}Mo-^{99m}Tc generator," *Journal of Nanoscience and Nanotechnology*, vol. 8, no. 9, pp. 4447–4452, 2008.

[160] R. Chakravarty, R. R. Shukla, R. Ram, A. K. Tyagi, A. Das, and M. Venkatesh, "Nanocrystalline zircona: a new sorbent for the preparation of ^{99}Mo-^{99m}Tc generators," *Journal of Labelled Compounds and Radiopharmaceuticals*, vol. 52, supplement 1, p. S500, 2009.

[161] R. Chakravarty, *Development of radionuclide generator for biomedical applications [Ph.D. thesis]*, Homi Bhabha National Institute, 2011.

[162] J. V. Evans and R. W. Matthews, "Technetium-99m generators," U.S. patent no. 4280053, July 1981.

[163] V. H. Tran and V. S. Le, "Activation analysis of trace elements in titanium-molybdate gel target used for pre-formed TiMo-gel-based ^{99m}Tc generator production and radionuclidic impurity of ^{99m}Tc pertechnetate eluate," in *Proceedings of the FNCA Workshop on the Utilization of Research Reactors*, pp. 105–111,

Japan Atomic Energy Research Institute, June 2004, JAERI-Conf 2004-010.

[164] R. Chakravarty, R. Ram, R. Mishra et al., "Mesoporous Alumina (MA) based double column approach for development of a clinical scale ^{99}Mo/^{99m}Tc generator using $(n,\gamma)^{99}$Mo: an enticing application of nanomaterial," *Industrial & Engineering Chemistry Research*, vol. 52, no. 33, pp. 11673–11684, 2013.

[165] A. Dash, F. F. (Russ) Knapp Jr., and M. R. A. Pillaia, "^{99}Mo/^{99m}Tc separation: an assessment of technology options," *Nuclear Medicine and Biology*, vol. 40, no. 2, pp. 167–176, 2013.

[166] V. S. Le and N. Morcos, "New SPE column packing material: retention assessment method and its application for the radionuclide chromatographic separation," *Journal of Radioanalytical and Nuclear Chemistry*, vol. 277, no. 3, pp. 651–661, 2008.

[167] I. Zolle, Ed., *Technetium-99m Radiopharmaceuticals: Preparation and Quality Control in Nuclear Medicine*, Springer, Berlin, Germany, 2007.

Review Article

Immobilisation of Higher Activity Wastes from Nuclear Reactor Production of ^{99}Mo

Martin W. A. Stewart, Eric R. Vance, Sam A. Moricca, Daniel R. Brew, Catherine Cheung, Tina Eddowes, and Walter Bermudez

Australian Nuclear Science and Technology Organisation (ANSTO), New Illawarra Road, Lucas Heights, NSW 2234, Australia

Correspondence should be addressed to Martin W. A. Stewart; mws@ansto.gov.au

A variety of intermediate- and low-level liquid and solid wastes are produced from reactor production of ^{99}Mo using UAl alloy or UO_2 targets and in principle can be collectively or individually converted into waste forms. At ANSTO, we have legacy acidic uranyl-nitrate-rich intermediate level waste (ILW) from the latter, and an alkaline liquid ILW, a U-rich filter cake, plus a shorter lived liquid stream that rapidly decays to low-level waste (LLW) standards, from the former. The options considered consist of cementitious products, glasses, glass-ceramics, or ceramics produced by vitrification or hot isostatic pressing for intermediate-level wastes. This paper discusses the progress in waste form development and processing to treat ANSTO's ILW streams arising from ^{99}Mo. The various waste forms and the reason for the process option chosen will be reviewed. We also address the concerns over adapting our chosen process for use in a hot-cell environment.

1. Introduction

^{99}Mo is produced in several countries; notably Belgium, Netherlands, Canada, and South Africa produce > 2,500 6dCi. (This refers to the number of curies of ^{99}Mo left 6 days after shipping from a production facility and is typically used during operation in allocating and pricing the shipment.) There are also smaller producers (300–1500 6dCi) in France, Russia, Czech Republic, Poland, Australia, and Argentina [1]. Wastes arising from ^{99}Mo production using nuclear reactor irradiation of enriched U-bearing targets range from ILW to LLW in both liquid and solid forms, according to current International Atomic Energy (IAEA) Classifications [2]. In ^{99}Mo production, the higher activity wastes would typically be classified as ILW, even after decaying for a few years. Traditionally [3], the boundary between ILW and high-level waste (HLW) was set at a heat output from the decay of radioisotopes of $2\,kW/m^3$ and the boundary between ILW and LLW was that at which shielding was required (contact dose of 2 mSv/hr).

Both HLW and ILW require shielding; however, ILW due to its lower heat output does not require controlled cooling during storage. In the updated version of the IAEA Classification System [2], the heat output has been omitted. This is because the new standard for classification and treatment is more closely related to the disposition options and the heat output limits for a waste package should now be linked to the safety cases for the storage/disposal facility.

Other methods of classification exist; for example, the British in determining the amount of waste to be returned to customers from its THORP reprocessing facility use the integrated toxic potential [5] methodology. This method is used as part of the UK waste allocation and substitution policy [6]. The USA operates under a different system to the IAEA. It developed prescriptive specifications for the operation of the Waste Isolation Pilot Plant (WIPP) [7] and the now halted Yucca Mountain geological repository [8] for high-level waste.

Typical waste compositions from ^{99}Mo production can be found in [9]. For irradiated U-Al alloy targets dissolution

is achieved via an alkaline-route; typically, this produces a 3.4–4 M NaOH plus 1–1.5 M $NaAlO_2$ plus fission products intermediate-level liquid waste (ILLW), with an activity of $\sim 10^{10}$-10^{11} Bq/L after ~3 years decay time from processing (Figure 1 and Table 1). The ILLW is subsequently adjusted to 5-6 M NaOH for tank storage to prevent the precipitation of gibbsite $(Al(OH)_3)$. From a long-term waste form storage and disposition viewpoint, ^{137}Cs and ^{90}Sr dominate the activity, although in alkaline waste streams the bulk of the Sr (~90–95%) remains with the U-rich filter cake. Separation of Cs and Sr was considered by ANSTO, but was rejected on the grounds that it would lead to two ILW waste streams that would need to be treated as the ILLW activity would remain above LLW limits beyond the design life of the holding tanks. Furthermore, ANSTO is building one plant to treat both alkaline and acidic wastes and a separations approach would require the construction of a second ion exchange route to remove the Cs and Sr from that. The result would be four waste streams to treat, four waste forms to qualify, and expensive additional hot-cell plant with its associated secondary waste streams.

Also produced are secondary wastes; the most predominant of these are a short-lived high activity liquid waste that decays below the intermediate-level waste limit of 10^8 Bq/L after ~4-5 years (Figure 1), plus a Na-U-O residue that also contains fission products, notably Sr. The options suggested for this residue include recycling to extract the enriched U, followed by reuse in new targets for ^{99}Mo production or disposition, with appropriate safeguards to allow for the fissile content. The latter may include dilution with depleted U or treatment to form a criticality safe and proliferation-resistant waste form.

UO_2 targets were used by ANSTO until 2005 and were dissolved in nitric acid, resulting in an intermediate level liquid waste (ILLW) that consists mainly of uranyl nitrate solution plus fission products in 0.5–1 M nitric acid (Table 2). Typically this consists of primary waste at 120–200 gU/L and secondary waste (wash), ~20 gU/L. The treatment of the intermediate-level wastes and the uranium filter cake wastes will be the focus of this paper.

In addition to these streams, additional wastes such as ion exchange columns (resin and/or alumina based), noble gases and iodine in the off-gas, and general low-level waste associated with processing are produced [9]. In the future there is the possibility of silicide targets being introduced to increase the target density [10], particularly with the push to move ^{99}Mo production from using highly enriched uranium (HEU) to <20% ^{235}U low enriched uranium (LEU) [11].

While the ILLW wastes will be considered separately in the first instance, we will also consider whether a single technology platform could be used for the individual wastes or waste mixtures. Candidate solids for immobilisation of the intermediate ILW or LLW within scope can be described as ceramics, glasses, glass-ceramics, or cementitious materials. While asphalt-based materials have been used by Belgium to immobilise LLW (not arising from ^{99}Mo production), the flammability of such material is highly undesirable from a risk aspect.

2. The Development of Waste Forms and Processes to Treat Radioactive Wastes

As early as 1953, researchers were showing concern about the need to immobilise radioactive wastes arising from the recently constructed nuclear reactors [12]. The waste of most concern is used UO_2 fuel in which most of the original fissile U was still present but in which the fission products caused so much neutron absorption that the fuel was no longer efficient. However, large amounts of waste that were a lot more dilute from a radioactive aspect were also generated. The initial concept to immobilise waste radionuclides was to add them to appropriate precursors for incorporation in leach-resistant clay minerals, followed by consolidation and burial in deep holes, an approach initially favoured at Chalk River, Canada, later that decade. Good leach resistance was needed to prevent the transport of radionuclides to the biosphere by groundwater. However, from the 1960s the favoured method for immobilisation of high-level nuclear waste (waste arising from used nuclear power plant fuel or primary fuel reprocessing waste) was incorporation in borosilicate glasses that could be melted and poured at temperatures of 1000–1200°C. The waste was calcined at ~600°C to remove nitric acid, water, and organics and then combined with glass frit and vitrified. Table 3 shows the typical chemical composition of HLW reprocessing waste.

The advantage of borosilicate glass was the fact that most fission products and process chemical wastes after calcination could be incorporated in the glass structure and the glass was reasonably resistant to leaching by groundwaters characteristic of deep (~1 km) geological repositories, with such repositories being generally agreed by the 1970s as the best way to deal with vitrified high-level waste. As an aside, it has been generally agreed for many years that spent fuel itself only needs encapsulation in metal containers for disposal in deep geological repositories. In the mid-1970s, university researchers devised the idea of atomically incorporating waste radionuclides in the crystalline lattices of certain minerals that were known to be very resistant to water leaching, as such minerals that incorporated small amounts of natural radioactivity in their structures could be shown to have survived in hot, wet environments for millions of years [13]. These minerals could then be produced by ceramic technologies and became alternative (to borosilicate glass) candidates for HLW immobilisation.

The optimisation of waste form design is achieved by optimising the waste form chemistry to achieve high waste loadings and applying appropriate noncomplex process technologies to derive an integrated solution to achieve maximum cost savings, whilst still retaining waste form performance. The following several key requirements were identified for a suitable waste form for Pu [14] but could equally apply to U-doped wastes, particularly HEU.

(1) High Waste Loading. The waste loading must be sufficiently high to make the waste form economic to process. It is the volume of waste form and packaging produced that determines the efficiency of the process. For instance, ceramics such as Synroc can have almost double the density

TABLE 1: Typical ILLW from alkaline-route ^{99}Mo production at ANSTO > 10 years after production.

Chemical composition		Main nuclides present	Half-life	Typical activity in ILLW waste (Bq/L)
NaOH	4–6 M	^{137}Cs	30.07 y	$1E + 10$
NaAlO$_2$	1–1.5 M	^{137m}Ba	2.552 m	$1E + 10$
Corrosion products		^{90}Sr	28.78 y	$5E + 08$
Fe, Cr, Ni	Traces	^{90}Y	64.1 h	$5E + 08$
		^{147}Pm	2.6 y	$1E + 08$
		^{125}Sb	2.77 y	$1E + 07$
		^{134}Cs	2.07 y	$9E + 6$
		^{155}Eu	4.96 y	$1E + 07$
		^{106}Rh	29.92 s	$3.5E + 06$
		^{106}Ru	1.02 y	$3.5E + 06$
		^{125m}Te	58 d	$3E + 06$
		^{99}Tc	213000 y	$3E + 04$

TABLE 2: Analysed ILLW compositions from tanks at ANSTO that were produced from irradiated LEU UO$_2$ target produced at ANSTO.

Chemical composition		Nuclide	Half-life	Analysed activity of primary ILLW waste (MBq/L)	Analysed activity of secondary ILLW waste (MBq/L)
U (primary waste)	70–200 g/L	^{144}Ce	284 d	10–3500	16–6000
U (secondary waste)	8–35 g/L	^{134}Cs	2.07 y	0.35–5.3	<DL–2.4
Mg	<0.02–0.6 g/L	^{137}Cs	30.07 y	2600–8000	170–1800
Fe	< 0.05–0.4 g/L	^{60}Co	5.27 y	0.6–2	0.1–1
NH$_4^+$	75–800 mg/L	^{155}Eu	4.76 y	<DL–90	<DL–20
HNO$_3$	0.6–0.8 M	^{95}Nb	35.06 d	1–80	4–1100
Al	<DL–0.6 g/L	^{106}Ru/^{106}Rh	1.02 y/29.6 s	<DL–970	<DL–420
		^{125}Sb	2.77 y	<DL–13	<DL–18
		^{95}Zr	64 d	0.6–50	1–610
		^{90}Sr	28.78 y	2600–7700	120–1700
		^{141}Ce	32.5 d	<DL–1.3	<DL–30
		^{91}Y	58.51 d	<DL–125	<DL–380
		^{103}Ru	39.35 d	<DL–1.5	<DL–32
		^{144}Pr	17.2 m	nd	<DL–6

Note: the data in this table are for from ~1 to 16 years after the tanks were filled. Lower activity values are generally from older waste. nd: not detected; DL: detection limit.

TABLE 3: Approximate composition (wt%) and half-lives[&] of main fission product and actinide oxides in PUREX fuel reprocessing HLW that has been stored for >10 years.

Fission product oxide Basis (wt%)[$]	Half-life of most abundant radioisotope (y)	Fission product oxide Basis (wt%)[$]	Half-life of most abundant radioisotope (y)
Cs$_2$O (6)	30	TcO$_2$ (6)	210000
SrO (3)	30	*AnO$_2$ (6)	>10000
BaO (4)	—	RuO$_2$ (10)	—
RE$_2$O$_3$ (15)	100[&]	PdO (6)	—
ZrO$_2$ (15)	—	Rh$_2$O$_3$ (2)	—
MoO$_3$ (15)	—		

Water excluded; *An: actinide. [$]Contains additional stainless steel corrosion products, RE: rare earth.
Group half-lives[&] are very approximate as they range from short to long times for different components. Absence of half-life value: stable elements.
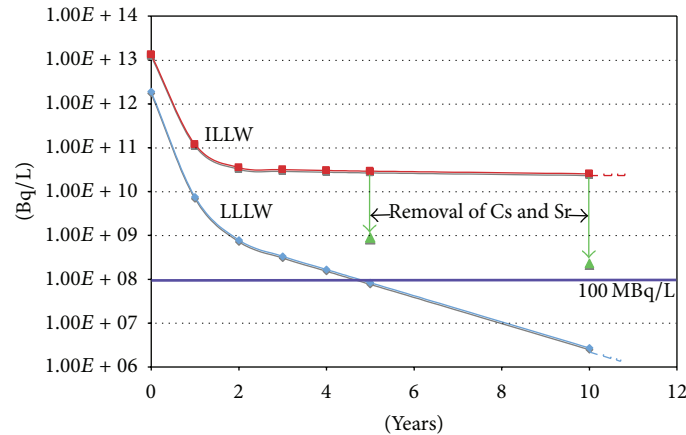
Figure 1: Typical calculated activity in Bq/L of the two liquid wastes from ^{99}Mo as a function of postproduction time. The intersections of the triangles represent the activity of ILLW if all Cs/Sr is removed after 5 and 10 years of storage, showing the ^{137}Cs and ^{90}Sr dominate the ILLW activity.

of borosilicate glass and hence an equal waste loading will produce less waste volume in the ceramic compared to the glass. Waste volume reduction significantly reduces life-cycle costs, particularly storage, transport, and repository costs; for instance, the disposition of one glass canister at Yucca mountain was estimated to cost $US 620,000 [15]. For instance, ANSTO demonstrated the production of a 40 kg hot-isostatically pressed waste form that had an 80 wt% waste loading of Idaho HLW calcines, far in excess of that achievable via glass melters [16]. The volume reductions achievable via this approach were independently estimated to have potential disposition cost savings over alternative routes for the calcines of $2–4.8 billion [15]. There are some limitations to waste loadings beyond just how much waste a waste form can incorporate and still remain durable. These include limits due to criticality concerns and limitations on heat loadings for the waste form and repository. The former can be overcome by the incorporation of neutron absorbers (e.g., Hf, Gd, Sm) into the same ceramic waste form phase as the fissile material and such an approach could be employed for ^{99}Mo production waste streams that contain HEU. Heat loading limits in HLW waste forms are constrained partly by the repository design and partly by the current baseline waste form technology, borosilicate glass, which undergoes devitrification at elevated temperatures and thus requires storage under controlled cooling for 30 years or more prior to disposition in a repository if it contains substantial amounts of HLW. The use of ceramic waste forms that are unaffected by moderate heat can enable higher levels of heat-producing isotopes; however ^{99}Mo production does not produce HLW according to current classifications [2, 3].

(2) The Waste Form must be Mechanically and Chemically Durable. It is important that the waste form retains the radioisotopes under storage and repository conditions. The waste form's ability to contain the radioactive isotopes under repository conditions is often measured by short-term leach testing, but also required is a measure of the long-term durability of the material, particularly when radiation damage and

annealing processes will be occurring over the waste form's lifetime. Modelling of the leaching of radionuclides and movement of them through a geological repository become part of the safety case for the repository. Typically, repositories are modelled on an ~10,000 y timeframe; however, recently there have been political drivers to have one million year time frames [17]. In the authors' opinion, this is likely to be unrealistic given the errors in potential models over such a time frame.

(3) Chemical Flexibility. The waste form has to be flexible enough to cope with "real," often variable, waste streams and processes. The waste form usually has to be able to incorporate significant amounts and types of impurities and process chemical additives without serious property degradation.

(4) Ease of Processing. Processing the waste to make the waste form needs to be cost effective, meet environmental and occupational health and safety norms (such as radiation doses to workers), and be technically feasible. Gamma emitting radioactive wastes, such as the ILLW from ^{99}Mo production, impose the need for remote operations in a hot-cell, which is expensive to build, operate, and maintain. Furthermore, characterisation of such wastes is difficult and expensive. Therefore, the process chosen must have process parameters that are broad enough to be practical and to cope with changes in the waste stream and enable easy operation of the remote process line.

(5) Proliferation Resistance. For fissile materials, such as HEU used in Mo-99 production, the waste form must have a good resistance to theft or diversion and it must be difficult to retrieve the actinides for reuse. Physical security in terms of storage and inspection by safeguards officers is required. In the longer term rendering the material unattractive for reuse by converting it to a waste form for disposition is desirable. There are usually two approaches to this: providing a radiation barrier coupled with physical security, and producing a waste form from which it is more difficult to extract the fissile

materials, for example, by requiring techniques other than existing, well-known reprocessing routes.

In all cases the aim to be achieved in selecting the waste form and process selection is to reduce risk. The primary risks are economic and safety/environmental. Economic risk can be managed by reducing life-cycle costs and using technology assessment processes [18]. Environmental risk can be dealt with by ensuring the waste form is durable and stable over long-time frames while meeting the appropriate standards and criteria for disposition and safety (using safety assessment processes) and applying principles such as, as low as reasonably achievable (ALARA) or practical (ALARP) to the design and operation.

2.1. Waste Forms for Molybdenum-99 Wastes. Nearly all [99]Mo producers use highly enriched U (HEU) and simply contain their waste in tanks (liquids) or as solids (e.g., used targets). However, from the 1970s to 2005, ANSTO produced [99]Mo from ~1.8 to 2.2% enriched UO_2 (LEU) targets irradiated in its HIFAR reactor at Lucas Heights. Until the early 1990s all the resultant nitric acid waste containing ~150–300 gU/L plus fission products was stored in tanks, but then a program was started to solidify this waste and contain the solids in metal cans [19]. ANSTO now has 560 kg of this solidified waste, but still has ~6000 L of liquid ILLW. The liquid waste consists of primary (95–195 gU/L) and secondary (9–35 gU/L) waste in tanks. In more recent times, however, plans have been made for immobilisation of this waste [20].

2.1.1. Ceramic Waste Forms for Legacy U-Rich ILW Arising from the Acidic Route for [99]Mo Production at ANSTO. The waste from the acidic route is principally uranyl nitrate plus a small amount of fission products and mostly is classed as ILLW (Table 2). To immobilise this a pyrochlore-rich ceramic was developed [20], which was similar to the pyrochlore-zirconolite-brannerite ceramics developed by ANSTO and the Lawrence Livermore National Laboratory (LLNL) in conjunction with Savannah River National Laboratory (SRNL) for the immobilisation of 17–30 tons of surplus weapons grade Pu, the Plutonium Immobilization Project (PIP) [21]. Initially a zirconolite-rich formulation was developed for the Pu immobilisation, and it also included Ba-hollandite and rutile. The hollandite would enable the incorporation of radioactive Cs and would form a radiation barrier to reuse. The material was extremely durable [22]. The zirconolite-rich laboratory samples were prepared via cold-pressing and pressureless sintering, and via hot-uniaxial pressing in graphite dies. For production purposes ANSTO proposed that this material would be produced via hot-isostatic pressing (HIPing) [23], which involves the simultaneous application of heat and pressure to consolidate materials. For containment of waste forms in metal cans for HIPing ANSTO typically used stainless steel cans; however, other alloys may be used, for example, Ni [24, 25] (Figures 2 and 3). The powder is fed into the bellows; the bellows are evacuated and then hermetically sealed before HIPing. A hot-isostatically pressed metal bellows (~0.4 kg) that contained ~50 g of PuO_2 plus several full-scale 9.5 kg

FIGURE 2: A hot Isostatic press located at ANSTO. This press can take up to a 30 cm diameter load. The machine consists of a pressure vessel in which a furnace is installed. Densification occurs under Ar at up to 200 MPa at the desired temperature.
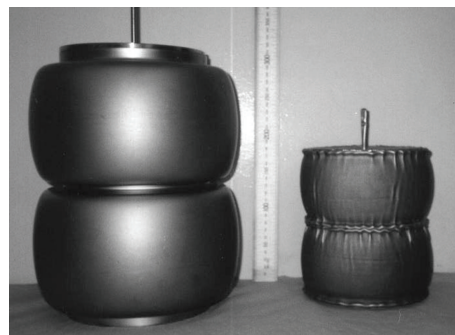
FIGURE 3: One of the many types of HIP can dumbbell designs showing how the can collapses to a near cylindrical shape (left before, right after HIPing). This 13.5 kg can contains Synroc-C. The HIPed can is 19 cm high by 15.5 cm in diameter.

bellows (12 cm dia. × 24 cm ht.) with Ce used as a Pu simulant were made.

Long-term criticality issues arising from the decay of [239]Pu to [235]U and the need to further discourage diversion led to the incorporation of significant amounts of depleted U. This reduced the waste loadings for Pu and hence pyrochlore-rich ceramics were developed containing ~10 wt% Pu, plus 20% U and equimolar amounts (to Pu) of Hf and Gd as neutron absorbers for criticality control both during processing and upon emplacement in a geological repository. A baseline formula of 0.9 $Ca_{0.89}Gd_{0.23}Hf_{0.23}Pu_{0.23}U_{0.44}Ti_2O_7$ + 0.1 $Ti_{0.9}Hf_{0.1}O_2$ was used [26]. This ceramic was shown to be capable of accommodating significant amounts of process chemicals and other variations in the Pu waste streams, having a wide range of ionic sizes and valences [27, 28]. The final formulations contained mixtures of pyrochlore, zirconolite, and brannerite (nominally UTi_2O_6) depending upon the feed chemistry. The process chosen was cold pressing and sintering of ~500 g pucks using a route similar to that used for mixed oxide (MOX) fuel.

Ceramics were chosen ahead of lanthanide borosilicate (LABS) glass for PIP [29], which was also a possibility for use in immobilising [99]Mo acidic ILLW if a melting-route

was chosen. While there were several factors influencing the decision to use a ceramic over a high-melting (1500°C) LABS glass [30] and one may have thought that the long-term durability of the ceramic phases (MCC-1 type leach tests produced very low normalized Pu leach rates of 10^{-5} to 10^{-6} g·m^{-2}·d^{-1} at 70°C in deionised water [22, 31]) would be critical, the two strong factors favouring the ceramic were its factor of ~7 lower neutron dose to workers (LABS glass contained boron which underwent (α, n) reactions); and its greater resistance to proliferation [32]; LABS could simply be dissolved in nitric acid and the Pu extracted by a PUREX-like process. Indeed, LABS glass was later developed as a means to store and transport actinides between US national laboratories [33, 34]. The processing options also favoured the ceramic in the fact that LABS glass was produced by melting at high temperatures (~1500°C) in costly platinum crucibles [35], and produced potential criticality risks from settling of PuO$_2$, in the crucible, whereas the ceramic was proposed to be produced using a process similar to mature mixed oxide fuel manufacturing technology. The leach resistance of the ceramic, particularly for actinides and U, was far greater than that of LABS glass [36]. However, another long-term issue was the potential rapid loss of highly leachable B, which with Gd also serves as a neutron absorber, from LABS glass over geological time frames, rendering it less intrinsically safe from a criticality viewpoint than the ceramic [37]. The ceramic contained both Gd and Hf. The leach rates of these are low and with Gd leach rates being slightly higher than that of Pu, particularly if the pH is low, and Hf lower or similar to that of Pu. Furthermore, the ceramics were shown to be durable even when radiation-damaged, with accelerated testing on samples doped with ^{238}Pu carried out at the Pacific Northwest National laboratory (PNNL) [38, 39].

Therefore, from a Mo-99 viewpoint the ceramic-route offers advantages over LABS glass in terms of U-durability, criticality safety, proliferation resistance, and processing. The higher processing temperatures needed for LABS glass production would increase volatile losses of fission products and complicate the high temperature off-gas system. Furthermore, ANSTO needed to treat additional waste streams and required one process line for these, and LABS glass was not considered suitable for both streams. The choice of plant is discussed later in this paper.

Following on from the plutonium immobilisation and work on U-doped zirconolite, in-house research into treatment of ANSTO's U-bearing wastes started in the late 1990s [40]. This work showed that simply mixing the waste with the Synroc-B precursor developed for the original Synroc-C, designed for immobilising PUREX-type HLW from nuclear power plant fuel reprocessing [41], and then calcining and HIPing the material in a manner similar to that for Synroc-C produced a durable waste form. However, to increase the waste loading the design was shifted from zirconolite as a host for actinides to the related pyrochlore (nominally (Ca,Zr,U,Gd,Hf)$_2$(Ti,Al)$_2$O$_7$) phase as a host for U [42, 43]. The waste form was somewhat similar to Synroc-F [44, 45], which was developed for the immobilisation of U-rich wastes such as those of the chemical composition of spent nuclear

fuel. The pyrochlore phase comprises ~80 wt% of the waste form. Hollandite and rutile (~10 wt% each) are present as secondary phases to assist in immobilising fission products present in ANSTO's legacy ILW [46], and small amounts of perovskite and brannerite may also form the final waste form matrix.

Although it would seem attractive to utilise a single ceramic phase for a given radwaste, real radwastes are inhomogeneous. So, the aim should be to create phase assemblages which can incorporate the full range of radionuclides, impurities, and process additives such that when the radwaste composition is variable the phase assemblage stays the same, but the phase proportions vary. Moreover, the waste form phase assemblage should be insensitive to variations in the waste/additives ratio as has been shown for Synroc-C and other Synroc systems.

The pyrochlore is nominally targeted as CaU$_{0.47}$Zr$_{0.53}$Ti$_2$O$_7$ with U in the tetravalent state, but ANSTO researchers have found that due to the presence of U^{5+} the pyrochlore contains additional Ca to maintain charge neutrality. This can also lead to the formation of brannerite. Figure 4 shows the microstructure of a sample produced via kneader drying. The sample was analysed in a scanning electron microscope and is composed of ~40–50 vol% pyrochlore (Ca$_{0.95}$Zr$_{0.09-0.12}$U$_{0.83-0.84}$Ti$_{1.99-2.04}$Al$_{0.05-0.07}$O$_7$); 30–40 vol.% brannerite (Ca$_{0.02}$U$_{0.97}$Ti$_{1.9}$Zr$_{0.04}$Al$_{0.01}$O$_6$); 5–10 vol% hollandite (Ba$_{1.13}$Ca$_{0.25}$Al$_{0.76}$Ti$_{6.72}$Zr$_{0.02}$O$_{16}$); 5–10 vol% Zr-doped rutile; plus ~1 vol% UO$_2$. This is an initial test sample for scale-up and shows some segregation of TiO$_2$, which explains the presence of more brannerite and some UO$_2$ than seen in laboratory samples which were more uniform [42]. This can be eliminated by improved drying techniques and improved precursor preparation. The samples produced were durable with low leach rates when tested using MCC-1 methodology (ASTM C1220-10 [47]). Measured leach rates for the HIPed sample shown in Figure 4 are given in Table 4. The result is consistent with unpublished data from small laboratory samples made earlier [4] (Table 4). The process is currently undergoing scale-up with full-scale testing to produce a 30L HIP can. The processing system will enable more homogeneous powders to be produced than those produced so far using small-scale and available mixers.

It has been shown at the laboratory scale that 100% dense ceramic samples containing around 40 wt% of U oxide plus fission products can be produced by HIPing at 1250°C/100 MPa for 2 h [20, 42] and that quite large variations in the additives and waste loading have little effect on the excellent leach properties. The advantages of HIPing have been described many times [16, 48, 49] and will be discussed below. In the process, an alkoxide-hydroxide precursor mix is prepared external to the hot-cell line. The preparation route for this precursor is the same as that used to produce Synroc-B [50, 51], the precursor used for the production of Synroc-C.

2.1.2. Ceramic and Glass-Ceramic Waste Forms for Alkaline ILLW Arising from ^{99}Mo Production.

With the closing down of the Australian Research Reactor in 2005 and

Table 4: Leach rates for the HIPed sample shown in **Figure 4**. MCC-1 replacement test 0-1 and 1–7 day periods, 90°C, deionised water. Data from earlier work (0–7 days) [4] are also given; note that after the 7 d leach period the leach rates drop to less than or close to the detection limit for all elements.

| Route | Normalised release rate ($g \cdot m^{-2} \cdot d^{-1}$) | | | | | | |
| | Latest data | | | Preliminary pyrochlore-rich work[#] [4] small-scale | | | |
	Kneader dried			Alkoxide-route			Microsphere
Waste loading	40 wt%	40 wt%	25 wt%	35 wt%	40 wt%	44 wt%	40
Leach period	0-1 d	1–7 d	0–7	0–7	0–7	0–7	0–7
Al	<DL	<DL	<0.01	0.05	<0.02	nm	0.05–0.3
Ba	0.65	0.11	0.04–0.1	0.005	<0.004	0.02	0.003–0.08
Ca	0.12	0.03	<0.01	0.01	0.02	nm	0.006–0.4
Cs	np	np	0.03–1	0.08	nm	0.10–0.13	0.2–7.3
Sr	np	np	0.04–1.4	0.08	0.03	0.08–0.12	0.04–0.3
Ti	0.005	0.00017	<0.01	<0.0001	<0.0001	<0.0001	<0.0001
U	0.008	0.0006	<0.01	<0.0001	<0.0001	<0.0001	<0.0001
Zr	0.010	0.0002	<0.01	<0.0001	<0.0001	<0.0001	<0.0001

Nm: not measured; np: not present.
[#]Note: data are varied because several different routes that produced differing degrees of homogeneity and some different processing conditions were tested. In addition variations in the waste composition were also tested. Only in a few samples where the redox was not controlled or the sample was inhomogeneous did the Cs and Ba leach rates increase. In all cases the U-leach rates remained low.
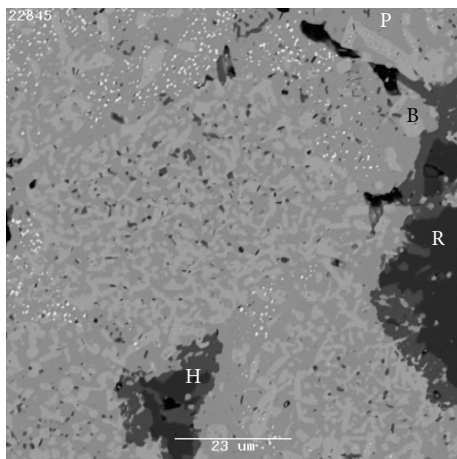

Figure 4: Microstructure of a baseline waste form designed to immobilise U-rich legacy waste at ANSTO. B = brannerite, H = hollandite, P = pyrochlore, R = rutile.

the construction of the new research reactor OPAL in 2006, ANSTO is now using 3% enriched UAl alloy targets and the Argentine/S. Africa/Belgium ^{99}Mo extraction methods, yielding alkaline ILW typically consisting of 5-6 M NaOH (after the addition of more NaOH for tank storage) plus 1.14–1.5 M $NaAlO_2$, plus fission products (Table 2). The waste form chemistry and its waste loading limits are therefore dominated by the Na in the waste stream.

Sodium can be incorporated into several ceramic phases. In Synroc-C, the waste loading is limited to ~2.5 wt% Na_2O, above which the leach rate increases as Na concentrates at the grain boundaries [52]. Other alternatives examined by the authors and others include, for example, perovskite $(Ca,Na,RE(III))TiO_3$ [53], freudenbergite $(Na_2(Al,Fe)_2Ti_6O_{16})$ [54], nepheline $(NaAlSiO_4)$ [55], NZP

$(NaZr_2P_3O_{12})$ [56, 57], and NTP $(NaTi_2P_3O_{12})$ [58]. However, the waste loading for Na in ceramics, especially after additional phases are added to host the waste ions, is limited, increasing the waste volumes produced, limiting plant throughput, and increasing life-cycle costs. Alternatives such as borosilicate glasses and glass ceramics were therefore examined.

Following initial forays into boroaluminosilicate glass consolidated by HIP rather than vitrification, we are now working with a glass-ceramic which can be HIPed at 1000°C/35 MPa with a 26 wt% oxide waste equivalent loading [20]. This has satisfactory leaching properties insofar as it will pass the Product Consistency Test (PCT) for HLW borosilicate glass [59] at 40 and 90°C and further optimisation and scale-up is in progress. We will discuss this further below.

Another alternative is bitumisation, carried out in Belgium [9] Japan, and elsewhere. However, such a plant did not match ANSTO's technical expertise and concerns exist about the storage and flammability and potential for self-ignition of such material, with accidents having already occurred [60]. Thus, there was no advantage in considering this route. Furthermore, from a long-term storage and repository perspective, the inclusion of large quantities of flammable materials may be deemed problematic.

2.1.3. Cementitious Options for ILLLW and LLLW Arising from ^{99}Mo Production. The alkaline-route ^{99}Mo production process also produces a similar amount of lower activity wastes to the volume of ILW produced. This waste is initially highly active but decays over ~3 years to below the ILW/LLW level. Of course cement is a popular solid waste form for low-temperature solidification and/or encapsulation of LLW. However, homogeneous incorporation of waste has some risk associated because the waste might seriously perturb the cement setting process. The cement cannot be dehydrated

by heating without detriment to its physical integrity, so radiolytic gas buildup as storage and disposal time is a serious factor to contend with. Also the fact that this waste is rich in Na is not a positive feature for cement; the large Na content would probably give rise to high leachability (the well-known alkali reaction problem for cement) unless the waste loading is kept very low. As a consequence, the waste volume would be considerably higher.

Alternative routes to ceramic immobilisation include drum drying of liquid waste followed by overpacking in concrete, which also acts as radiation shielding. This route is used by COVRA in The Netherlands. ANSTO looked at using this route but found that it would create 50,000 L/y of concrete waste for the ~2000 L/year production from its existing plant and much more (~112,000 L/y) from its planned future plant. The hot-isostatic pressing route chosen by ANSTO would produce only ~500 L per year of unshielded waste. The package size meant that the waste could be stored in existing facilities and hence eliminated the need to build a multimillion dollar waste store every 10 years. Furthermore, the number of shipments required to a future national store would be reduced by at least an order of magnitude. Given the several 1,000 km transportation distance in Australia, this cost saving was significant, but the decrease in political, environmental, and security risks by fewer shipments was also considered important. In addition, any final repository volume would also be significantly reduced, leading to life-cycle cost savings. While there are no published costs for an Australian repository/store the effect of volume reduction can be illustrated by considering the published US cost of $US602,000 per glass canister for disposition at Yucca Mountain [15] and around £18,000/m^3 to dispose of ILW in UK [61]. Using the UK figure the disposition savings from volume reduction alone would be around $3-4 million/yr. There are also other calculated benefits such as a reduction in life cycle CO_2 emissions. The Synroc route shows a significant reduction in CO_2 emission over the cementation process, although from an operational perspective the power consumption of producing synroc versus cement waste forms is similar with synroc being about 20% lower in the life cycle to storage. The significant CO_2 savings come from the size of the repository that is needed to be built to house and store the treated wastes, where the difference is around 20 times less for the synroc process compared to the cement option.

Geopolymers are low-temperature ceramics made by the action of highly alkaline silicate solutions on reactive aluminosilicate precursors, so the alkaline LLLW (Table 2) is attractive from this aspect. Geopolymer processing has many similarities to that of cement. Geopolymers are generally superior to cement in the radioactive context with respect to leachability (in addition to the absence of the alkali reaction problem). Cements are subject to radiolysis from nuclear waste and consequent weakening of the hydrous binding phase, whereas geopolymers do not rely on hydrous material for strength and can be carefully dehydrated by not-too-rapid heating without decrepitation or significant strength loss problems. It has been shown [62] that both the ILLW and LLLW from ^{99}Mo production can be incorporated in a metakaolin-based geopolymer and can pass the PCT leach test for deep disposal; however, the waste loadings on an oxide basis were somewhat below 10 wt% in both cases. The sulphate was precipitated as $BaSO_4$ to inhibit the SO_4^{2-} from interfering with the geopolymerisation process. More fundamental aspects of geopolymer leaching, notably temperature, pH dependence, and solution/volume ratio, have also been published by ANSTO workers [63]. The alkaline nature of geopolymers would suppress any potential for cyanide gas emissions from the KSCN present in the liquid LLW, even during dehydration at temperatures of ~300°C for example. Further optimisation studies are in progress.

However, nitrate waste streams are highly problematic for cement and geopolymer production would require front end treatment, calcination, or other denitrations, which would complicate the process. In addition the presence of water would also have criticality implications for HEU wastes requiring very low waste loadings and hence would produce large waste volumes if used to immobilise the U-rich wastes.

2.1.4. Immobilisation of Used UAl Alloy Targets. These consist mainly of $UO_2 + Na_2U_2O_7$, plus some fission products. A ceramic waste form approach could be the addition of Ca, rare earth, and Ti oxides to allow conversion into a perovskite-structured $(Na,RE)TiO_3$ + brannerite ceramic (nominally UTi_2O_6). Preliminary experiments have demonstrated the general feasibility of this approach. Depending on the enrichment of the U, the preferred rare earth would be Gd as a neutron absorber to inhibit the likelihood of criticality. While the U in the nominal brannerite is tetravalent, U^{5+} can also be accommodated, with the charge compensation provided by the addition of Gd^{3+} and other ions such as Ca^{2+} on the U site and Al^{3+} on the Ti site. Another alternative is a ceramic to immobilise U in brannerite and the Na in freudenbergite $(Na_2(Al,Fe,Cr,Ti)_2Ti_6O_{16})$.

A different approach would be to immobilise the Na in a glass and the uranium in a zirconolite/pyrochlore to make a glass-ceramic, similar in principle to work being undertaken by the UK National Nuclear Laboratory and ANSTO to immobilise Pu-residues wastes [64, 65].

2.1.5. Separation of Cs and Sr. Recent work appears to show highly efficient separation of Cs and Sr from ILLW [66], and several routes for both alkaline and acidic streams have been examined [67]. Also, *IONSIV* [68], the commercially available NaSiTiOx ion exchanger for separation of Cs and Sr from alkaline wastes, can be converted to a high-temperature ceramic with excellent leach resistance [69] or a glass [70]. The removal of the Cs and Sr may reduce the activity of the ILLW close to or below that of LLLW and the Cs and Sr could be incorporated in a relatively very small volume of waste form. Of course IONSIV is not able to immobilise the solid cake or any of the other ILW and the production of the highly radioactive waste form, such as the hollandite phase, would not be easy.

The principal disadvantage of separation technology is the fact that it requires the additional expensive hot-cell unit operations and you end up with two waste streams to treat,

plus additional secondary wastes. The reasons we did not pursue this option at ANSTO have already been summarised above.

2.2. ANSTO's Waste Treatment Plant for Treating ILLW. ANSTO undertook an assessment of options to treat both its legacy and alkaline wastes prior to commencement of the project. Some of the benefits have been discussed above in Part 3.1, in particular the life-cycle cost savings from waste volume reduction. After an assessment ANSTO chose a production route that included similar unit process operations to that used in the original Synroc Demonstration Plant (SDP), which was designed to process 10 kg/hr of Synroc-C [41]. Given the need to treat both acidic and alkaline streams and the desire to avoid costly off-gas systems, plus the relatively low throughput and currently proposed intermittent plant operation (3-4 days/week) compared to HLW glass melters, a melting-route was ruled out. As discussed above cementation was also ruled out on a life-cycle cost basis, because it could not handle all of the potential waste streams to produce a durable waste form and would therefore require additional front-end processing, produce a considerably larger waste volume, and could not use existing storage facilities. Given the lack of repository specification it was felt that an encapsulation approach was undesirable in an Australian context and that the fission products should be bound in the waste form.

HIPing, a technology that has matured considerably since the SDP was run in the 1980–90s, was employed as the consolidation step and its advantages are discussed below. In the SDP a hydraulic hot uniaxial press with induction heating was wed with metal bellows containing the processed synroc powder. The plant capital and operation have been costed for a plant with a 30-year design life with a planned maintenance schedule. The plant is designed to produce 150 30L HIP cans per year with a conservative maintenance and availability regime, but that is operating on a 3-4 day working week schedule and the plant has at least double that capacity. In addition, the plant could also be used to treat the lower activity liquid waste from the alkaline route and the U-rich filter cake. ANSTO is currently storing the latter with a view to either disposition or reuse after treatment.

Currently, the project is moving into the detailed design stage and the Environmental Risk Assessment is with the Australian regulator, the Australian Radiation Protection and Nuclear Safety Agency (ARPANSA) and has successfully undergone independent technical readiness level (TRL) assessment [71].

Although the compositions of the final waste forms for the legacy and alkaline wastes are different, the waste treatment steps are the same. Figure 5 illustrates the steps in the modern SYNROC HIP process. The durable synroc waste form is not produced until the calcined precursor powder has been HIPed. The process line is divided into sections for contamination control. In the first section the liquid waste is mixed with additives to get the chemistry of the waste form correct. This slurry is then dried to a free flowing powder. The front end will use fairly standard stainless steel tanks, mixing
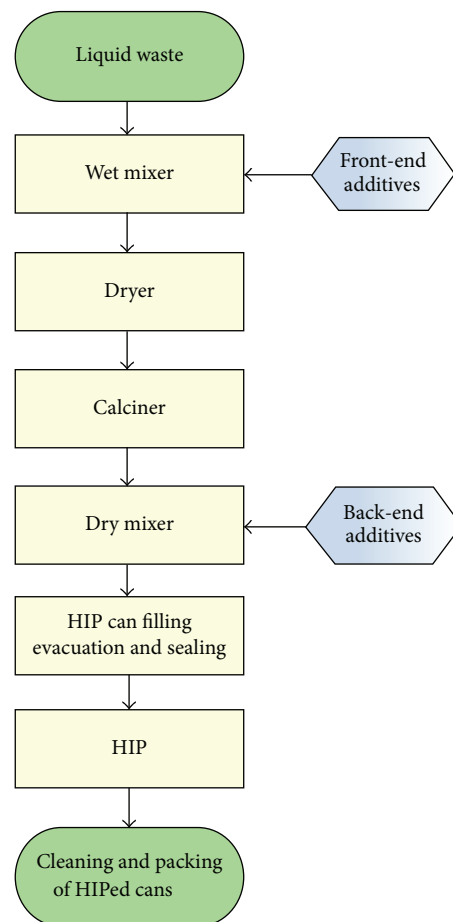

FIGURE 5: Schematic of the waste treatment steps.

and transfer systems that have been nuclearised for hot-cell maintenance and longevity. The powder is then heated in a calciner to remove species that may decompose and generate gas upon heating, such as chemically bound water, nitrates, and carbonate. ANSTO has examined a number of calciner options and has developed a proprietary system to replace the traditional rotary calciner. This system has a smaller footprint and will not require seal maintenance to prevent air ingress, as is the case with rotary calciners.

By using 3.5% H_2 in N_2, reducing conditions are maintained during calcination to reduce fission product volatility. There are limited data available at this stage on the specific plant dryer; however, work employing ^{134}Cs and ^{103}Ru radioactive tracers to measure volatilisation during the Synroc-C process, which has similar unit process steps and operating conditions to the current plant design (wet mixing, drying, calcining and hot-pressing), was undertaken. The dryer was a flash dryer with a measured loss of ~0.006% of Cs and 0.05% of Ru, but some of this was likely to be in fine particulates. The Cs loss during calcination during calcination at 750°C, in 3.5% H_2/N_2, was measured at 0.11% and this was mainly due to entrainment in/on the fine powder carried through by the process gas into the off-gas system [41]. In additional work by Woolfrey and Cassidy [72] the fines

were filtered from the off-gas and the measured Cs loss due to volatilisation was found to be much lower (0.0001%) and the Ru volatilisation was also lower (0.004%). We have undertaken some laboratory-scale work with nonradioactive Ru and have found little if any loss from the alkaline stream when dried and calcined. Further work is planned to be undertaken at scale to confirm this. As the plant off-gas will be filtered and the fines recycled, so the volatilisation is expected to be similar to the Synroc-C test figures. Technetium levels in the waste are small and the losses will also be minimised by processing under reducing conditions. ANSTO has prepared via sintering ^{99}Tc samples that retain the bulk of the Tc [73, 74]. Iodine is absent from the alkaline ILLW, but the off-gas system will be designed to remove I and any other volatiles carried over. The carryover waste will be treated via ANSTO's site management lines. With the use of HIPing inside a metal can for consolidation there will be considerably less off-gas compared to a melter route and hence the off-gas system for the ANSTO plant is considerably smaller than melters.

The resulting powder can then be mixed, if required, with back-end additives, such as metal getters for redox control; Ni and/or Ti are the most commonly used in Synroc. The calcined powder will be then loaded into the metal HIP can using ANSTO's proprietary designed filling and sealing system, that prevents contamination spread of the powder. The can is evacuated and sealed, and the seal welded. The can is decontaminated and passed through a lock into the next cell. For some plants there is the option to preheat the can or bake-out during evacuation, but this is not required for wastes in ANSTO's plant. The HIP can is placed inside an ACOP (Active Containment Over-Pack) [48] that provides another layer of protection for the HIP machine and the surrounding environment from the spread of contamination and damage to the furnace or pressure vessel should an unexpected failure of a HIP can occur.

The ACOP containing the filled HIP can is transferred to the HIP and processed under heat and pressure (using Ar) to produce a dense, durable glass-ceramic, or ceramic with a high waste loading. This is discussed in more detail below. The HIPed cans go through a further decontamination and check and are then loaded into bins for transfer to ANSTO's storage facilities.

The Synroc waste treatment plant will be operated to process around 5000 L of liquid waste per year with a higher capacity possible. The plant uses industrially mature plant and equipment that has been modified to be able to be operated remotely. The focus of the Synroc team's work in the past 2 years has been on developing the design to a high TRL to minimise technical risk involved in a "first of a kind" plant, and to optimise the processing parameters and determine the process windows. Preliminary engineering is at completion and the plant construction and commissioning is expected to be completed by 2016.

A conceptual design is shown in Figure 6. This design utilises a front-end with process equipment to mix the waste stream with additives and dry and calcine the product. The calcined powder is placed in a HIP can, which is then evacuated, sealed, and moved through decontamination cells into the HIP cell. The HIP cell is located such that contamination
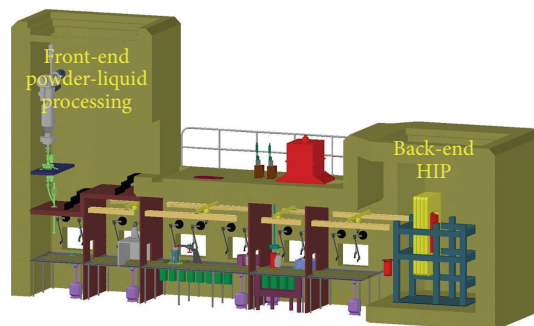

FIGURE 6: Initial conceptual plant design for the treatment of ILLW wastes at ANSTO.

control is maintained and access for maintenance is feasible. This design was ~18 m long. The final design will have triple the capacity to this design and will be only ~4 m longer and a little wider.

2.2.1. The Use of Hot-Isostatic Pressing to Treat Nuclear Waste. Hot-isostatic pressing (HIPing) technology was invented in the 1950s at the Battelle Memorial Institute (US) [75] and was used throughout the late 1950 and early 1960s as a research tool for fabricating experimental fuels and reactor materials [76, 77]. It involves the simultaneous use of heat and pressure to densify a material. Argon is the traditional gas medium used in commercial HIPs, but other gases have been employed for speciality materials or research purposes. The use of gas to transmit the pressure means that the material must either be contained within a sealed layer or first sintered to closed porosity, in order for densification to occur. To avoid high-pressure gas in pores or voids the container must be evacuated. The use of HIPing for the manufacture of radioactive waste forms was first proposed in the 1970s [78]. HIPing has been validated at the Idaho National Laboratory in the US as a credible (and advantageous) method of consolidating radioactive ceramic waste forms, with HIPing at the 100 kg scale of a zeolitic-type waste form and the use of an in-cell hot-isostatic press [79]. Moreover, the method is widely used in industry for preparing inactive ceramics. In the radioactive waste form field, Swedish workers were the first to use HIPing [80]. US workers HIPed experimental waste forms targeted to Savannah River wastes in the late 1970s and early 1980s [81] with Synroc-D developed at LLNL for US defence wastes [82, 83]. This was consolidated via HIPing or hot-uniaxial pressing in metal containers, which were favoured over pressureless sintering because this route gave a wider process window in which to achieve the required density rapidly (10 min. at 4000 psi (28 MPa) at 1100°C [84]) and could produce larger blocks of waste form. The cans also reduced the spread of contamination in the process line. HIPing demonstrations at 0.45 m dia. by 0.5 m high (50 kg) were undertaken [82] and bellows 26 "(0.67 m) in diameter by 58" (1.47 m) high proposed for a HIP plant [85]. A preliminary engineering layout was developed for

the Synroc-D process consisting of a wet mixer, a fluidised bed calciner, and a HIP to consolidate the material after it was loaded and welded into metal bellows [86]. The plant design capacity was ~1.45 tons/day.

For waste form processing ANSTO uses Ar as the pressure transmission medium. HIPs can be designed to operate above 2000°C, but processing temperatures for ceramic and glass-ceramic waste forms lie typically between 900 and 1300°C. HIP pressures up to 1000 MPa are possible with most general purpose laboratory HIPs operating around 100 MPa. Typical processing widows for waste forms are 20–100 MPa.

The metal HIP can is usually stainless steel, but it can be mild steel, nickel, or other metal as desired as mentioned in Section 2.1.1. The cans themselves are a few mm thick. The HIP can shape is tailored to suit the properties of the powder feed, the time-temperature-pressure cycle in the HIP, and the behaviour of the waste form during heating. It is advantageous to maximise the density of the calcined powder on loading the HIP can, to avoid undue rippling and substantial deviations from cylindrical geometry of the HIPed can; however, special designs are available for low-density powders. The dumbbell shaped can is designed to collapse to a near-cylindrical shape (Figure 3). The dumbbell design replaces earlier bellows designs and has the advantage of having the joins/welds in the can under compression. If a dumbbell can should fail or pinhole, high pressure gas can enter the can; on depressurisation of the HIP a dumbbell can will only expand to slightly bigger than its original shape and will therefore not damage the HIP furnace. ANSTO has undertaken experimental work to verify this. The bellows designs on the other hand are prone to failure at the tips of the bellows and if they fail they will expand considerably when depressurisation occurs, destroying the HIP furnace.

The can serves several roles. Its primary function is to act as a seal between the gas and powder allowing densification to occur during HIPing; it assists in maintaining the desired redox conditions during processing; it contains the waste form, preventing contamination spread, with minimal interaction. Testing has shown HIP that can interactions between the ceramic and glass-ceramic waste forms are minimal and not deleterious to the integrity of the waste form of HIP can [87, 88]. The can also retains volatile radioisotopes such as ^{99}Tc, ^{104}Ru, and ^{137}Cs during high-temperature consolidation. So the entire process produces off-gas only in the calcination stage where temperatures, <750°C, are much lower than those in the final consolidation, and reducing conditions further reduce the loss of volatile radioisotopes. While some credit may be possible for containment during storage of the waste form, ANSTO's approach is to rely on the waste form chemistry and use a transport container or overpack to provide mechanical protection.

For laboratory samples, the HIP can is usually evacuated after filling. The laboratory small cans typically contain a lid to which is attached an evacuation tube. However, production cans have a filling port and welding occurs on the lid. In laboratory samples the can often undergoes a bakeout cycle prior to sealing where it is heated to 300–600°C for several hours to remove gases adsorbed by the calcined powder when exposed to atmosphere. However, in production lines, where the unit process operations are interconnected and the atmosphere is controlled, this step may often be dispensed with.

2.2.2. Addressing Production Concerns Surrounding Use of HIPing in a Radioactive Environment.

Concerns have been expressed about the use of a high-pressure system in a radioactive environment and about the capacity of a HIP line to treat the volumes of nuclear waste, possibly because HIPing is a batch process, whereas its main competitor, glass melting, is semicontinuous and produces tonnes per day of glass waste form. Industrially large HIPs with hot zones of up to 2 m diameter with tonnes per day throughputs are in commercial operation. ANSTO has demonstrated that cans containing 100 kg of waste form are feasible (Figure 7) and has produced concept designs for treating ~10,000 m^3 per year of fuel pond sludges with two HIP units and another series of designs to treat the 6,600 tonnes of Idaho HLW calcines over a 6–12 year time frame. Industrially, cans containing several tons of material are processed.

The initial cans used in HIPing were of the bellows design used in hot uniaxial pressing. In the early 1980s ANSTO and LLNL [82, 89] studied synroc densification during HIPing using these types of cans and cylindrical tubes. These designs suffered from being inefficient in their use of space. Cylindrical cans deformed preferentially in the middle to give a "dog-bone" type shape. Bellows collapsed vertically leaving a relatively thick layer of compressed convolutions around the waste form. Bellows had an additional disadvantage in that the welds were placed in tension and if failure occurred (typically a pinhole failure), the Ar gas could enter the can. Upon decompression of the HIP this internal pressure would force the bellows to expand well beyond their original length often destroying the HIP furnace. To overcome this design deficiency ANSTO developed a dumbbell design [90]. These cans were designed to place the welds in compression to substantially reduce the risk of pin holing and if a dumbbell can failed it expands back to close to its original size and shape. The failed can may then be simply placed inside a bigger can, evacuated, sealed, and re-HIPed. ANSTO has tested this by deliberately inducing failure by putting a defect in the can wall; we have also examined failures due to defective welding. Once the waste form has densified there is no dust to leak out of the can. The dumbbell design had an added bonus of much more efficient packing. The dumbbell HIP cans have been designed with a 1/10,000 failure rate. They will be leak tested and the weld will be tested before use and the can marked for traceability.

The prevention of the loss of volatiles has also been mentioned and this considerably simplifies the off-gas system compared to a melter route. Recent laboratory-scale experiments at ANSTO have shown that the alkaline waste form process retained essentially all of the Cs and Ru from the wet mixing to the final HIPed waste form. Further tests at scale are planned. The segmented hot-cell design and decontamination systems also serve to mitigate the spread of contamination. As with all hot-cells the ANSTO line is connected to active ventilation systems that remove activity.

(a)   (b)

Figure 7: An ANSTO dumbbell design HIP can (100 L capacity) containing over 170 kg of Synroc waste form, before HIPing (a) and after HIPing (b), which was produced to demonstrate the scalability of HIPing.

The vent gases from the HIP are also passed through filtered systems. Water cooling in the HIP vessel design removes the heat from the vessel and hence the ventilation rates and temperature in the HIP hot-cell are within the normal operating parameters for hot-cells.

Control of radioactive contamination when handling powders is another concern. Dust is controlled by microfiltration on the dryer and calciner that recycles the particles back to the feed. The process lines are sealed with the units interconnected. The only decoupling occurs during HIP can filling or maintenance. Valving, and coupling design, plus washing procedures will be used to allow decoupling of equipment for removal or maintenance. ANSTO has a proprietary designed can filling system that replaces the earlier crimping and cutting system and prevents the calcined powder escaping during can filling. The use of an ACOP also provides another layer of protection for the HIP machine and the surrounding environment from the spread of contamination and damage to the furnace or pressure vessel, should an unexpected failure of a HIP can occur, containing both the can and its contents.

The two main HIP vessel designs are monolithic forged and wire wound pretensioned. The wire wound vessel has some fabrication advantages for the very large HIPs when compared to a monolithic forged vessel in terms of weight and size. However, ANSTO chose not to use a wire wound vessel because of some key potential risks, especially for radioactive environments. Concerns about the use of pressure needed to be addressed during the safety case for the ANSTO HIP. There have been two major vessel failures in the HIP industry. One was a noncoded monolithic pressure vessel that was improperly used, and the other, was a coded wire wound pressure vessel. Both resulted in damage to the surrounding infrastructure with the latter incident resulting in the death of a worker. In a radiological application the potential energy stored in a HIP system could in the event of failure pose a

hazard to the hot-cell structure and has the potential risk of the release of radioactive material to the surrounding building. ANSTO worked with the US HIP manufacturer American Isostatic Presses Inc. (AIP) to develop designs that mitigate the risk and make it possible to safely utilise HIP technology in a radioactive environment. ANSTO chose to use a forged vessel due to reasons discussed in detail in [48].

The ANSTO-AIP approach was to significantly increase the level of conservatism built into the pressure vessel design. By doing this, the subsequent major inspection interval for the vessel could be extended, even to the point that a properly designed hot-cell HIP that could complete the cleanup mission/campaign well before the first major vessel inspection is required. The additional cost of this is more than compensated for by reduced maintenance, replacement, and inspection costs, plus the reduced risk of radiation exposure to workers from such activities, even though the segregated hot-cell design and associated contamination control is such that it allows workers to enter the hot-cell that contains the HIP.

The first step in ensuring safety was to mandate the use of coded vessels designed, built, and tested in accordance with demanding specifications of the American Society of Mechanical Engineers (ASME) Pressure Vessel and Boiler Code, Section VIII, Division 2 and 3. ASME designed vessels can be designed for lives of 10,000–100,000 cycles at the maximum operating pressure, which would give a vessel 20–100 years of operation depending upon its duty cycles. The ASME lifetimes for a vessel are conservative and based on a presumed flaw in a pressure vessel. Such Division 2 coded vessels have a burst pressure of 2.4 times the design pressure, or roughly 2.5 times the normal operating pressure. The HIP in-built safety systems initiate well before the burst pressures are reached. A leak before burst design is also incorporated into the forged shell and heads without any high prestressing

requirements. In addition, it is possible to monitor crack growth in a forged vessel and hence determine its design life, repair the surface crack, or derate the vessel. The hot-cell is also designed against catastrophic failure. The ANSTO-AIP proprietary design has a design life of 10,000 cycles and will operate at a pressure well below its failure pressure. It also incorporates the leak before burst design which means that catastrophic failure is not possible. Safety analysis has indicated that failure of the proposed design nuclear HIP system is not credible.

While a pretensioned wire wound vessel, in theory, may also afford the leak before burst feature in the event of overheating, for example, due to cooling water loss, stress relaxation in the pre-tensioned wire winding could lead to significant distortion of the vessel. While one could put designs and systems in place to enable a wire wound vessel to have some of the advantages of the forged vessel, ANSTO's approach has been to use the passive safety implicit in a forged vessel design rather than rely solely on active systems, an approach that underpins the nuclear industry approach to design.

HIPing has several other advantages for use in a hot-cell: the process has a relatively small footprint, arising in the first instance because of the absence of off-gas in the hot-consolidation step. The HIP cans contain the fission products and, in conjunction with other methods, the HIP vessel can be kept relatively contamination free. The HIP pressure vessel is designed to exceed the life of the plant and because it is monolith contamination will be limited to the surface, which can be readily decontaminated. Thus, the secondary waste from the HIP plant will be far less than that from a glass melting route, which would produce several used glass melters, plus highly contaminated off-gas lines. The plant decommissioning will therefore be simpler.

For radioactive ceramic waste forms a prime advantage of HIPing is to achieve theoretical density of the waste form with minimum temperature and therefore minimum grain size, thereby adding to the overall strength and leaching resistance as well as reducing the potential of microcracking via polymorphic structural changes or radiation damage when the waste form contains a substantial amount of alphaemitting waste actinides.

The HIP process is scalable and can treat batches from a few grams to tons in the same unit. Because of this one process line could be used to treat multiple waste streams and ANSTO has design options to treat the ion exchangers, filter cake, and LLLW in the one plant. The scalability also means that small to large plants, tailored to a client's requirements, could be built.

For hot-cell operation ANSTO and AIP have designed remote loading and unloading systems, with a bottom loading approach used for the ANSTO line.

3. Conclusions

Higher activity LLLW and ILLW streams arising from ^{99}Mo production can be incorporated into several types of waste forms: ceramics, glass-ceramics, glasses, and in some cases cements or geopolymers. ANSTO is currently entering the detailed design stage of a Synroc plant to treat its legacy, current and future liquid wastes from ^{99}Mo production at its Lucas Heights site. For the legacy waste, which is mainly uranyl nitrate plus some fission products, ANSTO has chosen to use a pyrochlore-rich ceramic in which the U and fission products will be incorporated into titanate Synroc phases, pyrochlore, brannerite, hollandite, rutile, and perovskite. For the current and future waste arising from an alkaline route ANSTO will use a glass-ceramic. Both waste types will be processed in the one line, which has broadly similar unit operations to the original Synroc processing designs—liquid mixing, drying, calcining, and consolidation via hot-pressing. The plant will be the "first of a kind" incorporating a hot-isostatic press into the design. This was chosen because the route had significant life -cycle cost benefits for ANSTO and Australia, including a significant reduction in the volume of the waste that would need transporting to a National Store and future repository. The option of using the plant or similar designs to process other waste streams has also been examined and it is possible to utilise the technology to process other waste streams from ^{99}Mo production or from other waste inventories. The plant at ANSTO is currently entering the detailed design stage with a view to finishing construction by 2016.

References

[1] NEA, "The supply of medical radioisotopes—the path to reliability," NEA 6985, OECD, Paris, France, 2011.

[2] IAEA, *Classification of Radioactive Waste*, Safety Standards Series No. GSG-1, IAEA, Vienna, Austria, 2009.

[3] IAEA, *Classification of Radioactive Waste*, Safety Series No. 111-G-1.1, IAEA, Vienna, Austria, 1994.

[4] M. L. Carter, J. R. Bartlett, T. Eddowes et al., "^{99}Mo site waste immobilisation in pyrochlore/zirconolite-rich Synroc: wasteform development," Internal ANSTO Report, 2001.

[5] G. Varley and M. Kennard, *Review and Audit Report on Proposed Implementation of Radioactive Waste Substitution Arrangements Related to British Nuclear Group Overseas Reprocessing Contracts*, A report for the UK Nuclear decommissioning Authority, NAC International, 2006.

[6] "Review of radioactive waste management policy, final conclusions," White Paper Cm2919, 1995.

[7] "Transuranic waste acceptance criteria for the waste isolation pilot plant," Revision 7. 3 DOE/WIPP-02-3122, US-DOE, Carlsbad Field Office, 2013.

[8] OCRWM, "Civilian radioactive waste management system waste acceptance system requirements document," Revision 5 DOE/RW-0351 REV. 5, OCRWM, 2007.

[9] IAEA, "Management of radioactive waste from [99]Mo production," Tech. Rep. IAEA-TECDOC-1051, IAEA, Vienna, Austria, 1998.

[10] A. Leenaers, S. Van den Berghe, E. Koonen et al., "Microstructure of U_3Si_2 fuel plates submitted to a high heat flux," *Journal of Nuclear Materials*, vol. 327, no. 2-3, pp. 121–129, 2004.

[11] IAEA, "Non-HEU production technologies for molybdenum-99 and technetium-99m," IAEA Nuclear Energy Series NF-T-5. 4, IAEA, Vienna, Austria.

[12] L. P. Hatch, "Ultimate disposal of radioactive wastes," *American Scientist*, vol. 41, pp. 410–421, 1953.

[13] G. J. McCarthy, W. B. White, and D. E. Pfoertsch, "Synthesis of nuclear waste monazites, ideal actinide hosts for geologic disposal," *Materials Research Bulletin*, vol. 12, pp. 1239–1245, 1978.

[14] M. W. A. Stewart, B. D. Begg, R. A. Day, S. Moricca, E. R. Vance, and P. A. Walls, "Low-risk alternative waste forms for actinide immobilization," in *Proceedings of the Annual Waste Management Symposium (WM '05)*, Paper 5212, Tucson, Ariz, USA, February 2005.

[15] C/P/E Environmental Services, LLC, "Independent calcine disposition project review and cost estimate," US DOE Contract Report DE-AT07-06ID60550, 2006.

[16] B. D. Begg, R. A. Day, S. Moricca, M. W. A. Stewart, E. R. Vance, and R. Muir, "Low-risk waste forms to lock up high-level nuclear waste," in *Proceedings of the Annual Waste Management Symposium (WM '05)*, Paper 5364, Tucson, Ariz, USA, February 2005.

[17] US DOE, *Final Environmental Impact Statement for a Geologic Repository for the Disposal of Spent Nuclear Fuel and High-Level Radioactive Waste at Yucca Mountain, Nye County, Nevada*, Environmental Impact Statement U.S. DOE, Office of Civilian Radioactive Waste Management, 2001.

[18] US DOE, "US department of energy technical readiness assessment guide," Tech. Rep. DOE G 413. 3-4, US DOE, Washington, DC, USA, 2009.

[19] G. J. Parsons, "Solidification of acidic liquid waste from Mo-99 isotope production," IAEA International Conference on management of radioactive Waste from Non-Power Applications, Malta, November 2001.

[20] C. K. W. Cheung, E. R. Vance, M. W. A. Stewart et al., "The intermediate level liquid molybdenum-99 waste treatment process at the Australian nuclear science and technology organisation," *Procedia Chemistry*, vol. 7, pp. 548–553, 2012.

[21] M. W. A. Stewart, E. R. Vance, A. Jostsons, and B. B. Ebbinghaus, "Near-equilibrium processing of ceramics for actinide disposition," *Journal of the Australian Ceramic Society*, vol. 39, no. 2, pp. 130–148, 2003.

[22] K. P. Hart, E. R. Vance, M. W. A. Stewart et al., "Leaching behaviour of zirconolite-rich Synroc used to immobilize high-fired plutonium oxide," in *Proceedings of the MRS Symposium on Scientific Basis for Nuclear Waste Management XXI*, I. G. McKinley and C. McCombie, Eds., vol. 506, pp. 161–168, October 1998.

[23] H. V. Atkinson and S. Davis, "Fundamental aspects of hot isostatic pressing: an overview," *Metallurgical and Materials Transactions A*, vol. 31, pp. 2981–3000, 2000.

[24] E. R. Vance, A. Jostsons, S. Moricca et al., "Synroc derivatives for excess weapons plutonium," in *Environmental Issues and Waste Management Technologies IV, Ceramic Transactions*, J. C. Marra and G. T. Chandler, Eds., vol. 93, p. 323, American Ceramic Society, Westerville, Ohio, USA, 1999.

[25] M. W. A. Stewart, S. Moricca, T. Eddowes et al., "The use of hot-isostatic pressing to process nuclear waste forms," in *Proceedings of the 12th International Conference on Environmental Remediation and Radioactive Waste Management*, Paper ICEM2009-16253, Liverpool, UK, October 2009.

[26] B. B. Ebbinghaus, C. Cicero-Herman, L. Gray, and H. Shaw, "Plutonium immobilization project baseline formulation," Tech. Rep. UCRL-ID-133089, 1999.

[27] M. W. A. Stewart, E. R. Vance, R. A. Day et al., "Impurity incorporation in pyrochlore-rich ceramics," in *Environmental Issues and Waste Management Technologies In the Ceramic and Nuclear Industries V, Ceramic Transactions*, G. T. Chandler and X. Feng, Eds., vol. 107, p. 569, American Ceramic Society, Westerville, Ohio, USA, 2000.

[28] R. A. Van Konynenburg, B. B. Ebbinghaus, O. H. Kirkorian, S. I. Martin, F. J. Ryerson, and C. C. Herman, "Phase equilibria and impurity incorporation on the ceramic plutonium immobilization form," in *Proceedings of the 5th Annual Waste Management Symposium (WM '00)*, Tucson, Ariz, USA, February 2000.

[29] US DOE, "Record of Decision for the Storage and Disposition of Weapons-Useable Fissile Materials, Final Programmatic Environmental Impact Statement," 1997.

[30] S. G. Cochran, W. H. Dunlop, T. A. Edmunds, L. M. MacLean, and T. H. Gould, "Fissile material disposition program final immobilization form assessment and recommendation," UCRL-ID-128705, 1997.

[31] Y. Zhang, K. P. Hart, M. G. Blackford et al., "Durabilities of pyrochlore-rich titanate ceramics designed for immobilization of surplus plutonium," in *Proceedings of the Scientific Basis for Nuclear Waste Management XXIV, MRS Symposium*, K. P. Hart and G. R. Lumpkin, Eds., vol. 663, pp. 325–332, 2000.

[32] A. Macfarlane, "Immobilization of excess alternative to glass," *Science and Global Security*, vol. 7, pp. 271–309, 1998.

[33] A. P. Fellinger, M. A. Baich, B. J. Hardy et al., "Americium/curium vitrification process development," Tech. Rep. WSRC-MS-98-0475, WSRC, 1998.

[34] J. E. Marra, M. A. Baich, A. P. Fellinger et al., "A batch process for vitrification of americium/curium solutions," Tech. Rep. WSRC-MS-98-0475, WSRC, 1998.

[35] K. M. Marshal, J. C. Marra, J. T. Coughlin et al., "Development of the plutonium oxide vitrification system," in *Proceedings of the Annual Waste Management Symposium (WM '98)*, Tucson, Ariz, USA, March 1998.

[36] H. Xu, Y. Wang, P. Zhao, W. L. Bourcier, R. Van Konynenburg, and H. F. Shaw, "Investigation of pyrochlore-based U-bearing ceramic nuclear waste: uranium leaching test and TEM observation," *Environmental Science and Technology*, vol. 38, no. 5, pp. 1480–1486, 2004.

[37] OCRWM, "Degraded mode criticality analysis of immobilized plutonium waste forms in a geological repository," Predecisional Document A00000000-01717-5705-00014 REV 01, OCRWM, Washington, DC, USA, 1997.

[38] D. M. Strachan, A. E. Kozelisky, R. D. Scheele et al., "Radiation damage effects in candidate ceramics for plutonium immobilization: final Report," Tech. Rep. PNNL-14588, 2004.

[39] D. M. Strachan, R. D. Scheele, E. C. Buck et al., "Radiation damage effects in candidate titanates for Pu disposition: pyrochlore," *Journal of Nuclear Materials*, vol. 345, no. 2-3, pp. 109–135, 2005.

[40] E. R. Vance, G. R. Lumpkin, M. L. Carter et al., "Incorporation of uranium in zirconolite ($CaZrTi_2O_7$)," *Journal of the American Ceramic Society*, vol. 85, no. 7, pp. 1853–1859, 2001.

[41] A. E. Ringwood, S. E. Kesson, K. D. Reeve, D. M. Levins, and E. J. Ramm, "Synroc," in *Radioactive Waste Forms for the Future*, W. Lutze and R. C. Ewing, Eds., p. 233, North-Holland Publisher, Amsterdam, The Netherlans, 1988.

[42] M. L. Carter, H. Li, Y. Zhang, E. R. Vance, and D. R. G. Mitchell, "Titanate ceramics for immobilisation of uranium-rich radioactive wastes arising from ^{99}Mo production," *Journal of Nuclear Materials*, vol. 384, no. 3, pp. 322–326, 2009.

[43] M. James, M. L. Carter, Z. Zhang et al., "Crystal chemistry and structures of (Ca,U) titanate pyrochlores," *Journal of the American Ceramic Society*, vol. 93, no. 10, pp. 3464–3473, 2010.

[44] A. G. Solomah, T. S. Sridhar, and S. C. Jones, "Immobilisation of uranium-rich high-level radioactive waste in synroc-FA," *Advances in Ceramics*, vol. 20, p. 259, 1986.

[45] S. E. Kesson and A. E. Ringwood, "Safe disposal of spent nuclear fuel," *Radioactive Waste Management and the Nuclear Fuel Cycle*, vol. 4, no. 2, pp. 159–174, 1983.

[46] M. L. Carter, M. W. A. Stewart, E. R. Vance, B. D. Begg, S. Moricca, and J. Tripp, "HIPed tailored ceramic waste forms for the immobilization of Cs, Sr and Tc," in *Proceedings of the Advanced Nuclear Fuel Cycles and Systems (GLOBAL '07)*, pp. 1022–1028, Boise, Idaho, USA, September 2007.

[47] ASTM, "Static leaching of monolithic waste forms for disposal of radioactive waste," Tech. Rep. ASTM C1220-10, ASTM, 2010.

[48] S. Moricca, C. Orcutt, M. W. A. Stewart et al., "Hot isostatic pressing of synroc for nuclear waste disposal," in *Proceedings of the International Conference on Powder Metallurgy & Particulate Materials (PowderMet '12)*, Paper 0084, MPIF/APMI, Nashville, Tenn, USA, 2012 June.

[49] E. R. Vance, S. Moricca, B. D. Begg, M. W. A. Stewart, Y. Zhang, and M. L. Carter, *5th Forum on New Materials. Part B*, p. 130, Trans Tech Publications, 2010.

[50] W. J. Buykx, "Scale-up of Hydroxide-route," in *ANU, Nuclear Waste Immobilisation in SYNROC, NERDDP End of Grant Report Grant No. 83/3410 1986-88*, A. E. Ringwood and S. E. Kesson, Eds., p. 20, 1989.

[51] J. R. Bartlett, J. L. Woolfrey, and W. J. Buykx, "Production of synroc powders by alkoxide hydrolysis," in *Nuclear Waste Management III, Ceramic Transactions*, G. B. Mellinger, Ed., vol. 9, p. 45, American Ceramic Society, Westerville, Ohio, USA, 1990.

[52] E. R. Vance, M. W. A. Stewart, and G. R. Lumpkin, "Immobilization of sodium and potassium in Synroc," *Journal of Materials Science*, vol. 26, no. 10, pp. 2694–2700, 1991.

[53] E. R. Vance, K. L. Smith, G. J. Thorogood et al., "Alternative synroc formulations," in *Scientific Basis for Nuclear Waste Management, MRS Symposium Proceedings*, C. G. Sombret, Ed., vol. 257, p. 235, MRS, 1992.

[54] E. R. Vance, P. J. Angel, D. J. Cassidy, M. W. A. Stewart, M. G. Blackford, and P. A. McGlinn, "Freudenbergite: a possible synroc phase forsodium-bearing high-level waste," *Journal of the American Ceramic Society*, vol. 77, no. 6, pp. 2255–2264, 1994.

[55] P. E. D. Morgan, T. M. Shaw, and E. A. Pugar, "Ceramics for high waste loaded commercial radwaste disposal," *Advanced Ceramics*, vol. 8, pp. 209–221, 1983.

[56] R. Roy, E. R. Vance, and J. Alamo, "[NZP], a new radiophase for ceramic nuclear waste forms," *Materials Research Bulletin*, vol. 17, no. 5, pp. 585–589, 1982.

[57] B. E. Scheetz, D. K. Agrawal, E. Breval, and R. Roy, "Sodium zirconium phosphate (NZP) as a host structure for nuclear waste immobilization: a review," *Waste Management*, vol. 14, no. 6, pp. 489–505, 1994.

[58] L. J. Yang, S. Komarneni, and R. Roy, "Titanium-phosphate (NTP) waste form," *Advanced Ceramics*, vol. 8, p. 255, 1984.

[59] ASTM, "Determining chemical durability of nuclear, hazardous and mixed waste glasses and multiphase class ceramics: the Product Consistency Test (PCT)," Tech. Rep. ASTM C, 1285-02, ASTM, 2010.

[60] K. P. Zakharova and O. L. Masanov, "Bituminization of liquid radioactive wastes. Safety assessment and operating experience," *Atomic Energy*, vol. 89, no. 2, pp. 646–649, 2000.

[61] "Figures obtained from the UK Nuclear Decommissioning Authority as part of the NDA RFQ1850 Tender," February 2009.

[62] D. S. Perera, E. R. Vance, S. Kiyama, Z. Aly, and P. Yee, "Geopolymers as candidates for low/intermediate level highly alkaline nuclear waste," in *Scientific Basis for Nuclear Waste Management*, D. S. Dunn, C. Poinssot, and B. D. Begg, Eds., p. 361, Materials Research Society, Warrendale, Pa, USA, 2007.

[63] Z. Aly, E. R. Vance, D. S. Perera et al., "Aqueous leachability of metakaolin-based geopolymers with molar ratios of Si/Al = 1.5–4," *Journal of Nuclear Materials*, vol. 378, no. 2, pp. 172–179, 2008.

[64] M. W. A. Stewart, S. Moricca, E. Vance et al., "Glass-ceramic waste forms for uranium and plutonium residues wastes," in *Proceedings of the Annual Waste Management Symposium (WM '13)*, Paper 13164, Phoenix, Ariz, USA, February 2013.

[65] M. W. A. Stewart, S. A. Moricca, B. D. Begg et al., "Flexible process options for the immobilisation of residues and wastes containing plutonium," in *Proceedings of the 11th International Conference on Environmental Remediation and Radioactive Waste Management (ICEM '07)*, Paper ICEM07-7246, pp. 1453–1460, Oud Sint-Jan Hospital Conference CenterBruges, Bruges, Belgium, September 2007.

[66] L. Varshney, V. Venugopal, A. Kumar, V. Tessy, and S. D. Mishra, "Recovery of cesium from high level liquid nuclear waste by an advanced polymer composite," BARC Newsletter 327, 2012.

[67] E. D. Collins, G. D. Del Cul, and B. Moyer, *Advanced Separation Techniques for Nuclear Fuel ReprocessIng and Radioactive Waste Treatment*, K.L. Nash and G.L. Lumetta, Eds., p. 201, Woodhead Publishing, Cambridge, UK, 2011.

[68] M. Nyman, T. M. Nenoff, and T. J. Headley, "Characterization of UOP IONSIV IE-911," Tech. Rep. SAND2001-0999, 2001.

[69] E. R. Vance, *Environmental Issues and Waste Management Technologies in the Ceramic and Nuclear Industries XI*, C. C. Herman, S. L. Marra, D. Spearing, L. Vance and J. Vienna, Eds., p. 153, American Ceramic Society, Columbus, Ohio, USA, 2006.

[70] D. W. Hendrickson, R. K. Biyani, and J. B. Duncan, "Application of innovative sorbents in the removal of cesium from radioactive alkaline defense wastes," in *Proceedings of the Annual Waste Management Symposium (WM '98)*, http://www.wmsym.org.

[71] US DOE, "Technology readiness assessment guide," DOE G 413. 3-4, US DOE, Office of Management, 2011.

[72] J. L. Woolfrey and D. J. Cassidy, "Gas and volatiles evolved during synroc fabrication," SPN 47, Internal ANSTO Report, 1985.

[73] M. L. Carter, M. W. A. Stewart, E. R. Vance, B. D. Begg, S. Moricca, and J. Tripp, "HIPed tailored ceramic waste forms for the immobilization of Cs, Sr and Tc," in *Proceedings of the Advanced Nuclear Fuel Cycles and Systems (GLOBAL '07)*, pp. 1022–1028, Boise, Idaho, USA, September 2007.

[74] M. W. A. Stewart and E. R. Vance, "Titanate wasteforms for Tc-99 immobilization," in *Proceedings of the Annual Waste Management Symposium (WM '04)*, Paper 4362, Tucson, Ariz, USA, February 2004.

[75] "The Evolution of HIP—Commemorating the first hot and cold isostatic processing vessels," 1985, ASME paper, http://www.asme.com.

[76] A. N. Holden, *Dispersion Fuel Elements*, Gordon and Breach, New York, NY, USA, 1967.

[77] M. Padue, V. W. Storhok, and R. A. Smith, "Properties of plutonium mononitride and its alloys," in *Plutonium 1965*, A. E. Kay and M. B. Waldron, Eds., Chapman and Hall (Institute of Metals), London, UK, 1965.

[78] R. Tegman, "Hot-isostatic pressing of ceramic waste forms," *Interceram*, no. 3, p. 35, 1985.

[79] K. M. Goff, M. F. Simpson, K. J. Bateman, D. W. Esh, R. H. Rigg, and F. L. Yapuncich, "Unirradiated testing of the demonstration scale ceramic waste form at ANL-west," *Transactions of the American Nuclear Society*, vol. 77, p. 79, 1997.

[80] H. T. Larker, *Scientific Basis for Nuclear Waste Management I*, G. J. McCarthy, Eds., p. 207, Plenum, London, UK, 1979.

[81] P. D. E. Morgan, D. R. Clarke, C. M. Jantzen, and A. B. Harker, "High-alumina tailored nuclear waste ceramics," *Journal of the American Ceramic Society*, vol. 64, pp. 249–258, 1981.

[82] C. Hoenig, R. Otto, and J. Campbell, "Densification studies of synroc D for high-level defense waste," LLNL UCRL-53392, 1983.

[83] C. L. Hoenig and H. T. Larker, "Large scale densification of a nuclear waste ceramic by hot isostatic pressing," *American Ceramic Society Bulletin*, vol. 62, no. 12, pp. 1389–1390, 1983.

[84] J. H. Campbell, C. L. Hoenig, F. J. Ackerman, P. E. Peters, and J. Z. Grens, "Basalt Waste Isolation Project approach to develop models," in *Scientific Basis for Nuclear Waste Management V*, W. Lutze, Ed., p. 599, North Holland Publishing, New York, NY, USA, 1982.

[85] H. W. Newkirk, C. L. Hoenig, F. J. Ryerson et al., "SYNROC technology for immobilizing U.S. defense wastes," *American Ceramic Society Bulletin*, vol. 61, no. 5, pp. 559–566, 1982.

[86] R. B. Rozsa and C. L. Hoenig, "Synroc processing options," LLNL UCRL-53187, 1981.

[87] Y. Zhang, M. W. A. Stewart, H. Li, M. L. Carter, E. R. Vance, and S. Moricca, "Zirconolite-rich titanate ceramics for immobilisation of actinides: waste form/HIP can interactions and chemical durability," *Journal of Nuclear Materials*, vol. 395, pp. 69–74, 2009.

[88] M. W. A. Stewart, S. A. Moricca, E. R. Vance et al., "Hot-isostatic pressing of chlorine-containing plutonium residues and wastes," in *Proceedings of the Materials Science of Nuclear Waste Management Symposium (TMS '13)*, San Antonio, Tex, USA, March 2013.

[89] H. T. Larker, "HIP," in *Proceedings of the International Conference on Hot Isostatic Pressing, June 1987, Luleå, Sweden*, T. Garvare, Ed., p. 19, Centek Publication, Luleå, Sweden, 1988.

[90] E. J. Ramm and E. R. Vance, "In-bellows calcination of alkoxide precursor to synroc," in *Nuclear Waste Management III, Ceramic Transactions*, G. B. Mellinger, Ed., vol. 9, p. 57, The American Ceramic Society, Columbus, Ohio, USA, 1990.

Review Article

History and Actual State of Non-HEU Fission-Based Mo-99 Production with Low-Performance Research Reactors

S. Dittrich

GSG International GmbH, Eichenstr. 12, 8808 Pfaeffikon, Switzerland

Correspondence should be addressed to S. Dittrich; sven.dittrich@gsg-int.com

Fifty years ago, one of the worldwide first industrial production processes to produce fission-Mo-99 for medical use had been started at ZfK Rossendorf (now: HZDR, Germany). On the occasion of this anniversary, it is worth to mention that this original process (called LITEMOL now) together with its target concept used at that time can still be applied. LITEMOL can be adapted very easily to various research reactors and applied at each site, which maybe still of interest for very small-scale producers. Besides this original process, two further and actually proven processes are suitable as well and recommended for small-scale LEU fission Mo-99 production also. They are known under the names KSA/KSS COMPACT and ROMOL LITE and will be described below.

1. Introduction

"The IAEA's Coordinated Research Project (CRP) on "developing techniques for small-scale indigenous production of Mo-99 from low enriched uranium or neutron activation" has been working since 2005 to assist participating countries to assess, evaluate, and implement nuclear technology for producing Mo-99 without highly enriched uranium in order to meet local nuclear medicine requirements" [1]. Within that CRP, a fact-finding mission performed by experts of IAEA cooperating with other independent experts could be applied for such providing substantial help in analyzing the given situation at a research center and the country/region around. This paper describes two process technologies and one specially developed target the latter was especially suitable and proven for the use of very low enriched uranium, both supporting this CRP and its philosophy and tools at the same time.

During the sixties of last century, fission Mo-99 began its significant upturn lasting up to today ("Fission-produced ^{99}Mo (f.p. ^{99}Mo) of very high specific activity and alumina column based ^{99m}Tc generators have remained the mainstay in the field as "gold standard"." [2]), mainly due to the new cold KITs and their need of very high specific Tc-99 m solutions for labeling. About all research reactors, even those with thermal neutron flux densities down to 1×10^{13} n/(cm^{2}s),

are potential candidates for small-scale fission-based Mo-99 production covering the local or domestic demand of [^{99m}Tc] pertechnetate solutions of high specific activity for nuclear medicine diagnostic imaging procedures with homemade Tc-99 m generators. Adequate LEU targets are commercially available. An indigenous production of LEU targets as well as of very low enriched targets (0.72% ($^{nat.}$U) − 5% ^{235}U) is possible at local sites. Proven target manufacturing and Mo-99 processing technologies including waste management solutions fitting to the needs of small-scale producers are on the market, capable of establishing fission Mo-99 and Tc-99 m generator production cluster. Such clusters would allow countries and/or regions to develop indigenous production capacities to become independent from global Mo-99 market. This is especially helpful in cases of temporary world supply issues at which small generator producers and their customers suffer most. Furthermore, such initiatives will train indigenous specialists for broad applications at the national nuclear centers.

Although there are many attempts to classify research reactors [RRs], this paper will not look into those differences even if they may play a (smaller) role when irradiating uranium targets for radioisotope [RI] production. One aspect, however, is of some interest: the shape of RR-fuel, either clusters of (mostly) plates or single rods.

In terms of RI production, RRs will mainly be evaluated not only by their power density which determines the n-flux density, but also by the operation hours per week and their space which can be made available for targets to be irradiated, either in-core or at the core border or even inside the reflector.

Besides institutions which manufacture their own targets, there are target manufacturers on the market who are able to deliver proven targets suitable for the different RR types. Most common are plate-type targets with dispersion meat and Aluminum cladding and proven pin-type targets with uranium metal pellets or dispersion meat, with both Aluminum or steel cladding, all in quite different shapes. If a new target design is needed, the target has to be tested by the operator and certified by the responsible authorities.

2. Materials and Methods

Actually, there is a wide range of different target concepts for fission Mo-99 productions, mainly originating from HEU to LEU conversions of the fission targets. Still common in routine business are proven aluminum or aluminum-alloy cladded, (LEU- or HEU-) uranium aluminide or uranium alloy dispersion targets as straight plates or cylindrical—or (rarely) pin-type targets (pin-type targets are used, e.g., in RBT6 and RBT10 research reactor at RIAR, Russian Federation [3]). However, many other target concepts have been developed and undergone testing, for example, target with meats made of uranium metal foils, uranium metal pellets, uranium silicide dispersion, uranium oxide dispersion, and high density uranium aluminide dispersion.

Besides the target designs, manufacturing, and applications, during the last 50 years different processes for fission-Mo-99 production have been developed all over the world (in which each producer has its own process [4]), suited to dissolve one single or a group of similar targets, to remove all impurities out of the received Mo-99 solution, and to handle the wastes economically and safely. Alkaline and acidic solvents are in use, with or without additional oxidants and/or catalysts, in a single step or a two-step digestion. Using a two-step combination of alkaline solvent first and hydrofluoric acid with oxidant and catalyst afterwards, an ample scope of targets can be digested by one process [5], while alkaline nitrate solution has the ability to dissolute aluminum cladded, UAl_x-aluminum dispersion targets without hydrogen generation [6].

The need to convert Mo-99 production facilities worldwide from processing HEU targets to used LEU targets [7–9] has led to clearly favoring targets with high U-density [3, 10–15]. U-metal foils as targets are still struggling with encasing and handling issues [16]. The proven target with high U-density on the market is already the U_3Si_2-Al target, which can rely on a proven process as well (see below).

On occasion to the named 50th anniversary of one of the first industrial process for fission Mo-99 production [17], it is worth to have a look onto that target it started with.

2.1. Very Low Enriched Target with Uranium Metal Pellets. A decision for a small-scale fission Mo-99 production is an evident attempt to become independent from global fission Mo-99 market when trying to meet local or regional Mo-99 needs by our own capacities. Apart from the global market which did not exist in the early sixties of the last century, all these arguments remain valid for developing countries.

In this context, supply with adequate and sufficient targets is playing an important role, and an indigenous target production, if possible, seems to be the method of choice. Also, a complete technology for a closed LEU cycle is available (for details see Section 2.3.1), consisting of a proven uranium recycling process and a proven target reproduction for aluminum cladded uranium silicide dispersion targets.

As an alternative to a closed LEU cycle (LEU meaning nearly 20% enriched ^{235}U), the use of uranium metal pellets made of natural uranium or very low enriched uranium up to 5% ^{235}U is described here for two reasons, besides that, those targets can be produced easily: first, those targets had been the fundament of one of the named first industrial production processes of small-scale fission Mo-99, and secondly this target concept generally is very interesting for small-scale fission Mo-99 still using low-performance RRs with neutron flux densities down to 1×10^{13} n/(cm^{2}s). Moreover, those targets had permanently been used for around 15 years at ZfK Rossendorf (now: HZDR, Germany) [17].

Starting from metallic rods made of natural uranium (during the sixties imported from Russia, having diameters of 8.5 mm), small pellets had been manufactured on a lathe, having a thickness of 4.2 mm each. The pellets were placed in an aluminum tube with spacers of aluminum between them and at both ends, in order to get the fission heat distributed more homogenously inside the rod. This spacing of pellets had helped avoiding hot spots and providing better heat conduction to the outer surface of the Aluminum rod. After welding and leakage test(s), the target was ready for irradiation (see Figure 1).

From experiences made, very low ^{235}U enrichment should be adapted to the available thermal neutron flux density at the irradiation position. Table 1 could provide a first and very rough orientation of such adaption which is solely based on experience with heat removal out of the pellets preventing baking together with the spacers.

After irradiation and the mandatory cooling-down period, the tube can be easily cut-off and the uranium metal pellets can be separated and dissolved using an actual small-scale process like the KSS COMPACT described further down. Very high uranium density and no aluminum dissolution mean less process waste and processing of higher amounts of uranium during a certain time interval, shorter than with aluminum dispersion targets. These are reasons why even with natural uranium in moderate thermal neutron flux densities remarkable activities of fission Mo-99 can be achieved.

However, it has to be emphasized that this target as well as its processing (see Section 2.2) is basic (but proven) technology for Mo-99 production at small scale. Therefore, it should not be compared with other processes described in this paper based on dispersion targets using LEU at 20% enrichment.
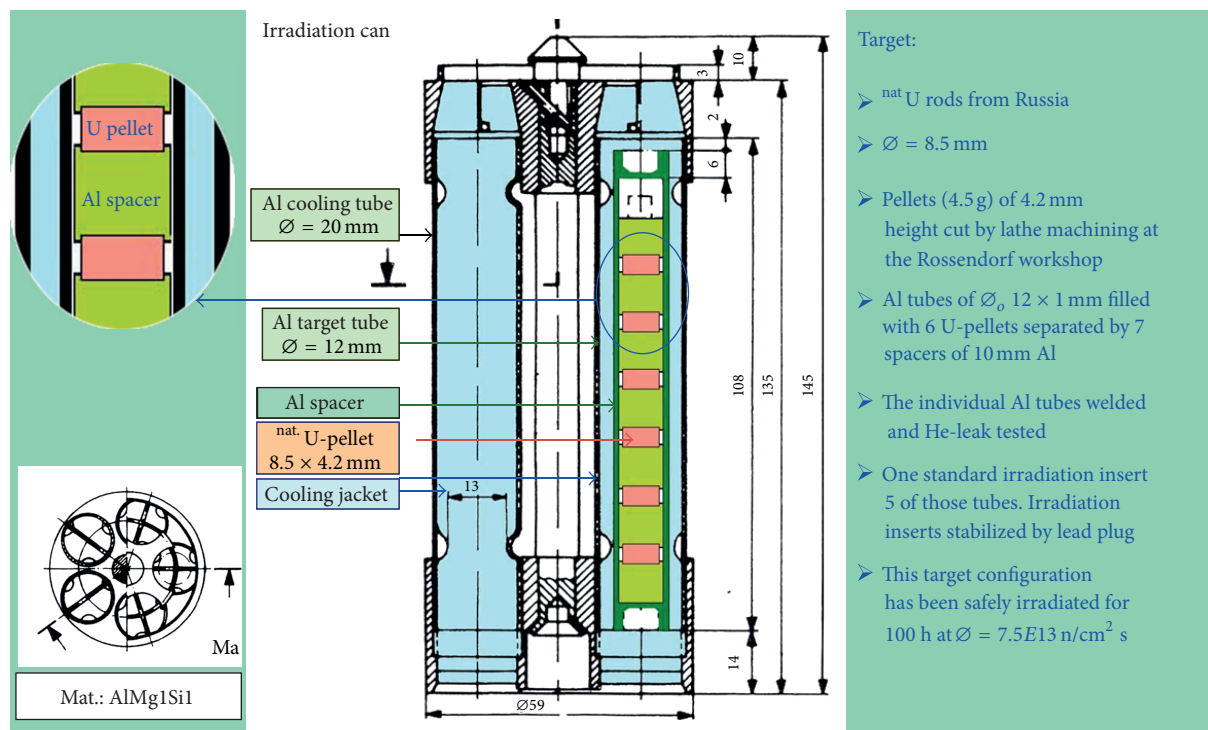
Figure 1: General design of an irradiation can with five very low enriched targets for fission Mo-99 production (taken from [18]).

Table 1: Flux density and corresponding U-enrichment for irradiation of very low enriched targets and given heat removal system capacity. Irradiating of 280 g of U-metal pellets over 100 h with subsequent 20 h cooling time and about 10 h processing time, resulting in 550–740 GBq (15–20 Ci) Mo-99 (calibrated 6 days after end of production), is expected to be delivered under given effective thermal neutron flux densities with the suggested ^{235}U enrichments.

nth-flux density [$n/(cm^2 s)$]	7E13	5E13	3E13	2E13	1E13
(^{235}U) enrichment [%]	0.7 (^{nat}U)	1.0	1.7	2.5	5.0

2.2. Historical Process: LITEMOL.

One of the first industrial processes for small-scale fission Mo-99 production had been originally developed for producing fission Te-132 to be used in Te-132/I-132 isotope generators. Under the economical restrictions during the cold war (during the early sixties of last century) and with limited availability of mainly "basic" chemicals, the process (now called LITEMOL) got the following design (see Figure 2).

This process with ~70% yield (decay corrected) [19] in combination with the very low enriched targets described above had produced enough fission Mo-99 for a country like the former German Democratic Republic (GDR) with around 17 million inhabitants under the conditions and requirements of last century's sixties and seventies. For actual need, some adaptions are necessary, but it will be possible to get this process modernised with some supplementary R&D.

2.3. Actual Processes: KSA/KSS COMPACT and ROMOL LITE.

KSA/KSS COMPACT and ROMOL LITE are small-scale adaptations of large-scale KSA/KSS (KSA/KSS are two sides of the same coin, where KS stands for KARLSRUHE-SAMEH technology developed by Sameh [20–25] at the Karlsruhe Research Center (FZK, now: KIT), Germany. This technology has been successfully used already in full-scale productions processes for uranium Aluminide dispersion targets (KSA version: KARLSRUHE-SAMEH ALUMINIDE) and for uranium Silicide dispersion targets (KSS version: KARLSRUHE-SAMEH SILICIDE, see Figure 3), but practically, all other targets can be processed with KS technology, too.) and ROMOL-99 processes, widely proven for processing plate type dispersion targets. Such proves are performed at and by (a) ROMOL-99 at Pakistan Institute of Nuclear Science and Technology (PINSTECH, Islamabad), (b) KSA at Karlsruhe Institute of Technology (KIT, formerly Forschungszentrum Karlsruhe (FZK)), Germany, and at Mallinckrodt Medical, Netherlands, (c) KSS at KIT, and (d) pin-type dispersion targets of different shapes applying ROMOL-99 at State Scientific Center-Research Institute of Atomic Reactors (RIAR), Russian Federation.

Whatever target concept will be realized for a future small-scale fission Mo-99 production facility, KSA/KSS COMPACT, using a two-step combination of alkaline solvent first and hydrofluoric acid with oxidant and catalyst afterwards, is able to dissolve almost all of these targets (In uranium metal foil targets, zinc or aluminum (instead of nickel due to its well-known resistance against hydrofluoric acid) has to be electroplated on uranium metal foils as recoil barrier and for preventing bonding with the aluminum cladding.) digesting the uranium compound to diuranate fast and under reduced pressure to extract high specific fission Mo-99 in pharmaceutical grade with ~90% yield

Irradiation, 180 g, ^{nat.} U-pellets,
Flux: 7.5E13, 100 h, 48 h cooling

Trapping Xe → ^{133}Xe

H$_2$-carrier gas
310 mL 10 M HCl → Dissolution in 310 mL
10 M HCl, dropwise → Trapping H$_2$Te → ^{132}Te/^{132}I-generator

N$_2$-carrier gas
50 mL conc. HNO$_3$ → Oxidation U^{4+} → UO$_2^{2+}$
50 mL conc. HNO$_3$ dropwise → Iodine trapping → Waste

200 mL 1 M HNO$_3$ → Evaporation-dilution
200 mL 1 M HNO$_3$

200 mL 1 M HNO$_3$
700 mL H$_2$O
100 mL 0.01 M NH$_4$OH
4 × 50 mL 2 M NH$_4$OH → Loading
Al$_2$O$_3$-column process
Washing
Elution → Liquid waste:
Uranium
Fission products

Evaporation
Sublimation

15–20 Ci Mo-99 (6 days)
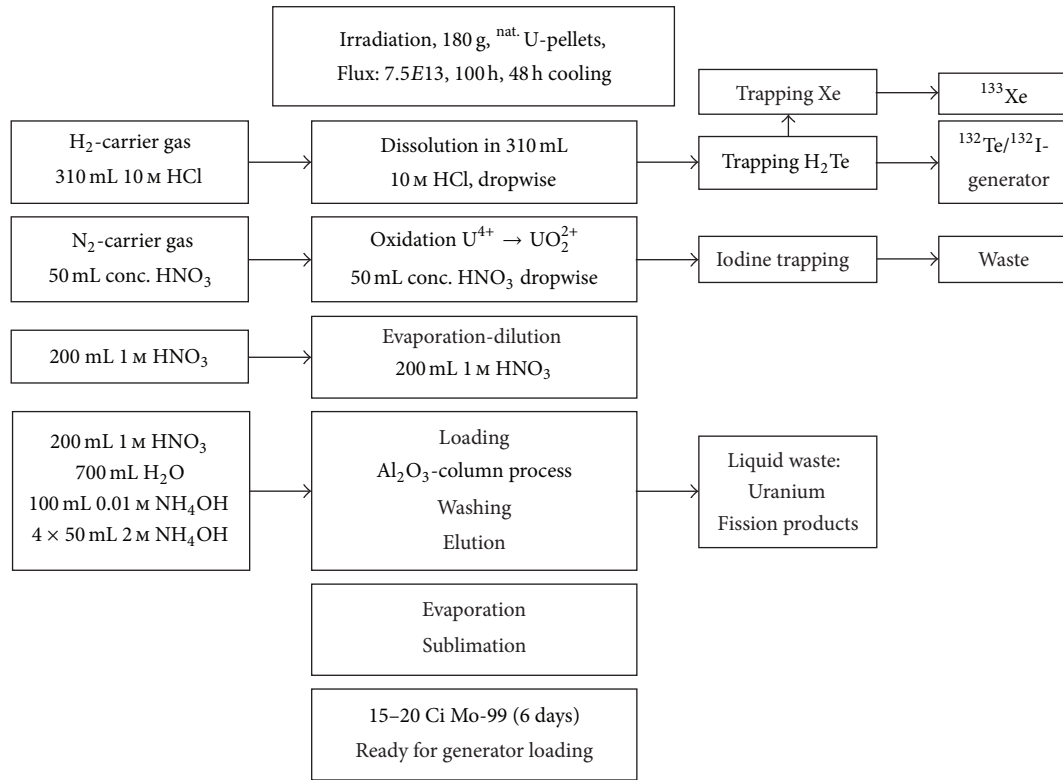Ready for generator loading

Figure 2: Process scheme (taken from [19]) describing one of the first industrial production processes for small-scale fission Mo-99 production (now called LITEMOL).
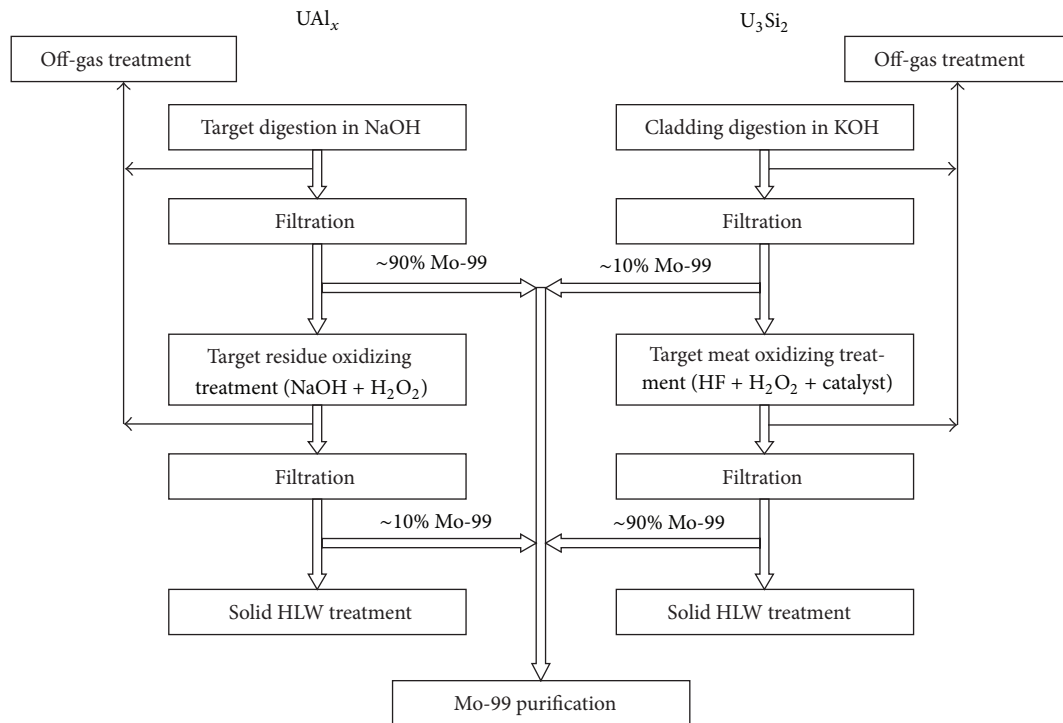
UAl$_x$ U$_3$Si$_2$

Off-gas treatment   Off-gas treatment

Target digestion in NaOH   Cladding digestion in KOH

Filtration   Filtration

~90% Mo-99   ~10% Mo-99

Target residue oxidizing
treatment (NaOH + H$_2$O$_2$)   Target meat oxidizing treatment (HF + H$_2$O$_2$ + catalyst)

Filtration   Filtration

~10% Mo-99   ~90% Mo-99

Solid HLW treatment   Solid HLW treatment

Mo-99 purification

Figure 3: Flow scheme (in detail) of KSA/KSS production process showing the chemical treatment of UAl$_x$ targets (left column) in comparison to other targets (right column, U$_3$Si$_2$ taken as example).

(decay corrected) [5] in an overall 12 h process with very low environmental impact.

On the other hand, a technology avoiding any Hydrogen generation became more and more interesting for Mo-99 producers in the last decade. For that reason, ROMOL LITE process with overall 12 h processing time had been developed as downscaled adaption of ROMOL-99 process with ~80% yield (decay corrected) [26] for dissolving LEU UAl$_x$ dispersion targets under reduced pressure and—as said—without any Hydrogen generation, using an alkaline Nitrate solution which has been already routinely used in fission Mo-99 production at PINSTECH, Pakistan [27] as well as at two large-scale fission Mo-99 production lines at RIAR, Russian Federation [3].

2.3.1. KSA/KSS COMPACT [20–25]. (This section is based on methods and processes developed by and proven under responsibility of Sameh et al. at Karlsruhe Institute for Technology (KIT) for large-scale Mo-99 production. The version for aluminum cladded UAl$_x$ dispersion targets (KSA) has been used since more than 15 years by Mallinckrodt Medical at Petten, The Netherlands, being second largest Mo-99 producer worldwide. For small-scale processes, KSA/KSS has been modified and simplified to a downscaled version called KSA/KSS COMPACT by Sameh.)

KSA/KSS process in its compact version for small-scale LEU fission Mo-99 production starts after transportation of the targets into the HC-line consisting of minimum two hot cells with a two-step digestion under reduced pressure to get target cladding completely dissolved and meat digested.

In case of aluminum or aluminum alloy cladded, uranium aluminide or uranium alloy dispersion (LEU) targets of plate- or pin-type, the proven KSA version could be the selected process. First step is a treatment in pure alkaline solution (6 m NaOH) dissolving the cladding plus digesting most of the meat of the target itself, followed by filtration. Around 90% of the Mo-99 is found in the solution. In a second step, some residues from meat material are digested in alkaline solution of hydrogen peroxide. A precipitate is filtered off (filter cake) consisting of uranium (as diuranate) and the bulk of other impurities (e.g., actinides and group II, III, IV, V, and VI elements).

In case of any other target concept, especially when using the available U$_3$Si$_2$-Al LEU targets with the so far highest U-density of all proven plate-type targets, KSS version of that process is considered as favorable solution for gain-based facilities.

In the KSS version of the described process, the first dissolution step is a treatment in pure alkaline solution using Potassium Hydroxide (6 M KOH) instead of sodium Hydroxide followed by filtration. Some Mo-99 will be found in the solution, but most of it remains in the nondissolved residue of the meat, which is treated in a second step with 5 M hydrofluoric acid supplemented by 7.5% hydrogen peroxide and halogen catalyst (0.02 M KIO$_4$).

Under reduced pressure, a smooth carrier gas stream (e.g., helium) takes all gaseous fission products and generated hydrogen out of the dissolvers passing a Copper-(II) oxide
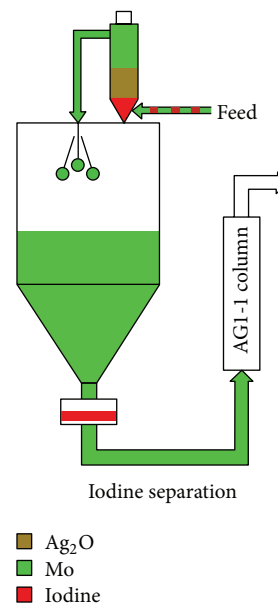

FIGURE 4: Separation of Iodine (taken from [23]) using a floating bed of hydrated Silver oxide and a filter, KSA/KSS process.

oven (for complete oxidization of hydrogen to water) with condenser (for drying the gaseous stream) into a vacuum tank for intermediate storage. After End of Production, the vacuum tank is evacuated for the next production and the gaseous fission products (mainly Xenon-isotopes) are retained on a battery of Charcoal columns cooled to 15°C, for decay. Alternatively, the radioxenon could be separated from the gaseous mixture for further use.

The acidic solution from the second digestion step of other than UAl$_x$ aluminum dispersion targets will be alkalized to 2-3 M KOH and some hydrogen peroxide is added before merging the two solutions from both digestion steps. Thus, after destroying some excess of hydrogen peroxide by boiling, alkaline solutions with some hydrogen peroxide added after filtration is the vantage for Mo-99 purification.

The subsequent Mo-99 purification is the same with KSA and KSS version of that process, independently from the targets mentioned. This is the main reason for putting both variants together as KSA/KSS process. The purification is started with Iodine separation on a floating bed of hydrated silver oxide, followed by four chromatographic steps and ending up in a high temperature treatment in Platinum crucibles. Solid waste (mainly filter cake and tubes) is locked out, taking the same way back which the targets came. Liquid waste is pumped into tanks below the hot cells for intermediate storage.

Alkaline filtrate of digested targets feeds a floating bed of hydrated silver oxide. The silver oxide is reduced by hydrogen peroxide to fine particles of silver metal and Iodine is strongly adsorbed on the silver surface. Bigger particle stays in the floating bed, smaller ones will be filtered off (see scheme of Figure 4). The silver metal/silver iodide mixture is ready for an easy fission-Iodine-131 production taking place in a separate hot cell or will be stored for decay, while
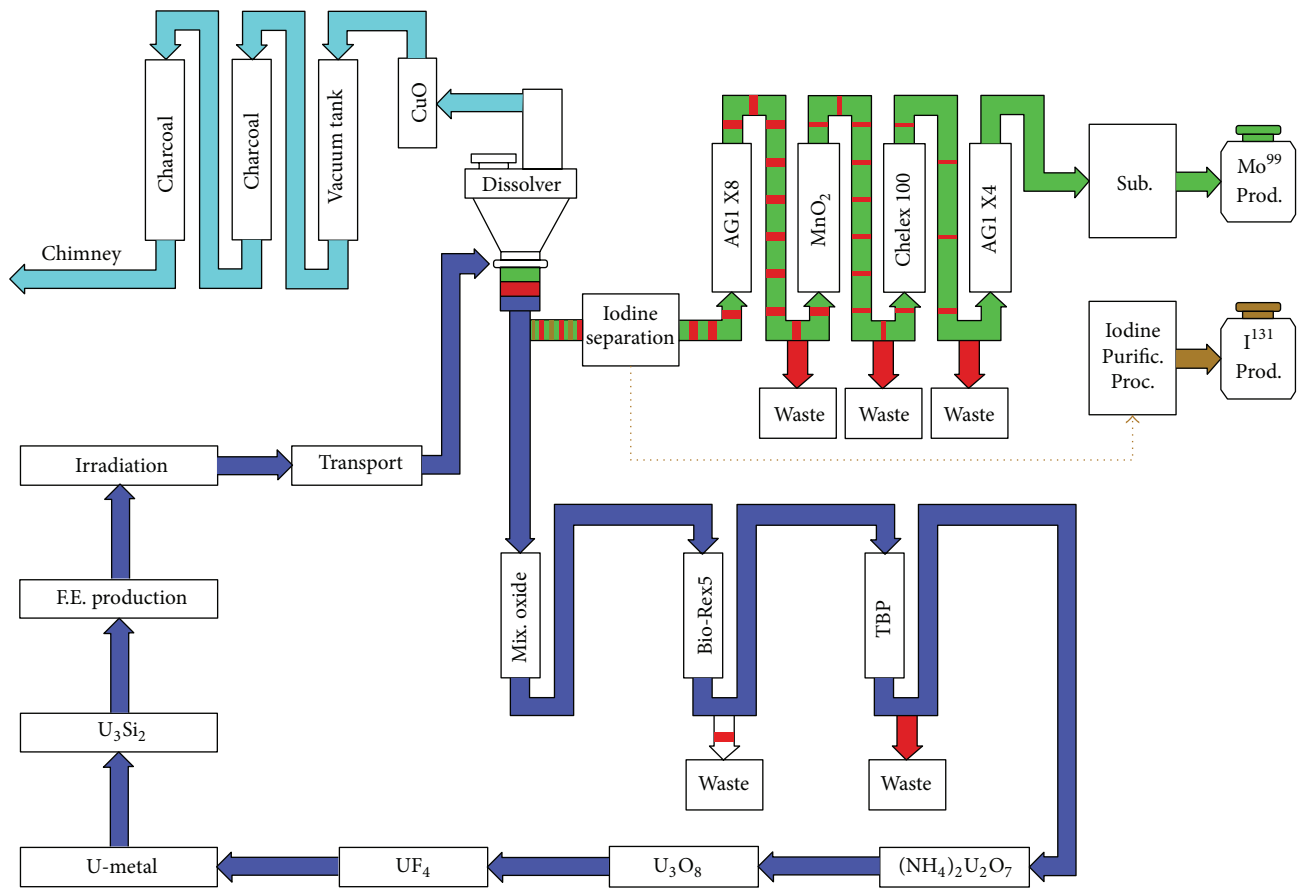
FIGURE 5: Process scheme of complete and closed KSS process variant (taken from [23]), completely proven with U_3Si_2-Al dispersion targets.

the filtrate feeds the first chromatographic column (AG1-X8, OH^--form, 200–400 mesh, Bio-Rad, USA), where Mo-99 is quantitatively retained as Molybdate. The feed solution is collected in an intermediate storage tank as liquid high-level waste (HLW).

AG1-X8 column is washed with 3 M KOH and molybdenum elution is carrying on using a 2 M sodium nitrate solution containing 1 M Nitric acid. This solution feeds the manganese dioxide column (hydrated manganese oxide, $MnO_2 \times nH_2O$, particle size of 0.2 to 0.5 mm (finer particles being removed by aqueous sedimentation)). In that column Mo-99 is quantitatively retained together with accompanying fission products, while all anionic species and the alkaline cations are removed with the feed solution and sucked into a slightly-evaporated intermediate storage tank for liquid low and intermediate level waste.

After washing the column with 1 M nitric acid and distillated water, the whole manganese oxide bed together with the molybdenum adsorbed is dissolved by a solution of 2 M Sulfuric acid supplemented by 0.2 M ammonia thiocyanate, 0.05 M sodium sulphite, and 0.001 M potassium iodide.

A Chelex 100 column is fed with that manganese oxide solution. Chelex 100 is a styrene divinylbenzene copolymer with iminodiacetate functional groups. Depending on the conditions, Chelex 100 can be used as weak cationic as well as

weak anionic exchanger. From the acidic solution, molybdenum is retained quantitatively as negatively charged molybdenum hexathiocyanato complex $[Mo(SCN)_6]^{3-}$, while manganese ions and fission product species are not adsorbed. The column is washed by Sulfuric acid supplemented by 0.2 M ammonia thiocyanate, pure Sulfuric acid, and water.

Molybdenum is easily desorbed from Chelex 100 under oxidizing alkaline conditions as Molybdate-(VI), with Chelex 100 meanwhile acting as a weak cationic exchanger. The desorption is carried out with sodium hydroxide solution containing some hydrogen peroxide which is becoming the feed solution for the last chromatographic column filled with AG1-X4 (OH^--form, 200–400 mesh, Bio-Rad, USA). This column is used for the desalination of the Mo-solution by washing with water before eluting the Mo-99 with Nitric acid to avoid the formation of mixed oxides with molybdenum.

The nitric acid solution of molybdenum is evaporated to dryness and subsequently the Mo(VI)-oxide sublimated at 1000°C in Platinum crucibles and condensed in a quartz condenser. This high temperature treatment ensures complete destruction of all organic impurities introduced during the process and eliminates possibly introduced corrosion products such as Iron, nickel, cobalt, or chromium by burning them to the so-called highly burned oxides. Mo(VI)-oxide
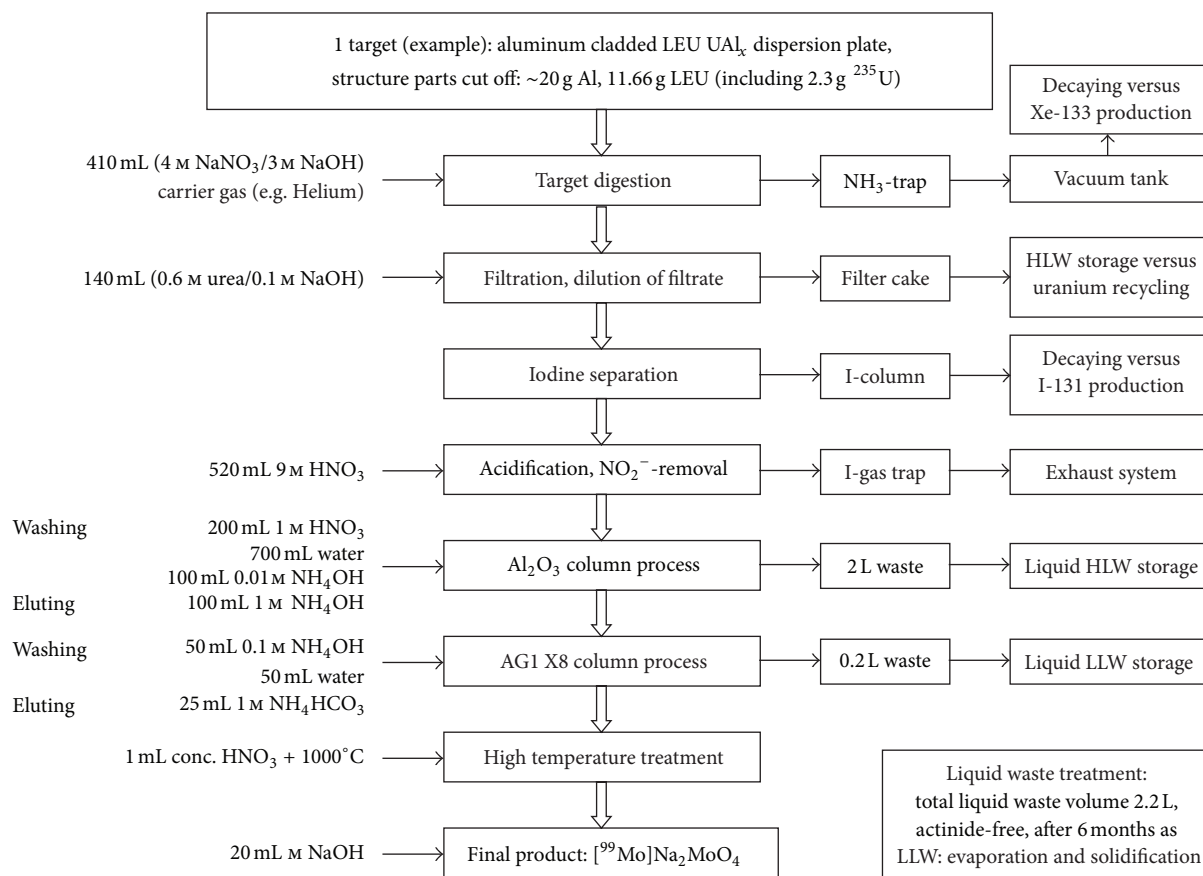
FIGURE 6: Process scheme for ROMOL LITE, example using one commercially available target plate. The processing of several plates is of course possible.

is dissolved in ammonia and finally adjusted with sodium hydroxide, while the ammonia is evaporated as very last step.

Due to the very low burn-up in LEU targets for small-scale fission Mo-99 productions, own target production based on a complete uranium recycling process might/should be considered. Figure 5 depicts the scheme of a closed process completely proven for U_3Si_2-Al dispersion targets being operated at KIT, Germany.

The off-gas treatment (described above), within KSA/KSS process which is used with the KSA version of the process by Mallinckrodt Medical at Petten under a KIT license for more than 15 years, is a unique technique leading to more than three orders of magnitude lower radioxenon release in comparison to other large-scale fission Mo-99 producers [28].

The idea of a worldwide voluntary limitation of radioxenon release to 5 GBq/day generated at WOSMIP [29, 30] for all Mo-99 producers is a reality for the operation at Petten site since 15 years—an advantage which certainly is as well available with the compact version foreseen for small-scale LEU fission Mo-99 producers.

2.3.2. ROMOL LITE. ROMOL LITE is the downscaled ROMOL-99 process; the latter developed and was proven for large-scale fission Mo-99 production comprising the special feature of dissolving UAl_x-Al dispersion targets without

hydrogen generation, but being limited to distinctly lower dense UAl_x-Al LEU targets than the a.m. KSS COMPACT process (see Figure 6).

Using alkaline solution (3 M sodium hydroxide) of 4 M sodium nitrate, the target(s) will be completely digested under reduced pressure at $(70 \pm 10)°$C. A smooth carrier gas stream (e.g., Helium) takes all gaseous fission products and generated ammonia out of the dissolver through an ammonia trap (filled with 5 M Sulfuric acid) and a condenser (to dry the gaseous stream) into a vacuum tank for intermediate storage. After end of production, the vacuum tank is evacuated again for the next production and gaseous fission products (mainly Xenon isotopes) are retained for decay on a battery of flasks filled with suitable zeolite.

A precipitate consisting of uranium (as di-uranate) and a bulk of other fission impurities (e.g., actinides and group II, III, IV, V, and VI elements) is filtered off. After decay of short lived isotopes (6 months after end of production) in a separate intermediate solid HLW storage at site, 99.4% activity of all wastes is accumulated in the filter cake, canned for long-term solid HLW storage (or used for re-cycling) in tight stainless steel boxes, while only 0.6% of the activity remains in the liquid ILW or LLW for further waste management [18].

Subsequently, the Mo-containing filtrate passes through a column filled with silver-coated acidic alumina [31] for

separation of Iodine isotopes and is acidified to 0.4 M Nitric acid afterwards. After adding on some urea, the solution is boiled under reflux to convert any nitrite into nitrogen.

Cooled down to ambient temperature, that acidic solution feeds an alumina column (aluminum oxide 90 active acidic (0.063–0.200 mm), Merck, Germany), where Mo-99 is absorbed as molybdate-VI. Washed first with 1 M nitric acid, water and 0.01 M ammonia, Mo-99 is eluted with 1 M ammonia.

That ammoniac eluate feeds the AG1 X8 column (AG1-X8, OH⁻-form, 200–400 mesh, Bio-Rad, USA) adsorbing molybdate-VI. After washing with water, molybdenum is desorbed by 1 M ammonium bicarbonate.

After adding some 1 m nitric acid, the solution is boiled and evaporated for destroying any organic impurities. Typically and at that stage already, the final product meets all requirements and is therefore solved in the solvent of choice, usually diluted sodium hydroxide. For getting rid of any impurities potentially having remained in the product, an optional high temperature treatment could be applied.

3. Results and Discussion

A widely variable adaption of both of the processes, KSA/KSS COMPACT and ROMOL LITE, to local conditions and requirements is possible despite their original design/development for large-scale production predominantly. Both being proven, first efforts have been made to scale them down during the last years. Thus, their scope of application now covers all sizes of production, from very small scale to very large scale. As an option, production supplemented by a complete uranium cycle (uranium recycling and target production on site) is well proven available, too.

A long-term proven target for natural or very low enriched uranium has been described. The use of uranium metal pellets and the possibility to separate the uranium from the aluminum spacers and the aluminum canning after irradiation allow small-scale production of remarkable activities of fission Mo-99 in RRs with thermal neutron flux densities down to about 1×10^{13} n/(cm²·s).

These technologies should enable operators of RRs of moderate performance to envisage production of indigenous fission Mo-99 for their countries/regions, in order to become independent from global market and to give their engineers and scientists an additional long-term perspective in their countries.

4. Conclusions

50 years ago, one of the worldwide first industrial production processes able to produce fission Mo-99 for medical use had come to life at ZfK Rossendorf (now: HZDR, Germany). It is around the occasion of this anniversary that original process (called LITEMOL now) together with its target concept used that time has been revived. The original target concept can be easily adapted to the conditions and needs of different research reactors and easily produced at their sites. Both process and target still may be of interest for very small-scale

producers of Mo-99, provided that some slight adaptions to the actual requirements have been performed. In order to deliver a complete picture of the possibilities of small-scale production in our days, the two proven and actually applied processes downsized for the so-called small-scale LEU fission Mo-99 production have been described in detail as well: KSA/KSS COMPACT and ROMOL LITE.

References

[1] I. N. Goldman, N. Ramamoorthy, and P. Adelfang, "Fostering new sources of Mo-99 for international nuclear medicine needs: the contribution of the IAEA coordinated research project on Molybdenum-99 production from LEU or neutron activation," in *Proceedings of the RETR International Meeting on Reduced Enrichment for Research and Test Reactors*, Washington, DC, USA, October 2008.

[2] N. Ramamoorthy, "Production and supplies of ⁹⁹Mo: lessons learnt and new options within research reactors and neutron sources community," in *Proceedings of the IAEA International Conference on Research Reactors*, Rabat, Morocco, November 2011.

[3] R. Kuznetsov and A. Svyatkin, "Mo-99 production at JSC "SSC RIAR": status, LEU conversion plan," in *Proceedings of the IAEA 1stCoordination Meeting on INT1056: Supporting Small Scale, Non-Highly Enriched Uranium (Non-HEU) Molybdenum-99 Production Capacity for Nuclear Medicine Applications*, Vienna, Austria, February 2013.

[4] G. F. Vandegrift, C. Conner, J. Sedlet et al., "Progress in chemical processing of LEU targets for ⁹⁹Mo production 1997," in *Proceedings of the International RERTR Meeting*, Jackson Hole, Wyo, USA, October 1997.

[5] A. A. Sameh, *Private Communication*, 2013.

[6] S. Dittrich, "Turn-key customized non-HEU fission Mo-99 production facilities (Small Scale)," in *Proceedings of the IAEA 1st Coordination Meeting INT1056: Supporting Small Scale, Non-Highly Enriched Uranium (Non-HEU) Molybdenum-99 Production Capacity for Nuclear Medicine Applications*, Vienna, Austria, February 2013.

[7] P. Staples, "GTRI Mo-99 Program," in *Proceedings of the IAEA 1st Coordination Meeting INT1056: Supporting Small Scale,*

Non-Highly Enriched Uranium (Non-HEU) Molybdenum-99 Production Capacity for Nuclear Medicine Applications, Vienna, Austria, February 2013.

[8] M. A. Pomper, "Time for an international commitment to end use of HEU for Mo-99," in *Proceedings of the Mo-99 Topical Meeting*, Chicago, Ill, USA, April 2013.

[9] M. Ahmad, "Molybdenum-99/technetium-99m management: race against time," *Annals of Nuclear Medicine*, vol. 25, no. 9, pp. 677–679, 2011.

[10] G. Ball, "Status update on the ^{99}Mo HEU/LEU conversion project in South Africa," in *Proceedings of the Mo-99 Topical Meeting*, Chicago, Ill, USA, April 2013.

[11] R. W. Brown, "Update on Mallinckrodt's low-enriched uranium (LEU) conversion project," in *Proceedings of the Mo-99 Topical Meeting*, Chicago, Ill, USA, April 2013.

[12] H. J. Ryu, M. S. Sim, J. M. Nam, S. J. Jang, C. K. Kim, and J. M. Park, "Characterization of dispersion Mo-99 targets using atomized powder," in *Transactions from European Research Reactor Conference*, pp. 69–74, Saint Petersburg, Russia, 2013.

[13] M. Ciocanescu and G. F. Vandegrift, "High density LEU annular target qualification," in *Proceedings of the Mo-99 Topical Meeting*, Chicago, Ill, USA, April 2013.

[14] V. Host, "Progresses on IRE's LEU conversion program," in *Proceedings of the Mo-99 Topical Meeting*, Chicago, Ill, USA, April 2013.

[15] G. F. Vandegrift, C. Conner, S. Aase et al., "RERTR progress in Mo-99 production from LEU," in *Proceedings of the 6th International Topical Meeting Research Reactor Fuel Management (RRFM '02)*, Gent, Belgium, March 2002.

[16] J. Creasy, "Update on the development, testing, and manufacture of high density LEU-foil targets and processing for the production of Mo-99," in *Proceedings of the Mo-99 Topical Meeting*, Chicago, Ill, USA, April 2013.

[17] O. Hladik, K. Jantsch, and G. Wagner, "Entwicklung der spaltproduktproduktion im ZfK rossendorf," *Isotopenpraxis*, vol. 19, no. 12, pp. 409–411, 1983.

[18] G.-J. Beyer, "German experiences in fission-based Mo-99 and recent revitalization by GSG," in *Proceedings of the Technical Meeting on Developing Techniques for Small Scale Indigenous Molybdenum-99 (Mo-99) Production Using Low Enriched Uranium (LEU) Fission or Neutron Activation*, Santiago, Chile, November 2010.

[19] D. Novotny and G. Wagner, "Procedure of small scale production of Mo-99 on the basis of irradiated natural uranium metal as target," in *Proceedings of the Consultants Meeting on "Small Scale Production of fission Mo-99 for Use in Tc-99m Generators"*, IAEA, Vienna, Austria, July 2003.

[20] W. Leifeld and A. A. Sameh, "Method for separation of molybdenum, USA 5.508.010," Patent DE4231955 (1994), 1996.

[21] A. A. Sameh, "Production of fission Mo-99 from LEU uranium silicide target materials," in *Invited Papers on Symposium on Isotope and Radiation Applications*, pp. 111–135, R.O.C, Lung-Tan, Taiwan, May 2000.

[22] A. A. Sameh, "Advances in Minimization of Fission Gas Release and Nuclear waste from Large Scale Fission Mo-99 Production Facilities," in *Proceedings of the Workshop on Signatures of Medical and Industrial Isotope Production (WOSMIP '09)*, Strassoldo, Italy, July 2009.

[23] A. A. Sameh, "Minimization of fission nuclide release from large-scale Mo-99 production facilities by combining processing and off gas handling technology," in *Proceedings of the Workshop on Signatures of Medical and Industrial Isotope Production II (WOSMIP II '11)*, Strassoldo, Italy, June 2011.

[24] Z. I. Kolar, W. J. C. Okx, and J. L. Kloosterman, "Assessment of molybdenum-99 production from high-enriched uranium (HEU) targets in comparison with that from low-enriched uranium (LEU) targets," Report, Delft University of Technology, Interfaculty Reactor Institute, Delft, Netherlands, 2002.

[25] A. A. Sameh and H. J. Ache, "Production techniques of fission molybdenum-99," *Radiochimica Acta*, vol. 41, pp. 65–72, 1987.

[26] R. Kuznetsov, *Private Communication*, RIAR, Dimitrovgrad, Russia, 2013.

[27] M. Ahmad, "Production of molybdenum-99 at PINSTECH, Islamabad," in *Proceedings of the IAEA Technical Meeting on Developing techniques for small scale indigenous Molybdenum-99 (Mo-99) production using low enriched uranium (LEU) fission or neutron activation: Specific waste and quality issues*, Santiago, Chile, November 2010.

[28] M. Matthews, P. Saey, T. Bowyer et al., "Workshop on signatures of medical and industrial isotope production—a review," PNNL 19294, 2010.

[29] I. M. Cameron, "Engagement between the medical isotope production and the nuclear explosion monitoring communities," in *Proceedings of the Mo-99 Topical Meeting*, Chicago, Ill, USA, April 2013.

[30] T. W. Bowyer, R. F. Kephart, P. W. Eslinger, J. I. Friese, H. S. Miley, and P. R. Saey, "Maximum reasonable radioxenon releases from medical isotope production facilities and their effect on monitoring nuclear explosions," *Journal of Environmental Radioactivity*, vol. 115, pp. 192–200, 2013.

[31] M. V. Wilkinson, A. V. Mondino, and A. C. Manzini, "Separation of iodine produced from fission using silver-coated alumina," *Journal of Radioanalytical and Nuclear Chemistry*, vol. 256, no. 3, pp. 413–415, 2003.

Research Article

Evaluation of ^{99}Mo and ^{99m}Tc Productions Based on a High-Performance Cyclotron

J. Esposito,[1] G. Vecchi,[1,2] G. Pupillo,[2] A. Taibi,[2] L. Uccelli,[3] A. Boschi,[3] and M. Gambaccini[2]

[1] *INFN, Laboratori Nazionali di Legnaro (LNL), Via dell'Università 2, 35020 Legnaro, Italy*
[2] *Dipartimento di Fisica, Università di Ferrara and INFN, Sezione di Ferrara, Via Saragat 1, 44122 Ferrara, Italy*
[3] *Dipartimento di Morfologia, Chirurgia e Medicina Sperimentale, Università di Ferrara e INFN, Sezione di Ferrara,*
Via Luigi Borsari 46, 44121 Ferrara, Italy

Correspondence should be addressed to J. Esposito; juan.esposito@lnl.infn.it

Following preliminary feasibility studies which started at Legnaro National Laboratories (LNL) in 2011, the Italian National Institute for Nuclear Physics (INFN) research activities are underway aiming at the alternative, accelerator-driven, ^{99}Mo / ^{99m}Tc production routes. One of the most promising approaches is to use ^{100}Mo-enriched (i.e., >99%) molybdenum metallic targets, bombarded with high-beam-current, high-energy proton cyclotrons. In order to get a comprehensive map of radionuclides expected, a detailed theoretical investigation has been carried out using the TALYS-TENDL 2012 excitation functions extended up to (p,6n), (p,p5n), and (p,2p4n) levels. A series of quality parameters have thus been calculated both at the end of beam (EOB) and at longer times. Results point out that accelerator-^{99}Mo is of limited interest for a possible massive production because of the quite low specific activity with respect to reactor-^{99}Mo. Accelerator-^{99m}Tc quality parameters (i.e., radionuclidic purity (RNP), isotopic purity (IP), and specific activities) calculated are instead quite close to the generator-Tc. Calculations at 15, 20, and 25 MeV have thus been performed to assess the best operative irradiation condition for ^{99m}Tc production while minimizing both the short-lived and long-lived Tc contaminant radionuclides. Although present in minimum quantities, Tc contaminants may indeed have an impact either on the pharmaceutical labeling procedures or on contributing to patient radiation dose during the diagnostic procedures.

1. Introduction

Nearly 80% of the radioisotopes used in nuclear medicine are currently produced by nuclear reactors. Among them, ^{99m}Tc (6.01 h half-life), a decay product of ^{99}Mo (65.94 h half-life), is the most important and widely used one. However, such a vital radionuclide is mainly supplied by two production facilities only, which cover about 65% of the ^{99}Mo world demand: the research reactor NRU at Chalk River, Ontario (Canada), and the HFR reactor at Petten (The Netherlands). The current ^{99}Mo mass production is indeed based upon the isotope separation from fission products by using the highly enriched uranium, weapons-grade (HEU-WG) material (^{235}U enrichment > 80%). Such a production is therefore subject to the strict international regulations and control actions against the proliferation of nuclear weapons. Both reactors have experienced in recent years (2009-2010) some long-scheduled/unscheduled shutdowns, which caused a temporary shortage of ^{99}Mo/^{99m}Tc radionuclides on the international market in 2010. Such an event has thus pushed new ideas about alternative arrangements, all based on accelerators, as well as making use of nonstrategic materials.

Since the early 1970s, ^{99m}Tc production through accelerator systems was demonstrated feasible, as proposed first by Beaver and Hupf [1], mainly by the ^{100}Mo(p,xn) reaction route. However, both excitation functions and production yields, due to the different Tc isotopes and isomeric states generated, still need to be made clearer. That is because of an unexpected spread in results, obtained over the past 40 years in different experimental campaigns. Results provided in the last 20 years, using nonstandard experimental procedures, and reported in different works [2–13] may give an idea about that and explain why further experimental investigations are demanded.

Moreover, labelling efficiency and biodistribution studies of some interesting radiopharmaceuticals have been recently carried out, using both cyclotron- and generator-produced ^{99m}Tc, as reported by Urbano et al. [14], Guérin et al. [15], and Targholizadeh et al. [16]. Such encouraging results have driven the first study aimed at the assessment of irradiation conditions for accelerator-based Tc production, as discussed by Celler et al. [17]. Based on the excitation functions from theoretical nuclear models, both the ^{99m}Tc production yields and a reduced map for other radioactive and long-lived generated isotopes (considering some simplified assumptions and constraints) have been determined.

In the framework of the (Laboratory of Radionuclides for Medicine) (LARAMED) project, funded by the Istituto Nazionale di Fisica Nucleare (INFN), a possible future supply of a set of radioisotopes in Italy, aimed at both research and medical application purposes, has been taken into account. This project derives from the installation at LNL in the near future of a high-performance cyclotron (proton output energy tunable in the range 35–70 MeV, maximum beam current 500 μA).

Taking into account the wide range of irradiation conditions which will be provided by such an accelerator, a theoretical assessment study has been preliminary carried out for both ^{99}Mo and ^{99m}Tc productions. Assuming a ^{100}Mo-enriched molybdenum metallic target, as currently available on the isotopes and pure materials market, a beam power areal density of 500 W/cm^2 and a beam current up to 500 μA, a series of parameters have been calculated for.

(i) *Optimal Molybdenum Layer Thickness.* Two basic configurations have been taken into account; in option 1, the incident beam energy down to the threshold for the reaction is considered, thus avoiding the useless heating due to the Bragg peak (i.e., thick target configuration). In option 2, a recommended thickness based on the estimation of yield distribution versus beam penetration depth is instead analyzed. In such a way, an optimized radionuclide production (i.e., avoiding the drop-off region because of cross section lowering) is achieved, with the minimum required thickness for the isotope-enriched material (not inherently thick target configuration).

(ii) *Different Proton Energies.* Taking advantage from the cyclotron directly tunable beam output energy, the reference cases at 40 and 70 MeV have been taken into account for ^{99}Mo production. ^{99m}Tc direct production at 15, 20, and 25 MeV has instead been investigated, in order to limit the amount of contaminant isotopes. Supposing, as reference, an energy degrader device made of 3.67 mm carbon layer, beam energy may be shifted from 35 MeV (i.e., the minimum cyclotron output energy) down to 20 MeV. In such a case, an approximate Gaussian energy spread ($\pm3\sigma$) of about ±1.25 MeV occurs. However, 90% of beam current (i.e., 450 μA) is within an energy window of just ±550 KeV which, through a Wien filter (if necessary), may be driven towards the target station at the accelerator beam exit.

(iii) *Different Irradiation Times.* 12 h, 24 h, and full saturation ($T_{irr} \sim 21$ d) for ^{99}Mo production, while several short irradiation times up to one half-life (i.e., 1 h, 2 h, 3 h, and 6 h) have been taken into consideration in case of ^{99m}Tc production. Irradiation times longer than $t_{1/2}$ are not convenient from the point of view of either the product final cost or the accumulation of useless longer-lived isotopes.

The isotopic composition of the enriched metallic molybdenum material, taken as reference in this study, is the one provided by the ISOFLEX company [18]: ^{100}Mo (99.05%), ^{98}Mo (0.54%), ^{97}Mo (0.07%), ^{96}Mo (0.11%), ^{95}Mo (0.10%), ^{94}Mo (0.05%), and ^{92}Mo (0.08%). The reaction yields for each Mo isotope have been estimated from the theoretical excitation functions leading to nuclei both in isomeric and ground states. For all nuclides, either directly produced following different reaction routes or generated as a decay product in any of the decay chains, the cumulative yields have been calculated.

Considering the direct ^{99m}Tc production, particular attention must indeed be paid to Tc contaminant radionuclides by reaction routes opened up by all Mo isotopes because of the same chemical species. Although present in rather low quantities, their contributions (except ^{100}Mo) are however not negligible in the overall yield estimation of accelerator-produced Tc. Optimal irradiation conditions (i.e., energy intervals, beam current, and irradiation time) are therefore needed in order to minimize their production. Finally, the long-lived ^{97g}Tc, ^{98}Tc, and ^{99g}Tc, having large cross sections and mean lives longer than 10^5 years, need to be produced in as low quantities as possible, having a direct impact on the specific activity of the final product and thus on the labelling procedures of the radiopharmaceutical preparation. Care has also to be taken of the productions of shorter-lived Tc isotopes (mainly ^{96}Tc) because of their contribution to extra radiation dose. However, such an issue is strictly related to the isotopic material composition made available by the supplier, rather than an optimal combination of irradiation time-beam energy parameters.

2. ^{99}Mo and ^{99m}Tc Production Routes

The ^{99}Mo mass production using the commercial proton-driven accelerators currently available, or next to be put into operation (as the one which will be installed at LNL), is known to be hardly achieved through neutron reaction routes, that is, using either the spallation reactions on heavy target systems or the relatively low energy beams driven by high intensity accelerators on light targets, as argued by Froment et al. [19] and Abbas et al. [20]. The radiative capture reaction (n,γ) on ^{98}Mo-enriched samples would provide ^{99}Mo production with good purity level. However, the resulting specific activities estimated and experimented are too low for a feasible massive production, even if 90% of neutrons are slowed down in the ^{98}Mo resonance energy interval (1–100 eV) [19, 20]. Moreover, exploiting the other possible (n,2n) inelastic scattering reaction on ^{100}Mo-enriched

samples, the limited neutron flux makes the expected ^{99}Mo production level poor. Some works are under way, as reported by Nagai and Hatsukawa [21] and Minato [22], although the approach followed to work out the low ^{99}Mo specific activity is to get the ^{99m}Tc through a thermal-induced sublimation of technetium from the irradiated molybdenum bulk targets.

On the other hand, the ^{235}U(n,f) ^{99}Mo fission reactions, that is, the subcritical version of the standard reactor-based route using accelerator-driven neutron multiplier systems, have also to be considered as long-term solutions because of the lack of information on production yields and economics, as discussed in NEA report [23]. For such reasons, only the proton-induced reactions ^{100}Mo(p,pn) ^{99}Mo and ^{10}Mo(p,2n) ^{99m}Tc are taken into account in the present study, being the best short-term solution to the possible future massive supply. The current cyclotrons have indeed the required beam current to ensure a high production level of these vital isotopes.

2.1. ^{99}Mo Production Route: The (p,pn) Reaction on ^{100}Mo.
^{99}Mo production may derive from two reaction routes: the main (p,pn) reaction and as a decay product of ^{99m}Nb ($t_{1/2} \simeq$ 15 s) and ^{99g}Nb ($t_{1/2} \simeq 2.5$ m), due to the additional (p,2p) reaction, when operating at proton beam energies above 10 MeV. Figure 1 shows a collection of the ^{100}Mo(p,pn) ^{99}Mo experimental excitation functions measured in the last two decades.

As can be observed, results are consistent up to $\approx$ 25 MeV, while at higher proton energies an unusual spread (i.e., uncertainty band) up to 100 mb (including error bars extension) may be noted among results obtained in different experimental campaigns. Moreover, even considering 100% of ^{100}Mo-enriched samples, additional reaction routes for the production of different Tc, Mo, and Nb isotopes (including Zr in case of a real $\geq$99% ^{100}Mo-enriched material) are already opened at proton energies higher than 10–15 MeV. The theoretical excitation functions available from the TENDL 2012 library [24] about the other Mo and Nb isotopes, yielded by other open reaction routes on ^{100}Mo, are shown in Figures 2 and 3, up to the (p,p5n) and (p,2p4n) levels, respectively. When available, experimental measurements are plotted as a benchmark.

Although predictions about the excitation functions for some reaction routes still need to be experimentally validated in the entire energy range, we are aware that a production of these nuclides is indeed energetically feasible. Nb and Tc isotopes expected to be yielded by open reaction routes on ^{100}Mo isotope only, are listed in Table 1 as reference, including decay modes. Similar considerations have been performed for the remaining Mo isotopes included in the enriched molybdenum material as well, in order to determine the whole list of nuclides (both stable and radioactive) generated by open reaction routes. The long-lived radioisotopes created, like ^{95}Nb and ^{96}Nb, ^{95m}Tc, ^{96g}Tc, ^{97}Tc, ^{98}Tc, and ^{99g}Tc, are however not considered to be a concern in the following chemical processing aimed at the preparation of
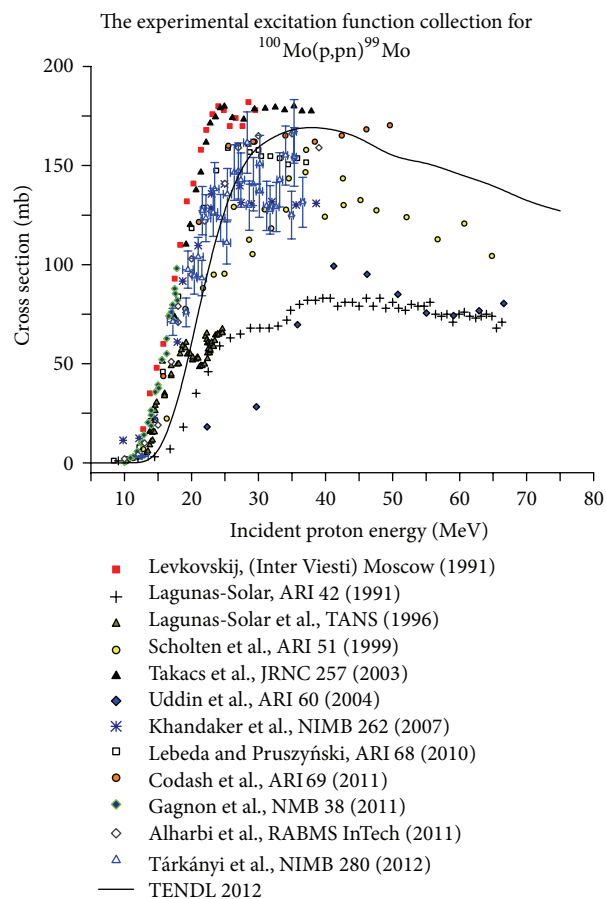

FIGURE 1: The collection of ^{100}Mo(p,pn) ^{99}Mo excitation functions experimentally measured in the last two decades. Error bars are shown for the most recent measurement only performed by Tárkányi (2012) [13]. The most recent theoretical excitation function by the TENDL 2012 library is also shown [24].

^{99}Mo/^{99m}Tc generator. The Nb, Tc, and even Rb elements may indeed be easily chemically separated from Mo for later reuse.

2.2. ^{99m}Tc Production Route: The (p,2n) Reaction on ^{100}Mo.
The excitation function ^{100}Mo(p,2n) ^{99m}Tc has been repeatedly measured over the past 40 years in different experimental campaigns (part of them shown in Figure 4), proving that within the energy range from 5 up to 70 MeV a single peak is present, centered around 15 MeV and estimated to be about 300 mb by Levkovskij [1] twenty years ago. The measurements repeated later by Scholten [4], Takacs et al. [5], and Khandaker et al. [7] have reduced such a value to about 200 mb. More recent evaluations point out higher peak values, about 250 mb, as reported by Lebeda and Pruszyński [9] and Tárkányi [13], later increased up to 300 mb by Gagnon et al. [12]. Even higher cross section peak values (i.e. >350 mb), originally measured by Lagunas-Solar et al. [11], more recently repeated by Challan et al. [8] are now considered not credible. Analyzing the different works performed, many reasons may be addressed to meet such an unusual spread observed, without a clear trend (i.e., different experimental
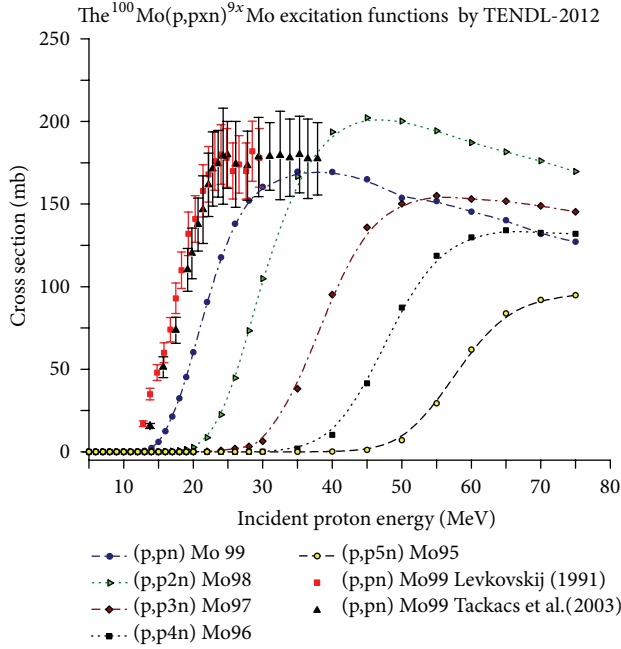
The ^{100}Mo(p,pxn)^{9x}Mo excitation functions by TENDL-2012

- –•– (p,pn) Mo 99
- ⋯▷⋯ (p,p2n) Mo98
- –◆– (p,p3n) Mo97
- ⋯■⋯ (p,p4n) Mo96
- –○– (p,p5n) Mo95
- ■ (p,pn) Mo99 Levkovskij (1991)
- ▲ (p,pn) Mo99 Tackacs et al.(2003)

FIGURE 2: The collection of ^{100}Mo(p,pxn)^{9x}Mo theoretical excitation functions from the TENDL 2012 library [24] up to the (p,p5n) level. The experimental measurements of ^{99}Mo by Levkovskij [2] and Takacs et al. [5] only are included for comparison.

TABLE 1: Niobium and technetium isotopes expected to be produced by the ^{100}Mo(p,x) reactions.

Reaction	Product	Decay	$t_{1/2}$	Daughter
p,α2n	^{95}Nb	β^-	34.99 d	^{95}Mo (stable)
p,αn	^{96}Nb	β^-	23.35 h	^{96}Mo (stable)
p,α	^{97}Nb	β^-	72.1 m	^{97}Mo (stable)
p,2pn	^{98}Nb	β^-	2.9 s	^{98}Mo (stable)
p,2p	^{99}Nb	β^-	15 s	^{99}Mo
	^{99m}Nb	β^-	2.6 m	^{99}Mo (96.2%)
		IT		^{99g}Nb (3.8%)
p,6n	^{95m}Tc	EC	61 d	^{95}Mo (96.1%) (stable)
		IT		^{95g}Tc (3.9%)
	^{95g}Tc	EC	20 h	^{95}Mo (stable)
p,5n	^{96m}Tc	EC	51.5 m	^{96}Mo (2.0%) (stable)
		IT		^{96g}Tc (98.0%)
	^{96g}Tc	EC	4.28 d	^{96}Mo (stable)
p,4n	^{97g}Tc	EC	$4.2 \cdot 10^6$ y	^{97}Mo (stable)
	^{97m}Tc	IT	91 d	^{97g}Tc (96.1%)
		EC		^{97}Mo (3.9%) (stable)
p,3n	^{98}Tc	β^-	$4.2 \cdot 10^6$ y	^{98}Ru (stable)
p,2n	^{99m}Tc	IT	6.01 h	^{99g}Tc (99.9963%)
		β^-		^{99}Ru (0.0037%) (stable)
	^{99g}Tc	β^-	$2.1 \cdot 10^5$ y	^{99}Ru (stable)
p,n	^{100}Tc	β^-	15.46 s	^{100}Ru (99.9982%) (stable)
		EC		^{100}Mo (0.0018%) (stable)

set-ups, target material purity, contaminant levels, isotopic compositions, and *ad hoc* procedures followed during sample
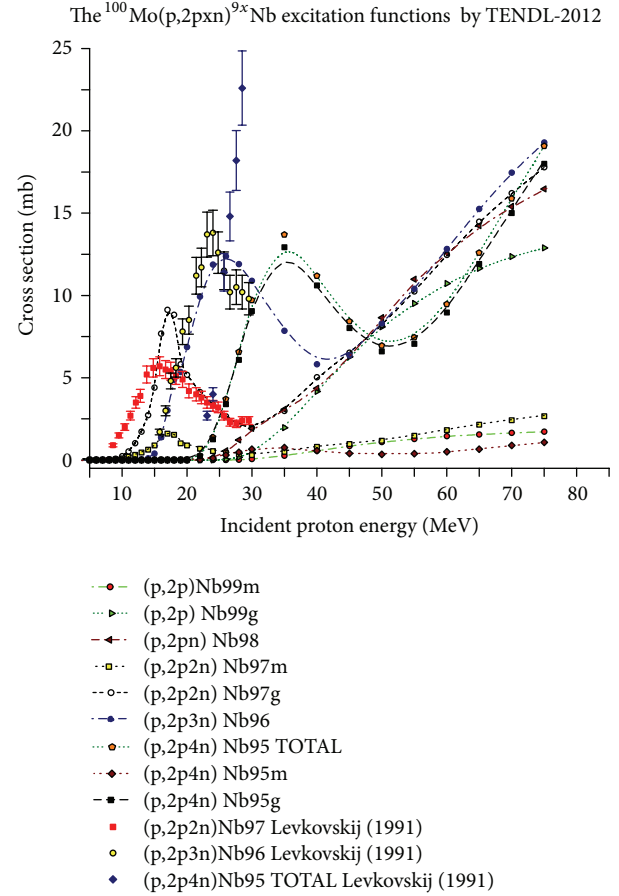

The ^{100}Mo(p,2pxn)^{9x}Nb excitation functions by TENDL-2012

- –•– (p,2p)Nb99m
- ⋯▷⋯ (p,2p) Nb99g
- –◀– (p,2pn) Nb98
- ⋯□⋯ (p,2p2n) Nb97m
- ⋯○⋯ (p,2p2n) Nb97g
- –•– (p,2p3n) Nb96
- ⋯●⋯ (p,2p4n) Nb95 TOTAL
- ⋯◆⋯ (p,2p4n) Nb95m
- –■– (p,2p4n) Nb95g
- ■ (p,2p2n)Nb97 Levkovskij (1991)
- ○ (p,2p3n)Nb96 Levkovskij (1991)
- ◆ (p,2p4n)Nb95 TOTAL Levkovskij (1991)

FIGURE 3: The collection of ^{100}Mo(p,2pxn)^{9x}Nb theoretical excitation functions from the TENDL 2012 library [24] up to the (p,2p4n) level. The available experimental measurements by Levkovskij [2] for $^{95m+g}$Nb, ^{96}Nb, and ^{97}Nb nuclides are included for comparison.

irradiations and detection methods). Moreover, different correction methods are applied in calculating the ^{99m}Tc activity, as deduced by the 140 keV photon peak emissions through gamma spectrometry measurements.

Considering such a production route, particular care has indeed to be taken of the Tc contaminants (see in Table 1 those yielded by ^{100}Mo) since they would remain in the final Tc product. In order to minimize them, irradiation energies at 15, 20, and 25 MeV only have been investigated in this work. In Figure 5, the theoretical excitation functions from the TENDL 2012 library [24], concerning the ^{100}Mo(p,X) reaction routes for additional Tc isotopes production, both in ground and isomeric states, are plotted up to the (p,6n) level. The experimental excitation functions measured for ^{99m}Tc by Takacs et al. [5] and for ^{100}Tc by Skakun [25] are shown for comparison as well. In Figure 5, one can notice that only the long-lived contaminants ^{99g}Tc, ^{98}Tc, and ^{97g}Tc will be produced by ^{100}Mo isotope up to 25 MeV.

Figure 5 also shows the first experimental evaluation of the ^{100}Mo(p,2n)^{99g}Tc excitation function, performed in the energy range 8–18 MeV and reported by Gagnon et al. [12], from which a general agreement may be found with the
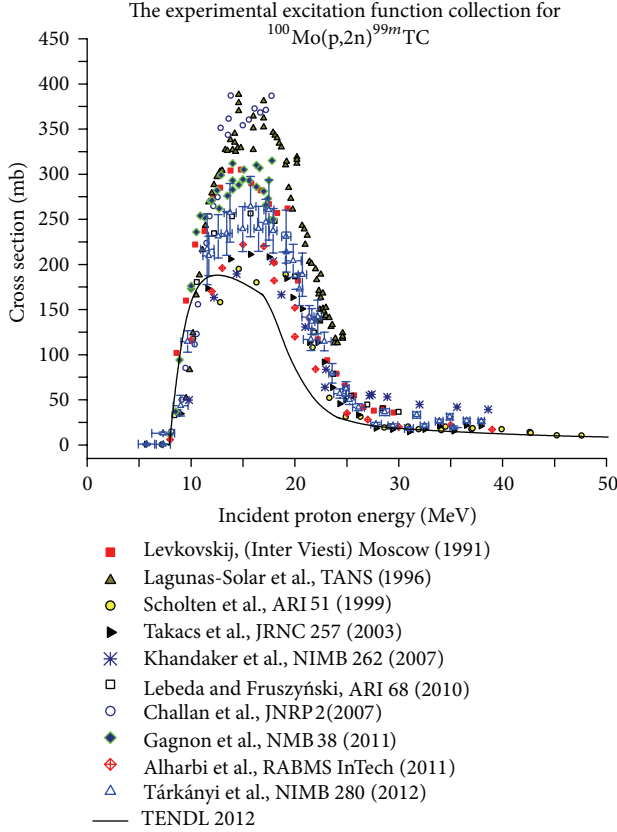
FIGURE 4: The collection of ^{100}Mo(p,2n)^{99m}Tc excitation functions experimentally measured in the last two decades. Error bars are shown for the most recent measurement only performed by Tárkányi (2012) [13]. The most recent theoretical excitation function by the TENDL 2012 library is also shown [24].

FIGURE 5: The collection of ^{100}Mo(p,pxn) ^{xx}Tc theoretical excitation functions from the TENDL 2012 library [24] up to the (p,6n) level. The experimental measurements for ^{99g}Tc (Gagnon et al. [12]), ^{100g}Tc (Skakun et al. [25]), and ^{99m}Tc (Takacs et al. [5]) productions are included for comparison.

theoretical one. Being the largest Tc contaminant produced, further studies and experimental campaigns are however requested, mainly to validate the ^{99g}Tc excitation function in the entire energy range of interest.

Moreover, an additional issue to be assessed is the necessary reuse of the ^{100}Mo-enriched material (quite expensive) in case of direct ^{99m}Tc production. The Mo isotopic composition of the original enriched target material is indeed expected to be modified, if multiple reuse is planned due to economic reasons. In this regard, a preliminary investigation has been carried out on irradiated ^{100}Mo-enriched metal samples, but considering only one recycling stage, as reported by Gagnon et al. [26]. Such a test basically demonstrated the feasibility of molybdenum recovery from the chemical point of view but is however not able to provide a final answer to such a question. The issue about how many times the molybdenum material recovered might be reused, before an impact on the accelerator produced Tc quality becomes critical, still needs to be defined.

3. Materials and Methods

3.1. Decay Chain Calculations.

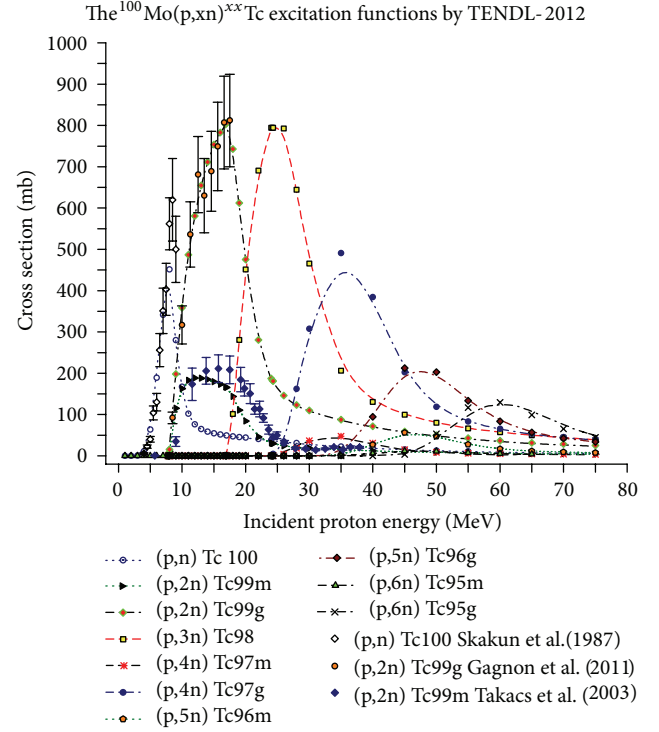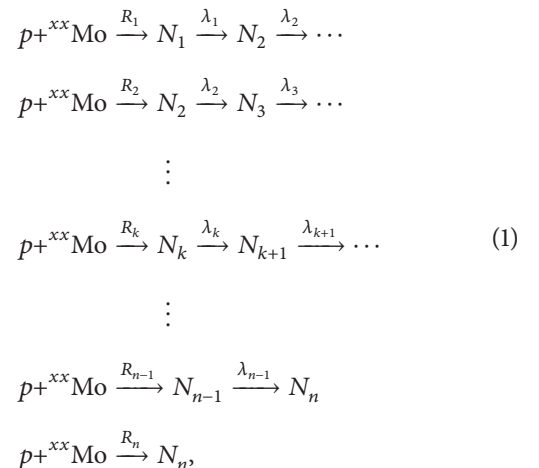When molybdenum targets are irradiated, some of the reaction routes lead to the production of different radioactive isotopes, thus resulting in different radioactive decay chains. Since the same radionuclide may be created through a number of production-decay routes, all of them must be accounted for when estimating the final number of atoms and activity (relative to radioactive ones) available inside the target. The total number of any atom species present at time t, $N(t)$, and the activity $A(t)$ may be obtained by summing up values from the contributing chains. The general production-decay scheme of a single radioactive chain is therefore the following:

$$
\begin{aligned}
p+{}^{xx}\text{Mo} &\xrightarrow{R_1} N_1 \xrightarrow{\lambda_1} N_2 \xrightarrow{\lambda_2} \cdots \\
p+{}^{xx}\text{Mo} &\xrightarrow{R_2} N_2 \xrightarrow{\lambda_2} N_3 \xrightarrow{\lambda_3} \cdots \\
&\quad\vdots \\
p+{}^{xx}\text{Mo} &\xrightarrow{R_k} N_k \xrightarrow{\lambda_k} N_{k+1} \xrightarrow{\lambda_{k+1}} \cdots \\
&\quad\vdots \\
p+{}^{xx}\text{Mo} &\xrightarrow{R_{n-1}} N_{n-1} \xrightarrow{\lambda_{n-1}} N_n \\
p+{}^{xx}\text{Mo} &\xrightarrow{R_n} N_n,
\end{aligned}
\tag{1}
$$

where N_k are the number of radioactive products of a given chain, λ_k is the corresponding decay constants, N_n is the number of the last (stable) nuclide, and R_k is the yield rate for the formation of the first nuclide of each chain directly produced. Since the (p,X) cross sections are relatively low (hundred mb as order of magnitude), only nuclear reactions on target nuclei were considered in calculations. Any secondary reaction that may occur at each level of the newly produced isotopes has been ignored. Likewise, the change in the number of target nuclei during the irradiation process has been considered negligible (i.e., R_k are time constants).

For each decay chain, the variation in the number of nuclei versus time is described by the general set of differential equations. In case of more than one decay mode of a given radionuclide, every branch of the chain has been considered as a different, independent chain according to the branching ratio f_k. Consider

$$\frac{dN_1}{dt} = R_1 - \lambda_1 N_1,$$

$$\frac{dN_2}{dt} = R_2 + f_1 \lambda_1 N_1 - \lambda_2 N_2,$$

$$\vdots$$

$$\frac{dN_k}{dt} = R_k + f_{k-1} \lambda_{k-1} N_{k-1} - \lambda_k N_k,$$

$$\vdots$$

$$\frac{dN_n}{dt} = R_n + f_{n-1} \lambda_{n-1} N_{n-1}$$

with boundary conditions for each equation given by

$$N_k (t = 0) = N_k^0. \tag{3}$$

Such initial conditions are the most general possible, since at starting irradiation time $t = 0$, a certain amount N_k^0 of each (radioactive) nuclide species might be present inside the target material (i.e., in case of multiple reuse of target material). During calculation runs, however, all initial amounts for radioactive species have been set to zero, since only stable molybdenum isotopes were supposed to be included inside the target material, and a unique irradiation run was considered.

In the first one of (2), N_1 is the number of nuclei of a given species yielded as a result of the nuclear reaction. If such a nuclide species is radioactive, the number of nuclei available at any time t is thus a balance between the production rate R_1 and the radioactive decay with constant λ_1. The solution for N_1 can be easily obtained by multiplying both sides of the equation by $e^{\lambda_1 t}$ and then integrating the following

$$\int_{N_1^0}^{N_1(t)e^{\lambda_1 t}} d\left(N_1 \left(t' \right) e^{\lambda_1 t'} \right) = \int_0^t R_1 e^{\lambda_1 t'} dt',$$

$$N_1 (t) e^{\lambda_1 t} - N_1^0 = \frac{R_1}{\lambda_1} \left[e^{\lambda_1 t} - 1 \right] \tag{4}$$

which leads to

$$N_1 (t) = N_1^0 e^{-\lambda_1 t} + \frac{R_1}{\lambda_1} \left[1 - e^{-\lambda_1 t} \right]. \tag{5}$$

On the other hand, if the N_1 nuclei are stable, then $N_1(t)$ increases linearly with time and is given by

$$N_1 (t) = N_1^0 + R_1 t. \tag{6}$$

Likewise, the remaining equations may be analytically solved by direct integration, once the solution for the previous nuclide of the chain has been determined. Consider the following for the generic N_k and N_n nuclides.

$$\int_{N_k^0}^{N_k(t)e^{\lambda_k t}} d\left(N_k \left(t' \right) e^{\lambda_k t'} \right)$$

$$= \int_0^t \left(R_k e^{\lambda_k t'} + f_{k-1} \lambda_{k-1} N_{k-1} \left(t' \right) e^{\lambda_k t'} \right) dt',$$

$$\int_{N_n^0}^{N_n(t)} d\left(N_n \left(t' \right) \right)$$

$$= \int_0^t \left(R_n + f_{n-1} \lambda_{n-1} N_{n-1} \left(t' \right) \right) dt'. \tag{7}$$

After analyzing both stable and unstable solutions for decay chains as long as 6 elements, two general and compact solutions have been obtained, which represent the number of nuclei of, respectively, the unstable N_k and the stable N_n elements of a given decay chains. Consider

$$N_k (t) = \sum_{i=1}^{k} \left\{ N_i^0 \cdot \prod_{l=i}^{k-1} (f_l \lambda_l) \cdot \sum_{j=i}^{k} \left[\frac{e^{-\lambda_j t}}{\prod_{\substack{m=i \\ m \neq j}}^{k} \left(\lambda_m - \lambda_j \right)} \right] \right.$$

$$+ \frac{R_i}{\lambda_k} \prod_{l=i}^{k-1} (f_l)$$

$$\left. \cdot \left[1 - \sum_{j=i}^{k} \left[e^{-\lambda_j t} \cdot \prod_{\substack{m=i \\ m \neq j}}^{k} \left(\lambda_m - \lambda_j \right) \right] \right] \right\},$$

$$N_n (t) = \sum_{i=1}^{n} \left\{ N_i^0 \cdot \prod_{l=i}^{n-1} (f_l) \right.$$

$$\cdot \left[1 - \sum_{j=i}^{n-1} \left[e^{-\lambda_j t} \cdot \prod_{\substack{m=i \\ m \neq j}}^{n-1} \left(\frac{\lambda_m}{\lambda_m - \lambda_j} \right) \right] \right]$$

$$+ R_i \prod_{l=i}^{n-1} (f_l)$$

$$\left. \cdot \left[t - \sum_{j=i}^{n-1} \left[\frac{\left(1 - e^{-\lambda_j t} \right)}{\lambda_j} \cdot \prod_{\substack{m=i \\ m \neq j}}^{n-1} \left(\frac{\lambda_m}{\lambda_m - \lambda_j} \right) \right] \right] \right\}. \tag{8}$$

The estimation of every nuclide produced by any decay chain has been thus calculated at any given irradiation time. For each decay chain, the nuclide number $N_k(t)$ and the related radioactivity $A_k(t)$ have been calculated, adding up the different contributions to a given nuclide species. Once the irradiation time is over ($t = $ EOB), the nuclide yields by nuclear reactions stop, while the decays still continue. All R_k for each decay chain are therefore set to zero, and the same set of equations may be solved to calculate both the nuclide number and activity change against the decay time $t_D = $ EOB $+ t$.

3.2. The Estimations of ^{99}Mo and ^{99m}Tc Yields Expected inside Irradiated Samples.

As a starting approach, the ^{99}Mo production level expected at EOB on ^{100}Mo-enriched molybdenum metallic targets has been estimated at 40 MeV and 70 MeV proton energies, while for the direct ^{99m}Tc production 15, 20, and 25 MeV have been instead considered. In both cases, the maximum of 500 μA beam current has been assumed as a reference. Yields expected at different beam currents anyway may be easily inferred through simple scaling calculations.

For the thick-target configuration, the required thickness for the molybdenum material has to be primarily assessed both at the minimum and the maximum proton energies, in order to limit the amount of ^{100}Mo and, consequently, the material cost. This can be done assuming, as a starting step, that the proton beam hits the molybdenum sample in normal direction and using tabulated data on stopping power values and projected ranges calculated by SRIM 2012 code [27] or taken by the PSTAR database of the National Institute for Standards and Technology (NIST) website (NIST-STAR database [28]). The estimated metallic molybdenum thickness to fully stop 70 MeV protons turns out to be about 7.1 mm, while 2.6 mm is instead needed when using 40 MeV protons. When the incident energy optimized for ^{99m}Tc production is instead considered 0.48 mm, 0.78 mm, and 1.1 mm are enough to fully stop 15, 20, and 25 MeV proton beams, respectively.

Such penetration thicknesses for protons are actually needed also in other irradiation conditions (tilted targets). The proton energy loss per unit path, as well as the corresponding energy drop off versus penetration depth, has been calculated. Since the sample thickness T_0 required to fully stop the beam is much lower than the maximum linear size (radius) of the target material in the hypotheses of cylindrical configuration, an analytical calculation approach, based on a slab geometry model, may be used in such a case with good approximation (see Figure 6).

The estimation of local yield contribution dY_i, that is, the nuclide species i produced inside the given infinitesimal thickness dt at depth t of the target material, is described by the following equation:

$$dY_i = n_{\text{Mo}} \cdot \sigma_i \left(E_0 - \int_0^t \frac{dE}{dx} dx \right)$$
$$\cdot \frac{I_0}{Q} \left(\prod e^{-n_{\text{Mo}} \sigma_R (E_0 - \int_0^x (dE/dx') dx') dx} \right)_t \cdot dt, \tag{9}$$
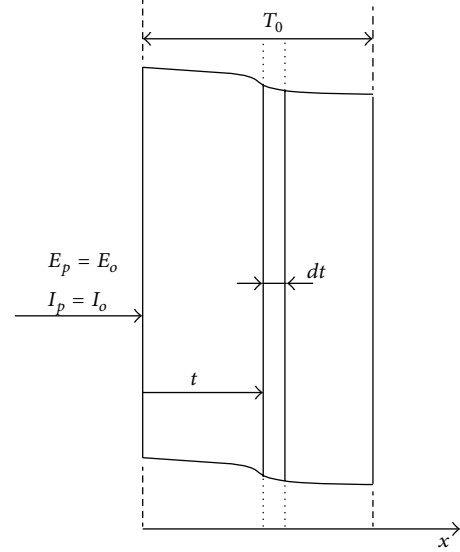

FIGURE 6: The main parameters in the slab approximation geometry for the calculation of yield distributions inside molybdenum sample thickness.

where n_{Mo} is the atomic density of the enriched molybdenum target material (i.e., $n_{\text{Mo}} = \rho_t f_x (N_A/M_{\text{mol}})$) with ρ_t the target density, f_x the weight fraction of the ^{9x}Mo isotope considered, N_A the Avogadro number, and M_{mol} the molar mass of the target. Then, $\sigma_i(E(t))$ is the ^{9x}Mo(p,x) cross section for the production of the given nuclide species, as a function of the proton energy E at each thickness t (estimated by an iterative calculation process once known the proton stopping power dE/dx and the incident proton energy E_0). The proton beam current I_0 divided by the electric charge unit Q is the n_p number of protons per unit time, hitting the target ($n_p = I_0/Q$).

The product expression within brackets is the fraction of incident protons, available at the generic depth t inside the sample, because of the contribution of the exponential attenuations in any single infinitesimal slab. The removal cross section $\sigma_R(E(t))$ takes into account all the reaction routes that remove protons from the main stream.

The resulting contribution of the exponential, for each infinitesimal thickness inside samples, however turns out to be basically constant and quite close to unity, mainly because of the order of magnitude of the cross section involved (i.e., 10–100 mb). Expression (9) may therefore be simplified to a very good approximation in the next one. The overall nuclide production dY_i, normalized for incident proton, is obtained by integrating (9) over the whole target thickness T_0 and dividing by n_p as follows:

$$\frac{Y_i}{n_p} = n_{\text{Mo}} \cdot \int_0^{T_0} \sigma \left(E_0 - \int_0^t \frac{dE}{dx} dx \right) dt. \tag{10}$$

Equation (10) was used for later calculations of the in-target production of any Mo, Nb, Zr and Tc nuclides. The theoretical excitation functions for the reaction routes of interest, involving up to 6 emitted particles (i.e., protons
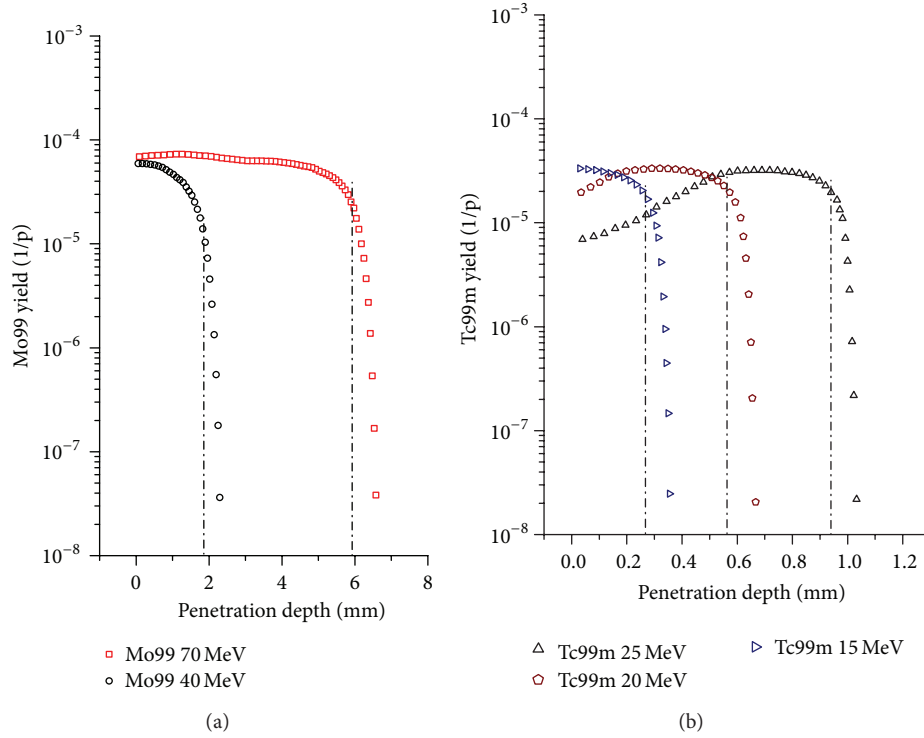
(a)

(b)

FIGURE 7: The distributions of the nuclide yields, normalized per incident proton, versus penetration depth, calculated inside 99.05% ^{100}Mo-enriched samples: (a) 70 MeV and 40 MeV are considered for ^{99}Mo production; (b) the same plot for 15, 20, and 25 MeV beam, in case of direct ^{99m}Tc production. The eye-guide vertical lines show the recommended sample thicknesses to get an optimized production.

and/or neutrons), have been taken into account as provided by the TENDL 2012 library and available as output by TALYS code. The excitation functions for both isomeric and ground states may therefore be calculated taking into account a complete set of nuclear models developed (i.e., optical model, direct reactions, compound reactions, etc.). Further information may be found in [24].

4. Results and Discussion

^{99}Mo and ^{99m}Tc yields versus sample thicknesses calculated, normalized per incident proton, are plotted in Figure 7 for the energies concerned. As can be noticed, values are within one order of tenth, up to the point where the yield drop off starts down to the corresponding energy threshold for the reaction (i.e., energy exit without the useless heat power deposition corresponding to the Bragg peak). Figure 7 also shows the recommended thicknesses for an optimized production, saving the target material.

In Table 2, the isotope productions expected by both thick and optimized target thicknesses, normalized per incident proton, are reported for the selected proton energies. As can be seen, the accelerator production of ^{99}Mo is interesting at energies larger than 40 MeV, in order to operate in the most useful energy range for the the excitation function (see Figure 2).

As for the direct ^{99m}Tc production, the quality parameters (i.e., the ^{99m}Tc / $^{(99m+g)}$Tc and the ^{99m}Tc/$\sum$ ^{xx}Tc nuclei

ratios) have been calculated and listed. Such parameters, which directly relate the ^{99m}Tc production quality expected to the proton beam energy selected, have to be as high as possible. Almost all of the Tc nuclides directly yielded at 15 MeV, caused by ^{99m}Tc and ^{99g}Tc mainly, with a contribution of about 10% from the short-lived ^{100}Tc, are shown in Table 2, in case of the optimized target configuration. At 20 and 25 MeV, significant contributions are instead from other Tc contaminants (i.e., mainly from ^{98}Tc, $^{(97m+g)}$Tc $^{(96m+g)}$Tc, and at lesser extent by $^{(95m+g)}$Tc $^{(99m+g)}$Tc) produced by the reaction routes due to the other Mo target isotopes, which basically cause a decrease of the ^{99m}Tc /$\sum$ ^{xx}Tc ratio. The contribution from Tc nuclides other than $^{(99m+g)}$Tc, compared with ^{99m}Tc, indeed increases to about 17% and 37%, respectively.

On the basis of these considerations, it may be inferred that the best irradiation energy which should be considered for the accelerator ^{99m}Tc production is 15 MeV. However, the ^{99m}Tc production rate is about 2.0 times lower at this energy than expected at 20 MeV. A weighted balance, between the ^{99m}Tc yield ratio and production yield expected, is therefore needed at such an energy range. The production at 25 MeV should instead be avoided because of the low ^{99m}Tc /$\sum$ ^{xx}Tc ratio (basically the half with respect to 15 MeV) which is available just from direct reactions only. It has anyway to be kept in mind that once produced, the compositions of different Tc nuclides are continuously modified by the decay

TABLE 2: The integral production yields (normalized per incident proton) estimated on ^{100}Mo-enriched sample thicknesses both for ^{99}Mo and ^{99m}Tc productions. Additional production quality parameters for ^{99m}Tc are listed as well.

Proton energy	Target for ^{99}Mo (mm)	Target for ^{99m}Tc (mm)	^{99}Mo/p (adu)	^{99m}Tc/p (adu)	^{99m}Tc/$^{99m+g}$Tc yield ratio	^{99m}Tc/all Tc yield ratio
70 MeV	Optimized 5.93	/	$5.52 \cdot 10^{-3}$	/	/	/
	Thick 6.74	/	$5.67 \cdot 10^{-3}$	/	/	/
40 MeV	Optimized 1.82	/	$1.66 \cdot 10^{-3}$	/	/	/
	Thick 2.47	/	$1.72 \cdot 10^{-3}$	/	/	/
25 MeV	Optimized 0.66	0.94	$2.75 \cdot 10^{-4}$	$6.70 \cdot 10^{-4}$	0.187	0.117
	Thick 1.00	1.04	$2.78 \cdot 10^{-4}$	$7.03 \cdot 10^{-4}$	0.191	0.115
20 MeV	Optimized 0.46	0.57	$5.83 \cdot 10^{-5}$	$5.65 \cdot 10^{-4}$	0.198	0.170
	Thick 0.63	0.65	$5.83 \cdot 10^{-5}$	$5.97 \cdot 10^{-4}$	0.203	0.161
15 MeV	Optimized 0.14	0.26	$1.95 \cdot 10^{-6}$	$2.84 \cdot 10^{-4}$	0.235	0.211
	Thick 0.33	0.35	$1.99 \cdot 10^{-6}$	$3.23 \cdot 10^{-4}$	0.244	0.185

TABLE 3: The ^{99}Mo production yields expected at EOB for different irradiation conditions, based on 99.05% ^{100}Mo-enriched metallic molybdenum (thick and optimized target configurations), 500 μA proton current, and 500 W/cm^2 mean areal power density on target.

^{99}Mo production	$E_P = 70$ MeV		$E_P = 40$ MeV	
Beam power on target (kW)	35		20	
Target configuration	Thick	Optimized	Thick	Optimized
Beam power deposited in target (kW)	31.1	24.1	16.1	10.1
Irradiation time: 12 h				
Integral yield (mCi/μA)	119.5	116.5	34.7	34.5
In-target activity (Ci)	59.7	58.3	17.4	17.3
Specific activity (mCi/g)	119.8	136.5	159.5	205.2
Irradiation time: 24 h				
Integral yield (mCi/μA)	224.8	219.2	65.4	65.1
In-target activity (Ci)	112.4	109.6	32.7	32.6
Specific activity (mCi/g)	225.4	256.9	300.0	386.0
Saturation: ≈ 21 d				
Integral yield (mCi/μA)	1003.3	978.3	291.9	290.5
In-target activity (Ci)	501.6	489.2	145.9	145.3
Specific activity (mCi/g)	1011.4	1152.3	1345.4	1731.1

chain contributions during the irradiation time, up to the EOB and for times longer, as discussed later in a more detailed way. In other words, the yield ratio numbers listed in Table 2 are the upper values for the isotopic purity (IP) parameter that may be achieved in the theoretical approach concerned.

Table 3 reports the ^{99}Mo in-target yields estimated at EOB for different irradiation conditions, taking into account the contribution from the decay of parent nuclides $^{(99m+g)}$Nb. The proton beam spot size and energy, resulting from the mean areal power density, uniquely defines the size and mass of the requested samples (thick or optimized), thus allowing to estimate the specific activity as well.

Table 4 reports the ^{99m}Tc production yields estimated at EOB at 15 and 20 MeV for the optimized sample configuration at the irradiation times as long as $t_{1/2}$ (1 h, 2 h, 3 h, and 6 h). The ^{99m}Tc specific activity (in isotopic carrier condition) is estimated as well. Moreover, all technetium radionuclides, as well as ^{99m}Tc activity, versus activities of all radioactive

species, are calculated. The specific activity, the radionuclidic purity (i.e., $\text{RNP}(t) = A(t)_{99m\text{Tc}} / \sum A(t)_{xx\text{Tc}}$), and the isotopic purity (i.e., $\text{IP}(t) = N(t)_{99m\text{Tc}} / \sum N(t)_{xx\text{Tc}}$) expected at EOB are also listed, taking into account the contributions from all the radioactive chains available.

As may be observed, almost all of the in-target radioactivity produced at EOB is due to Tc radioisotopes (i.e., about 98% at 15 MeV and 95% at 20 MeV, resp.). The ^{99m}Tc radionuclidic purity (RNP) is however relatively low (around 20–30%), even considering the best irradiation combination (e.g., 15 MeV proton beam and the short irradiation times in order to get the highest IP). The reason for that is basically the contribution of the quite short-lived ^{100}Tc, the presence of which may not be avoided. At both energies considered, the ^{100}Tc activity contribution ranges from 5 times larger to values almost equal to that provided by ^{99m}Tc, at increasing irradiation times.

TABLE 4: The ^{99m}Tc production yields estimated at EOB for different irradiation times at 15 and 20 MeV proton beams on 99.05% ^{100}Mo-enriched metallic molybdenum and optimized target configuration. 500 μA proton current and 500 W/cm^2 mean areal power density are considered on target. A series of production quality parameters are calculated and listed (see body text).

^{99m}Tc production	$E_P = 15$ MeV			
Beam power on target (kW)	7.5			
Beam power deposited inside Mo sample (kW)	1.41			
Irradiation time	1 h	2 h	3 h	6 h
Integral yield (mCi/μA)	5.32	10.05	14.28	24.38
In-target activity (Ci)	2.66	5.03	7.14	12.2
Specific activity (Ci/g)	$1.16 \cdot 10^6$	$1.10 \cdot 10^6$	$1.04 \cdot 10^6$	$8.86 \cdot 10^5$
Tc/Total activity	0.9877	0.9853	0.9848	0.9861
^{99m}Tc/Total activity	0.1809	0.2929	0.3693	0.4984
^{99m}Tc/$^{99m+g}$Tc	0.2224	0.2103	0.1990	0.1699
Isotopic purity (IP)	0.2200	0.2081	0.1970	0.1682
Radionuclidic purity (RNP)	0.1831	0.2973	0.3750	0.5055
^{99m}Tc production	$E_P = 20$ MeV			
Beam power on target (kW)	10.0			
Beam power deposited inside Mo sample (kW)	3.95			
Irradiation time	1 h	2 h	3 h	6 h
Integral yield (mCi/μA)	10.35	19.58	27.81	47.56
In-target activity (Ci)	5.17	9.79	13.90	23.78
Specific Activity (Ci/g)	$8.96 \cdot 10^5$	$8.47 \cdot 10^5$	$8.01 \cdot 10^5$	$6.84 \cdot 10^5$
Tc/Total activity	0.9573	0.9488	0.9468	0.9491
^{99m}Tc/Total activity	0.2006	0.3162	0.3926	0.5190
^{99m}Tc/$^{99m+g}$Tc	0.1862	0.1760	0.1665	0.1420
Isotopic purity (IP)	0.1698	0.1606	0.1520	0.1297
Radionuclidic purity (RNP)	0.2095	0.3333	0.4147	0.5468

As a reference, in Table 5, the calculated integral yields (mCi/μA) at 3 and 6 hours irradiation, from all of the Tc radioactive products expected at EOB inside the thin target configuration, are listed at the three bombarding energies of 15, 20, and 25 MeV.

Based on all the calculations performed, the resulting ^{99}Mo activity expected after 24 h irradiation inside sample at EOB is 109.6 Ci, considering an optimized target configuration under 70 MeV beam, while the specific activity is being 256.9 mCi/g. When 40 MeV protons are instead taken into account, 32.6 Ci activity is estimated at EOB, with a specific activity increase to 386.0 mCi/g.

Although these in-target ^{99}Mo activity levels seem to be enough to cover a regional demand, it should be however noted that the resulting specific activities are a factor of 10^4 lower than the one present inside the current Mo/Tc generators, achieving levels of about 10^4 Ci/g. If the current industrial method for Mo/Tc generator manufacturing has to be maintained, the accelerator ^{99}Mo production is therefore not a favourable option of practical interest, considering the high cost of the target material, the very large alumina column needed, and the resulting large elution volumes, as discussed by Morley et al. [29].

When the ^{99m}Tc direct production is instead taken into account in the range 15–25 MeV, the estimation of the resulting specific activity (see Table 4) is similar to the one

provided by the current Mo/Tc generators, which turns out to be about $1.5 \cdot 10^6$ Ci/g at any standard 24 h elution. Table 5 shows that the major contribution to the Tc-produced activity at EOB is from the short-lived ^{100}Tc and the production energy range of which is only partly included in the optimized target configuration. Although the exit proton energy, at the indicated target thicknesses reported in Table 2, turns out to be around 9.6 MeV, its production may not be avoided. Because of the quite short mean life, ^{100}Tc does not play a disturbing role in the final Tc contaminants. Just a few minutes after EOB, the ^{100}Tc activity indeed drops off, transmuting in the stable ^{100}Ru which may be later separated in the chemical process of the target dissolution. The contributions from other main Tc contaminants to the overall Tc activity which, instead, remain in the final Tc solution are, in order of decreasing activity (reference case at 20 MeV protons and 3 hrs irradiation), ^{96m}Tc, ^{94g}Tc, ^{92}Tc, ^{94m}Tc, ^{93g}Tc, ^{95g}Tc, ^{93m}Tc and ^{96g}Tc. On the other hand, the activity contribution from the long-lived ^{99g}Tc, ^{98}Tc, and ^{97g}Tc, which are produced in larger amounts because of the highest values of the excitation functions, is minimal and therefore irrelevant for dosimetry considerations. Nevertheless, their impact on the ^{99m}Tc isotopic purity level is not negligible and may affect the radiochemical quality of the accelerator-Tc labelled pharmaceuticals.

TABLE 5: The calculated integral yields (mCi/μA) at EOB after 3 and 6 hours irradiations for the expected Tc radioactive species inside the target. 99.05% ^{100}Mo-enriched metallic molybdenum in the optimized target configuration irradiated at 15, 20, and 25 MeV is considered. The whole list of all Mo, Nb, and Zr radioactive yields is not reported here for the sake of brevity.

Product	$t_{1/2}$	3 h irradiation			6 h irradiation		
		15 MeV	20 MeV	25 MeV	15 MeV	20 MeV	25 MeV
^{100}Tc	15.46 s	$2.357E + 01$	$3.871E + 01$	$5.427E + 01$	$2.357E + 01$	$3.871E + 01$	$5.427E + 01$
^{99m}Tc	6.01 h	$1.428E + 01$	$2.781E + 01$	$3.321E + 01$	$2.438E + 01$	$4.756E + 01$	$5.707E + 01$
^{99g}Tc	$2.1 \cdot 10^5$ y	$1.867E - 07$	$4.525E - 07$	$5.804E - 07$	$3.871E - 07$	$9.339E - 07$	$1.204E - 06$
^{98}Tc	$4.2 \cdot 10^6$ y	$3.696E - 11$	$2.383E - 09$	$1.737E - 08$	$7.392E - 11$	$4.766E - 09$	$3.475E - 08$
^{97m}Tc	91 d	$2.122E - 04$	$4.792E - 04$	$6.994E - 04$	$4.241E - 04$	$9.580E - 04$	$1.398E - 03$
^{97g}Tc	$4.2 \cdot 10^6$ y	$4.037E - 11$	$1.197E - 10$	$2.156E - 10$	$8.075E - 11$	$2.394E - 10$	$4.312E - 10$
^{96m}Tc	51.5 m	$8.741E - 02$	$1.567E - 01$	$4.117E - 01$	$9.516E - 02$	$1.706E - 01$	$4.483E - 01$
^{96g}Tc	4.28 d	$3.230E - 03$	$6.209E - 03$	$2.294E - 02$	$7.040E - 03$	$1.345E - 02$	$4.846E - 02$
^{95m}Tc	61 d	$7.551E - 05$	$1.849E - 04$	$2.806E - 04$	$1.509E - 04$	$3.696E - 04$	$5.607E - 04$
^{95g}Tc	20 h	$1.722E - 02$	$4.414E - 02$	$7.529E - 02$	$3.275E - 02$	$8.393E - 02$	$1.431E - 01$
^{94m}Tc	52 min	$2.744E - 02$	$6.489E - 02$	$9.470E - 02$	$2.993E - 02$	$7.078E - 02$	$1.033E - 01$
^{94g}Tc	293 min	$3.409E - 02$	$1.094E - 01$	$1.951E - 01$	$5.637E - 02$	$1.809E - 01$	$3.225E - 01$
^{93m}Tc	43.5 min	$6.191E - 04$	$1.525E - 02$	$3.005E - 02$	$6.543E - 04$	$1.612E - 02$	$3.176E - 02$
^{93g}Tc	2.75 h	$2.318E - 03$	$4.935E - 02$	$1.218E - 01$	$3.476E - 03$	$7.426E - 02$	$1.824E - 01$
^{92}Tc	4.25 min	$5.181E - 02$	$1.017E - 01$	$1.152E - 01$	$5.181E - 02$	$1.017E - 01$	$1.152E - 01$
^{91m}Tc	3.3 min	$0.000E + 00$	$0.000E + 00$	$2.595E - 03$	$0.000E + 00$	$0.000E + 00$	$2.595E - 03$
^{91g}Tc	3.14 min	$0.000E + 00$	$9.369E - 06$	$1.190E - 02$	$0.000E + 00$	$9.369E - 06$	$1.190E - 02$

As recalled, a key parameter to be carefully assessed considering the ^{99m}Tc accelerator production is the ground state ^{99g}Tc, which is useless for the diagnostic procedures. In the report by the european commission [30], a limiting purity of the end product, approximately composed by 25% ^{99m}Tc and 75% ^{99g}Tc (i.e., ^{99m}Tc / $^{(99m+g)}$Tc ratio equal to 0.25), is reported to interfere with the function of some labelled radiopharmaceuticals, thus reducing the effectiveness of Tc-based scans. Unfortunately, it is not clear in [30] how such an IP level should affect the diagnostic procedures, as neither the radiolabelling processes nor the resulting SPECT images quality are mentioned.

In order to get a reference, when technetium ($^{99g+99m}$Tc), under pertechnetate form (TcO$_4^-$), is eluted as a sterile solution from a standard Mo/Tc generator after intervals of 24 h, the maximum ^{99m}Tc activity is reached and the corresponding isotopic purity IP turns out to be about 0.26, as may be inferred by the considerations reported by Alfassi et al. [31]. On the other hand, on the basis of our theoretical approach it can be noted that such a ratio is never higher than 0.22 (see Table 4). It has to be reminded that the ^{99m}Tc excitation function from the TENDL 2012 library shows the peak located at the bottom of the uncertainty band from the experimental measurements, as shown in Figure 4. Therefore, it has to be reasonably expected that an IP value similar to Tc generators might be obtained at both short irradiation times and low bombarding energies (i.e., 1-2 hr, 15 MeV).

Once produced, and eventually chemically separated from other radioactive and stable isotopes of other chemical species, the expected evolution of both the isotopic purity (IP) and the radionuclidic purity (RNP) for the accelerator-produced ^{99m}Tc, against the decay time after EOB, is finally shown in the three plots of Figure 8. The sharp increase of RNP, with respect to the ones enlisted in Table 4 up to values higher than 95%, occurs in just a few minutes, mainly because of the quick decay of ^{100}Tc. The decays of other short-lived Tc isotopes lead the RNP increase to values as high as 99% in about 1 hour after EOB, considering the reference case of 3 h irradiation at 20 MeV energy. RNP values above 99% for accelerator-produced Tc are quite important, considering that the same parameter from the generator-produced Tc is about 99.99%. Such a limit is basically approached (i.e., 99.58%) if the irradiations at proton energies as low as 15 MeV are performed, whatever the irradiation time chosen. Moreover, the accelerator produced ^{99m}Tc, having RNP values never higher than 99% and IP ones always lower than 10% 1 h after EOB, clearly points out that irradiations at 25 MeV have to be avoided, even using highly enriched molybdenum material.

Some experimental investigations have been performed in recent times to assess the influence of the IP parameter on radiolabelling procedures, using ^{99m}Tc from standard Mo/Tc eluates at times as long as after 3 days from the previous elution. In a recent study performed by Urbano et al. [14], the ^{99g}Tc and oxidizing impurities amounts present in different eluates were accurately determined and their influence in radiochemical purity determination of different radiopharmaceuticals, for example, ^{99m}Tc-DTPA (diethylenetriaminepenta-acetic acid), ^{99m}Tc-MIBI (methoxyisobutylisonitrile), and ^{99m}Tc-HMPAO (hexamethylpropylene amine oxime), was carefully evaluated. It was found that the radiolabelling procedures of these commercial
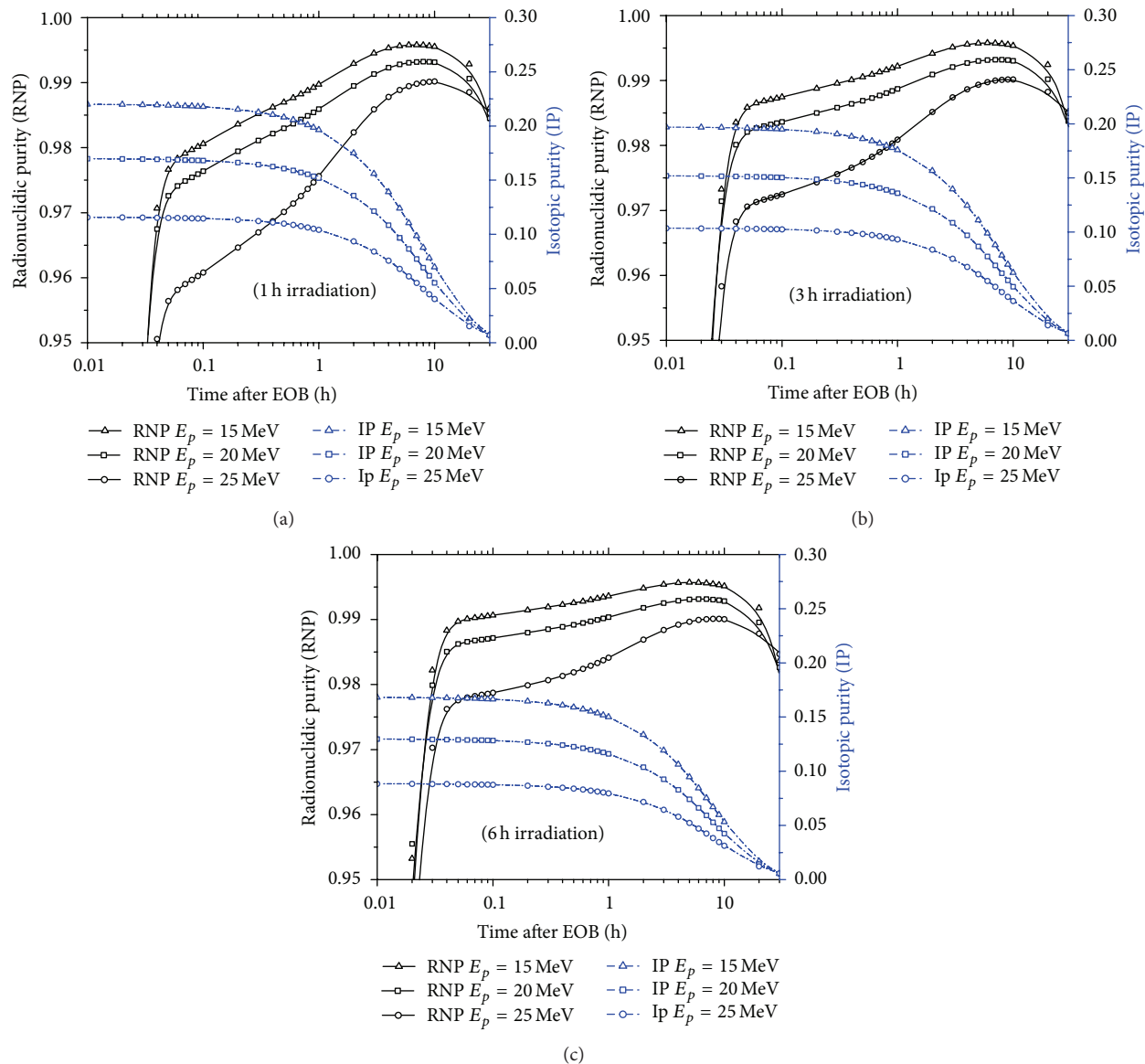
FIGURE 8: The evolution of ^{99m}Tc isotopic purity (IP) and radionuclidic purity (RNP) expected inside the target (or supposing a quick chemical separation process of accelerator Tc produced) versus the decay time after EOB. 99.05% ^{100}Mo-enriched metallic molybdenum in optimized sample configuration bombarded at 15, 20, and 25 MeV protons and 1, 3, and 6 h irradiation times has been considered.

kits were not affected when using eluates at 72 h and at longer times from the previous one (i.e., solutions with an IP value as low as about 0.08). Moreover, the USP requirements were fulfilled in all the cases considered, even with those radiopharmaceuticals whose stannous contents were low (i.e., MIBI and HMAPO). Such a consideration suggests that, as shown in Figure 8, the useful time-window (1–10 h) after EOB for labelling procedures may be fulfilled by accelerator-produced Tc at energies below 20 MeV and irradiation times within 3 h.

It has to be noted that some interesting imaging *in vivo* tests have also been performed on healthy rats, to get a comparison between the generator-produced against the cyclotron-produced ^{99m}Tc, as reported in a newsline of JNM by Guérin et al. [15]. After short irradiations (1.5–3 h) at 17 MeV using 99.5% ^{100}Mo-enrichment, the resulting labeling, the resulting labelling efficiencies of ^{99m}Tc-MDP and ^{99m}Tc-MIBI were above the USP requirements (>90%), and identical patterns were found for the cyclotron- and the generator-produced ^{99m}Tc radiopharmaceuticals, within normal individual variations between each pair of animals.

Moreover, *in vivo* biodistribution studies in rats were performed, using the cyclotron-produced ^{99m}Tc-BRIDA pharmaceutical, whose radiochemical purity after the technetium labelling procedure was above 97%, finding agreement with the expected time behaviour of the kit in different organs (Targholizadeh et al. [16]). Therefore, it may be concluded that the long-lived isotopes ^{99g}Tc and ^{98}Tc, certainly present

in the radiopharmaceuticals, seem to induce a marginal effect (if any) on the results of the diagnostic procedures. Additional and more accurate investigations are however needed in order to have clearer indications.

It should at last be reminded that the chemical separation process described by Chattopadhyay [32, 33] may be completed very quickly, just within 1 h from EOB, as confirmed by Guérin et al. [15]. In case of a direct ^{99m}Tc accelerator production, it must be assumed that a fully dedicated radiochemical plant for separation and purification processes, up to the final radionuclides in GMP chemical form ready for use, should be available in the same regional area of the production site. In such a way, the already established distribution network for short-lived radionuclides may be exploited.

5. Conclusions

In this work, a comprehensive feasibility study, aimed at the ^{99}Mo / ^{99m}Tc alternative production through high-performance cyclotron-based proton accelerators up to 70 MeV, has been presented. For such a purpose, a wide set of TENDL 2012 theoretical excitation functions have been used, available for the reaction routes on all Mo isotopes present inside ^{100}Mo-enriched molybdenum metallic material, up to (p,6n), (p,p5n), and (p,2p4n) levels. No simplified constraints, about either the magnitude of cross section values for the various isotope productions (both ground or isomeric states) or assumptions about jumps on the different decay chains (based on the short mean life of radionuclide concerned) have been adopted, thus following the most general theoretical approach.

The estimated theoretical yields obtained in this study are, on the whole, consistent with the previous ones performed by Celler et al. [17], based on a different theoretical approach. An agreement with the experimental results reported in the works by Scholten [4], Takacs et al. [5], and Gagnon et al. [12], mainly about the ^{99}Mo and ^{99m}Tc and ^{99g}Tc yields by direct reactions on ^{100}Mo, has been found. For all of the theoretical excitation functions taken into account about the Mo isotopes present inside the target material, a benchmark study has been performed as well in the EXFOR database [34], collecting all of the experimental nuclear reaction data available. A general agreement (although with some deviations) has been found, as may be seen in Figures 2, 3, and 5 for the case of ^{100}Mo isotope, thus confirming the general reliability of the TENDL 2012 theoretical excitation functions.

This study proves that the expected in-target specific activities for the ^{99}Mo production (mainly in the 40–70 MeV energy range), even using the incoming high-performance cyclotron at LNL, are about a factor of 10^4 lower than the one currently available inside the standard Mo/Tc generators. Although the in-target yields estimated for the irradiation parameters investigated may be considered enough, such a route is however not interested as a production way, if maintaining the current standard Mo/Tc generators manufacturing because of the high cost of the target material.

On the contrary, the direct proton-driven ^{99m}Tc production is feasible and quite interesting. Although the in-target yields are improved moving towards beam energies higher than 20 MeV, the production of other Tc contaminants starts increasing to levels that are not negligible. Some impacts may therefore occur on the quality of accelerator-Tc radiopharmaceuticals, as well as on dosimetric aspects. The calculation results clearly show that the energy region of 15–20 MeV is the best operative solution for the accelerator production of ^{99m}Tc. In such a, case the main quality-related parameters, that is, the isotopic purity (IP) as well as the resulting radionuclidic purity (RNP) evolution some hours after EOB, are indeed closer to the generator-produced ^{99m}Tc if short irradiations (i.e., not longer than 3 h) are chosen. Moreover, results also show that the expected specific activity at EOB is similar to the one available from the current Mo/Tc generators, that is, around 10^6 Ci/g for 15–20 MeV proton beam. A good balance between production yields and isotopic/radionuclidic purities concern is therefore likely to be found within such constraints. A series of short irradiations are thus preferable instead of a unique per day, in order to minimize the amount of Tc-contaminants. Moreover, a key parameter is the production of the ground state ^{99g}Tc that has a strong influence on the IP parameter. Although recent studies have shown that labelling procedures performed on some commercial kits were not affected using eluates from the standard Mo/Tc generator at 72 h and longer from the previous one, such a consideration suggests that a time window, ranging from 2 h and up to 10 h after EOB, may be exploited for medical procedures with the accelerator-^{99m}Tc pharmaceuticals. Further studies and experimental campaigns are however requested to validate the ^{100}Mo(p,2n) ^{99g}Tc excitation function in the entire energy range and to find out the acceptable IP and RNP limits preferably through imaging *in vivo* tests. These basic aspects will be the subject of future experimental investigations as well as the evaluation of the amount of other technetium isotopes produced (e.g., ^{95,96,97,98}Tc) from the irradiation of available enriched ^{100}Mo targets.

References

[1] J. E. Beaver and H. B. Hupf, "Production of ^{99m}Tc on a medical cyclotron: a feasibility study," *Journal of Nuclear Medicine*, vol. 12, no. 11, pp. 739–741, 1971.

[2] N. Levkovskij, "Middle mass nuclides ($A = 40 \pm 100$) activation cross sections by medium energy ($E = 10 \pm 50$ MeV) protons and α-particles (experiment and systematics)," (Moscow: Inter-Vesti) p. 155, 1991.

[3] P. Chodash, C. T. Angell, J. Benitez et al., "Measurement of excitation functions for the ^{nat}Mo(d,x) ^{99}Mo and ^{nat}Mo(p,x)

^{99}Mo reactions," *Applied Radiation and Isotopes*, vol. 69, no. 10, pp. 1447–1452, 2011.

[4] B. Scholten, R. M. Lambrecht, M. Cogneau, H. Vera Ruiz, and S. M. Qaim, "Excitation functions for the cyclotron production of ^{99m}Tc and ^{99}Mo," *Applied Radiation and Isotopes*, vol. 51, no. 1, pp. 69–80, 1999.

[5] S. Takacs, Z. Szucs, F. Tarkanyi, A. Hermanne, and M. Sonck, "Evaluation of proton-induced reactions on ^{100}Mo: new cross sections for the production of ^{99m}Tc and ^{99}Mo," *Journal of Radioanalytical and Nuclear Chemistry*, vol. 257, pp. 195–201, 2003.

[6] M. S. Uddin, M. Hagiwara, F. Tarkanyi, F. Ditroi, and M. Baba, "Experimental studies on the proton-induced activation reactions of molybdenum in the energy range 22–67 MeV," *Applied Radiation and Isotopes*, vol. 60, no. 6, pp. 911–920, 2004.

[7] M. U. Khandaker, M. S. Uddin, K. S. Kim, Y. S. Lee, and G. N. Kim, "Measurement of cross-sections for the (p,xn) reactions in natural molybdenum," *Nuclear Instruments and Methods in Physics Research B*, vol. 262, pp. 171–181, 2007.

[8] M. B. Challan, M. H. N. Comsan, and M. A. Abou-Zeid, "Thin Target yields and EMPIRE-II predictions on the accelerator production of Technetium-^{99}m," *Journal of Nuclear and Radiation Physics*, vol. 1-2, pp. 1–12, 2007.

[9] O. Lebeda and M. Pruszyński, "New measurement of excitation functions for (p,x) reactions on natMo with special regard to the formation of ^{95m}Tc, $^{96m+g}$Tc, ^{99m}Tc and ^{99}Mo," *Applied Radiation and Isotopes*, vol. 68, no. 12, pp. 2355–2365, 2010.

[10] A. A. Alharbi, A. Azzam, M. McCleskey et al., "Medical radioisotopes production: a comprehensive cross-section study for the production of Mo and Tc radioisotopes via proton induced nuclear reactions on ^{nat}Mo, dioisotopes—applications," in *Bio-Medical Science*, N. Singh, Ed., pp. 748–742, InTech, 2011.

[11] M. C. Lagunas-Solar, N. X. Zeng, I. Mirshad, and T. Grey-Morgan, "An Update on the Direct Production of ^{99m}Tc with Proton Beams and enriched ^{100}Mo targets," *Transactions of the American Nuclear Society*, vol. 74, p. 137, 1996.

[12] K. Gagnon, F. Bénard, M. Kovacs et al., "Cyclotron production of ^{99m}Tc: experimental measurement of the ^{100}Mo(p,x) ^{99}Mo, ^{99m}Tc and ^{99g}Tc excitation functions from 8 to 18 MeV," *Nuclear Medicine and Biology*, vol. 38, no. 6, pp. 907–916, 2011.

[13] F. Tárkányi, F. Ditrói, A. Hermanne, S. Takács, and A. V. Ignatyuk, "Investigation of activation cross-sections of proton induced nuclear reactions on ^{nat}Mo up to 40 MeV: new data and evaluation," *Nuclear Instruments and Methods in Physics Research B*, vol. 280, pp. 45–73, 2012.

[14] N. Urbano, S. Modoni, M. Guerra, and M. Chinol, "Evaluation of fresh and old eluate of ^{99}Mo/^{99m}Tc generators used for labeling of different pharmaceutical kits," *Journal of Radioanalytical and Nuclear Chemistry*, vol. 265, no. 1, pp. 7–10, 2005.

[15] B. Guérin, S. Tremblay, S. Rodrigue et al., "Cyclotron production of ^{99m}Tc: an approach to the medical isotope crisis," *Journal of Nuclear Medicine*, vol. 51, no. 4, pp. N13–N16, 2010.

[16] H. Targholizadeh, G. Raisali, A. R. Jalilian, N. Rostampour, M. Ensaf, and M. K. Dehghan, "Cyclotron production of technetium radionuclides using a natural metallic molybdenum thick target and consequent preparation of [Tc]-BRIDA as a radio-labelled kit sample," *Nukleonika*, vol. 55, no. 1, pp. 113–118, 2010.

[17] A. Celler, X. Hou, F. Bénard, and T. Ruth, "Theoretical modeling of yields for proton-induced reactions on natural and enriched molybdenum targets," *Physics in Medicine and Biology*, vol. 56, no. 17, pp. 5469–5484, 2011.

[18] Isoflex Batch, "Certificate of Analyses Mo-100 enriched molybdenum metallic material," (ISOFLEX-USA), 2012.

[19] P. Froment, I. Tilquin, M. Cogneau, T. Delbar, J. Vervier, and G. Ryckewaert, "The production of radioisotopes for medical applications by the adiabatic resonance crossing (ARC) technique," *Nuclear Instruments and Methods in Physics Research A*, vol. 493, no. 3, pp. 165–175, 2002.

[20] K. Abbas, S. Buono, N. Burgio et al., "Development of an accelerator driven neutron activator for medical radioisotope production," *Nuclear Instruments and Methods in Physics Research A*, vol. 601, no. 3, pp. 223–228, 2009.

[21] Y. Nagai and Y. Hatsukawa, "Production of ^{99}Mo for nuclear medicine by ^{100}Mo(n, 2n) ^{99}Mo," *Journal of the Physical Society of Japan*, vol. 78, no. 3, Article ID 033201, 2009.

[22] F. Minato and Y. Nagai, "Estimation of production yield of 99Mo for medical use using neutrons from ^{nat}C(d,n) at Ed = 40 MeV," *Journal of the Physical Society of Japan*, vol. 79, no. 9, Article ID 093201, 2010.

[23] Nuclear Energy Agency, Organisazion for economic co-operation and development 2010 The supply of medical isotopes—review of potential molybdenum-99/technetium-99m production technologies, http://www.oecd-nea.org/med-radio/reports/Med-Radio-99Mo-Prod-Tech.pdf.

[24] A. J. Koning, D. Rochman, S. van der Marck et al., TENDL-2012: TALYS-based evaluated nuclear data library, www.talys.eu/tendl-2012.html.

[25] E. A. Skakun, V. G. Batij, Y. N. Rakivnenko, and O. A. Rastrepin, "Excitation functions and isomer ratios for up-to-9 MeV proton interactions with Zr and Mo isotope nuclei," *Soviet Journal of Nuclear Physics*, vol. 46, no. 17, 1987.

[26] K. Gagnon, J. S. Wilson, C. M. B. Holt et al., "Cyclotron production of ^{99m}Tc: recycling of ^{100}Mo metal targets," *Applied Radiation and Isotopes*, vol. 70, pp. 1685–1690, 2012.

[27] SRIM, "Particle interactions with matter," 2012, http://www.srim.org.

[28] NIST Physical Laboratory, STAR database, http://www.nist.gov/pml/data/star/index.cfm.

[29] T. J. Morley, M. Dodd, K. Gagnon et al., "An automated module for the separation and purification of cyclotron-produced ^{99m}TcO$_4^-$," *Nuclear Medicine and Biology*, vol. 39, no. 4, pp. 551–559, 2012.

[30] European Commission, "Health and consumers directorate general preliminary report on supply of radioisotopes for medical use and current developments in nuclear medicine," Tech. Rep., SANCO/C/3/HW, 2009.

[31] Z. Alfassi, F. Groppi, M. Bonardi, and J. Goeij, "On the artificial nature of Tc and the carrier-free nature of ^{99m}Tc from ^{99}Mo/^{99m}Tc generators," *Applied Radiation and Isotopes*, vol. 63, pp. 37–40, 2002.

[32] S. Chattopadhyay, S. S. Das, M. K. Das, and N. C. Goomer, "Recovery of ^{99m}Tc from Na$_2$[^{99}Mo]MoO$_4$ solution obtained from reactor-produced (n,γ)^{99}Mo using a tiny Dowex-1 column in tandem with a small alumina column," *Applied Radiation and Isotopes*, vol. 66, no. 12, pp. 1814–1817, 2008.

[33] S. Chattopadhyay, S. S. Das, and L. Barua, "A simple and rapid technique for recovery of ^{99m}Tc from low specific activity (n,γ)^{99}Mo based on solvent extraction and column chromatography," *Applied Radiation and Isotopes*, vol. 68, no. 1, pp. 1–4, 2010.

[34] Experimental Nuclear Reaction Data (EXFOR), http://www-nds.iaea.org/exfor/exfor.htm.

Research Article

Production Cycle for Large Scale Fission Mo-99 Separation by the Processing of Irradiated LEU Uranium Silicide Fuel Element Targets

Abdel-Hadi Ali Sameh

Zellmarkstraße 7, 76275 Ettlingen, Germany

Correspondence should be addressed to Abdel-Hadi Ali Sameh; a.a.sameh@gmx.de

Uranium silicide fuels proved over decades their exceptional qualification for the operation of higher flux material testing reactors with LEU elements. The application of such fuels as target materials, particularly for the large scale fission Mo-99 producers, offers an efficient and economical solution for the related facilities. The realization of such aim demands the introduction of a suitable dissolution process for the applied U_3Si_2 compound. Excellent results are achieved by the oxidizing dissolution of the fuel meat in hydrofluoric acid at room temperature. The resulting solution is directly behind added to an over stoichiometric amount of potassium hydroxide solution. Uranium and the bulk of fission products are precipitated together with the transuranium compounds. The filtrate contains the molybdenum and the soluble fission product species. It is further treated similar to the in-full scale proven UAl_x process. The generated off gas stream is handled also as experienced before after passing through KOH washing solution. The generated alkaline fluoride containing waste solution is noncorrosive. Nevertheless fluoride can be selectively bonded as in soluble CaF_2 by addition of a mixture of solid calcium hydroxide calcium carbonate to the sand cement mixture used for waste solidification. The generated elevated amounts of LEU remnants can be recycled and retargeted. The related technology permits the minimization of the generated fuel waste, saving environment, and improving processing economy.

1. Introduction

Particularly for the large scale producers, the conversion of the production targets for fission Mo-99 presents a serious challenge for keeping economical conditions for operating their plants. The uranium enrichment dropping from ~90% to ~19.8% demands modifications on process operation to compensate for the resulting loss in output. Evaluations based on keeping the production process proven since decades unchanged and just increasing the amount of processed targets are not realistic in general. The dominant reasons are limitations on efficient irradiation positions in the available research reactors plus drastically increased processing and waste costs.

The idea of maintaining the current production process [1–8] by increasing fuel densities of the targets exploiting the progress in target technology from actually ~1 gU/cm³

for highly enriched uranium (HEU) to approximately 2.6 gU/cm³ for low enriched uranium (LEU) targets can be classified as a compromise. Such compromise is appropriate for several small- and medium-scale facilities but not for large scale producers of batch sizes in the average of 4000 Ci of Mo-99 at End of Production (EOP). When keeping the same amount of targets, the predictable loss of produced activity will be—under optimal conditions—more than 30%. The described drawback can be prevented by applying LEU targets of factor 5 higher fuel contents than the actual HEU-based targets. Actually, that condition can be fulfilled by two types of targets. One of them is made from U-metal foil tightly enclosed in aluminum. The dissolution process related to these targets is applying nitric acid, respectively, low basic carbonate solution and anodic oxidation of uranium [9–11]. The other target is manufactured from uranium silicide fuel cladded with aluminum, derived from the MTR type fuel

developed for research reactor core conversions. Dissolution experiments of U_3Si_2 in alkaline media by H_2O_2 [12–15] showed promising results on small scale productions which could not be confirmed in larger scale. Main reason for that lack of larger scale is the aggressive decomposition of H_2O_2 in presence of the alloy. With respect to the experienced problem, the process presented below follows another concept.

The publication has focused on the processing of irradiated LEU targets of uranium silicide for the large scale production of fission Mo-99. Silicide targets were favored because of their proven and reliable operation as research reactor fuels during decades and their commercial availability on the world market. Moreover, the results achieved with the presented dissolution process [15–20] favored that selection. As the silicide compound is not attacked by caustic solution applied for the target digestion, a selective dissolution process for the remaining silicide meat had to be developed. Evident condition was and still is that the new process steps are fitting to the proven HEU-based production process operating with UAl_x-Al targets from HEU. Originally the up-to-date process was developed and operated at KFK as an integral part of a closed cycle. Figure 1 shows the scheme of the UAl_x production cycle.

The part of that process related to the Mo-99 separation and the off-gas handling technology is actually operated at the Mallinckrodt Medical Facility at Petten, The Netherlands. Figure 2 shows a simplified scheme of the process operating at Petten. It was established there by a licensing and know-how transfer agreement contracted with KFK. The Petten facility is producing approximately 25% of the world market which is estimated to be 12,000 Ci 6 days precalibrated weekly. The operation reliability and the environmental impact of this installation are exceptional worldwide with an average annual release of 7.3×10^{11} Bq of Xe-133. All data mentioned above were investigated, respectively, determined by the CTBTO and published by PNNL [21].

Already during the development and testing at KFK, implementation of the silicide fuel and related modifications of the original (UAl_x) process had to fit to the proven process concept. At KFK, the investigation program was successfully completed and the process modifications were demonstrated, with both fitting to a later scale of 1,000 6d-Ci Mo-99 at EOP. Keeping the proven concept, the new process has been integrated in a closed fuel cycle. That cycle was demonstrated repeatedly. The Mo-99 separation process is started by alkaline digestion of the irradiated silicide targets. The remaining silicide residue is dissolved in hydrofluoric acid under oxidizing conditions [22, 23].

2. Considerations on Processing Operation

2.1. Uranium Silicide as Target Compound

(i) Processing of irradiated silicide fuels permits the adaptation of major parts of the original HEU process for the production of fission Mo-99 from irradiated UAl_x targets. The selection of U_3Si_2 as the fuel compound for the LEU targets had the same background as had the choice of UAl_x as the fuel compound for the HEU fuel. Both selected target types presented just the adaptation of the type of research reactor fuel throughout applied for the related U-enrichment, resulting in UAl_x-based targets for HEU and U_3Si_2 based for LEU.

(ii) Since some decades, silicide-based fuel elements are presenting the standard nuclear fuels for high and medium flux material test reactors (MTRs). That fuel combines high fuel density with high thermal and dimensional stability and provides operations safety up to burn up of around 80% [15, 17, 19].

(iii) Already the regularly applied standard uranium density of U_3Si_2 fuel of 4.8 gU/cm^3 permits full compensation of the uranium content originating from the conversion from HEU to LEU, for fuel elements as well as for irradiation targets.

(iv) Cladding material and dimensions of the U_3Si_2-based LEU targets are very similar to the processed UAl_x-based HEU targets. That fact prevents expensive modifications of the proven hardware devices used for carrying out the reactor irradiations and handling the production targets in hot cells.

(v) The potential of silicide fuels enables the production of fuel elements and irradiation targets of even higher U-densities, up to 5.8 gU/cm^3. Such fuels were produced from the same named compound and were also successfully irradiated to average burn-ups of above 50% without any deviation in their dimensional and thermal stability [18–20]. The potential for higher U-loading is of relevance with respect to future recycling of the uranium from spent targets and retargeting of the purified fissionable material.

(vi) From economic point of view, recycling and retargeting are essential, particularly for large scale producers.

2.2. Evaluations of Dissolution Process.

The dissolution of the short-time cooled irradiated targets presents a sensitive operation step regarding the high inventory of volatile and radio-toxic fission nuclides contained in the fuel matrix (meat). Operational safety and public acceptance concerns demand the minimization of the potential contamination as well as hazards from emissions of volatile fission products into the environment. Most efficient precaution measure is the implementation of advanced processing and off-gas handling technologies. Both measures are interacting with each other. Essential precondition for the minimized release of iodine is the exclusion of any acidic operation as long as iodine activity is in the system. Another concern is related to elevated releases of the isotopes Xe-133 and Xe-135 to the environment. The most efficient and economical way of handling those issues is applying a combination of advanced process operation technology and efficient xenon retention, respectively, delay on charcoal columns. For safety reasons, any application of charcoal filters is strictly prohibiting the presence of nitrogen oxide in the off-gas stream. Thus, any dissolution of irradiated fuel in nitric acid would be most critical as nitric acid is always accompanied by NO_2
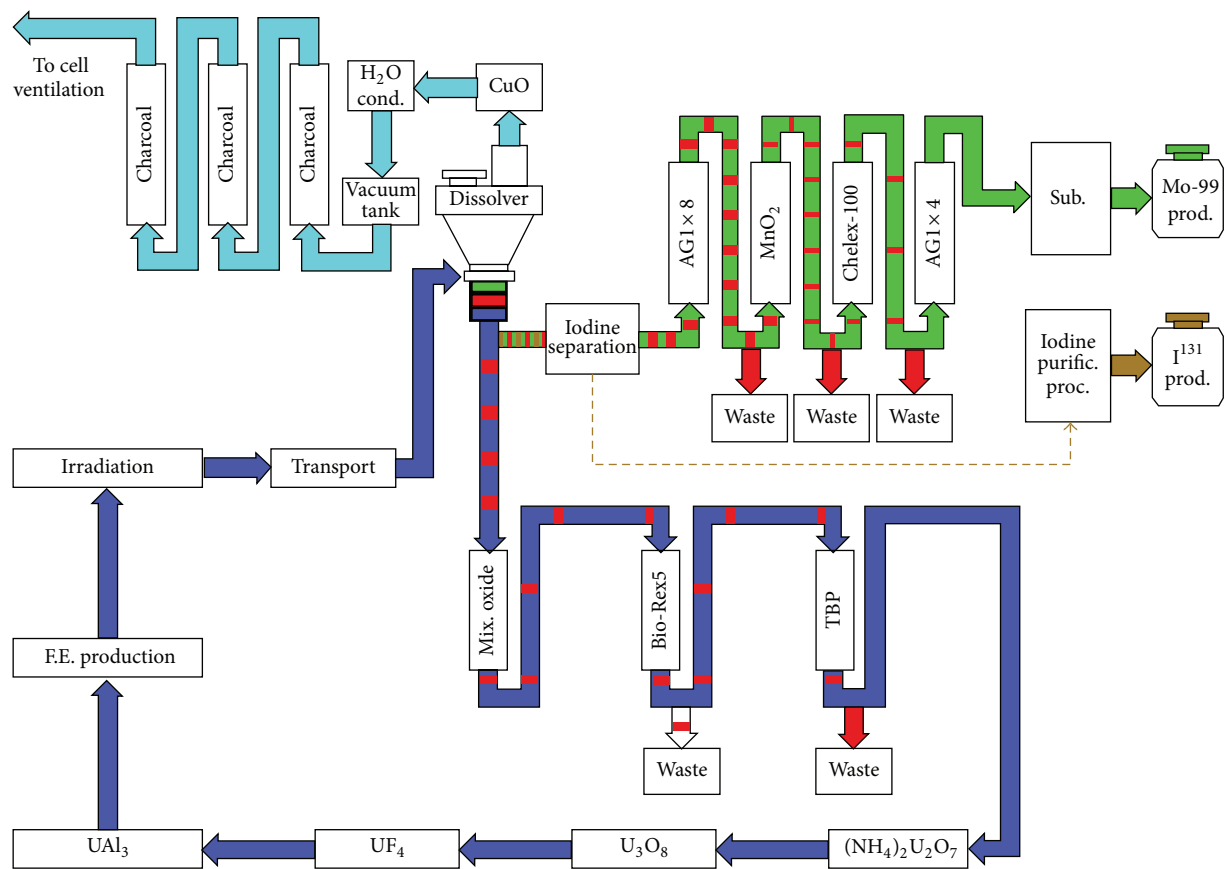
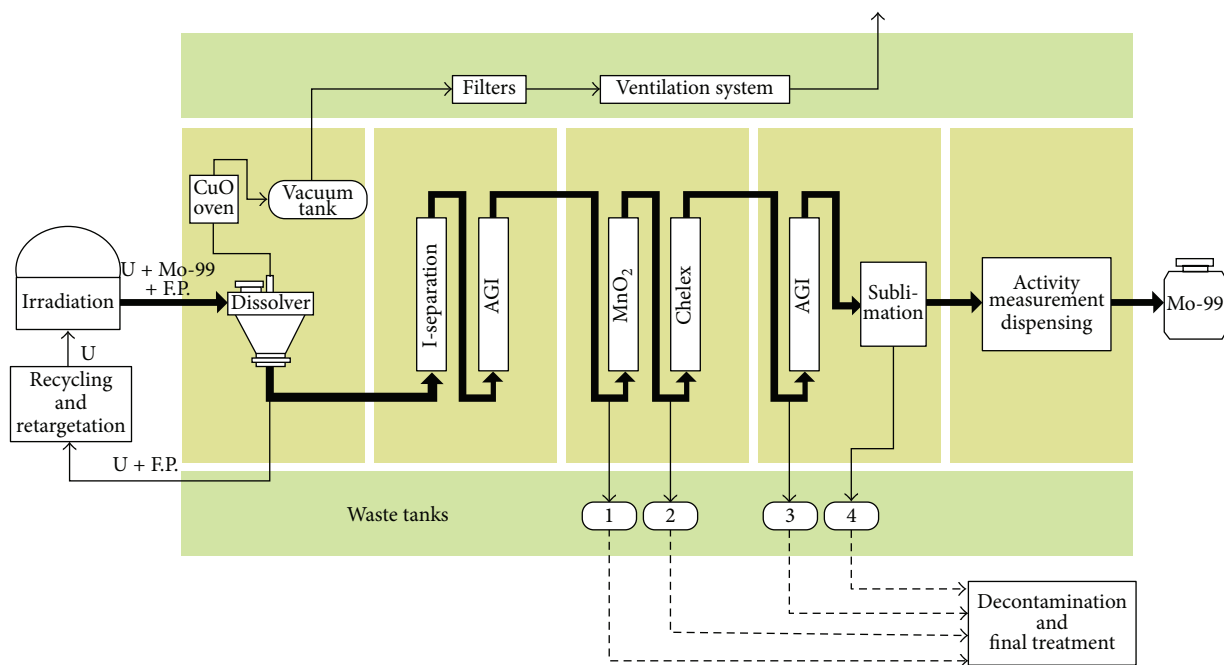FIGURE 1: Production cycle of HEU-based UAl$_x$- plate-type targets.

FIGURE 2: Schemes of the HEU-based fission Mo-99 production process from irradiated UAl$_x$ targets.

permanently generated during such operation by radiation degradation of HNO_3.

The described drawbacks are major reasons for a strong preference for the alkaline processing starting by the alkaline digestion of the target. The digestion is fully sufficient to get the molybdenum into solution as it is attacking the aluminide compound. Subsequently the silicide is dissolved by an oxidizing acid treatment at room temperature. The selected solvent HF is proved to be efficient as well as excellent to handle by using related proven materials inside the hot cell such as Hastelloy. Hastelloy has been applied for the production of hundreds of tons of HF per year by chemical industry. The described drawbacks of applying HNO_3 accompanied by its degradation products are prevented by the KFK-developed processing system. As HF is one of the most resistant chemicals, it is not decomposing by radiation and it is excellent to be washed out of the off-gas stream by passing through a solution of KOH. The dissolution process is carried out at room temperature within 60 minutes. In the subsequent purification process the acidic solution has not to be handled as it is converted to alkaline after the dissolution step. Fluoride anions in the alkaline solution are neither corrosive nor disturbing the following purification of the product stream. Further, fluoride anions in the alkaline media are not disturbing the Mo-retention on the anion exchanger AG1 (see Figures 1 and 2). Nitrates as added by some producers to the digesting solution are the blocking highly efficient and economical purification systems such as AG1 and Chelex-100. To prevent hydrogen formation during the alkaline digestion step of the aluminum alloy of the target cladding and the UAl_x meat, in some processes, nitrate is added. The alternative hydrogen oxidation to water on copper oxide as applied at KFK never created any problem with all users. For the described reasons all large scale producers including the Petten facility never added nitrate to the caustic solution. A final aspect of the KFK designed and developed processing is related to the waste treatment. For the silicide process the alkaline waste stream is solidified in cement similar to the comparable UAl_x process. In case of the silicide dissolution, the fluoride content in the alkaline solution is—with solid mixture of $Ca(OH)_2$ and $CaCO_3$ added to the cement—forming insoluble CaF_2.

Back to the dissolution part of the processing, both the digestion of the target and the subsequent HF-dissolution step are operated in a Hastelloy dissolver. The filtration unit connected to the dissolver is also made from Hastelloy. The Mo-separation process is started by the alkaline digestion of the aluminum cladding (preferably "AlMg1") together with Al-matrix of the meat, the fueled part of the target, in 6 M KOH. Aluminum and the fission products located at the surface of the insoluble silicide particles are dissolved. These are mainly cesium, strontium, iodine, molybdenum, and small contaminations of other fission products such as lanthanides, ruthenium, and zirconium. The off-gas of the alkaline digestion contains hydrogen generated by the aluminum dissolution to aluminate and the magnesium conversion to the hydroxide together with approx. 10% of the noble gas activity. The major radioactivity of the gas stream is originating from Xe-133 and Xe-135. The noble gases leave the dissolver together with the hydrogen at its upper end, driven by helium or nitrogen gas which is constantly metered into the dissolver. Hydrogen is oxidized to water via a copper oxide "oven." That oven is a heated device containing CuO. The formed water steam is condensed in a related device. Xenon is collected together with the driving gas in preevacuated stainless steel tanks and pumped into a xenon delay section later on passing cooled deep bed carbon filters on its way. The described operation, which is similar to the UAl_x digestion, is schematically presented in Figure 3.

The filtrate of the alkaline digestion contains approx. 10% of the Mo-99 generated by fission together with the related soluble fission-generated nuclides. To collect the included Mo-activity the filtrate is undergoing the same purification procedure as the molybdenum bulk later on. Therefore the filtrate is fed through a floating silver oxide column where iodine is retained. Figure 4 is showing a simplified scheme of the iodine separation on this advanced system. The named column is located above a stainless steel (SS) device provided with a filtration and collecting unit. The column is connected with the device below by an SS-valve. That valve to the vessel is closed during feeding the process solution. After ending loading of the iodine containing solution the valve to the vessel is opened. The floating silver oxide is washed into the vessel. The collected silver oxide is reduced to silver by a solution of H_2O_2. The previously retained iodine remains loaded over silver metal as silver iodide. It can be stored for safe iodine decay or further used for the separation of I-131 on commercial base.

The passing through solution which contains the Mo-activity is loaded on the strongly basic anion exchanger AG1. The operation step described in the previous section is repeated with the alkaline bulk resulting from the silicide dissolution. The Mo-bulk is also fed through the same AG1 column after completion of the above described iodine separation step on silver oxide. The eluate of AG1 contains the combined two Mo-streams. In order to improve the purification efficiency and to reduce the amount of higher active solid waste, the AG1 operation is split into two AG1 columns connected and acting behind each other. The first AG1 is made of stainless steel and the second being a larger column is of propylene (PP). As experienced, contaminants (on top of all iodine) and soluble ruthenate compounds reduced to ruthenium dioxide on the organic resin are retained at the entering side on the first column. Molybdenum is moved by the alkaline process solution and the following washing KOH solution through the first column to the second and larger column connected behind. After disconnecting of the first column being loaded with contaminants, the elution of molybdenum from that second column is initiated. With respect to the minimization of higher active waste, the small column is made of stainless steel to permit long-term radiation resistant storage of the tightly enclosed contaminants. The larger column behind is of PP. It is cheaper to purchase and far more economical to treat as waste. The experience achieved with this modification is highly positive from all sides. The same concept is applied by the final AG1 system (see Figure 2) as the potential contamination hazard is very low. Here the entering small column is of PP already.
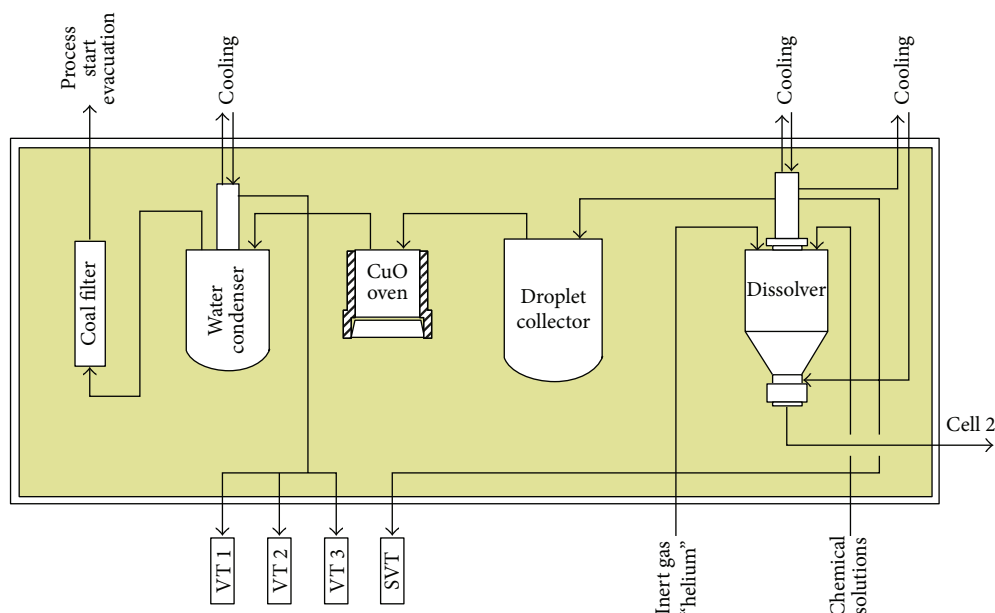
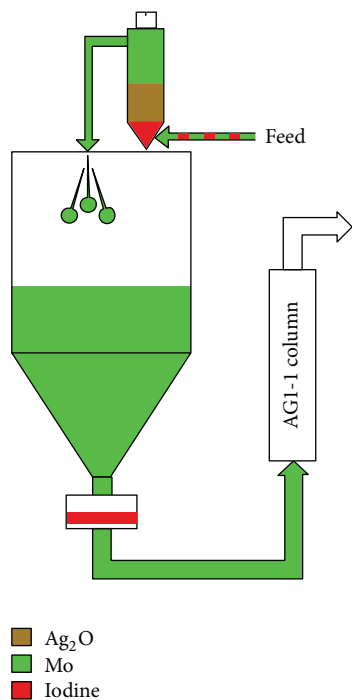FIGURE 3: Treatment of the off-gas generated during alkaline digestion of U_3Si_2 and AlMg1-cladding.
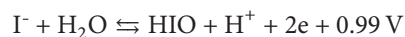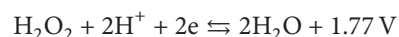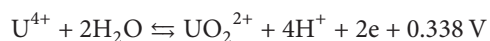

FIGURE 4: Separation of iodine on the floating silver oxide column.

2.3. Dissolution of Silicide Meat in HF/H_2O_2.

The silicide particles of the meat remaining on the sinter metal filter are dissolved in ~6 M HF under catalyzed oxidation conditions [23]. The oxidation agent is hydrogen peroxide. Suitable catalytic agents are KI, KBr, and KCl or higher oxidation states of halogen compounds such as hypochlorite, hypobromite, or KIO_3. The dissolution is carried out at ~20°C. The oxidation agent is needed to oxidize the primary formed insoluble layer of UF_4 to soluble UO_2F_2. The oxidation with H_2O_2 in absence of the catalyzing agent is inefficient because a major amount of the H_2O_2 is just decomposed without significant impact. Fully different is the situation in presence of the mentioned halide compounds. All these compounds are oxidized by H_2O_2 which acts as strong oxidizing agent in acidic solutions. The following formula and the related redox potentials underline the oxidation efficiency of hydrogen peroxide in acidic media.

Redox potentials of H_2O_2 and related catalysing compounds used for the oxidation of U^{IV} to U^{VI} and its solution in hydrofluoric acid:

$$U^{4+} + 2H_2O \leftrightarrows UO_2^{2+} + 4H^+ + 2e + 0.338\,V$$

$$H_2O_2 + 2H^+ + 2e \leftrightarrows 2H_2O + 1.77\,V$$

$$Cl^- + H_2O \leftrightarrows HClO + H^+ + 2e + 1.50\,V \qquad (1)$$

$$Br^- + H_2O \leftrightarrows HBrO + H^+ + 2e + 1.33\,V$$

$$I^- + H_2O \leftrightarrows HIO + H^+ + 2e + 0.99\,V$$

The oxidized halogen compounds oxidize efficiently UF4 to soluble UO_2F_2 following the chemical formula:

$$UF_4 + HIO \longrightarrow UO_2F_2 + HI + 2HF \qquad (2)$$
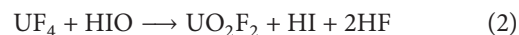
The complete dissolution formula for the silicide alloy is

$$U_3Si_2 + 18HF + 6H_2O_2 \longrightarrow 3UO_2F_2 + 2H_2SiF_6 + 6H_2 \qquad (3)$$
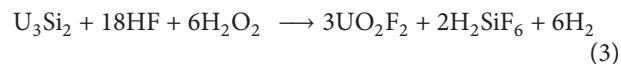
Following the formula, 18 moles of HF is needed for the dissolution of 768.5 g of the alloy. A full scale production of about 4,000 Ci at EOP demands around 200 g of 19.75%

enriched U_3Si_2, assuming similar irradiation conditions as applied for an equivalent amount of HEU, 93% enriched. The dissolution of the HEU-related amount demands far less hydrofluoric acid.

The dissolution of the silicide is completed within ~60 minutes. The solution is pressed through the sinter metal filter and fed in to an over stoichiometric amount of ~8 M KOH solution. The KOH excess is adjusted to a final total molarity of ~3 M KOH. Uranium is precipitated as potassium uranate together with the insoluble hydroxides and oxide hydrates of the related fission products and higher actinides. The alkaline filtrate contains all in the fuel still remaining Mo-99 activity. This amount presents 90% of the in total by fission generated Mo-99 activity. The solution also contains the related soluble fission products iodine, cesium, partially strontium, and contaminants of further fission products, mainly ruthenium and antimony.

The above described HF treatment is operated in Hastelloy devices. Also the acidic filtrate is fed through a Hastelloy pipe in to the precipitation vessel, below the surface of the KOH solution. All tubes used for feeding the acidic solution are treated behind with alkaline solution. All operations under alkaline conditions are carried out in stainless steel devices.

The uranium precipitate is boiled for 20 minutes to insure the decomposition of the formed soluble peroxide compounds of uranium. The Mo-containing filtrate is fed through the floating silver oxide column as described before (see Figure 4). The filtrate of the formed Ag/AgI_ precipitate is fed through the same AG1 column which the first 10% of generated Mo had been loaded on. The described operation and the specific treatment of the dissolver exhaust gases both during the HF operation [23] are schematically presented in Figure 5.

2.4. Elution of the AG1 Column.

The loaded AG1 is washed by minimal 3-column volumes of 3 M KOH to ensure efficient replacement of the fluoride anions. The resin bed is emptied from residual amounts of the KOH solution by passing air through. The elution is initiated by a solution of 1 M NaOH and 2 M NaNO$_3$. The solution is fed from the bottom to the top of the column to achieve optimal contact between eluent and resin. The introduction of nitric acid and nitrate ensures excellent elution yields for this operation. The positive influence of nitrate on the Mo-elution from AG1 turns to the negative for the subsequent purification step on Chelex-100. Thereto molybdenum is loaded on Chelex-100 from a reducing and complex forming media. Nitrate must be avoided in the whole system by loading of the cationic molybdenum compounds on a stationary phase, followed by washing out the NO_3^-/HNO_3.

2.5. Mo-Loading on Hydrated MnO$_2$ and Dissolution of the Loaded Matrix.

The eluate of the AG1 column is acidified by HNO$_3$ to a final acidity of ~1 molar. The adjusted Mo-solution is fed through a column of hydrated MnO$_2$. Molybdenum is retained as cationic molybdenyl compound on the inorganic exchanger. The Mo-loaded stationary phase is washed with a solution containing ~0.01 M K$_2$SO$_4$. The amount of the washing solution is adjusted such that the passing through solution is free of nitrate. The addition of K$_2$SO$_4$ is needed to stabilize the lattice of the MnO$_2$ matrix by the larger potassium cation.

The introduction of the MnO$_2$ column offers additional benefits on top off all the concentration of molybdenum and compact feed for the following purification step. The purified product is released from the column, free of losses by a unique operation [24]. Thereto the loaded matrix is directly dissolved in the feeding solution prior to the subsequent purification step on Chelex-100. The resulting solution consists of sulfuric acid, thiocyanate, sodium sulfite, and potassium iodide. The final molarity of the major compound is ~2 M H$_2$SO$_4$. Under these conditions the molybdenum is reduced and forms the extremely stable anionic complex $[Mo(SCN)_6]^{-3}$. The Mo-complex is retained on Chelex-100 with a distribution coefficient of about 5×10^4. In absence of the exchanger, Mo-compounds of different oxidation stages below 6 are formed. In presence of the exchanger the equilibrium is moved to the complex of the highest negative charge. This compound is the red $[Mo(SCN)_6]^{-3}$ complex. Higher Mo-oxidation stages have lower specific electrical charges. When the preferred compound is retained on the matrix, the dynamic equilibrium is moving in the described direction.

2.6. Purification on Chelex-100 Column.

The purification of molybdenum on Chelex-100 offers outstanding decontamination efficiency [25].

This fact is underlined by the extremely high distribution coefficient for molybdenum thiocyanate compound on the resin of around 5×10^4, while the distribution coefficients of the related fission products species are in the average of 1 [4]. Most relevant for this part of operation are contaminations of lanthanides, ruthenium, and zirconium. The realized separation factors for the mentioned contaminations are ~10^4.

2.7. Final Chromatographic Purification on AG1 Column.

The following operation is introduced as a preparatory step for the sublimation of MoVI oxide. The sublimation presents the ultimate purification of the product from organic and inorganic impurities.

Organic impurities are originating from flexible connecting tubes and applied organic exchangers. Such impurities present potential reducing agents and are the cause for lower elution yields of technetium from the generators at a later stage.

Inorganic impurity traces of iron, nickel, cobalt, and chromium are brought in the product solution by applied metallic hardware components. The presence of such impurities in the final product is the major reason for elevated breakthrough of molybdenum during loading and elution of the Tc-generator columns. Such phenomenon can be explained by the instability of the related cations under low acidic loading and almost neutral pH-values during elution of the generators. The formed colloids in the solution adjusted for generator loading retain the molybdenum compounds on
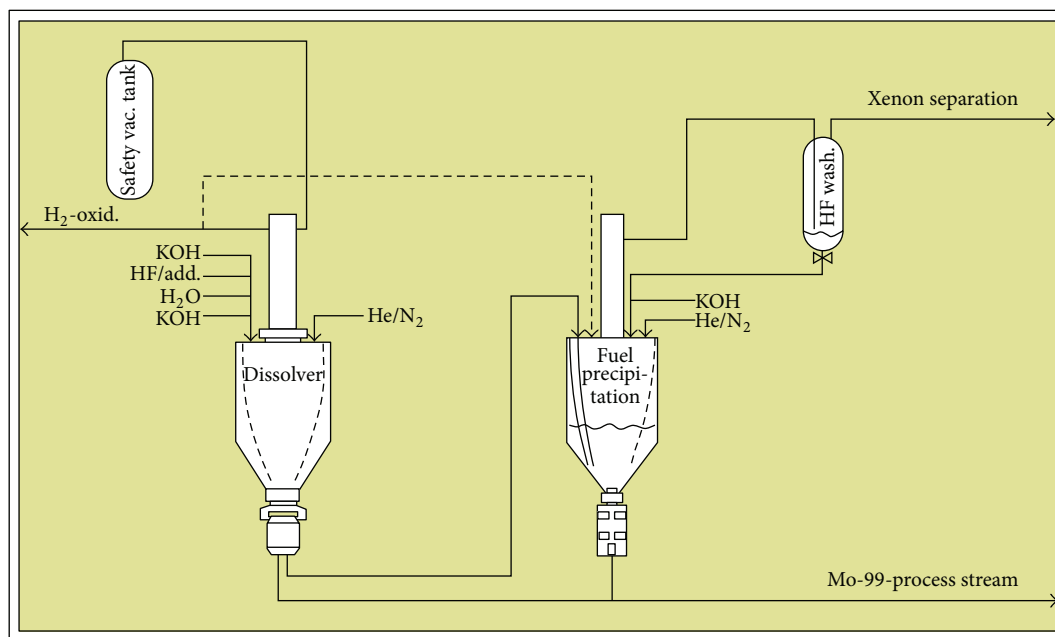
FIGURE 5: Combined operation of U_3Si_2 dissolution and precipitation.

their surface and pass, loaded with molybdenum, through the generator column.

The gradual thermal treatment of the dried product of up to ~1,000°C at which the sublimation is completed decomposes the organic compounds and converts the inorganic impurities to the insoluble and chemically resistant so-called highly burned oxides. The oxides remain in the crucible while molybdenum oxide is sublimated. The resulting product shows excellent behavior during transportation of the bulk solution to the users and on the generators.

The sublimation step demands the preseparation of the major bulk of the cations, mainly of sodium from the Mo-containing solution. The presence of sodium in the Mo-solution would lead to the formation of mixed oxides with molybdenum. The volatilization of MoVI-oxide from such compound demands for higher temperatures than salt-free systems. The purification of the Mo-solution is achieved by loading of molybdenum on an AG1 column. The stationary phase is washed by feeding of the sufficient amount of water through its resin bed.

The molybdenum elution is carried out by slow metering of highly pure 2–4 M HNO_3 through the column.

2.8. Sublimation of MoVI-Oxide and Final Product Preparation.

The nitric eluate is filled into a platinum/iridium crucible and evaporated to dryness. The operation is carried out in controlled ventilated quartz equipment. The acid vapor is driven out of the evaporation equipment by a metered nitrogen gas stream. The gas stream is directly fed through washing devices to prevent the contamination of the cell environment with acid and nitrogen oxide. After completed evaporation the crucible with the included dried MoVI-nitrate is placed in the quartz sublimation device. The complete unite is then placed into the sublimation oven. The temperature in the

oven is gradually increased up to ~1,000°C. The sublimated Mo-oxide is collected in the quartz condenser above the crucible. The sublimation device is taken out of the oven for cooling in cell atmosphere. After a cooling time of ~15 min the condensed Mo-oxide is dissolved in ammonia solution.

The Mo-solution is transferred into a round bottom flask. After adding a mixture of sodium hydroxide and sodium nitrate as calculated for the amount of final product, the ammonia is trapped out by smooth boiling. Both compounds are added to the final product solution to stabilize the molybdate in the high active solution and to prevent the precipitation of Mo-compounds of lower oxidation level, mainly consisting of hydrated MoO_2. The addition of nitrate is also recommended to reduce the amount of hydrogen generated by radiation degradation of water in the product flask. The nitrate anions act as a radical catcher for hydrogen radicals, forming nitrite anions and water.

2.9. Recycling of Uranium from the Spent Fuel Residue.

The uranium recycling process is initiated by dissolution and purification of the uranium stored in the collecting sinter metal filters. Those filters carry about 98% of the initially irradiated uranium as alkali uranate together with the insoluble fission products and the transuranium elements. The U-decontamination is carried out after an approximate cooling time of 6 months. During this period U-237 and the shorter living fission products have decayed. The remaining radiation dose of the residue is mainly caused by the fission product nuclides ruthenium, zirconium, niobium, and the lanthanides. The residue includes also the generated plutonium as oxide/oxide hydrate. The dissolution concept aims for the selective dissolution of uranium by keeping the bulk of the activity carriers and particularly plutonium in the residue.

According to those considerations, a suitable process was developed and demonstrated at KFK [26]. The process is based on the basic dissolution of uranium by formation of the soluble anionic uranyl-tricarbonate complex $[UO_2(CO_3)_3]^{-4}$. The dissolution is carried out in hydrogen carbonate, carbonate, or mixed solutions of both. Hydrogen peroxide is added to the solution for the oxidation of U-species of lower oxidation stages potentially formed by radiation. The dissolution is carried out at temperatures between 20 and 40°C. Figure 6 shows the dissolution behavior of ammonium diuranate as a function of CO_3^{-2} concentration.

Figure 6 delivers the maximum uranium solubility of this system being at 48 gU/L. For practical operation conditions a U-solubility of 40 gU/L should be considered. The limited solubility of uranium in the HCO_3^-/CO_3^{-2} is by far overcompensated by the achieved advantages, which are as follows.

(i) Efficient decontamination of the uranium stream already by the dissolution process, in contradiction to the common fuel dissolution in nitric acid in which the uranium and nearly the whole contaminants are dissolved. The realized decontamination factors for uranium in the hydrogen-carbonate/carbonate system are in the average of 100. The high separation efficiency also includes the decontamination from the generated transuranium elements neptunium and plutonium. Both are retained in the residue when the basic solution is boiled for 30 minutes.

(ii) Safe processing conditions, such as carbonate solutions being absolutely noncorrosive and requiring uncomplicated off-gas treatment measures only.

(iii) Quick and economical predecontamination of the uranium stream on compact, radiation resistant inorganic adsorbers.

2.10. Chromatographic Decontamination of the Uranium Tricarbonate Stream.

In spite of the high decontamination of uranium by the carbonate dissolution, fission product carbonate ions are codissolved. Possibilities for their pre-separation on selective, radiation-resistant inorganic exchangers [26] were experimentally investigated. Static distribution experiments of the relevant fission nuclide ions on inorganic exchangers showed promising separation options for carbonate media. The preselected exchangers were further tested under dynamic conditions in absence—and later on also in presence—of uranium in the solution. The determined retention efficiencies of the relevant fission nuclides on the investigated exchangers are composed in Table 1. The retention efficiencies of the related fission products on the different columns are expressed in % of the original activity in the solution.

The data above show the efficiency of several inorganic exchangers for the separation of the investigated fission products in this system. Regarding these data, ruthenium is not completely retained on the related exchangers only. The successful adaptation of these promising systems under real process conditions depends on further information such as

TABLE 1: Dynamic retention behavior of fission product traces on inorganic exchanger columns: loading solution: 10 mL, washing solution: 15 mL, total HCO_3^-/CO_3^{-2} content: 1 M, column diameter: 9.7 mm, bed volume: 5.5 mL, adsorber weight: 5 g, loading speed: 30 cv/h.

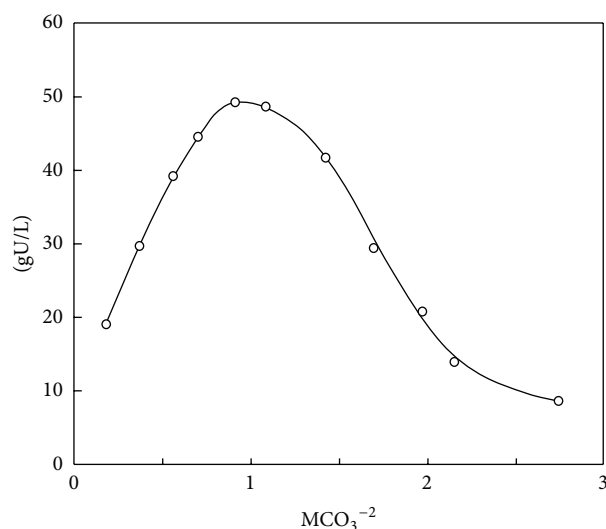| Fiss. Prod.	Ce	Cs	Ru	Sb	Sr	Zr
Al_2O_3	100	60	94	38	100	0
MnO_2	100	7	82	100	100	100
SnO_2	95	0	6	0	100	63

FIGURE 6: Dissolution of ammonium diuranate at varying CO_3^{-2} concentrations.

the specific retention capacity of each nuclide in presence of uranium under real operation conditions.

Figure 7 shows the corresponding data for cerium on MnO_2 as the stationary phase, Ce-141 being added as an indicator. The figure shows the high efficiency of hydrated MnO_2 as a matrix for the chromatic separation of cerium from hydrogen-carbonate/carbonate containing solutions.

Comparable data were achieved for the other fission nuclides. All except ruthenium could be separated at one step on MnO_2 columns. The deviating behavior of ruthenium is related to its ability to form varying complexes simultaneously. Even in presence of an adsorber retaining the preferred complex, the equilibrium adjustment is too slowly.

Interesting is the observed increase of the fission product retention in presence of uranium. The most probable explanation for this behavior is the decrease in concentration of free HCO_3^-/CO_3^{-2} ions caused by the complex formation with uranium. Higher HCO_3^-/CO_3^{-2} concentrations lead to the formation of negative charged fission product ions which are not retained on the adsorber. The reduced retention efficiency of ruthenium is also improved by the presence of uranium in the system but still remains lower than of all nuclides tested for the data of Table 1. Therefore additional purification steps are needed for the complete decontamination of the process stream from the rest activity of ruthenium remaining in the solution. The deviating behavior of ruthenium is also
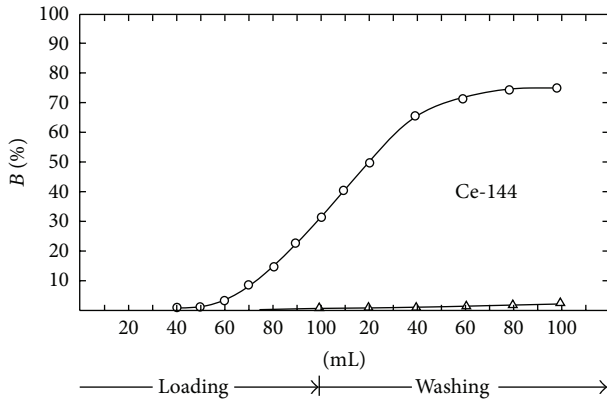
FIGURE 7: Breakthrough of cerium during the loading and washing on hydrated MnO_2 column from hydrogen-carbonate/carbonate containing solution: HCO_3^-/CO_3^{-2}, ratio: 95/5, total molarity: 1 M, cerium-concentration: 1 mg/L, U-concentration: 35 g/L, column inner diameter: 9.7 mm, bed volume: 5.5 mL, adsorber weight: 5.5 g MnO_2, and loading speed: 30 cv/h. Ce-141 was added to the loading solution as a radioactive indicator.
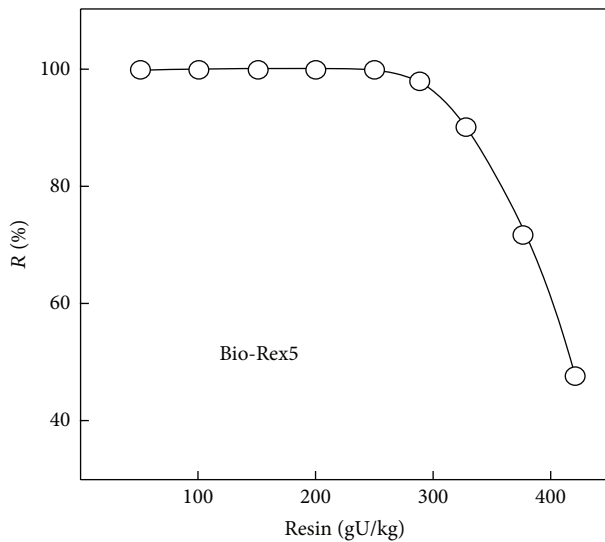

FIGURE 9: U-elution with 4 M HNO_3.

FIGURE 8: U-loading on Bio-Rex5 U 1: 3 HCO_3^-/CO_3^{-2}.
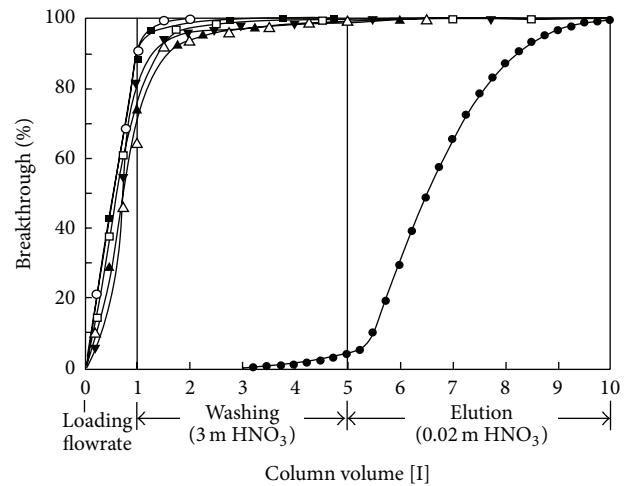
Breakthrough after washing:

- □ Ce-144: 99.4%   △ Ru-106: 99.4%
- ■ Cs-137: 99.9%   ○ Sb-125: 100.0%
- ▼ Nb-95: 99.0%   ● Uran: 3.8%
- ▲ Zr-95: 99.4%

FIGURE 10: Decontamination of uranium from fission product species on TBP loaded SM-7 column.

experienced in different systems, for example, nitric acid. In the latter, 21 species of ruthenium were determined, anionic, neutral, and cationic. The latter is a reason too that the complete separation of ruthenium demands a series of steps.

2.11. Uranium Concentration and Final Purification. The decontaminated fuel solution still has to undergo a final purification process in which the alkaline salt content and the still remaining fission product nuclides are separated. Under such conditions best results are achieved by the proven PUREX-process [27, 28]. Uranium is extracted from nitric acid solution in tributyl phosphate. Optimal extraction conditions are obtained by the extraction of uranium from approximately 3 M HNO_3 in an organic phase containing 30 vol% TBP in kerosine. The liquid/liquid extraction system

is the best solution for middle to large scale batches and can be operated continuously. The situation is different for the recycling of the U-batches needed for Mo-99 production targets. Batch sizes of 1,000 g are optimal to be operated in laboratory scale. The most practical operation is achieved by using the solid-bed extraction technique [29, 30]. It is based on the extraction of $UO_2(NO_3)_2$ dissolved in nitric acid in undiluted TBP. TBP is loaded on a macroporous nonpolar matrix of polystyrene-divinyl benzene such as Bio-Beads SM-2 and SM-4 (Bio-Rad, Richmond, VA, USA) or on the intermediate
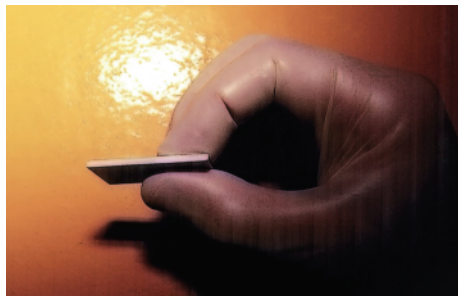
FIGURE 11: Side view of the fuel rectangle.

FIGURE 12: Surface view of the fuel rectangle.

FIGURE 13: Preparation of the uranium silicide target plate.

polar acrylic ester matrix SM-7 (Bio-Rad). The described technique combines the high decontamination efficiency of the TBP/HNO_3 system with the simple handling of chromatographic operations. Favored operation conditions for the solid bed extraction are achieved from feed solutions of higher U-concentrations. Under such conditions the extraction of contaminants such as ruthenium and zirconium is efficiently reduced. As previously described, the U-solubility in carbonate solutions is limited to 45 gU/L. Optimal decontamination of uranium on TBP loaded solid-bed columns is achieved at U-concentrations in the average of 200 g/L. Such conditions are realized most practical by loading of the U-tricarbonate species on the intermediate basic exchanger Bio-Rex5 (Bio-Rad) which permits the loading of approx. 300 g of uranium on 1 kg of the resin. The elution is carried out by 4 M HNO_3 from the bottom to the top of the column to prevent overpressure formation by the released CO_2. The eluent acid concentration also presents the optimal loading HNO_3 molarity for the solid-bed extraction. Figure 8 shows the U-loading on Bio-Rex5 from the carbonate solution. Figure 9 shows the U-elution with 4 M HNO_3 from the Bio-Rex5. The elution with 4 M HNO_3 considers acid losses by adsorption during elution of the exchanger, resulting in an approximate HNO_3 molarity of 3 in the U-eluate presenting the optimal molarity for the solid-bed extraction.

Subsequently the U-containing nitric acid solution is fed through the TBP loaded solid-bed column. Uranium is extracted under the optimized loading conditions as a sharp yellow band on the stationary phase while the fission products leave the column at the upper end. After washing the stationary phase with 3 M HNO_3, uranium is eluted by 0.02 M HNO_3. Figure 10 shows typical solid-bed extraction curves
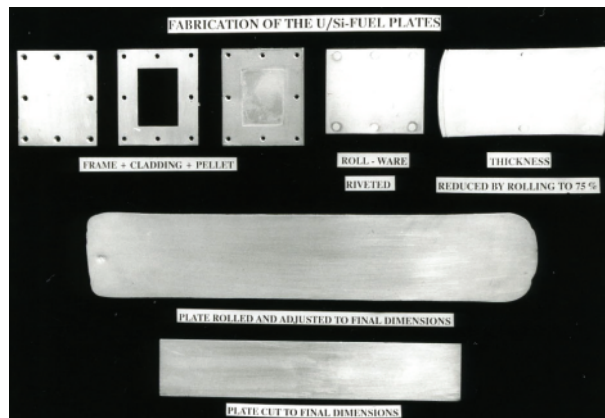
for uranium and potentially accompanying fission products on a TBP loaded SM7 column.

Uranium is precipitated by ammonium hydroxide. The ammonium diuranate precipitate is centrifuged, dried, and finally calcined at 800°C to U_3O_8.

2.12. Preparation of the Uranium Silicide Alloy. The uranium oxide is transferred to a nickel crucible and converted to UF_4 by treatment with a gas mixture of hydrogen and hydrogen fluoride in argon atmosphere at 650°C. The reaction is performed in a nickel oven. The UF_4-powder is transferred to KUF_5 by melting the tetrafluoride with the stoichiometric amount of potassium fluoride in the same oven at 850°C. The conversion to KUF_5 is carried out in argon atmosphere in a graphite crucible. The product is powdered and added in small portions to a melting electrolysis bath of a salt mixture of 50 weight% NaCl and KCl in which the graphite crucible is acting as anode. A molybdenum sheet is used as the cathode. The process is carried out in argon atmosphere at 800°C. The U-loaded cathode is replaced frequently and washed after subsequent cooling with ethyl-alcohol containing few percent of water and cold water to dissolve the uranium accompanying salt in an ultrasonic bath. The described procedure is carried out in argon atmosphere. The dried U-powder is finally melted in argon atmosphere under low pressure with silicon to U_3Si_2. The melting procedure is carried out in a high-frequency oven at 1,850°C.

2.13. Fuel Targeting. The alloy is transferred into a glove box line in which the U_3Si_2 is grounded in a hard metal swinging mill. All following operations up to the fuel meat encapsulation are carried out in argon atmosphere. The milled alloy is sieved. Only particles with grain sizes below 40 micrometers were mixed with aluminum powder of the same particle size. Aliquots of this mixture are pressed to rectangles which will present the meat zone in the final plate. Figures 11 and 12 show photographs of formed rectangles from 2 directions. Figure 13 shows the target preparation steps starting by the formed rectangle.
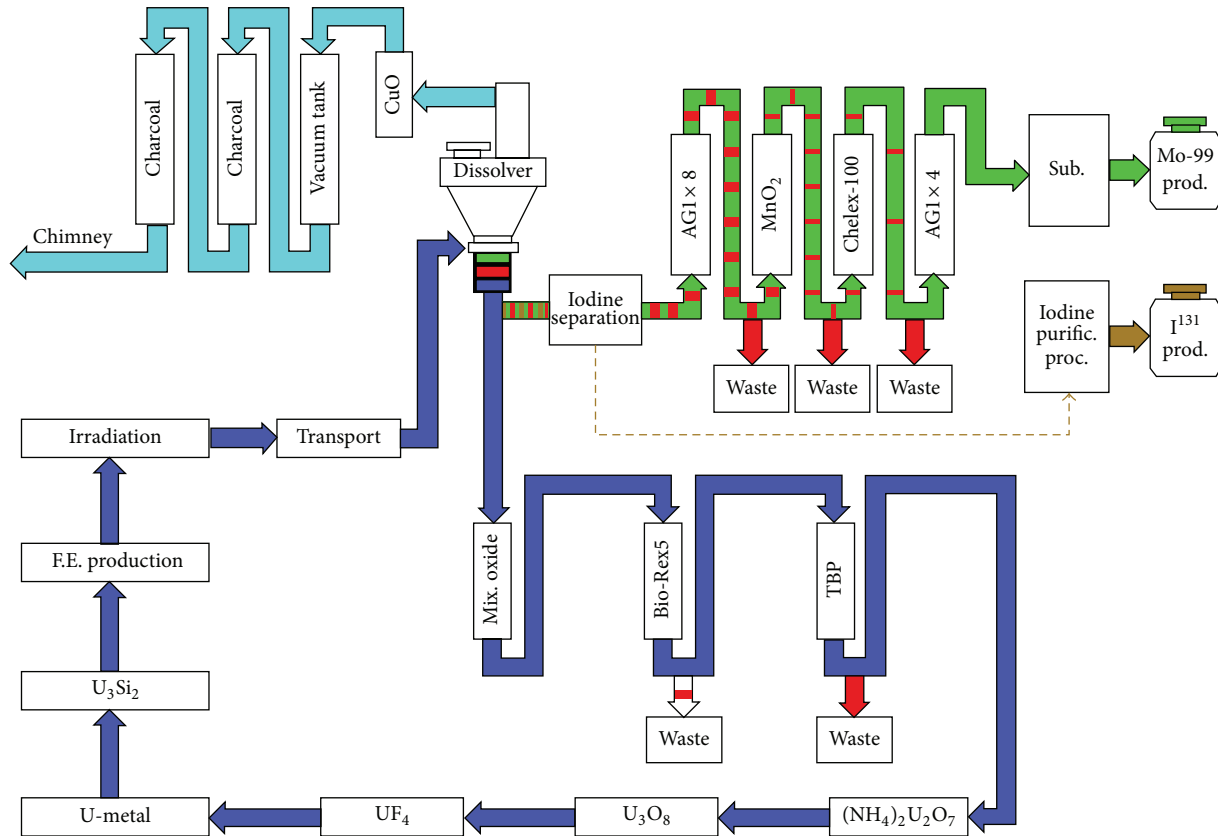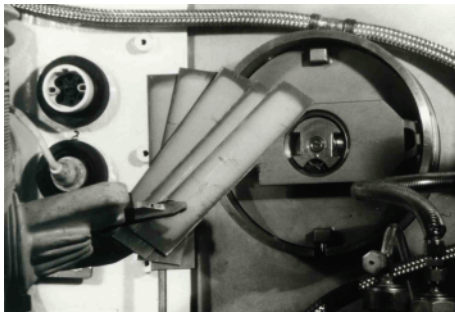
FIGURE 14: Simplified scheme of the U_3Si_2 production cycle.

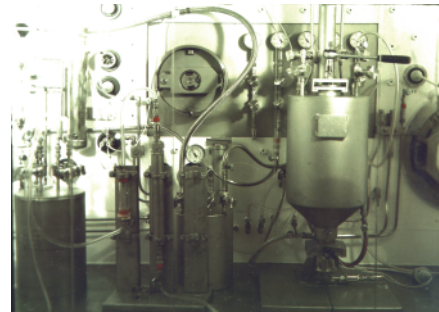FIGURE 15: Irradiated silicide-based fuel targets prior to starting the dissolution process at KFK.

FIGURE 16: Dissolution cell and the applied hardware devices for process operation at KFK.

Each rectangle (meat) is placed into a suitable frame of an aluminum-magnesium alloy, for example, AlMg1. Then the combined frame + meat is covered on both sides with plates of the same alloy. The package is riveted together and stepwise rolled to the final thickness. Before each rolling step the fuel package is heated up to 400–450°C before each rolling step. The fuel zone is marked under an X-ray screen. After cutting to the final shape, surface treatment completes the manufacturing. Figure 13 depicts the parts and steps of target manufacturing. The manufacturing technology follows related experiences at KFK [31, 32].

2.14. Target Irradiation and Processing. Hundreds of targets were produced from natural uranium in order to develop and verify production technique and fulfillment of the required quality standards. The target qualification standards were identical to those of regular MTR-fuel elements qualification standards.

Fuel densities were varying between 1.5 and 5.0 gU/cm³. Natural uranium targets were also used for the development and cold testing of the new silicide treatment process. The uranium precipitates generated by cold testing have been recycled. The prepared silicide fuel was applied for the
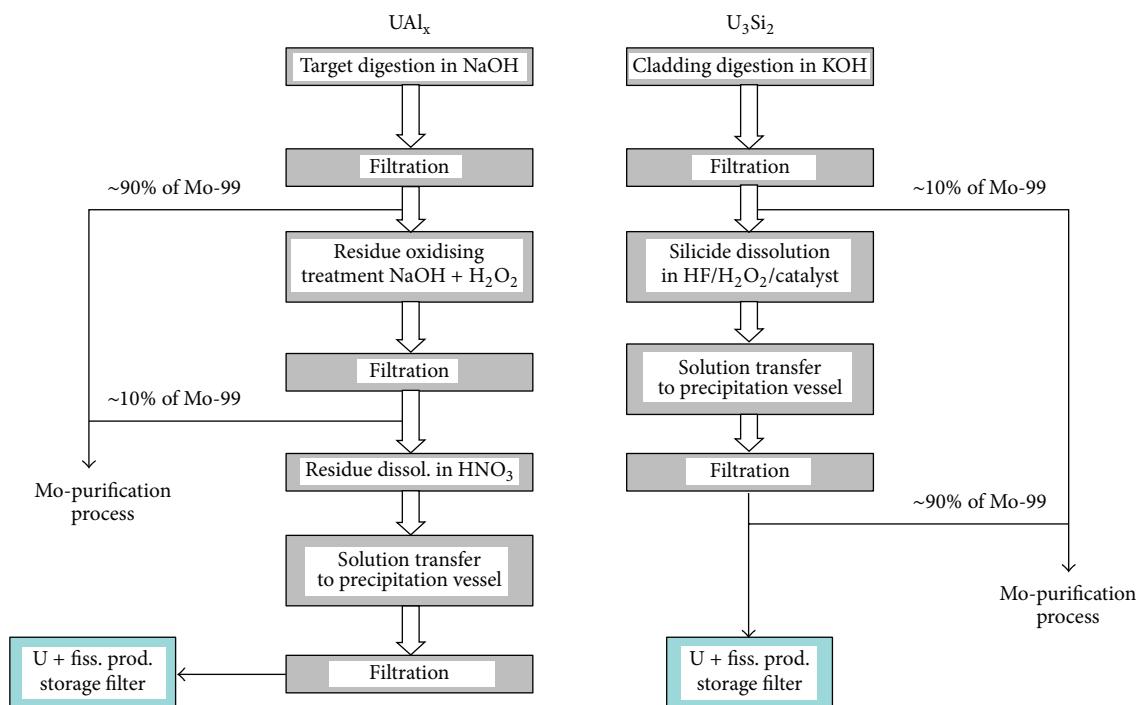
FIGURE 17: Fission Mo-99 production flow sheets for irradiated UAl_x and U_3Si_2 fueled targets.

preparation of new targets again and had to undergo the fuel qualification needed for irradiation. The qualified targets were again dissolved without being irradiated. The material was repeatedly recycled and processed.

The achieved experience was applied for the preparation of those LEU targets foreseen for irradiation and hot process demonstration. The produced LEU targets comprised varying densities up to 5.0 gU/cm^3. The U-densities of all irradiated targets were 3 gU/cm^3. The uranium enrichment of the targets was 19.75%. It was adjusted by blending of recycled HEU fuel of 91% enrichment with natural uranium. The blending was carried out by adding of a solution of uranyl nitrate of the natural uranium to a part of the uranium eluate of the TBP solid-bed column at the end of purification cycle. The mixture was precipitated as ammonium diuranate and further treated up to metal as described.

The silicide production cycle of Figure 14 was completed by demonstration tests at KFK, operated at 1,000 Ci of Mo-99 at EOP. Figure 15 shows 5 of the used irradiated silicide fuel targets prior to starting the dissolution process. Figure 16 shows the applied dissolution cell and major components of the hardware devices applied for the hot demonstration operations.

The hot experiments with U_3Si_2-based targets showed, except the dissolution and the related off-gas handling operations, no difference to the processing of the UAl_x-based fuels. The latter were frequently operated on similar scale for over 100 production runs. The dissolution tests of the silicide targets showed no difference in solubility between irradiated and nonirradiated silicide nor with fuel densities varying from 1.5 to 5.0 gU/cm^3. The achieved results were not surprising, as in extensive cold dissolution experiments pure silicide grains of several millimeters diameter were smoothly dissolved in the developed system.

3. Conclusions

The described experiments and related high-active demonstrations underlined the advantage of uranium silicide fuels as an outstanding target material for the production of fission Mo-99. Silicide targets combine remarkable features predestinating them as starting up materials for the large scale production of fission nuclides when starting from LEU. Among others these features are as follows.

(i) The full compensation of the enrichment drop from HEU to LEU in the production targets.

(ii) Long term proven excellent behavior in irradiation as MTR-fuel, which simplifies their acceptance in all involved research reactors supplementary.

(iii) Qualification on large scale and to high burn-ups as nuclear fuels up to uranium densities of 5.8 gU/cm^3 which even permits outstanding recycling potential for the generated spent fuel.

(iv) Reliable and reproducible production quality, which can be easily supervised with view to settled standards.

(v) Contamination and off-gas free handling before starting up the chemical process regarding the fact that no mechanical target dismantling is needed.

The demonstrated process for the production of fission Mo-99 and the integrated fuel cycle, both as described, is

designed for the long-term large scale operation. Relevant features are as follows.

(i) Complete separation of the nuclear fuel from the Mo-stream, already at the beginning of the separation process, combined with the quantitative retention and the safe enclosure of the nuclear fuel together with the bulk of fission products.

(ii) Exceptional low environmental impact comparable to that UAl_x process operating on full scale at Petten, The Netherlands.

(iii) Uncomplicated and economical to handle, noncorrosive, and nuclear fuel free alkaline waste.

(iv) Reliable immobilization of the fluoride content in the alkaline waste by formation of calcium fluoride during solidification, CaF_2 being a mineral "fluorite" of very low solubility.

(v) Efficiently reduced nuclear waste amounts by recycling and retargeting of the spent fuel.

(vi) Shorter operation times for the silicide fuel in comparison to the processing of similar fuel amounts of UAl_x. Figure 17 shows the operations needed for both fuel target types and demonstrates the related processing schemes for UAl_x and U_3Si_2. In case of the UAl_x processing, the needed final treatment for safe spent fuel enclosure as diuranate is an additional operation but integral part of the silicide processing already.

Acknowledgment

References

[1] C. J. Fallias, A. More de Westgaver, L. Heeren, J. M. Baugnet, J. M. Gandoflo, and W. Boeykens, "Production of radioisotopes with BR2 facilities," in *Proceedings of the BR-2 Reactor Meeting*, INIS MF 4426, pp. 1–11, Mol, Belgium, 1978.

[2] R. O. Marques, P. R. Cristini, H. Fernandez, and D. Marziale, "Operation and installation for fission for fission ^{99}Mo production in Argentina. Fission molybdenum for medical use," in *Proceedings of the Technical Committee Meeting Organized by the International Atomic Energy Agency*, IAEA-TECDOC-515, pp. 23–33, Karlsruhe, Germany, October 1987.

[3] J. Salacz, "Processing of irradiated ^{235}U for the production of ^{99}Mo, ^{131}I, and ^{133}Xe radioisotopes. Fission molybdenum for medical use," in *Proceedings of the Technical Committee Meeting Organized by the International Atomic Energy Agency*, IAEA-TECDOC-515, pp. 149–154, Karlsruhe, Germany, October 1987.

[4] A. A. Sameh and H. J. Ache, "Production techinques of fission molybdenum-99," *Radiochimica Acta*, vol. 41, pp. 65–72, 1987.

[5] A. Mushtaq, "Specifications and qualification of uranium/aluminum alloy plate target for the production of fission molybdenum-99," *Nuclear Engineering and Design*, vol. 241, no. 1, pp. 163–167, 2011.

[6] K. L. Ali, A. A. Khan, A. Mushtaq et al., "Development of low enriched uranium target plates by thermo-mechanical processing of UAl2-Al matrix for production of ^{99}Mo in Pakistan," *Nuclear Engineering and Design*, vol. 255, pp. 77–85, 2013.

[7] G. Ball, "Status update on the ^{99}Mo HEU/LEU conversion in South Africa," in *Proceedings of the NNSA 2nd Mo-99 Topical Meeting on Molybdenum-99 Technological Development*, Chicago, Ill, USA, April 2013.

[8] M. Druce, "Manufactoring Mo-99 from LEU for Australian market," in *Proceedings of the NNSA 2nd Mo-99 Topical Meeting on Molybdenum-99 Technological Development*, Chicago, Ill, USA, April 2013.

[9] G. F. Vandegrift, J. L. Snelgrove, S. Aase, M. M. Bretschner, and B. A. Buchholz, "Converting targets and process for fission-product ^{99}Mo from high to low enriched uranium," IAEA TECODOC, 1997.

[10] J. Jerden, J. Baily, L. Hafenrichter, and G. F. Vandegrift, "Full-scale testing of the ambient pressure,acid-dissolution front-end process for the current Mo-99 recovery process," *Chemical Science and Engineering*. In press.

[11] A. Guelis, G. Vandegrift, and S. Wiedmeyer, "Uranium anodic dissolution under slightly alkaline conditions," ANL Progress Report, Argonne, 2012.

[12] J. D. Kwok, G .F. Vandegrift, and J. E. Matos, "Processing of low-burnup LEU silicide targets," in *Processedings of the 1988 International Meeting on Reduced Enrichment for Research and Test Reactors*, ANL/RERTR/TM-13, CONF-880221, pp. 434–442, San Diego, Calif, USA, 1993.

[13] Cols, P. R. Cristini, and R. O. Marques, "Preliminary investigations on the use of uranium silicide targets for fission Mo-99 production," in *Proceedings of the 1994 International Meeting on Reduced Enrichment for Research and Test Reactors*, ANL/RERTR/TM-20, Williamsburg, Va, USA, September 1994.

[14] G. F. Vandegrift, A. V. Gelis, S. B. Aase, A. J. Bakel, E. Freiberg Y Koma, and C. Conner, "ANL progress in developing a target and process for converting CNEA Mo-99 production to low-enriched uranium," in *Proceedings of the 2002 International Meeting on Reduced Enrichment for Research and Test Reactors*, San Carlos de Bariloche, Argentina, November 2002.

[15] J. P. Durand, Y. Fanjas, and A. Tissier, "Development of higher-density fuel at CERCA status as of Oct.1992," in *Proceedings of the 1992 International Meeting on Reduced Enrichment for Research and Test Reactors-Status*, Roskilde, Denmark, September-October 1992, Argonne National Laboratory Report ANL/RERTR/TM-19, CONF-9209266.

[16] A. A. Sameh and A. Bertram-Berg, "HEU and LEU MTR fuel elements as target materials for the production of fission molybdenum," in *Proceedings of the 1992 International Meeting on Reduced Enrichment for Research and Test Reactors*, Roskilde, Denmark, September-October 1992, Argonne National Laboratory Report.

[17] J. P. Durand, J. C. Cottone, M. Mahe, and G. Ferraz, "LEU fuel development at CERCA-status as of October 1998," in *Proceedings of the 1998 International Meeting on Reduced Enrichment for Research and Test Reactors*, Sao Paulo, Brazil, October 1998, Argonne National Laboratory Report.

[18] A. A. Sameh, "Production of fission Mo-99 from LEU uranium silicide target materials," in *Proceedings of the 2000 Symposium on Isotope and Radiation Applications*, Institute of Nuclear Energy Research, Lung-Tan, Taiwan, May 2000.

[19] J. L. Snelgrove, *Qualification Status of 6-GU/Cm3 U3Si2 Dispersion Targets for 99Mo Production*, Argonne National Laboratory, 2011.

[20] *Workshop on Signatures of Medical and Industrial Isotope Production (WOSMIP '09)*, Friuli-Venezia Giulia, Italy, July 2009, PNNL-19294.

[21] A. A. Sameh, "KIT Process operating at Petten-the Netherlands," in *Proceedings of the Workshop on Signatures of Medical and Industrial Isotope Production (WOSMIP '10)*, Friuli-Venezia Giulia, Italy, June 2010, PNNL-21052.

[22] A. A. Sameh and A. Bertram-Berg, "Process for treating dissolution residues," Patent DE4241955, US5419881 ,1995.

[23] A. A. Sameh, "Processing and off gas handling of irradiated LEU uranium silicide," in *Proceedings of the Workshop on Signatures of Medical and Industrial Isotope Production (WOSMIP '11)*, Friuli-Venezia Giulia, Italy, June 2011.

[24] A. A. Sameh and W. Leifeld, "Process for separation of molybdenum," Patent DE4231955, USA 5.508.010, 1996.

[25] A. A. Sameh, J. Hoogveldt, and J. Reinhardt, "Process for recovering molybdenum-99 from a matrix containing neutron irradiated fissionable materials and fission products," Patent DE 2758783, 1994.

[26] A. A. Sameh and J. Haag, "Process for the separation of large amounts of uranium from small amounts of radioactive fission products, which are present in basic, aqueous carbonate containing solutions," Patent DE3428877, USA 4696768, 1987.

[27] R. G. Wymer and B. L. Vondra, *Light Water Reactor Fuel Cycle*, CRC Press, Boca Raton, Fla, USA, 1981.

[28] H.-J. Bleyl, D. Ertel, H. Goldacker, G. Petrich, J. Romer, and H. Schmieder, "Recent experimental findings on the way to the one-cycle Purex process," *Kerntechnik*, vol. 55, no. 1, pp. 21–26, 1990.

[29] R. Kröbel and A. Maier, *International Solvent Extraction Conference*, Lyon, France, 1974.

[30] H. Eschrich and W. Ochsenfeld, "Application of extraction chromatography to nuclear fuel reprocessing," *Separation Science and Technology*, vol. 15, no. 4, pp. 697–732, 1980.

[31] S. Nazare, G. Ondracek, and F. Thümler, "UAl3-Al als Dispersionsbrennstoff für Höchstflussreaktoren," KFK, 1252, 1970.

[32] S. Nazare, Private communication and advice on silicide preparation and targeting (1988–1990).

Research Article

Assembly and Irradiation Modeling of Residual Stresses in Low-Enriched Uranium Foil-Based Annular Targets for Molybdenum-99 Production

Srisharan G. Govindarajan, Brian S. Graybill, Philip F. Makarewicz, Zhentao Xie, and Gary L. Solbrekken

Department of Mechanical and Aerospace Engineering, University of Missouri, E2413 Lafferre Hall, Columbia, MO 65211, USA

Correspondence should be addressed to Srisharan G. Govindarajan; sgkff@mail.missouri.edu

This paper considers a composite cylindrical structure, with low-enriched uranium (LEU) foil enclosed between two aluminum 6061-T6 cylinders. A recess is cut all around the outer circumference of the inner tube to accommodate the LEU foil of open-cross section. To obtain perfect contact at the interfaces of the foil and the tubes, an internal pressure is applied to the inner tube, thereby plastically and elastically deforming it. The residual stresses resulting from the assembly process are used along with a thermal stress model to predict the stress margins in the cladding during irradiation. The whole process was simulated as a steady-state two-dimensional problem using the commercial finite element code Abaqus FEA. The irradiation behavior of the annular target has been presented, and the effect of the assembly residual stresses has been discussed.

1. Introduction

The majority of the molybdenum-99 (Mo-99) produced internationally is extracted from high-enriched uranium (HEU) dispersion targets that have been irradiated. Mo-99 is the parent isotope of the radioactive tracer, technetium-99 m, which is used in medical imaging procedures. The high concentration U-235 in HEU-based targets makes them potential items of interest for rogue individuals. To alleviate the potential of proliferation issues, low-enriched uranium (LEU) targets are being mandated. Unfortunately the conversion of HEU- to LEU- based dispersion targets is accompanied by a reduction in Mo-99 production given today's dispersion target technology. An increase in the density of uranium is needed in LEU-based targets in order to recover the loss in Mo-99 production per target [1]. One strategy to increase the uranium density is to use an LEU metal foil placed within the 6061-T6 aluminum cladding [2]. A second advantage of the LEU foil-based target is that it allows for the potential of the LEU foil to be removed after

irradiation so that it can be dissolved by itself, reducing the liquid waste that would be generated by dissolving the entire target, including the 6061-T6 aluminum cladding. In this paper the aluminum 6061-T6 cladding will be simply referred to as "aluminum cladding."

The function of the target is to contain the fission products and to effectively dissipate the generated fission heat to the reactor coolant. For dispersion target designs there is generally little concern about heat getting dissipated to the coolant as the target structure offers little resistance to heat transfer. However, for the disassemble-able LEU foil target; there is a potential of the cladding to separate from the LEU foil and significantly increase the thermal resistance between the LEU and cladding. The increase in thermal resistance could lead to a rise in LEU temperature that might exceed the limits set forth by the reactor. An analysis needs to be conducted on this target structure to ensure safe usage both during assembly and irradiation.

The target is assembled by wrapping a thin nickel foil (~15 μm) around the LEU foil and placing it on the outer

circumference of the inner aluminum tube. The width of the foil is such that it does not wrap all the way around the inner tube, leaving a gap, as illustrated in Figure 1. The gap provides a cutting street for postirradiation disassembly of the target. An aluminum outer tube is slid over the inner tube and the Ni-wrapped LEU foil. The nickel acts as a recoil barrier to prevent the LEU foil from bonding with the cladding, while aluminum is used as the cladding material due to its small neutron absorption cross-section [3].

An internal pressure is applied to the inner surface of the inner tube to close the gap between the foil and the outer tube. The internal pressure can be applied by either a draw plug or by using a pressurized hydraulic fluid [4]. The internal pressure applied to the inner cylinder causes it to expand and plastically deforms it. The magnitude of the required internal pressure is calculated by applying the condition that at the end of the process the LEU foil and the outer tube share a common interface. This assembly process creates a sandwiched structure where the interfaces between all the target components are in contact with one another.

By design, the assembly process leaves residual stresses in the aluminum cladding. Previous thermal-mechanical analysis on annular targets with zero residual stresses has shown that there is a tendency for a gap to open up between the foil and the outer tube [2]. Hence, it is important to model the irradiation process by including the assembly residual stresses and to design the assembly process such that the residual stresses help prevent any gaps from forming. It has been shown that based on the direction of heat flow in a sandwich cylinder, contact can be established or withdrawn [5]. Though these annular targets have been safely irradiated in the past [6], the magnitude of the resulting thermal stresses is unknown. This paper will seek to establish, by means of numerical analysis, the thermal stress margins in these annular targets by including the residual stresses from the assembly process.

2. Numerical Model

A numerical model of the annular target assembly was created using the commercial finite element code Abaqus FEA [7]. A three-step analysis was created to model the assembly of the tubes, the residual stresses, and the irradiation process. In the first step, the hydroforming assembly process is simulated by the application of a calculated internal fluid pressure. The second step is a zero pressure step, where the applied internal pressure is removed and the target is allowed to relax. Any remaining stresses in the target are the residual stresses that will help to keep gaps from forming between the LEU and cladding. The final step simulated is the irradiation heat generating process. This step is simulated by applying a volumetric heat generation rate to the LEU foil.

The finite element mesh used in the analysis, consisting of 16000 elements and 51221 nodes with 10 elements through the thickness of each assembly component, is illustrated in Figure 2. Thus, the final assembly consisted of 30 elements through all the components. It is important to note that the assembly and the residual stress part were modeled as a
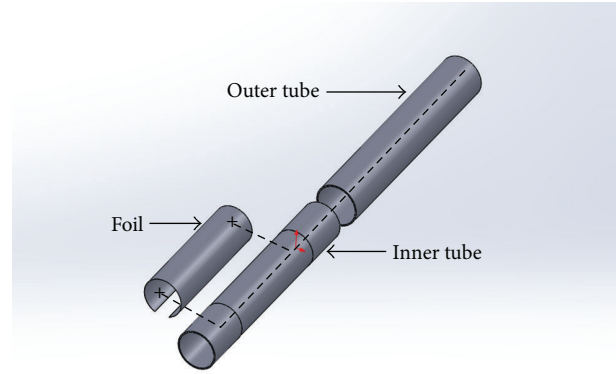

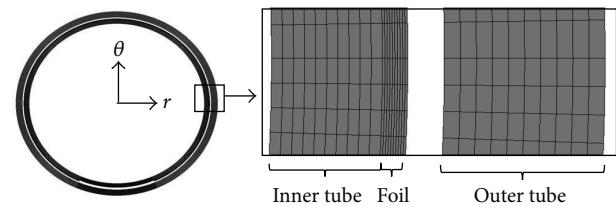Figure 1: Exploded view of the target assembly.

Figure 2: Finite element mesh used in the three-step analysis.

fully coupled thermal stress problem instead of a static stress analysis. This makes it easier to add a third step to run the irradiation analysis. If a static stress analysis type is used for the first two steps, an Abaqus script file is required to input the residual stress data into the irradiation model which uses a fully coupled thermal stress step. Fully coupled quadratic reduced integration elements of type CPE8RT were used in the analysis.

2.1. Assembly and Residual Stress Model. The development of the assembly model follows directly from the Argonne National Lab (ANL) target design [6]. Since the mechanical model was constructed in two dimensions, the relevant cross-sectional area of the target occurs at the midpoint of the target's length, such that the inner tube, outer tube, and uranium foil are all present in the model, as illustrated in Figure 3.

As the model is based on the ANL target, all the tube dimensions are precisely those described by the technical drawing of that target. Again, because the cross-section occurs at a length along the target that includes the uranium foil, the dimensions of the inner tube correspond to the ANL foil relief specifications. In addition, it should be noted that the foil is assumed to be in perfect initial contact with the inner tube. While this is not necessarily the case with physical specimens, it is an essential simplification to the model. The assembled stress state of a target is important as it can either aid or hinder the disassembly process. In order to achieve a stress state that encourages the target to open after being cut longitudinally, the inner tube must be plastically deformed and the outer tube must be only elastically deformed. To
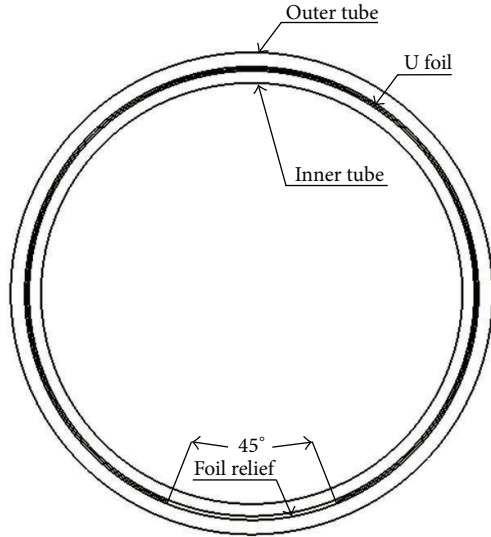
Notes:

(1) Foil thickness: 125 μm

(2) Inner tube ID: 26.210 mm

(3) Inner tube OD: 27.714 mm

(4) Outer tube ID: 28.220 mm

(5) Outer tube OD: 30.000 mm

Figure 3: Drawing of the geometry used for the assembly model in the first analysis step.

simulate plastic deformation, a plastic material model must be defined within Abaqus. This data must be given in the form of true stress and plastic strain. In some cases, it may be necessary to convert engineering stress and strain to true stress and plastic strain. However, as the tube material being investigated at the University of Missouri-Columbia is Al 6061-T6, the true stress and plastic strain data for aluminum 6061-T6 was obtained from [8], while the flow curve equation based on [9] was used to construct the true stress versus plastic strain curve for uranium as illustrated in Figure 4.

The plasticity data supplied by [9] is in the form of strength coefficients and hardening exponents, K and n. For unalloyed uranium, the alloy used in this study, K and n, is 1.14 GPa and 0.23, respectively. These values are used in the plastic flow equation given by the following:

$$\sigma = K\varepsilon^{n},\tag{1}$$

where σ is true stress and ε is plastic strain. It should be noted that according to [9] the values of the strength coefficient and strain hardening exponent are only valid for plastic strains between 0.001 and 0.01. The elastic material definitions are much simpler to create, requiring only the elastic modulus and Poisson's ratio. For the aluminum tubes, the values used were 68.9 GPa and 0.33, respectively. The elastic modulus for uranium used was 208 GPa, and Poisson's ratio was 0.23 (typical for unalloyed metals).

The desired internal pressure for hydroforming was determined through a combined analytical and experimental

approach. According to analytical plastic theory, the critical pressure which will cause yielding is given by the following as

$$P = \frac{\sigma_o}{2}\left(\frac{b^2/a^2 - 1}{b^2/r^2}\right),\tag{2}$$

where P is the critical pressure, σ_o is the yield stress, b is the outer diameter of a cylinder, and r is the location of interest through the cylinder wall. Assuming r to be the inner diameter ($r = a$) reduces (2) to

$$P = \frac{\sigma_o}{2}\left(1 - \frac{a^2}{2b^2}\right).\tag{3}$$

Using the dimensions of the inner tube previously described and a typical yield stress for Al 6061-T6 of 255 MPa, the calculated critical pressure using (3) is 13.75 MPa. This is the pressure that will initiate yielding in the inner tube. The corresponding displacement for the critical pressure is determined. A parametric study is performed to determine the pressure that will nearly close the gap between the foil and the outer tube and is found to be 16.3 MPa. However, this 16.3 MPa does not induce enough plastic deformation to keep the gap closed after unloading. After analytically determining the proper order for internal pressure, several tests were conducted to precisely determine the internal pressure required to close the gap. This was accomplished using a hydroforming test bench developed at the University of Missouri. Hydroforming provides an advantageous testing method because only the internal pressure is required to assemble the target.

Through the experiments run with the hydroforming test bench (Figure 5), the maximum allowable pressure (i.e., the maximum pressure that does not rupture the target) was determined to be 36.4 MPa. Thus, the internal pressure applied to the Abaqus model in the assembly step was 36.4 MPa as illustrated in Figure 6. It should be noted that above this pressure, the targets ruptured, with both the inner and outer tubes splitting along the longitudinal relief where the inner and outer tubes were in direct contact, without uranium in between. The application of the internal pressure only constitutes the first step of the multistep model. Simulation of the assembly requires the addition of a step in which the internal pressure is returned to zero. There are two purposes for the pressure relaxation step. First, this simulates the actual target assembly process: an internal pressure is applied to assemble the tube and foil and then removed in order to remove the target from the hydroforming rig. Because, at the applied pressures, the outer tube is not plastically deformed, there is some elastic recovery upon removal of the internal pressure. The remaining stresses in the target are known as residual stresses, leading to the second purpose for simulating the pressure relaxation. The residual stresses are of interest in the assembly process as the residual state can either aid or hinder the disassembly process. If tensile stresses remain in the outer tube, it will "spring" open when cut along the longitudinal relief for retrieval of the uranium foil. However, compressive residual stresses will cause the outer tube to collapse, increasing the time and
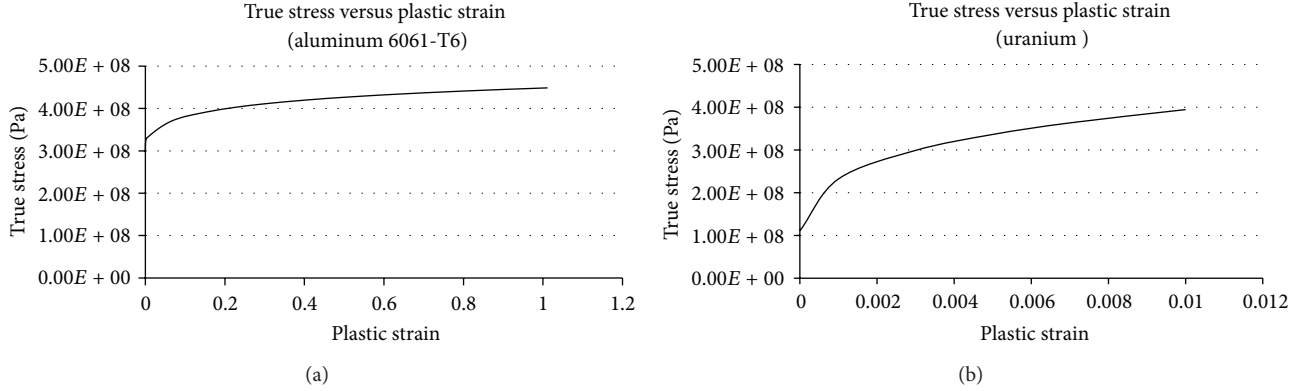
True stress versus plastic strain
(aluminum 6061-T6)

(a)

True stress versus plastic strain
(uranium)

(b)

FIGURE 4: True stress and plastic strain data for aluminum 6061-T6 and uranium.
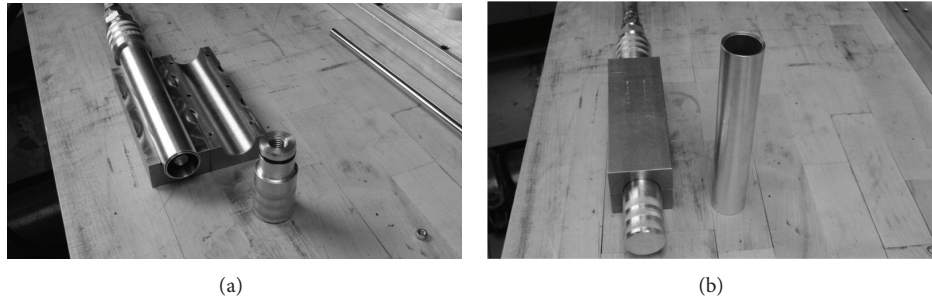

(a)

(b)

FIGURE 5: (a) Hydroforming test rig with annular target in place. (b) Assembled hydroforming test rig.

effort required to remove the irradiated foil from the target. Thus, the simulation of pressure relaxation serves to verify a favorable residual stress state, improving production.

2.2. Irradiation Model. To model the irradiation behavior which takes into account the residual stresses from the assembly process, a fully coupled thermal stress step was added after the residual stress step. The loading conditions and the contact definitions from the first two steps were suppressed. A heat generation rate of 1.6×10^{10} W/m^3 was applied to the foil, which corresponds to a heat flux of 100 W/cm^2 incident on the outer surface of the inner tube and the inner surface of the outer tube. Water coolant flow at 323 K through the inner and along the outer tubes was simulated by defining a surface heat transfer coefficient and a sink temperature. The heat transfer coefficient of 19000 W/m^2 K corresponds to a flow velocity of 0.83 m/s through the inner tube and 1.86 m/s along the outer tube. The loading and boundary conditions for the irradiation model are illustrated in Figure 7.

New contact definitions had to be made for the irradiation model due to the different contact interaction property for the normal behavior. For the irradiation model it is assumed that the tubes may have a tendency to separate after they come in contact, whereas for the hydroforming part, the normal behavior does not allow any separation once the tubes are in contact. This is the main difference in the mechanical contact definition properties for the assembly and the irradiation

part. Due to the composite structure of the model and the presence of interfaces, a thermal conductance had to be defined while defining the contact interaction properties. As the magnitude of the thermal conductance is unknown, an infinite conductance was specified at zero clearance, and for a clearance of 0.01 m the thermal conductance is assumed to be zero. Abaqus interpolates between these values to obtain the thermal conductance for any interfacial gap in the model. It is assumed that there is conduction through the air, and the effects of heat redistribution have not been considered in modeling the gap.

3. Results

Figure 8 illustrates the displacement contour after the first assembly step, which simulates the hydroforming process. Though the applied internal pressure closes the gap between the foil and the outer tube, a gap ($\sim 200\,\mu$m) still remains close to the edges of the foil, in the region between the inner and the outer tubes. The maximum displacement occurs in the inner tube at 180° as illustrated in Figure 8.

Figure 9 illustrates the equivalent plastic strain across the thickness of the annular target assembly. The Abaqus parameter name for this is "PEEQ" and is used to evaluate the yield condition. For isotropic hardening and Von Mises plasticity, PEEQ is defined as $\sqrt{(2/3)d\varepsilon^{\mathrm{pl}} : d\varepsilon^{\mathrm{pl}}}$. It is essentially a scalar measure of all components of equivalent plastic strain in a model, and a value of PEEQ greater than zero
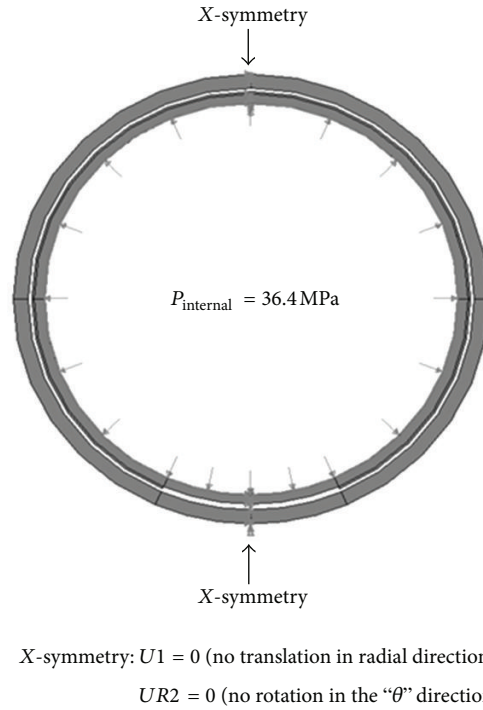
X-symmetry

X-symmetry

$P_{\text{internal}} = 36.4\,\text{MPa}$

X-symmetry: $U1 = 0$ (no translation in radial direction)

$UR2 = 0$ (no rotation in the "θ" direction)

FIGURE 6: Loading and boundary conditions for the hydroforming model in the first analysis step.

X-symmetry boundary

Inner tube (Al 6061-T6)

Outer tube (Al 6061-T6)

LEU heat generation
$q_{\text{gen}} = 1.6 \times 10^{10}\,\text{W/m}^3$

Coolant at 323 K
$h_{\text{out}} = 19000\,\text{W/m}^2\,\text{K}$

X-symmetry boundary

Coolant at 323 K
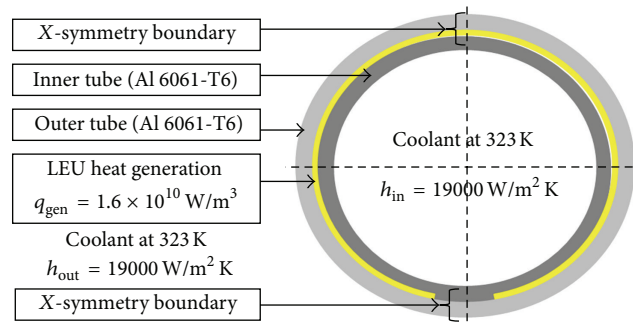$h_{\text{in}} = 19000\,\text{W/m}^2\,\text{K}$

FIGURE 7: Loading and boundary conditions for the irradiation model in the third analysis step.

indicates that the material has already yielded. As expected, the combined effects of heating and assembly stresses result in a higher plastic strain at the end of the irradiation step than in the previous steps. Also, the plastic strain remains the same during the pressure relaxation step. This is because, when the applied load is removed the inner tube elastically recovers, but the plastic deformation due to the hydroforming process remains in the inner tube. Figure 9 also illustrates the plastic deformation in the outer tube. For the irradiation step, there is a small amount of plastic deformation in the outer tube, while there is zero plastic deformation in the outer tube for the first two steps. This means that the plastic deformation in the outer tube at the end of the irradiation step is purely due to thermal effects.

One of the goals of the hydroforming process is to close the gap between the foil and the outer tube by plastically deforming the inner tube. The magnitude of the applied hydroforming pressure should be such that it should be able to close the gap between the foil and the outer tube and induce sufficient plastic deformation in the inner tube so that even during elastic recovery an interfacial bond is maintained between the foil and the outer tube. Figure 10 illustrates the separation between the outer tube and the foil. For the hydroforming and the pressure relaxation step there is zero separation. This means that the applied hydroforming pressure of 36.4 MPa is sufficient to maintain the contact between the foil and the outer tube when elastic recovery occurs. However, a gap does open up during the irradiation step due to thermal expansion mismatch and radially outward heat flow.

Figure 11 illustrates the radial temperature distribution in the inner tube and outer tube cladding. The temperature
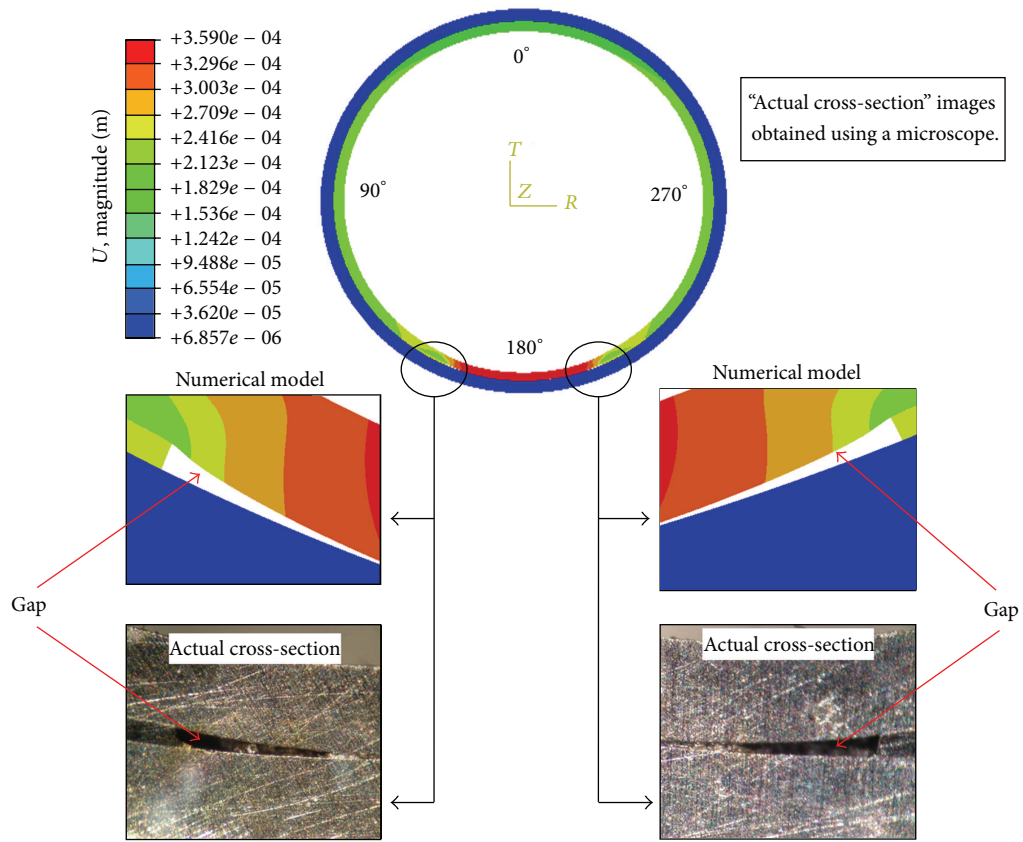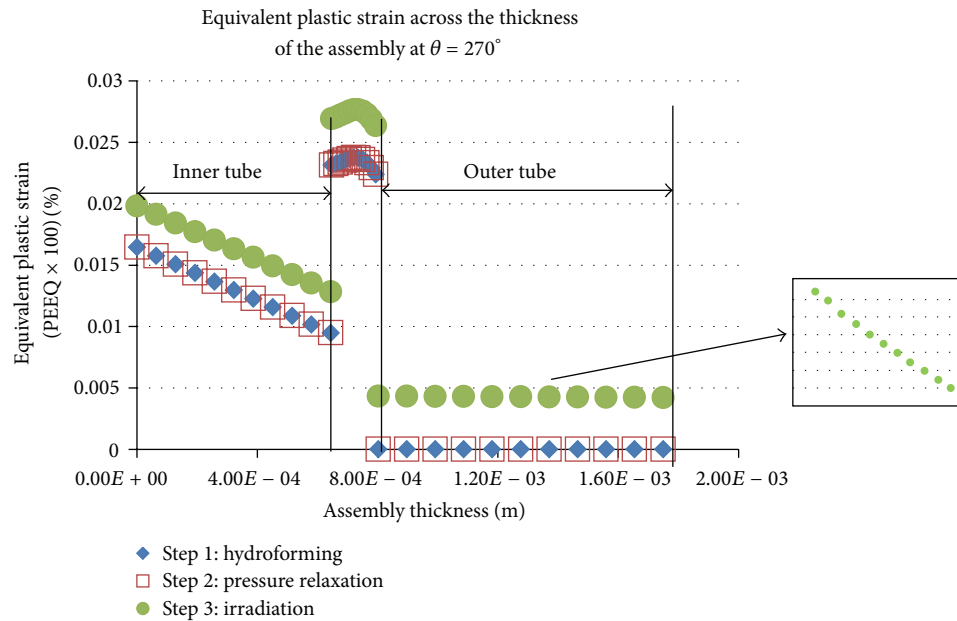
FIGURE 8: Postassembly numerical displacement contour and microscope images.

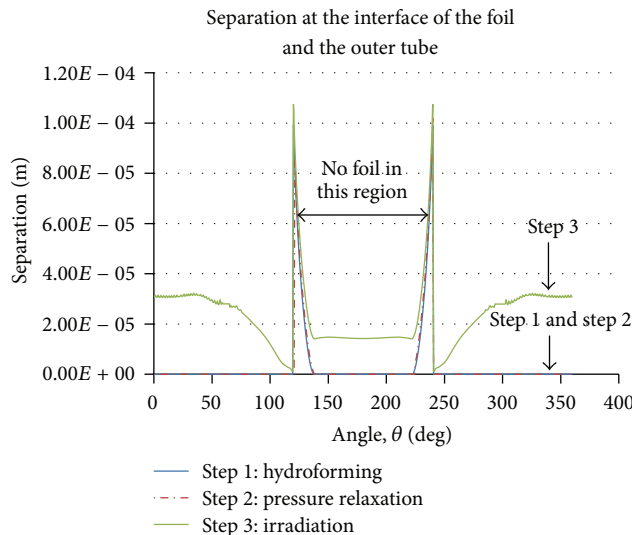FIGURE 9: Equivalent plastic strain across the assembly radius at $\theta = 270°$.

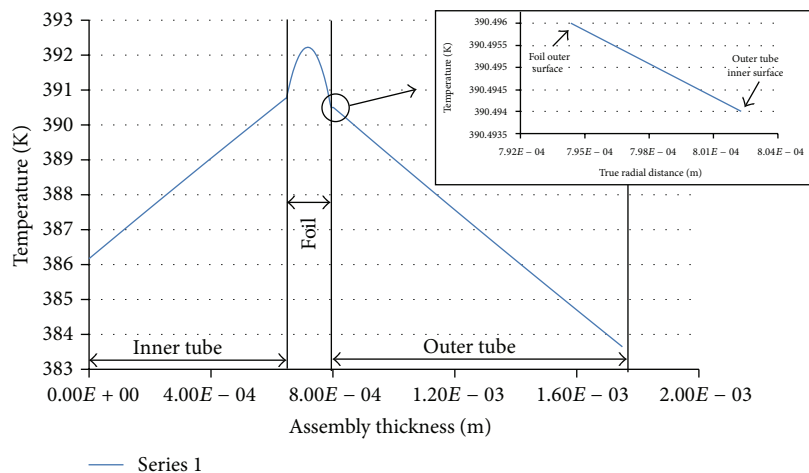FIGURE 10: Separation at the interface of the foil and the outer tube after the various modeling steps.

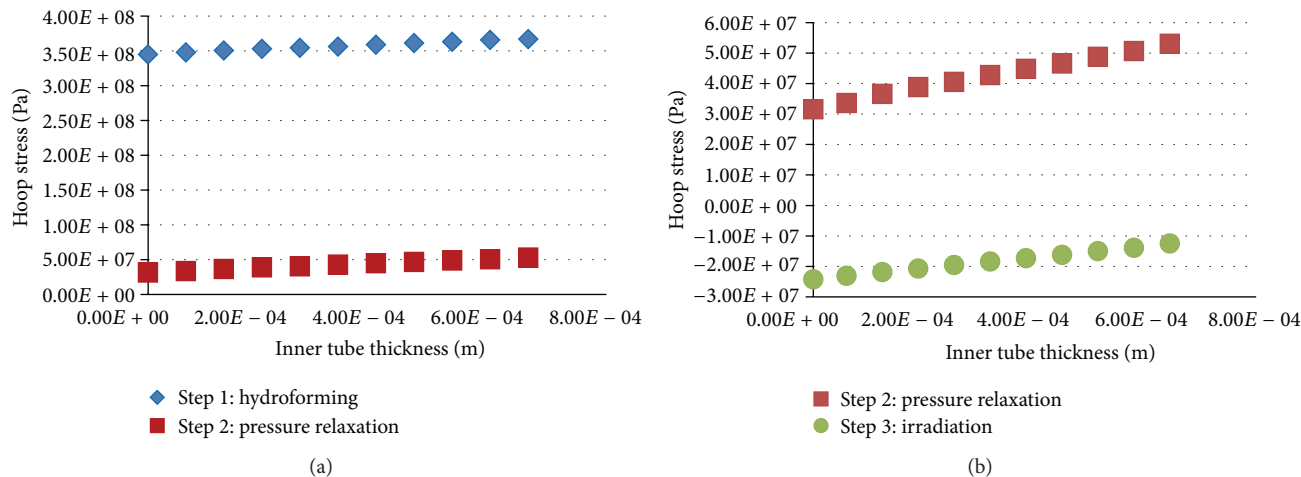FIGURE 11: Radial temperature distribution across the inner and outer cladding.

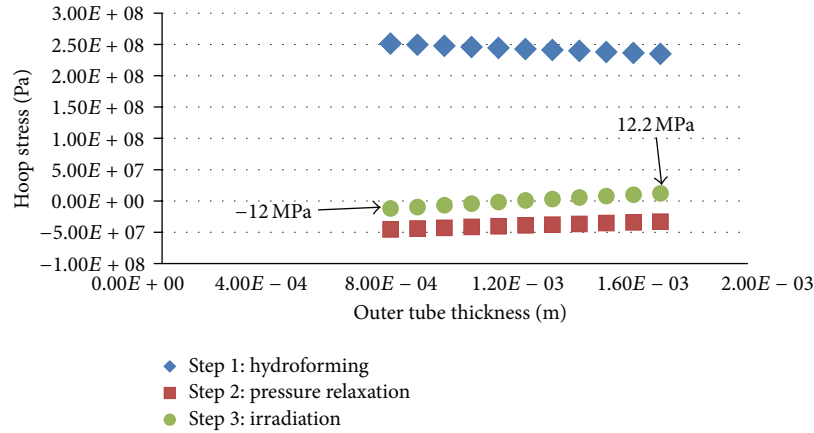FIGURE 12: Hoop stress distribution in the inner tube through various modeling steps at $\theta = 270°$.

FIGURE 13: Hoop stress distribution in the outer tube through various modeling steps at $\theta = 270°$.

decreases from the outer surface to the inner surface for the inner tube for radially inward heat flow and from the inner surface to the outer surface for the outer tube for radially outward heat flow. Due to the separation between the foil and the outer tube, there is a small temperature drop at this interface as illustrated in Figure 11. All the modeling was done by assuming a heat generation value that corresponds to a surface heat flux of $100 \, \text{W/cm}^2$. Using this value of heat flux along with the small temperature drop shown in Figure 11 results in a negligibly small value of thermal contact resistance. However, it remains to be seen if such a small value of thermal contact resistance is significant. Efforts are currently underway [10] at the University of Missouri to experimentally quantify the thermal contact resistance using surrogate foils.

Figure 12 illustrates the hoop stress across the inner tube radius for all the steps in the model. Beginning with the hydroforming step (Figure 12(a)), the hoop stress is greater on the outer surface than on the inner surface of the inner tube. As the load is removed, the resulting residual hoop stresses drop by an order of magnitude. Figure 12(b) illustrates the variation of residual hoop stresses during the pressure relaxation step and during the irradiation step. These residual hoop stresses are compressive in the inner surface, and the magnitude of compressive stress gradually decreases across the thickness. The maximum compressive stress is on the inner surface as this is where yielding begins. Previous analysis [2] has shown that for an elastic irradiation model of an annular target that begins from a zero residual stress state, the hoop stresses in the inner tube are completely compressive and increase towards the outer surface of the inner tube. This behavior can be obtained from Figure 12(b) by subtracting the residual stresses from the postirradiation hoop stresses. This would effectively give the hoop stresses in a tube for zero residual stress state. Thus the tensile residual stresses reduce the amount of postirradiation hoop stresses in the inner tube.

The hoop stresses in the outer tube through the three modeling steps have been illustrated in Figure 13. For the hydroforming process, the hoop stresses are greater on the inner surface than on the outer surface of the outer tube. The

internal pressure applied during the hydroforming process causes the outer surface of the foil to be displaced towards the inner surface of the outer tube. When these interfaces meet, the inner surface of the outer tube is displaced outwards resulting in compressive stresses. The residual stresses from the assembly process are completely compressive in the outer tube with the hoop stresses being higher on the inner surface. The resulting hoop stresses from the final irradiation step are compressive on the inner surface and tensile on the outer surface. This can be attributed to radially outward heat flow through the outer tube. The outer surface of the outer tube is unrestrained and therefore free to expand. The free expansion of the outer surface results in tensile stresses being generated across the outer half of the tube, but expansion of the inner surface is resisted by the elements across the thickness of the tube.

4. Conclusions

The goal of this paper was to integrate the assembly process of the annular target along with the irradiation analysis to analyze the behavior of the target and assess the effect of residual stresses. A three-step elastoplastic model was built using the commercial finite element code Abaqus FEA [7]. The first analysis step simulated the hydroforming process using an internal pressure of 36.4 MPa, and this was followed by a pressure relaxation step to simulate the recovery. The third step simulated the irradiation process by including the residual stresses from the previous step.

The results from the analysis show that the applied internal pressure is adequate to induce enough plastic deformation to maintain the bond at the interface of the foil and the outer tube. The residual stresses from the assembly process tend to negate and decrease the hoop stresses in the inner and outer tubes at the end of the irradiation step. This is favorable from a material standpoint as the inner and outer tubes are unlikely to fail under the applied heat generation of $1.6 \times 10^{10} \, \text{W/m}^3$. This corresponds to a heat flux of $100 \, \text{W/cm}^2$ incident on the outer surface of the inner tube and the inner surface of the outer tube. The postirradiation compressive hoop stresses

in the inner tube are greater than the stresses in the outer tube, which move from being compressive to tensile across the thickness. Hence, the inner tube is likely to dictate the failure of the target.

Acknowledgments

References

[1] K. K. Turner, G. L. Solbrekken, and C. W. Allen, "Thermal-mechanical response of non-uniformly heated nominally flat and curved LEU foil based target," in *Proceedings of the ASME International Mechanical Engineering Congress & Exposition*, Paper IMECE2012-88939, Houston, Tex, USA, November 2012.

[2] S. G. Govindarajan, G. L. Solbrekken, and C. W. Allen, "Thermal-mechanical analysis of a low-enriched uranium foil based annular target for the production of molybdenum-99," in *Proceedings of the ASME International Mechanical Engineering Congress and Exposition*, Paper IMECE2012-86921, Houston, Tex, USA, November 2012.

[3] US. Department of Energy, *DOE Fundamentals Handbook—Material Science*, vol. 2 of *Claddings and Reflectors*, US. Department of Energy, Washington, DC, USA, 2010.

[4] A. S. El-Gizawy, J. K. Berlin, and B. S. Graybill, "Robust design of assembly process of targets carrying LEU foils for production of Mo-99," in *Proceedings of the ANS Winter Meeting and Nuclear Technology Expo, Technical Conference Proceedings: The Status of Global Nuclear Deployment*, Washington, DC, USA, November 2011.

[5] C. V. Madhusudana, "Thermal conductance of cylindrical joints," *International Journal of Heat and Mass Transfer*, vol. 42, no. 7, pp. 1273–1287, 1999.

[6] A. Mutalib, B. Purwadi, H. G. Adang et al., "Full scale demonstration of the cintichem process for the production of molybdenum-99 using a low enriched uranium target," in *Proceedings of the International Meeting on Reduced Enrichment for Research and Test Reactors*, Sao Paulo, Brazil, October 1998.

[7] "Abaqus FEA," Version 6.12-2, D S Simulia, DassaultSystemes, 2002–2013.

[8] R. K. S. Racha, *Damage characterization of four wrought aluminum alloys [M.S. thesis]*, Tennessee Technological University, 2008.

[9] G. R. Caskey Jr., "Memo to P.H. Permar," Technical Division Savannah River Laboratory, Aiken, SC, USA, 1965.

[10] P. F. Makarewicz, S. G. Govindarajan, and G. L. Solbrekken, "Experimental testing of annular target surrogates for the production of molybdenum-99," in *Proceedings of the ASME International Mechanical Engineering Congress & Exposition*, Paper IMECE2012-87783, Houston, Tex, USA, November 2012.

Research Article

The Fission-Based ^{99}Mo Production Process ROMOL-99 and Its Application to PINSTECH Islamabad

Rudolf Muenze,[1] Gerd Juergen Beyer,[1] Richard Ross,[2] Gerhard Wagner,[1] Dieter Novotny,[1] Erik Franke,[1] Mustansar Jehangir,[3] Shahid Pervez,[4] and Ahmad Mushtaq[4]

[1] *GSG International GmbH, Eichenstraße 12, 8808 Pfäffikon, Switzerland*

[2] *IAF Radioökologie GmbH, Karpatenstraße 20, 01326 Dresden, Germany*

[3] *Foundation University Islamabad, 44000 Islamabad, Pakistan*

[4] *Isotope Production Division, Pakistan Institute of Nuclear Science and Technology (PINSTECH), P.O. Nilore Islamabad, 45650 Nilore, Pakistan*

Correspondence should be addressed to Gerd Juergen Beyer; gerd.beyer@gsg-int.com

An innovative process for fission based ^{99}Mo production has been developed under Isotope Technologies Dresden (ITD) GmbH (former Hans Wälischmiller GmbH (HWM), Branch Office Dresden), and its functionality has been tested and proved at the Pakistan Institute of Nuclear Science and Technology (PINSTECH), Islamabad. Targets made from uranium aluminum alloy clad with aluminum were irradiated in the core of Pakistan Research Reactor-1 (PARR-1). In the mean time more than 50 batches of fission molybdenum-99 (^{99}Mo) have been produced meeting the international purity/pharmacopoeia specifications using this ROMOL-99 process. The process is based on alkaline dissolution of the neutron irradiated targets in presence of $NaNO_3$, chemically extracting the ^{99}Mo from various fission products and purifying the product by column chromatography. This ROMOL-99 process will be described in some detail.

1. Introduction

The present sources of molybdenum-99 (^{99}Mo; $T_{1/2} = 66$ h) are research reactors by neutron-induced fission of ^{235}U, which results in high-specific activity ^{99}Mo, or using the (n, γ) nuclear reaction with ^{98}Mo (natural Mo or enriched ^{98}Mo = 24%), resulting in low-specific activity ^{99}Mo. Generally, the specific activity of molybdenum produced by fission is more than 1000 times higher than that obtained by $(n; \gamma)$ process. The almost universal means by which technetium-99m (^{99m}Tc; $T_{1/2} = 6$ h) is made available for clinical applications is from the elution of generators containing high-specific activity fission-based ^{99}Mo.

The first chemical process for separation of fission ^{99}Mo was described by the Brookhaven group, USA [1]. In this process the target (93% enriched U-235 alloyed with Al) was dissolved in 6 M nitric acid catalyzed by mercuric nitrate. In the former Zentralinstitut für Kernforschung (ZfK) Rossendorf,

a fission-based ^{99}Mo separation technology became operationally ready in 1963 which was actually the basis of the first fission-based ^{99}Mo/^{99m}Tc generator in Europe. Metallic natural uranium pellets were used as target material and the dissolution of the irradiated U-pellets was done with concentrated HCl. Quartz and glass apparatus was used in chemical processing, and yield of ^{99}Mo was ~70% [2]. In 1980, this process was replaced by the AMOR process (AMOR: Anlage zur Mo Production Rossendorf), developed in the same institute [3]. The AMOR process made use of original fuel elements of the RF-reactor as qualified target which was dissolved in HNO_3/Hg. Batch-wise adsorption at Al_2O_3 and sublimation technique were used for separation and purification of the ^{99}Mo. This process was in operation until the shut-down of the Rossendorf Research Reactor in 1991.

Another small-scale production process for fission ^{99}Mo was proposed by the Rossendorf group in which natural uranium as uranium oxide was used as target material [4]. This procedure was particularly interesting for those which

do not dispose of enriched nuclear fuel material. Approximately 400 g of uranium oxide enclosed in irradiation cans are dissolved in nitric acid after irradiation for 100 hrs at a neutron flux of 5×10^{13} cm^{2}s^{-1} in a research reactor. The separation of ^{99}Mo from the fuel-fission product solution is performed by ion exchange with alumina in a chromatography column. Final purification includes the repeated chromatography separation and subsequently a sublimation stage.

Based on their own long-term experiences and considering international achievements in ^{99}Mo production, scientists of the Radio-Isotope department of the former Rossendorf institute ZfK designed a new process for fission-based ^{99}Mo production named ROMOL-99 [5–7]. The basic principles of this process are as follows (see also the flow scheme, **Figure** 1).

  (i) The dissolution of the UAlx/Al-clad targets shall be performed in a mixture of NaOH/NaNO$_3$ without H$_2$ generation, under reduced pressure conditions.

  (ii) The Xe shall be trapped cryogenically after passing a gas treatment line.

  (iii) The NH$_3$ generated in the dissolving process shall be separated prior to Mo separation.

  (iv) The radioiodine shall be separated prior to ^{99}Mo-separation as well.

  (v) During dissolving process nitrite is generated which shall be eliminated prior to the ^{99}Mo separation.

The basic parameters of this process has been developed with modern nonradioactive analytical techniques by the IAF-Radioökologie GmbH Dresden, while the active testing and optimization of the process has been carried out at PINSTECH Islamabad under supervision of the German scientists. In this paper the chemical process of the ROMOL-99 technology will be described in some detail.

2. Materials and Methods

All chemicals were purchased from E. Merck (Germany) and were of guaranteed reagent grade (GR) or analytical reagent (AR) grade. Al$_2$O$_3$ (90 active acidic for column chromatography, 70–230 mesh ASTM) was used. Silver-coated alumina was freshly prepared at institute. Organic anion-exchange resin was purchased from BioRad, USA.

The non-radioactive development work was performed using uranium-free Al-plates (purchased from PINSTECH) having the same composition as the material used for the original targets.

Tracer experiments were performed using ^{131}I tracer activities which were taken from the PINSTECH routine ^{131}Iodine production, and the ^{99}Mo tracer was taken from the routine PAKGEN ^{99m}Tc generator production (^{99}Mo imported from South Africa).

2.1. Irradiation of Target.
Qualified HEU/Al alloy clad with high purity aluminum target plates [8] were irradiated for 12–18 h at a neutron flux of $\sim1.5 \times 10^{14}$ cm^{-2}s^{-1} inside the
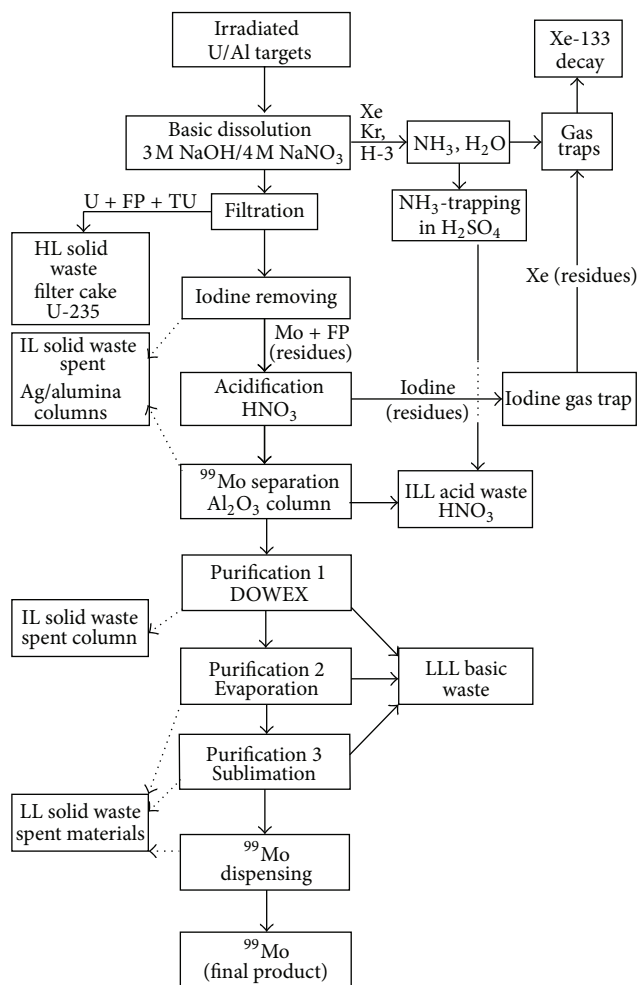

Figure 1: Process flow scheme of the ROMOL-99 process.

core of the Pakistan Research Reactor-1 (PARR-1). After 24 h cooling, the irradiated target plates were transferred to the ^{99}Molybdenum Production Facility (MPF) for separation of ^{99}Mo from the uranium, actinides, and fission products. For the warm test runs, targets were irradiated for short times at lower flux density, but the target composition was identical with those for production runs. The irradiation conditions were chosen in a way that the total activity inventory for the development work was of the order of 4 GBq.

2.2. Process Control and Quality Control.
Gamma ray spectroscopy high-purity Ge detector (Canberra Series 85 multichannel analyzer) was used to determine the activity balance during all process steps and for the determination of radionuclide impurities in the final ^{99}Mo product. This concerns mainly ^{131}I and ^{103}Ru, ^{132}Te. Beta counting of ^{89}Sr and ^{90}Sr was done by a liquid scintillation analyzer (Tri-Carb 1900 TR, Packard Canberra Company) after separation by ion-exchange and precipitation with the aid of carrier. Contamination of alpha emitters was done with the α-counter (UMF-200). Radiochemical purity of [^{99}Mo] molybdate was determined by means of paper chromatography with a

mixture of hydrochloric acid, water, ether, and methanol (5 : 15 : 50 : 30) as mobile phase. The chemical purity was occasionally determined after decay by optical emission spectrometry (Optima 3300XL, Perkin Elmer). It was used for the determination of toxic elements such as Cr, Co, As, Sn, Cd, Pb, and U; the detection limits in ppm were 2, 5, 5, 5, 1, 5, and 2, respectively.

The final ^{99}Mo product was dispensed and assayed by means of a calibrated ionization chamber. Radioactivity concentration (MBq/cm^3) was calculated by dividing the total product activity by the final volume of the product solution. All required nuclear data were taken from NuDat 2.5 [9].
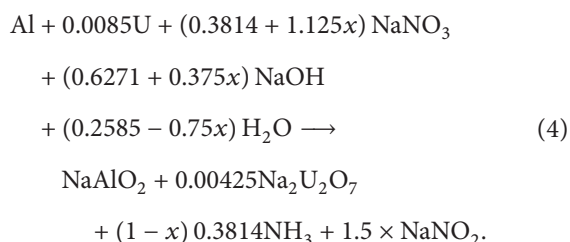
3. Results and Discussion

3.1. The Dissolving Process. When dissolving the target plates in the solvent, 3 M NaOH/4 M NaNO$_3$, 3 reactions must be considered leading to different reaction products as follows:

$$8Al + 3NaNO_3 + 5NaOH + 2H_2O \longrightarrow \tag{1}$$
$$8NaAlO_2 + 3NH_3,$$

$$Al + 1.5NaNO_3 + NaOH \longrightarrow \tag{2}$$
$$NaAlO_2 + 1.5NaNO_2 + 0.5H_2O,$$

$$Al + NaOH + H_2O \longrightarrow NaAlO_2 + 1.5H_2, \tag{3}$$
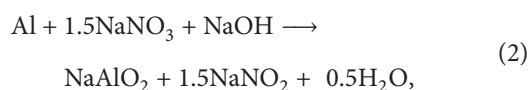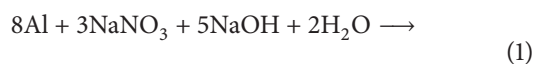
The most important is reaction (1), where the Al reduces the nitrate ion down to NH$_3$. Close to the end of the dissolving process the nitrate is reduced only to nitrite (2). This fraction is of the order of 10 to 15%. The theoretically possible reduction (3) generating hydrogen is nearly suppressed. Gas chromatographic determination of hydrogen in the off-gas from the dissolving process did not show any signal for H$_2$, meaning, the upper limit for H$_2$ generation is <2% and is therefore without any danger.

Under the conditions that x represents the mass unit of the target matrix that undergoes to nitrite formation and consequently $(1 - x)$ represents the mass units of the target matrix that undergoes under NH$_3$ formation, we obtain the "master equation" for dissolving the targets following:

$$Al + 0.0085U + (0.3814 + 1.125x)\, NaNO_3$$
$$+ (0.6271 + 0.375x)\, NaOH$$
$$+ (0.2585 - 0.75x)\, H_2O \longrightarrow \tag{4}$$
$$NaAlO_2 + 0.00425Na_2U_2O_7$$
$$+ (1 - x)\, 0.3814NH_3 + 1.5 \times NaNO_2.$$

The value x, representing the fraction of the aluminum that is dissolved under nitrite formation, ranges between $0.1 < x < 0.16$.

The solvent volume needed for the process is determined by the solubility of the sodium aluminate (NaAlO$_2$) which is 2.1 M/L corresponding to 57 g/L Al. Furthermore, the Na concentration should be kept as high as possible, in order to reach safely the saturation concentration for the precipitate

Na$_2$U$_2$O$_7$. A high nitrate concentration is needed for avoiding the formation of hydrogen, while the viscosity of the solution should be suitable for easy filtration. We found a composition of 3 M NaOH/4 M NaNO$_3$ as most suitable for the dissolving process.

The dissolving process is strong exothermic (close to 600 kcal are generated for dissolving 100 g Al), and in addition the dissolving speed increases with the second power of the temperature. Thus, the reaction is self-accelerating. Following the experiences collected in Dresden (IAF) and PINSTECH, the control of the dissolving process is easy and safely possible by short heating and cooling pulses. With these techniques one can easily adjust the dissolving temperature at around 70–80°C. Furthermore, the process can be performed at slightly reduced pressure conditions (see Figure 2). The dissolving process is performed in a special, dissolving vessel, equipped with heater and cooling jacket.

3.2. NH$_3$ Distillation. Since the iodine shall be removed from the process solution using a silver-coated column material, the NH$_3$ is recommended to be eliminated because it has potential to influence the efficiency of the iodine removal at the Ag-coated column. The simplest way to separate the NH$_3$ is the distillation from strong basic solution. Preliminary experiments have shown that 150–200 mL distilled volume is sufficient. This volume can be distilled off from the target solution within about 20 minutes. In the production runs, the distilled NH$_3$ is trapped in 5 N H$_2$SO$_4$ solution.

3.3. Filtration. The precipitate that is formed during the dissolving process is composed of mainly 2 components: the Na-diuranate and in addition the nonsoluble hydroxides, oxides or carbonates of several alloying metals of the Al-matrix that are coprecipitated together with the Na$_2$U$_2$O$_7$. Based on analytical data of the Al-matrix material used for the target preparation, the following quantities for the precipitate should be expected (Table 1).

Assuming a density of the precipitate of 4.4 g/cm^3 (based on ~30% porosity) and the uranium in the form of Na$_2$U$_2$O$_7 \times$ 6 H$_2$O, one would obtain a precipitate volume of ~2.37 cm^3, which corresponds to a filter bed thickness of $d \leq 1.5$ mm.

The target element uranium after dissolution must be present exclusively in the chemical form of Na$_2$U$_2$O$_7$ because it is well known that uranium species of lower oxidation stage absorb ^{99}Mo and consequently lower the production yield. Dissolving the same targets alone in NaOH or KOH (without NaNO$_3$) [10], an additional oxidation process (usually H$_2$O$_2$) is required to reach the oxidation stage of +6 for both of the U and the Mo.

As shown from the crystallographic analysis, the target element uranium was found after our ROMOL-99 dissolving process straight as sodium diuranate (Na$_2$U$_2$O$_7$) in the precipitate (Figure 3) without any further treatment.

The time needed for filtration is mainly determined by the surface area and the porosity of the used filter plate and the filter cake, the viscosity of the solution and the filtration pressure. The filter plate consists of a 3 mm thick metallic (INOX) sinter plate with a porosity of ~30 μm. The cold
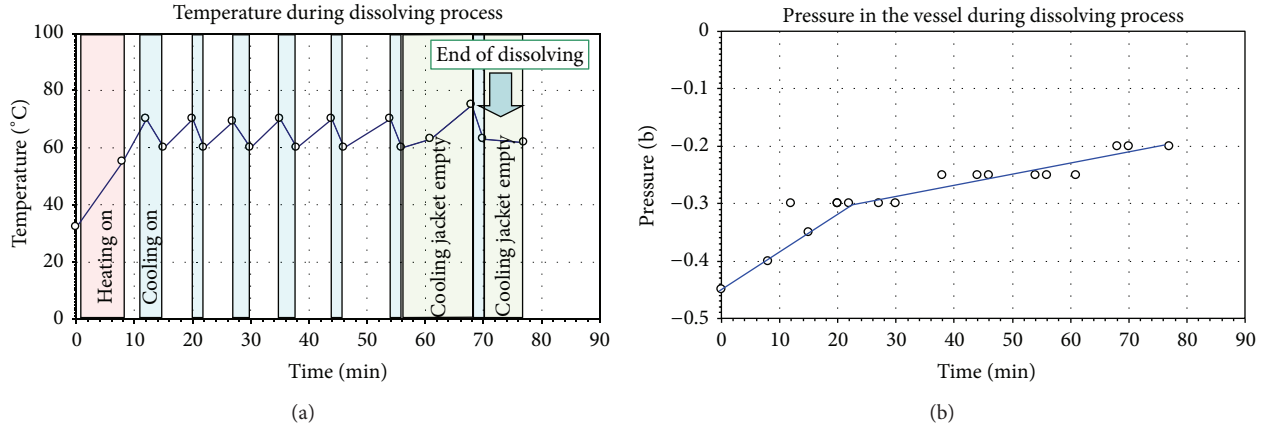
FIGURE 2: Temperature gain during controlled dissolving process (a) and the pressure situation during the dissolving process (b).

TABLE 1: Composition of the target material and the related composition of the precipitate after the dissolving process.

| Alloying element	Content (% of Al-weight)	Content in (mg) for 3 targets	Precipitated species	Precipitate in (mg) for 3 targets
Fe	0.14	128,8	$Fe(OH)_2$	207.14
Mn	0.002	1,84	$Mn(OH)_2$	3.03
Si	0.01	9,20	SiO_2	19.33
Ca	0.16	147,2	$CaCO_3$	950.43
C	0.1	92	C	92.00
U	5.16	5100	$Na_2U_2O_7$	6814.85

and hot runs showed that first of all the precipitate can be filtrated from the target solution with the above given alloying components, and in addition sufficient filtration speed (200–300 mL/min) is achieved in 10–20 min at a temperature of around 50°C.

3.4. Iodine Removal. In order to minimize the risk of iodine release in later production steps and waste, the adsorption on silver is the most promising approach for trapping the radioiodine before the ^{99}Mo is separated. During the production process, we have to deal with ^{132}I (2.3 h half-life, daughter of ^{132}Te), ^{133}I (20.8 h half-life), and ^{131}I (8.02 d half-life). Freshly prepared silver-coated Al_2O_3 material has shown to be the most appropriate material; this material has been prepared according to the Wilkinson et al. method [11]. The iodine removal process is performed by controlled filtration of the filtrated target solution over a column filled with this material. The flow rate needs to be controlled. Since the optimal flow rate for high iodine trapping efficiency is identical with the speed for introducing the basic target solution into the strong acid reaction vessel (next process step); there is no technological separation of both steps, thus, while transferring the basic solution into the nitric acid for acidification the radioiodine is removed simultaneously. The transfer process lasts for about 60–90 minutes. The efficiency

for iodine trapping has been determined to be >98%. The Ag-column also traps a good fraction of the Ru (see Figure 4); ^{99}Mo could not be detected within a detection limit of 3%.

3.5. Acidification and Nitrite Destruction. For the main separation step—the separation of the ^{99}Mo from the process solution after iodine removal—Al_2O_3 column chromatography has been selected. Molybdate is adsorbed from weak HNO_3-acid media at Al_2O_3 (this principle is used in the ^{99}Mo/^{99m}Tc-generator technology). Thus, the strong basic process solution needs to be acidified. This is not an easy step, since the Al-concentration is high. An anion-exchange process, as it is used in cases were only NaOH or KOH is involved for dissolving the targets under H_2 generation, is not possible due to the high NO_3^- concentration. Many test experiments have been performed in order to determine the optimal conditions for this step. When introducing strong basic aluminate solution into strong acid HNO_3 solution in the first step, $Al(OH)_3$ is precipitated. This hydroxide needs to dissolve immediately, otherwise it may transmute into nonsoluble configurations which may create problems in the further production steps. When the basic solution is introduced with moderate speed (50–70 mL/min) under strong mixing, one observes first a thick white precipitate that is redissolved relatively fast. Due to neutralization heat the solution is warming up. In order to bring the solution to boil additional heating is required.

As said before, we also have nitrite in the system, which is recommended to be destroyed. Simultaneously with the acidification process the nitrite is reduced with urea under nitrogen formation according to

$$(NH_2)_2CO + 2HNO_2 \longrightarrow 2N_2 + CO_2 + 3H_2O. \quad (5)$$
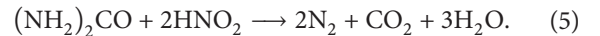
In test experiments, this gas generation looked like very fine silk. This gas generation is mixing the solution only a little, because of the microscopic fine bubbles, this effect is by far insufficient; additional strong stirring is required. The complete nitrite destruction and the re-dissolving of the primary precipitated hydroxides require refluxing under stirring for one additional hour after complete solvent transfer.
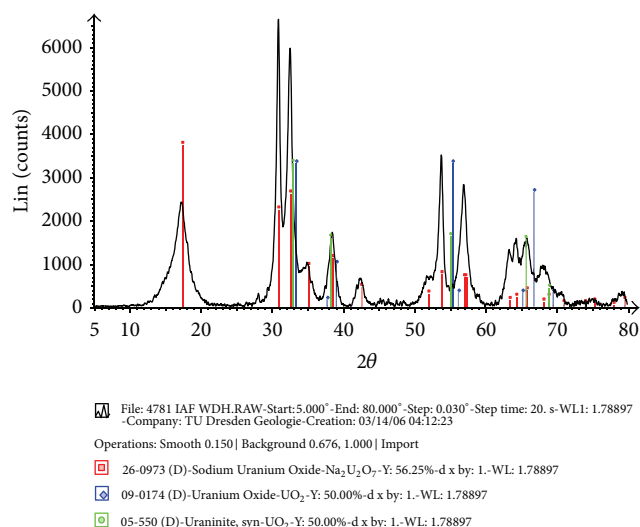
FIGURE 3: X-ray diffraction patterns of the uranium precipitate that show only the reflections of $Na_2U_2O_7$ and excluded other uranium species to be present. This X-ray diffractogram was performed by TU Dresden/Geologie.
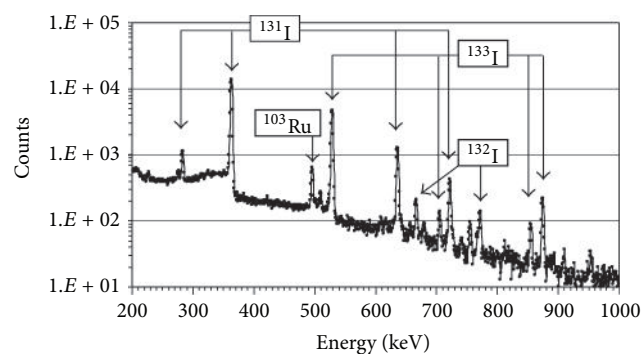

FIGURE 4: Gamma spectrum of the Ag-coated Al_2O_3 column after passing the filtrated target solution. The measurement was done from large distance. Only gamma signals from iodine radionuclides and Ru could be identified.

The reaction gases of this acidification process and in addition a slight carrier gas flow release also remain volatile iodine species (from iodine residue and decay of Te-parent nuclides) and radio Xe (mainly from ^{133}I-decay). The radio iodine is retained in a gas adsorption trap filled with Ag-IONEX. This is a Zeolite exchange material that adsorbs at $T > 100°C$ volatile inorganic and organic iodine species that is widely used in fuel reprocessing process for decontamination of acid off-gases. After passing the IONEX filter, off-gas from the acidification process that still may contain some Xe is introduced into the gas process line for further treatment.

When the nitrogen formation and iodine release is finished, the solution is cooled down to room temperature and is ready for the Al_2O_3 column process.

3.6. Alumina Column Process. The separation of the ^{99}Mo from the acidified target solution is achieved via anion
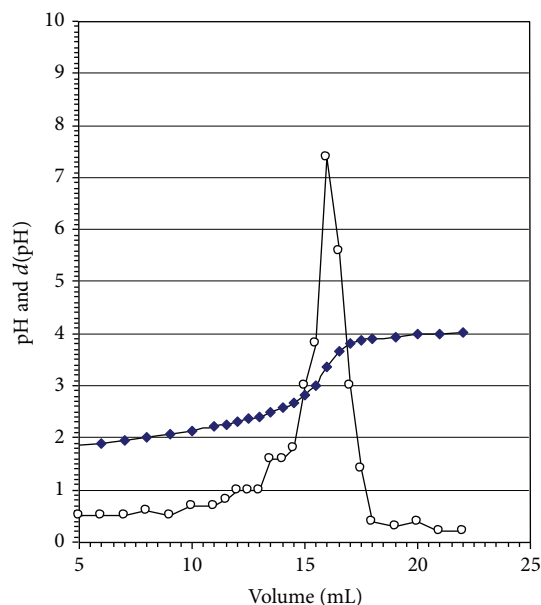

FIGURE 5: Potentiometric titration of 1 mL of the acidified target solution after nitrite destruction diluted to 100 mL with 0.100 N NaOH.

exchange chromatography using week acid Al_2O_3 as column material. The adsorption efficiency for Mo depends mainly on the salt concentration and the acidity of the solution and not so much on the absorber material itself. For the optimization of the column parameters, the control of the free acidity in the FEED solution played an important role. Due to the high salt concentration (especially that of Al^{3+}), a direct pH-measurement is not possible. A potentiometric titration did not show the required precision (see Figure 5).

The safe and better is to dilute a sample of the solution by a factor 1 : 100 with distilled water. This solution could perfectly undergo a pH measurement with an ordinary glass electrode. The pH determined in this way was always in the region of $2.2 < pH < 2.6$, which means that the free acid concentration in the original FEED solution under practical conditions was in the range of about $0.15 < [H^+] < 0.7$ M.

Under practical conditions, the volume of the loading solution (FEED) is around 6 L (for ~100 g target material). After the loading process, the column shall be washed with 0.5–1.0 L of 0.5 M HNO_3 500 mL water and then with 1500 mL 0.01 M NH_4OH. The ^{99}Mo is then eluted with up to 2000 mL of 1 M NH_4OH solution. One obtains a raw ^{99}Mo product of already ≫99% radionuclide purity.

In order to define the optimal Al_2O_3 column parameters one needs to consider

(i) the adsorption capacity of the exchange material Al_2O_3,

(ii) the selectivity related to the separation from radioactive contaminations,

(iii) the possible and needed loading- and elution speed which is relevant for the duration of the process.

TABLE 2: Optimal parameters for the alumina column process.

Al$_2$O$_3$ column	About 50 mm × 145 mm, bottom G 3 frit
Al$_2$O$_3$ weak acid material	250 g, size ~60 μm, density 1.25 mL/g, porosity 0.875
Loading process:	FEED volume ~5.8 L, 0.15 < [H$^+$] < 0.7 M, ~120 min
(1) Wash process	1000 mL 0.5 M HNO$_3$, time about 15 min
(2) Wash process	500 mL water, time about 7 min
(3) Wash process	1000 mL 0.01 M NH$_3$, time about 15 min
Liquid waste volume:	8300 mL
Elution	1000 mL 1-2 M NH$_3$, time about 30 min
Alumina column process:	Total time about 3 h.

FIGURE 6: Elution profile for ^{99}Mo elution from the Al$_2$O$_3$ column with 1 M NH$_3$ using the parameters shown in Table 2.

The capacity of Al$_2$O$_3$ for Mo adsorption is known to be ~30 mg Mo/g Al$_2$O$_3$ column material. In test experiments using 50 mL of model-target solutions containing a Mo-concentration of 20–33 mg Mo/L and columns with 2 g Al$_2$O$_3$ column material (0.7 × 5.6 cm column dimension) using a flow rate of 7 cm/min corresponding to 2.7 mL/min the Mo could be adsorbed with an average yield of >90%. Thus, in these experiments only a small fraction (1.5–2.5%) of the capacity of the exchanger has been utilized. This corresponds to 0.5–0.8 mg Mo/g Al$_2$O$_3$. Based on this data one would need for processing of 3 target plates theoretically 140 g of Al$_2$O$_3$ corresponding to 152 mL Al$_2$O$_3$ for the separation process.

For defining the column dimensions one needs to find a compromise between the needed amount of the Al$_2$O$_3$ material and reasonable high applicable elution speed. Furthermore one has to consider losses due to irreversible bound Mo with increasing Al$_2$O$_3$ quantities. Assuming the following practical conditions:

(i) the total volume of liquids that has to pass the column is ~11 L composed from 5.8 L acidified target solution, 3.3 L wash solutions, and 2.0 L elution volume,

(ii) the linear filtration speed is 7 cm/min (50 mL/min for loading and eluting and 80 mL/min washing),

(iii) the diameter of the column shall be 5 cm,

one obtains a volume flow speed of 137 mL/min under practical conditions.

Considering the previous determined 140 g or 152 mL Al$_2$O$_3$ absorber material, one would obtain an absorber bed height of 7.8 cm. If one increases the dimensions by at least a factor 2 for compensating not optimal conditions, the length of the Al$_2$O$_3$ column becomes 15.6 cm filled with 304 mL Al$_2$O$_3$ absorber material.

During the commissioning, it has been demonstrated that a 250 g alumina column bed is acceptable which corresponds to a column bed volume of about 275 mL. Table 2 summarizes the Al$_2$O$_3$ column process parameters.

Using the parameters shown in Table 2, the profile for eluting the ^{99}Mo from the Al$_2$O$_3$ column has been performed. As seen in Figure 6, the ^{99}Mo is eluted in a relatively sharp peak and 1000 mL of 1.0 M NH$_3$ solution is sufficient.
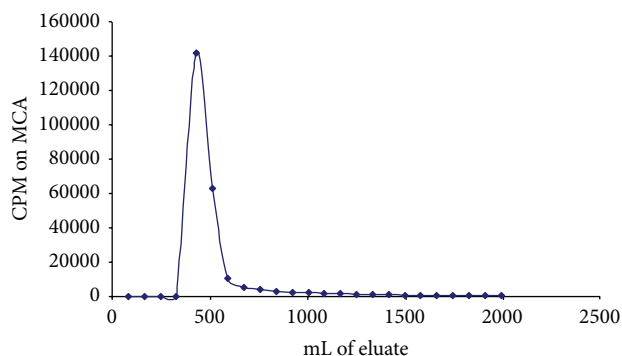
The ^{99}Mo retention at the column using model solutions was practically 100%, and the ^{99}Mo recovery was measured to be 91.2%.

The Al used in the target material contains some quantities of Si. It is well known that Si forms very unpleasant nonsoluble Mo Si-species which may cause dramatic losses in the ^{99}Mo yield. Certain limited quantities of Mo-carrier can help solving this problem. The other way around would be to elute the Al$_2$O$_3$ column with higher-concentrated NH$_3$ (2 M instead of 1 M) or with NaOH.

3.7. DOWEX-1 Column Process. Molybdenum in its anionic form MoO$_4$$^{2-}$ is adsorbed directly from the ammonia solution eluted from the Al$_2$O$_3$ column at strong basic anion exchange resins as DOWEX-1 (configuration OH$^-$). The distribution coefficients has been determined to be $K_D = 270$ for adsorption from 1 M NH$_4$OH and $K_D = 0.8$ for the desorption with 1 M (NH$_4$)$_2$CO$_3$ solution.

The dimensions of a suitable DOWEX-1 column and its operation parameters are determined in a similar way as demonstrated for the Al$_2$O$_3$ column. For a column of about 26 × 120 mm, a linear flow speed of 13 cm/min is the maximum. If the volume of the Mo solution is 2000 mL one would need theoretically 54.6 g of the ion exchange resin. DOWEX-1 in the dry form. Considering the density of 0.65 g/mL resin, this would give an 84 mL volume of the resin. For rinsing the column, 4 bed volumes are required which correspond to 340 mL. Table 3 summarizes the parameters for the DOWEX column process. The corresponding elution profile is shown in Figure 7.

3.8. Evaporation Step. The purification step at the DOWEX column delivers 200 mL of the ^{99}Mo molybdate in 1 M (NH$_4$)$_2$CO$_3$ solution. In the following step this eluted solution is evaporated to the dryness in a special evaporator, with condenser. During evaporation, the (NH$_4$)$_2$CO$_3$ is being decomposed; thus no additional salts are introduced into the final configured [^{99}Mo] molybdate solution.

The residue is redissolved in the desired volume of diluted NaOH solution forming the final product solution

TABLE 3: Optimal parameters for the DOWEX-1 column process.

DOWEX-1 column	About 26 mm × 120 mm, bottom G 3 frit
Loading process:	^{99}Mo-solution in 1 M NH$_3$ volume ~1.0 L, ~15 min
(1) Wash process	170 mL water, time about 3 min
(2) Wash process	170 mL water, time about 3 min
Liquid waste volume:	~1.4 L (depending on FEED and wash volume)
Elution	200 mL of 1 M (NH$_4$)$_2$CO$_3$ solution, time about 10 min
DOWEX column process:	Total time about 35–40 min
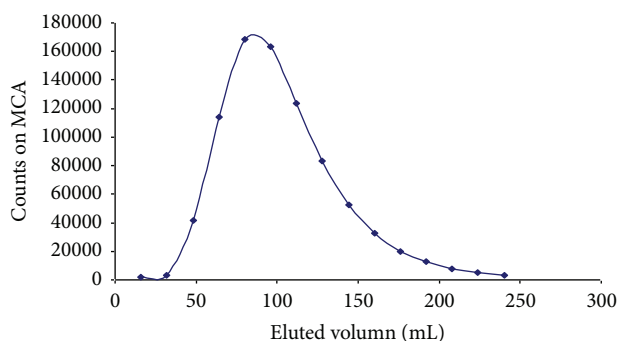
FIGURE 7: ^{99}Mo elution profile from the DOWEX-1 column with 1 M (NH$_4$)$_2$CO$_3$-solution using the parameters shown in Table 3.

[^{99}Mo]Na$_2$MoO$_4$. This final product solution is then transferred into a corresponding plastic vial and transferred into the hot cell 3 for further processing, precise measurement and distribution.

A sublimation step (at 1000°C) is foreseen as an additional reserve for improving purity, if required. In this case the residue after evaporation shall be redissolved in diluted HNO$_3$ or NH$_4$OH.

3.9. Radioactivity Balance during the Process. Careful studies have been performed to obtain a full picture on the behavior of the ^{99}Mo, of the most important impurities in ^{99}Mo preparations, for other fission products, and for the target element itself. On one hand, tracer activities of ^{99}Mo and ^{131}I have been used, and after having optimized the separation conditions the same full protocol has been applied to study the separations technology with weak irradiated original target material (activity level ~4 GBq). Figure 8 summarizes gamma-spectroscopic measurements that illustrate how powerful the individual separation steps are. Segments of original measured gamma spectra are shown in one graph. Signals of the most critical radionuclides are clearly identified. In order to have a good overview, the original data of the different spectra have been expanded using a factor shown in the graph.

The upper spectrum has been taken from a small fraction of the filter cake (precipitate) followed by the spectrum from a sample from the filtrate. It is clearly seen that only few gamma lines are left in the filtrate, which correspond to ^{99}Mo,
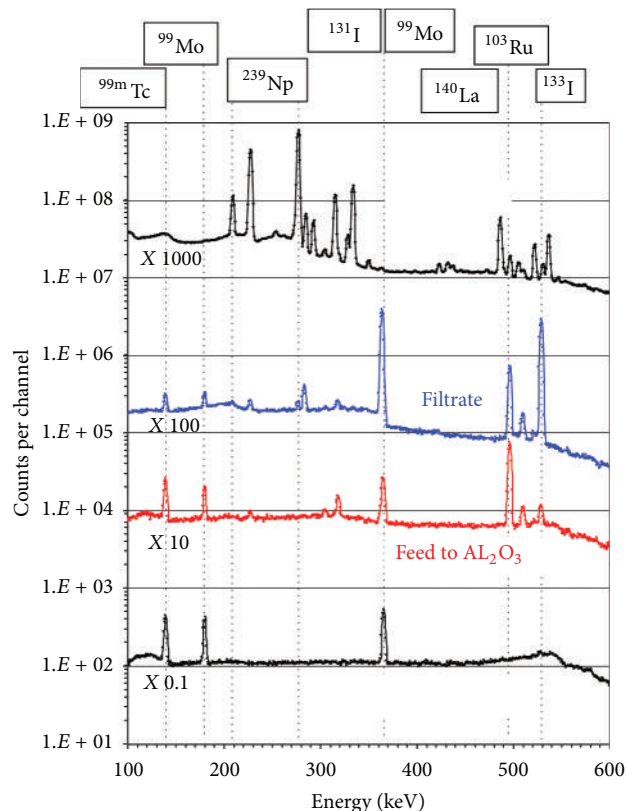

FIGURE 8: Gamma spectra of samples from the precipitate, filtrate, FEED solution (filtrate after iodine removal), from the final product illustrating the different separation and purification steps (for more details see text).

its daughter ^{99m}Tc, the radioiodine's, and some fractions of Ru. The strongest signals in the precipitate (^{239}Np, and ^{140}La) are not seen in the filtrate solution. As said before the filtrate is passed through a silver-coated Al$_2$O$_3$ column prior to the acidification process. Thus comparing the spectra 2 and 3, one clearly sees that iodine is missing in the FEED solution (see also Figure 4). When interpreting spectrum 3, one needs to consider that the strongest gamma signal from ^{99}Mo is 739 keV with the branching of 12.13% (not shown in this graph). The two gamma lines here at 181 keV and 366 keV have a branching of only 5.99 and 1.19%, respectively. Finally the last spectrum below is taken from a sample of the final ^{99}Mo preparation. All measurements have been performed using a Pb absorber to suppress the strong gamma signal from ^{99m}Tc (and other low-energetic radiation).

3.10. Radioactivity Distribution between Precipitate and Filtrate. In total the precipitate collects more than 60% of the radioactivity formed in the nuclear process in the chemical form of hydroxides, oxides, or carbonates of the fission products. This corresponds to the fission products of Ba and Sr, the rear earth elements and actinides, Zr/Nb. Te and Sb are nearly quantitatively collected in the precipitate. The results of a corresponding tracer experiment, are summarized

TABLE 4: Radioactivity distribution between precipitate and filtrate after dissolving irradiated $^{nat.}$U-targets of original composition.

Nuclide	Precipitate (%)	Solution (%)
^{239}Np	100	$\ll 1$
^{132}Te	100	< 3
^{143}Ce	100	$\ll 1$
^{141}Ce	100	$\ll 1$
^{140}Ba	100	$\ll 1$
^{140}La	100	$\ll 1$
^{131}I	0.60	99.39
^{103}Ru	20–40	60–80
^{99}Mo	0.57	99.43

Note: Ru behaves in different experiments differently, thus these data provide just an estimate.

TABLE 5: Radioactivity distribution of ^{99}Mo and the most important impurities during the process.

	^{99}Mo	^{103}Ru	^{132}Te	^{131}I
Filter cake	<0.5%	19.20%	96.30%	n.d.
Filtrate	**>99.5%**	**80.70%**	**3.70%**	**100%**
Ag-column	n.d.	22.70%	1.00%	>98%
FEED	>99%	66.90%	1.60%	<2%
Al_2O_3 column	10.6%	0.10%	1.10%	n.d.
Al-waste	n.d.	75.40%	n.d.	n.d.
DOWEX column	0.003%	0.06%	n.d.	n.d.
Final	86.5%	<0.001%	<0.001%	<0.001%

The % values relates to the individual content of the specified nuclide and not to ^{99}Mo.
(n.d.: not detected).

in Table 4. In this experiments target plates of the original composition were used.

The most important impurities have been followed up quantitatively throughout the process as good as gamma-spectroscopy could do under practical conditions with limited measuring time. The results are summarized in Table 5. The FEED solution (filtrate after passing the silver column) contains already relatively clean ^{99}Mo, however in presence of high salt concentration (Al, Na including ^{24}Na and fission-Cs). Up to 80% of the Ru is found in the filtrate, at the silver column already about 22% are retained. The remaining Ru is passing the Alumina column during the loading procedure. Careful washing avoids the transfer of Ru to the next purification steps. Ru shows a nonstandard behavior, sometimes we observed significant higher Ru-retention in the filter cake.

The ^{132}Te is nearly quantitatively coprecipitated. The highest ^{132}Te-content in the filtrate was 3.7% of the original quantity. About half of this fraction is retained at the silver column, the other half fraction at the Alumina column. In the filtrate and wash solutions from the Alumina column the ^{132}Te could not be detected any more (with the applied spectrometric parameters).

The iodine is nearly quantitatively retained at the silver column. The small fraction that is passing the silver column

TABLE 6: Quality parameters of fission ^{99}Mo produced at PINSTECH meeting international standard.

Gamma	^{131}I	$\leq 5 \times 10^{-2}$ MBq/GBq ^{99}Mo
	^{103}Ru	$\leq 5 \times 10^{-2}$ MBq/GBq ^{99}Mo
Beta	^{89}Sr	$\leq 6 \times 10^{-4}$ MBq/GBq ^{99}Mo
	^{90}Sr	$\leq 6 \times 10^{-5}$ MBq/GBq ^{99}Mo
Alpha		$\leq 1 \times 10^{-6}$ MBq/GBq ^{99}Mo
Other gamma		$\leq 1 \times 10^{-1}$ MBq/GBq ^{99}Mo

is then distributed throughout the system, mainly in the waste solutions through the washing procedures of the columns. Summarizing, the separation and purification process is efficient and easy.

3.11. ^{99}Mo Production Facility at PINSTECH. The ^{99}Mo Production Facility (MPF) is installed at PINSTECH Phase-1 building near reactor hall of PARR-1. The technical realization of the ROMOL-99 process in a semiautomated separation facility has been carried out by ITD Dresden GmbH (former Hans Wälischmiller (HWM) GmbH, Branch office Dresden). The main working areas of this facility are the Hot Cell complex (3 Hot Cells), interim liquid storage tanks, charcoal filter beds for iodine retention, xenon delay tanks, and the operator and service areas interconnected with it. Additionally, there are the so-called lock rooms through which the activated targets, the final product, and solid and liquid wastes are moved. Still, there are areas for personnel, preparation of reagents, storage, dosimetry, measurement, and decontamination. Further equipment in other rooms or buildings, which participate in the ^{99}Mo production, is the existing equipment of the main exhaust system with filter chamber, Secomak blowers and the main exhaust blower. The spent target material (loaded filter plates enclosed in screw shut cans) is stored in Spent Fuel bay of PARR-1. The solid low-radioactive wastes (spent ion-exchange columns, tubes, interconnections, and other one-way materials) are stored, while decayed radioactive liquid waste is cementized in the radioactive waste management Group building.

More than 50 commercial batches of fission based ^{99}Mo using ROMOL-99 process have been successfully completed. After the evaporation step, the residue is dissolved in the desired volume of diluted NaOH solution forming the final product solution $[^{99}$Mo]Na$_2$MoO$_4$. This final product solution is then transferred to the PAKGEN ^{99m}Tc generator production site at PINSTECH. These generators are then distributed to the 35 nuclear medical centers in Pakistan. The performance of these generators is comparable to that of generators produced from imported fission ^{99}Mo. The quality of the ^{99}Mo preparations produced at PINSTECH corresponds to the required international standard (Table 6). Details about the preparation of PAKGEN ^{99m}Tc generators and their quality control have already been reported [12]. The next steps at PINSTECH related to the routine ^{99}Mo-production are upscaling the production capacity and transmutation to LEU (low enriched uranium) as target fuel.

4. Conclusion

The ROMOL-99 process allows dissolving UAlx/Al clad dispersion targets under reduced pressure conditions without generation of hydrogen at temperatures between 70 and 80°C. The technology implements the separation of NH_3 and radio-iodine prior to the ^{99}Mo separation. Generated nitrite is safely destroyed during the acidification process by urea to N_2. The technical realization of the ROMOL-99 process in a semiautomated separation facility has been carried out by ITD Dresden GmbH (former Hans Wälischmiller (HWM) GmbH, Branch Office Dresden). More than 50 commercial batches of fission-based ^{99}Mo using the ROMOL-99 process have been successfully completed at PINSTECH. PAKGEN ^{99m}Tc generators were prepared by using this locally produced high purity fission ^{99}Mo and distributed to 35 nuclear medical centers in Pakistan. The performance of these generators is comparable to that of generators produced from imported fission ^{99}Mo.

Conflict of Interests

The authors declare that they have no conflict of interests.

References

[1] L. G. Stang, BNL 864 (T-347), 1964.

[2] D. Novotny and G. Wagner, "Procedure of small scale production of Mo-99 on the basis of irradiated natural uranium targets," in *Proceedings of the IAEA Consultancy Meeting on Small Scale Production of Fission Mo-99 for Use in Tc-99m Generators*, Vienna, Austria, July 2003.

[3] R. Muenze, O. Hladik, G. Bernhard, W. Boessert, and R. Schwarzbach, "Large scale production of fission ^{99}Mo by using fuel elements of a research reactor as starting material," *International Journal of Applied Radiation and Isotopes*, vol. 35, no. 8, pp. 749–754, 1984.

[4] O. Hladik, G. Bernhardt, W. Boessert, and R. Muenze, "Production of fission ^{99}Mo by processing irradiated natural uranium targets," Fission Molybdenum for Medical Use, IAEA-TECDOC-515, IAEA, Vienna, Austria, 1989.

[5] G. J. Beyer, R. Muenze, D. Novotny, A. Mushtaq, and M. Jehangir, "ROMOL-99—a new innovative small-scale LEU-based Mo-99 production process," in *Proceedings of the 6th International Conference on Isotopes*, Seoul, Republic of Korea, May 2008.

[6] G. Beyer, R. Muenze, D. Novotny, M. Ahmad, and M. Jehangir, "S8-4 ROMOL-99: a new innovative small-scale LEU-based Mo-99 production process," in *Proceedings of the International Meeting on Reduced Enrichment for Research and Test Reactors (RERTR '08)*, Washington, DC, USA, October 2008.

[7] G. Beyer, R. Muenze, D. Novotny, M. Ahmad, and M. Jehangir, "S13-P6 ROMOL-99: a new innovative small-scale LEU-based Mo-99 production process," in *Proceedings of the 31th International Meeting on Reduced Enrichment for Research and Test Reactors (RERTR '09)*, Beijing, China, November 2009.

[8] A. Mushtaq, "Specifications and qualification of uranium/aluminum alloy plate target for the production of fission molybdenum-99," *Nuclear Engineering and Design*, vol. 241, no. 1, pp. 163–167, 2011.

[9] NuDat 2.5, www.nndc.bnl.gov/nudat2/.

[10] A. A. Sameh and H. J. Ache, "Production techniques for fission molybdenum -99," *Radiochimika Acta*, vol. 41, pp. 65–72, 1987.

[11] M. V. Wilkinson, A. V. Mondino, and A. C. Manzini, "Separation of iodine produced from fission using silver-coated alumina," *Journal of Radioanalytical and Nuclear Chemistry*, vol. 256, no. 3, pp. 413–415, 2003.

[12] A. Mushtaq, S. Pervez, S. Hussain et al., "Evaluation of Pakgen ^{99m}Tc generators loaded with indigenous fission ^{99}Mo," *Radiochim Acta*, vol. 100, pp. 793–800, 2012.

Research Article

Influence of the Generator in-Growth Time on the Final Radiochemical Purity and Stability of ^{99m}Tc Radiopharmaceuticals

L. Uccelli,[1] **A. Boschi,**[1] **M. Pasquali,**[1] **A. Duatti,**[1] **G. Di Domenico,**[2] **G. Pupillo,**[2] **J. Esposito,**[3] **M. Giganti,**[1] **A. Taibi,**[2] **and M. Gambaccini**[2]

[1] *Dipartimento di Morfologia, Chirurgia e Medicina Sperimentale, Sezione di Diagnostica per Immagini, Università di Ferrara and INFN, Sezione di Ferrara, Via Luigi Borsari 46, 44121 Ferrara, Italy*

[2] *Dipartimento di Fisica e Scienze della Terra, Università di Ferrara and INFN, Sezione di Ferrara, Via Saragat 1, 44122 Ferrara, Italy*

[3] *INFN, Laboratori Nazionali di Legnaro (LNL), Via dell'Università 2, 35020 Legnaro, Italy*

Correspondence should be addressed to A. Boschi; alessandra.boschi@unife.it

At Legnaro laboratories of the Italian National Institute for Nuclear Physics (INFN), a feasibility study has started since 2011 related to accelerated-based direct production of ^{99m}Tc by the ^{100}Mo(p,2n) ^{99m}Tc reaction. Both theoretical investigations and some recent preliminary irradiation tests on ^{100}Mo-enriched samples have pointed out that both the ^{99g}Tc/^{99m}Tc ratio and the ^{99m}Tc specific activity will be basically different in the final accelerator-produced Tc with respect to generator-produced one, which might affect the radiopharmaceutical procedures. The aim of this work was to evaluate the possible impact of different ^{99g}Tc/^{99m}Tc isomeric ratios on the preparation of different Tc-labeled pharmaceutical kits. A set of measurements with ^{99m}Tc, eluted from a standard ^{99}Mo/^{99m}Tc generator, was performed, and results on both radiochemical purity and stability studies (following the standard quality control procedures) are reported for a set of widely used pharmaceuticals (i.e., ^{99m}Tc-Sestamibi, ^{99m}Tc-ECD, ^{99m}Tc-MAG3, ^{99m}Tc-DTPA, ^{99m}Tc-MDP, ^{99m}Tc-HMDP, ^{99m}Tc-nanocolloids, and ^{99m}Tc-DMSA). These pharmaceuticals have been all reconstituted with either the first $[^{99m}$TcO$_4]^-$ eluate obtained from a ^{99}Mo/^{99m}Tc generator (coming from two different companies) or eluates after 24, 36, 48, and 72 hours from last elution. Results show that the radiochemical purity and stability of these radiopharmaceuticals were not affected up to the value of 11.84 for the ^{99g}Tc/^{99m}Tc ratio.

1. Introduction

^{99m}Tc, with its peculiar physical-chemical properties, still continues to be the most important radionuclide used in diagnostic nuclear medical procedures. In particular, the developments of technetium chemistry have opened new perspectives in the field of diagnostic imaging [1]. More than 80% of the radiopharmaceuticals are currently labeled with this radionuclide [1] by reconstitution with sodium pertechnetate [2–4] [Na^{99m}TcO$_4$] commercial kits containing in lyophilized form the various reagents required for the preparation of each radiopharmaceutical. Its routine applications are ensured by the availability of portable ^{99}Mo/^{99m}Tc generators in which ^{99}Mo is bound as molybdate anion

to alumina columns. Current global interruptions of ^{99}Mo supply that involved uranium fission of highly enriched ^{235}U targets, aging reactors, and the staggering costs of their maintenance, focused on the search for alternative method of the ^{99}Tc production [5]. One of the possibilities is to replace the reactors with particle accelerators, aiming at a regional production and distribution. At Legnaro laboratories of the Italian National Institute for Nuclear Physics (INFN), a feasibility study related to accelerated-based direct production of ^{99m}Tc by the ^{100}Mo(p,2n) ^{99m}Tc reaction [6, 7] has started since 2011. Theoretical investigations and some recent preliminary irradiation tests on ^{100}Mo-enriched samples point out that both the ^{99g}Tc/^{99m}Tc ratio and ^{99m}Tc specific

TABLE 1: Radiopharmaceuticals used in the study.

Name	Radiopharmaceutical
Neurolite (Brystol-Myer Squibb)	^{99m}Tc-ECD (^{99m}Tc-Bicisato)
Cardiolite (Brystol-Myer Squibb)	^{99m}Tc-SESTAMIBI
Stamicis (IBA)	^{99m}Tc-SESTAMIBI
Technemibi (Mallinckrodt)	^{99m}Tc-SESTAMIBI
TechneScan (Mallinckrodt)	^{99m}Tc-MAG3
Pentacis (IBA)	^{99m}Tc-DTPA
Medronato II (GE Healthcare)	^{99m}Tc-MDP
Osteocis (IBA)	^{99m}Tc-HMDP
Nanocoll (GE Healthcare)	^{99m}Tc-nanocolloids
Renocis (IBA)	^{99m}Tc-DMSA

activity will be basically different in the final accelerator-produced Tc with respect to generator-produced one, due to the concomitant production of Tc contaminant nuclides, such as ^{99g}Tc, ^{98}Tc, ^{97m}Tc, and ^{97g}Tc. In particular, the amount of the ground-state long-lived β^- emitter ^{99g}Tc, useless for diagnostic procedures, might have a negative effect in the radiopharmaceutical procedures going to compete with ^{99m}Tc for the formation of the corresponding chemically identical radiopharmaceuticals. The presence of an excess of ^{99g}Tc might be responsible for a value of radiochemical purity lower than the standard required for some radiopharmaceutical preparations. In fact, the ^{99g}Tc present in solution could consume reagents of reaction, and in particular the reducing agent ($SnCl_2$). As a result, unreacted $[^{99m}TcO_4]^-$ may remain in the solution, or radioactive by-products not useful for the specific diagnostic procedure may be formed. The quality of ^{99m}Tc is then fundamental for the assurance of radiopharmaceuticals quality [8–10]. The aim of this work was therefore to perform a set of measurements with ^{99m}Tc, eluted from a standard ^{99}Mo/^{99m}Tc generator, in order to first check possible impact of different ^{99g}Tc/^{99m}Tc isomeric ratios on the preparation of different Tc-labeled pharmaceutical kits. Results on both radiochemical purity and stability studies (following the standard quality control procedures) are reported for a set of widely used pharmaceuticals (i.e., ^{99m}Tc-Sestamibi, ^{99m}Tc-ECD, ^{99m}Tc-MAG3, ^{99m}Tc-DTPA, ^{99m}Tc-MDP, ^{99m}Tc-HMDP, ^{99m}Tc-nanocolloids, and ^{99m}Tc-DMSA). These pharmaceuticals have been all reconstituted with either the first $[^{99m}TcO_4]^-$ eluate obtained from the ^{99}Mo/^{99m}Tc generator (coming from two different companies) or eluates after 24, 36, 48, and 72 hours from last elution.

2. Materials and Methods

The preparation of radiopharmaceuticals reported in Table 1 was carried out with sodium pertechnetate eluates coming from two different ^{99}Mo/^{99m}Tc generators: a "dry" DRYTEC generator (GE Healthcare, Via Galeno 36 20126, Milan), and a "wet" Elumatic III generator (IBA-CIS Bio International, Route Nationale 306, Saclay BP 32, 91192 GIF SUR YVETTE, Cedex France).

All generators, with ^{99}Mo calibrated activity of 10 GBq, were eluted with 5 mL of saline solution as indicated by each manufacturer. From each generator, we analyzed and compared the three first elutions, performed just after generator delivery (time elapsed between manufacturing and first use can be estimate in 2-3 days), and 3 elutions were carried out after 36, 48, and 72 hours from the previous elution.

2.1. Quality Control of ^{99}Mo/^{99m}Tc Generator Eluates. Generator eluates have been subjected to all the tests [11] required by European Pharmacopoeia [14], and Italian Pharmacopoeia, 12th edn., Norme di Buona Preparazione dei Radiofarmaci per Medicina Nucleare, All. A, p.to A.2 "Generatore di ^{99}Mo/^{99m}Tc (molibdeno/tecnezio)".

2.1.1. Generator Elution Yield. It was expressed as % of the ratio between the eluate radioactivity measured immediately after elution using a dose calibrator (V_M) and the theoretical radioactivity (V_C) calculated on the basis of the date of calibration and multiplied by the factor 100 [3]. The elution efficiency should be within the range of 90%–110%.

2.1.2. Eluate Visual Inspection. All eluates were visually inspected, pulling the vial from its shielded container. The operation was performed within an adequately shielded cell for radiopharmaceuticals manipulation; the vial containing the pertechnetate eluate was manipulated by operators using a pair of pliers to guarantee an adequate distance from the hands of the operator.

2.1.3. Eluate pH. Generator eluate is itself a preparation for injection; ideally it should have a pH as close as possible to the physiological, between 7 and 8. The Pharmacopeia requires that eluates have pH values within the range of 4–8. Since the molybdenum is adsorbed onto the alumina in an acid environment, the pH values of eluates are slightly acid (4.5–6). It was measured by means of pH usual indicator strip (range 0–14) and checked by electronic pH-meter.

2.1.4. Aluminum Content. It was determined by a semiquantitative procedure employing indicator strips (Tec-Control Biodex Medical, New York, USA) together with standard aluminium solution [12, 13]. A drop of standard solution with a concentration less than $5 \mu g \, mL^{-1}$ of aurintricarboxylic acid was deposited on indicator paper; subsequently, by side a drop of eluate was deposited. If the coloration produced by the latter is lower than the one produced by the standard solution, it can be assumed that the concentration of aluminium in the eluate is less than the maximum acceptable level of $5 \mu g \, mL^{-1}$ provided by Official Pharmacopoeia [14].

2.1.5. Radionuclidic Purity. Radionuclidic purity is the percentage of total radioactivity which may be attributed to the daughter radionuclide. In the case of fission-produced generator, the largest potential source of contamination that could exceed the minimum value detectable can be due to the parent (^{99}Mo) [15]. Trace amount of other fission impurities [16, 17] may be usually present in negligible amounts.
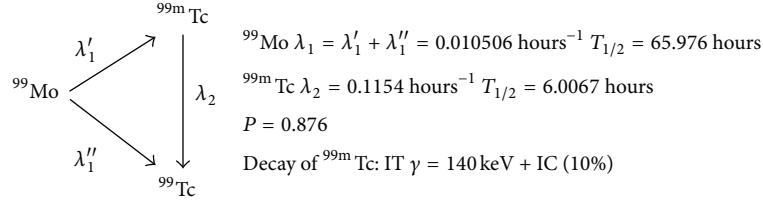
FIGURE 1: Simplified decay scheme of ^{99}Mo to ^{99g}Tc.

The early and quick evaluation of the eluate content of ^{99}Mo was provided by the following procedure, which involved the use of a lead shield of appropriate thickness (0.6 mm of lead) in order to attenuate ^{99m}Tc emission [18]. The activity contained in the unshielded elution vial was measured with a dose calibrator (PET-dose, Comecer, Castelbolognese, Italy); for measuring ^{99}Mo activity, the elution vial was then placed within the lead shield and its activity was recorded. The thickness of the shield was enough to largely attenuate the 140 keV photons [19], and only partly those greater than 700 keV. The measured activity, multiplied by a suitable correction factor which accounts for the attenuation of 740–780 keV photons due to the lead shielding, provides an estimation of the ^{99}Mo activity. This value should not exceed 0.1% of the ^{99m}Tc activity according to the European Pharmacopoeia.

For a more accurate determination of the radionuclidic purity [17, 20], the same eluate sample was examined again (reassayed) after 7–15 days by means of high-resolution gamma spectrometry using a solid-state, high-purity germanium detector [16].

2.1.6. Radiochemical Purity. It was checked by paper chromatography, Whatman no.1 paper strips and saline as mobile phase. According to this procedure, ^{99m}TcO$_4^-$ migrates with the solvent front ($R_f = 1$), whereas reduced hydrolyzed ^{99m}Tc remains at the origin ($R_f = 0$). The radioactivity distribution was measured by a scanning radiochromatography detection system for thin layer chromatography (Cyclone instrument equipped with a phosphor imaging screen and an OptiQuant image analysis software (Packard, Meridien, CT)). Eluate radiochemical purity should be greater than 95%.

2.1.7. ^{99g}Tc to Active ^{99m}Tc Ratio. ^{99}Mo decays to ^{99g}Tc (12.4%) and ^{99m}Tc (87.6%), and the latter, with a physical $T_{1/2}$ of 6.0067 h, decays to ^{99g}Tc ($T_{1/2}$ = 211,100 years). Due to this particular branching decay of ^{99}Mo, even fresh elutions from a generator always contain both isotopes (^{99m}Tc and ^{99g}Tc), indistinguishable from the chemical point of view. The amount (μg) of total technetium present in the eluate is directly related to the amount of ^{99}Mo atoms present on the column (i.e., ^{99}Mo activity) and the time that elapsed since the previous elution. The total number of Tc atoms, namely, the sum of ^{99g}Tc and ^{99m}Tc, has been calculated as follows:

$$N_{\text{Tc(total)}} = N^\circ_{^{99}\text{Mo}} \left(1 - e^{-\lambda_1 t}\right), \qquad (1)$$

where $N^\circ_{^{99}\text{Mo}}$ is the initial ^{99}Mo atoms number present on the column, λ_1 is the decay constant of ^{99}Mo (0.0105 hours^{-1}), and t is the time that elapsed since the last elution. The number of ^{99m}Tc atoms has been calculate as follows:

$$N_{^{99m}\text{Tc}} = P \frac{\lambda_1}{\lambda_2 - \lambda_1} N^\circ_{^{99}\text{Mo}} \left(e^{-\lambda_1 t} - e^{-\lambda_2 t}\right), \qquad (2)$$

where λ_2 is the decay constant of ^{99m}Tc (0.1149 hours^{-1}) and P is the decay probability ($P = 0.876$). A simplified decay scheme of ^{99}Mo to ^{99g}Tc is shown in **Figure 1**. From the above equations the number of ^{99g}Tc atoms can be easily calculated as follows:

$$N_{^{99g}\text{Tc}} = N_{\text{Total Tc}} - N_{^{99m}\text{Tc}} \qquad (3)$$

and thus the ^{99g}Tc to active ^{99m}Tc ratio can be estimated.

The determination of the ^{99g}Tc content in a fresh eluate requires an immediate measurement after the elution of the ^{99m}Tc activity and a later measurement of the total activity of ^{99g}Tc (in a few months almost all the ^{99}Mo and ^{99m}Tc atoms decay into ^{99g}Tc). The evaluation of ^{99m}Tc activity in the sample has been performed by using a dose calibrator (PET-dose, Comecer, Castelbolognese, Italy), while the evaluation of ^{99g}Tc activity has been performed using the TRI-CARB 2810TR liquid scintillation analyzer (Perkin Elmer Inc., Monza, Italy). The samples for ^{99g}Tc activity measurements were prepared taking an aliquot of 0.8 mL from an eluate decayed for 60 days (total volume of the eluate: 5 mL) and adding 5.4 mL of liquid scintillator (Ultima Gold LLT cocktail, Perkin Elmer Inc., Monza, Italy). The measurement of ^{99g}Tc activity was performed using the 0–295 keV energy window.

2.2. Radiopharmaceuticals Labeling. The elutions were used to label different commercial kits (Table 1). Kits reconstitution was performed according to the methods described in the package included within the commercial kits. The radiochemical purity (RCP) of radiopharmaceuticals was evaluated immediately after preparation ($t = 0$) and at the end of the stability period indicated by the manufacturer. The radiochemical purity and stability were measured using methods specified by manufacturer, with the exception of TechneScan (Mallinckrodt) for which the following chromatographic system was used [21]: mobile phase, 54/45/1 (physiological/methanol/glacial acetic acid) and stationary phase, RP-18 (Merck). Thin-layer chromatography plates were analyzed with a Cyclone instrument equipped with a

Table 2: pH, ^{99}Mo, ^{103}Ru, and ^{131}I amounts and radiochemical purities (mean ± standard deviation) of the evaluated generators' elutions.

Type of generator	Type of elution	pH	^{99}Mo %	^{103}Ru %	^{131}I %	RCP %
Drytec-GE	1° eluate	6.0 ± 0.3	$(2.1 ± 0.2) × 10^{-2}$	$(1.9 ± 0.2) × 10^{-6}$	$(1.4 ± 0.4) × 10^{-7}$	99.8 ± 0.3
	36 h	6.0 ± 0.4	$(3.9 ± 0.5) × 10^{-2}$	—		99.7 ± 0.3
	48 h	6.1 ± 0.3	$(3.7 ± 0.4) × 10^{-2}$	—		99.8 ± 0.2
	72 h	6.0 ± 0.2	$(3.1 ± 0.2) × 10^{-2}$	—		99.7 ± 0.3
Elumatic III	1° eluate	6.2 ± 0.1	$(2.7 ± 0.3) × 10^{-2}$	$(1.7 ± 0.5) × 10^{-7}$	$(2.2 ± 0.3) × 10^{-7}$	99.8 ± 0.1
	36 h	6.2 ± 0.3	$(2.5 ± 0.5) × 10^{-2}$	—		99.8 ± 0.3
	48 h	6.2 ± 0.4	$(2.5 ± 0.1) × 10^{-2}$	—		99.6 ± 0.2
	72 h	6.1 ± 0.2	$(2.5 ± 0.3) × 10^{-2}$	—		99.4 ± 0.1
E.P.		4.8–8.0	<0.1%	$<5 × 10^{-3}$	$<5 × 10^{-3}$	≥95.0

E.P.: European pharmacopoeia; 36, 48, and 72 h indicate the time from the previous elution; the amount of ^{99}Mo represents the % of total radioactivity in the generators' eluates determined with "rapid method"; ^{103}Ru (0.497 MeV) and ^{131}I (0.365 MeV) are the most common gamma radionuclide detectable by gamma spectrometry, and in the table are reported the % of total radioactivity in the generators' eluates.

Table 3: RCP of radiopharmaceuticals at $t = 0$, prepared with generator DRYTEC GE Healthcare eluates at time superior to 24 h from the last elution.

Commercial name	Radiopharmaceuticals	RCP_{36}	RCP_{48}	RCP_{72}	RCP requirements
Neurolite	^{99m}Tc-ECD	98.57 ± 0.45	99.41 ± 1.51	98.73 ± 1.85	≥90%
Cardiolite	^{99m}Tc-Sestamibi	97.91 ± 0.38	98.35 ± 1.02	99.40 ± 1.23	≥ 94%
Stamicis	^{99m}Tc-Sestamibi	97.88 ± 0.28	97.90 ± 0.15	98.16 ± 0.11	≥94%
Technemibi	^{99m}Tc-Sestamibi	98.18 ± 0.23	97.77 ± 0.33	98.53 ± 0.27	≥94%
TechneScan	^{99m}Tc-MAG3	98.89 ± 0.64	99.10 ± 0.44	99.31 ± 0.14	≥95%
Pentacis	^{99m}Tc-DTPA	98.84 ± 1.01	98.91 ± 0.24	99.12 ± 0.33	≥95%
Medronato II	^{99m}Tc-MDP	99.01 ± 0.24	98.44 ± 0.16	99.63 ± 0.64	≥95%
Osteocis	^{99m}Tc-HMDP	99.22 ± 0.14	98.01 ± 0.52	99.13 ± 0.11	≥95%
Nanocoll (PRC = 40 min)	^{99m}Tc-nanocolloids	99.34 ± 0.09	99.38 ± 0.16	98.94 ± 0.41	≥95%
Renocis	^{99m}Tc-DMSA	99.55 ± 0.08	99.22 ± 0.77	99.11 ± 0.03	≥95%

$RCP_{36,48,72}$ indicate the radiochemical purity carried out with eluates obtained 36, 48 and 72 hours after the previous elution.

phosphor imaging screen and an OptiQuant image analysis software (Packard, Meridien, CT).

2.3. Imaging Studies. Three ^{99m}Tc eluates produced by ^{99}Mo/^{99m}Tc generator with different ^{99g}Tc/^{99m}Tc ratio R were used for imaging studies; the R values were 4.16, 9.51, and 15.2, respectively. Each tomographic acquisition has been performed by filling a NEMA phantom NU 4-2008 with 74 MBq of ^{99m}Tc-pertechnetate solution, and the data have been acquired with the YAP-(S)PET small animal scanner prototype [22] and reconstructed by using an EM-ML algorithm.

3. Results and Discussion

The results of the quality control (Table 2) performed on all eluates obtained from two different generator (DRYTEC GE Healthcare and Elumatic III IBA) are consistent with the European Pharmacopoeia requirements [12]. For simplicity, data of visual inspection, yield of elution, and the aluminum content in eluates are not reported, because they fell within European Pharmacopoeia requirements.

The radiochemical purity (RCP) values of all radiopharmaceuticals labeled with each eluate are reported in Tables 3 and 4. Results refer to the RCP evaluated immediately after the preparation ($t = 0$). For simplicity, data at the end of the stability period specified by the manufacturer are not reported, because they fell within the specifications required by the manufacturer. Tables 5 and 6 report the RCP data obtained from reconstitution of the kits with the first eluate. The values refer to the checks carried out immediately after the preparation ($t = 0$) and at the end of the stability period specified by the manufacturer in the package insert of each radiopharmaceutical. The values of radiochemical purity are always superior to the standards required by the manufacturer. The results show that the total amount of technetium (^{99g}Tc + ^{99m}Tc) present in the first eluate and in the eluates obtained at longer intervals, from 24 h up to 72 h, did not affect the radiochemical purity of the final products. Table 7 shows an estimation of the total amount of technetium present in an eluate obtained from a ^{99m}Tc generator with ^{99}Mo calibrated activity of 10 GBq. The ratios R of three ^{99m}Tc eluates at 24 hours and two ^{99m}Tc first eluates at 48 hours have been measured, and the results have been $R_{24\,h} = 3.23 ± 0.15$ and $R_{48\,h} = 6.68 ± 0.31$, respectively. While

TABLE 4: RCP of radiopharmaceuticals at $t = 0$, prepared with generator Elumatic III (IBA) eluates at time superior to 24 h from the last elution.

Commercial name	Radiopharmaceutical	RCP_{36}	RCP_{48}	RCP_{72}	RCP requirements
Neurolite	^{99m}Tc-ECD	98.77 ± 0.89	99.21 ± 0.71	98.68 ± 0.95	≥90%
Cardiolite	^{99m}Tc-Sestamibi	97.88 ± 0.78	98.83 ± 0.92	99.13 ± 0.63	≥94%
Stamicis	^{99m}Tc-Sestamibi	98.78 ± 0.23	98.90 ± 0.20	98.00 ± 0.19	≥94%
Technemibi	^{99m}Tc-Sestamibi	98.45 ± 0.09	98.17 ± 0.23	98.11 ± 0.06	≥94%
TechneScan	^{99m}Tc-MAG3	99.79 ± 0.64	98.10 ± 0.44	99.44 ± 0.14	≥95%
Pentacis	^{99m}Tc-DTPA	99.14 ± 0.12	98.88 ± 0.15	98.12 ± 1.03	≥95%
Medronato II	^{99m}Tc-MDP	99.11 ± 0.33	99.44 ± 0.15	99.11 ± 0.43	≥95%
Osteocis	^{99m}Tc-HMDP	99.01 ± 0.24	98.44 ± 0.16	99.63 ± 0.64	≥95%
Nanocoll (PRC = 40 min)	^{99m}Tc-nanocolloids	98.99 ± 0.03	99.18 ± 0.49	98.11 ± 0.11	≥95%
Renocis	^{99m}Tc-DMSA	99.35 ± 0.22	98.67 ± 0.17	99.03 ± 0.29	≥95%

$RCP_{36,48,72}$ indicate the radiochemical purity carried out with eluates obtained 36, 48 and 72 hours after the previous elution.

TABLE 5: RCP of radiopharmaceuticals at $t = 0$ and at the expired time specified by the manufacturer, prepared with the first eluate obtained from DRYTEC GE Healthcare generator.

Commercial name	Radiopharmaceutical	RCP ($t = 0$)	RCPex	RCP requirements
Neurolite	^{99m}Tc-ECD	99.17 ± 0.25	99.13 ± 0.21	≥90%
Cardiolite	^{99m}Tc-Sestamibi	97.67 ± 1.24	97.71 ± 1.13	≥94%
Stamicis	^{99m}Tc-Sestamibi	98.65 ± 0.40	98.57 ± 0.57	≥94%
Technemibi	^{99m}Tc-Sestamibi	98.15 ± 0.11	98.01 ± 0.04	≥94%
TechneScan	^{99m}Tc-MAG3	98.79 ± 0.02	98.11 ± 0.15	≥95%
Pentacis	^{99m}Tc-DTPA	99.03 ± 0.24	99.88 ± 0.11	≥95%
Medronato II	^{99m}Tc-MDP	98.10 ± 0.13	98.02 ± 0.15	≥95%
Osteocis	^{99m}Tc-HMDP	99.23 ± 0.18	98.15 ± 0.16	≥95%
Nanocoll (PRC = 40 min)	^{99m}Tc-nanocolloids	98.22 ± 0.13	98.33 ± 0.39	≥95%
Renocis	^{99m}Tc-DMSA	99.28 ± 0.07	98.55 ± 0.21	≥95%

RCPex indicates the radiochemical purity at the end of the expired time.

TABLE 6: RCP of radiopharmaceuticals at $t = 0$ and at the expired time specified by the manufacturer, prepared with the first eluate obtained from Elumatic III (IBA) generator.

Commercial name	Radiopharmaceuticals	RCP ($t = 0$) ($n = 3$)	RCPex ($n = 3$)	RCP requirements
Neurolite	^{99m}Tc-ECD	98.38 ± 0.54	98.74 ± 0.25	≥90%
Cardiolite	^{99m}Tc-Sestamibi	97.68 ± 0.56	97.77 ± 0.88	≥94%
Stamicis	^{99m}Tc-Sestamibi	98.42 ± 1.02	99.03 ± 0.48	≥94%
Technemibi	^{99m}Tc-Sestamibi	97.99 ± 0.11	98.15 ± 0.14	≥94%
TechneScan	^{99m}Tc-MAG3	98.11 ± 0.62	98.43 ± 0.29	≥95%
Pentacis	^{99m}Tc-DTPA	99.16 ± 0.32	99.19 ± 0.11	≥95%
Medronato II	^{99m}Tc-MDP	99.13 ± 0.04	98.77 ± 0.08	≥95%
Osteocis	^{99m}Tc-HMDP	99.17 ± 0.12	98.76 ± 0.29	≥95%
Nanocoll (PRC = 40 min)	^{99m}Tc-nanocolloids	98.79 ± 0.16	98.92 ± 0.59	≥95%
Renocis	^{99m}Tc-DMSA	99.11 ± 0.35	99.01 ± 0.32	≥95%

RCPex indicates the radiochemical purity at the end of the expired time.

TABLE 7: Evaluation of total technetium amount in ^{99m}Tc eluates coming from a generator with ^{99}Mo calibrated activity of 10 GBq, at different times by previous elution.

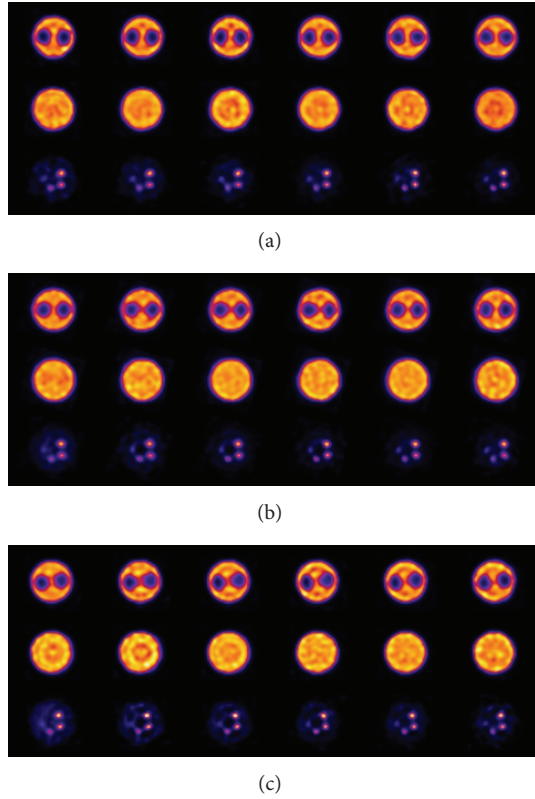| Time by the previous elution	Amount of total Tc calculated	^{99g}Tc/^{99m}Tc ratio calculated	Amount of total Tc found	^{99g}Tc/^{99m}Tc ratio found
72 h	0.30 μg	11.84		
48 h	0.22 μg	6.50	0.22 ± 0.01	6.68 ± 0.31
36 h	0.18 μg	4.34		
24 h	0.13 μg	2.54	0.12 ± 0.01	3.23 ± 0.15

(a)

(b)

(c)

FIGURE 2: Reconstructed SPECT trans-axial slices of NEMA NU 4-2008 filled with ^{99m}Tc-pertechnate solution. Top images (a) have $R = 4.16$, middle images (b) have $R = 9.51$, and bottom images (c) have $R = 15.2$.

the experimental value of first eluates at 48 hours is in good agreement with thetheoretical value of 6.5, the experimental value of eluates at 24 hours shows a large difference with respect to the theoretical value of 2.55. This discrepancy could be explained by taking into account the elution efficiency $\varepsilon = 0.91$ of ^{99}Mo generators used in our work. Indeed, the recalculated ratio R at 24 hours is included in the range (2.78–3.38) and depends on temporal sequence of previous elutions. The reconstructed SPECT images of NEMA phantom, for the different ^{99g}Tc/^{99m}Tc ratios R used, are shown in Figure 2. The average reconstructed activity along the phantom axis, for the three values of R, is shown in Figure 3. The visual inspection on the images doesn't show significant difference in image quality and radioactivity distribution. Currently, CERETEC is the only commercial product for which the use of a fresh eluate, obtained from a generator eluted for not more than 24 hours, is required. This exception is linked to the low amount of tin chloride dehydrate in its formulation (7.6 μg), which makes its radiochemical purity strongly influenced by the amount of ^{99g}Tc present in the eluate. All formulations studied possess significantly higher amount of tin. A further limitation to the use of eluates characterized by greater amount of ^{99g}Tc (elution intervals > 24 h) could be due to radioprotection reasons related to the physical characteristics of ^{99g}Tc ($t_{1/2} = 2 \times 10^5$ y, $\beta_{max} = 292$ keV). However

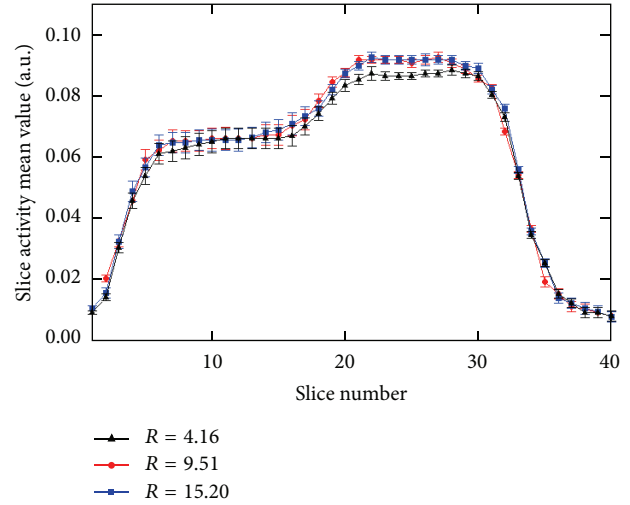

FIGURE 3: The average activity for reconstructed 40 slices of NEMA NU 4-2008 phantom filled with ^{99m}Tc-pertechnate solution having $R = 4.16$, $R = 9.51$, and $R = 15.2$.

the amount of radioactivity associated with the mass value is very low (e.g., 1 μg of ^{99g}Tc corresponds to 630 Bq).

4. Conclusion

In order to first check the possible impact of different ^{99g}Tc/^{99m}Tc isomeric ratios on the preparation of different Tc-labeled pharmaceutical kits, the radiochemical purity and stability of ^{99m}Tc-Sestamibi, ^{99m}Tc-ECD, ^{99m}Tc-MAG3, ^{99m}Tc-DTPA, ^{99m}Tc-MDP, ^{99m}Tc-HMDP, ^{99m}Tc-nanocolloids, and ^{99m}Tc-DMSA were studied by using ^{99m}Tc eluates coming from ^{99}Mo/^{99m}Tc generator eluted at different times from the previous elution. The results prove that radiochemical purity and stability of these radiopharmaceuticals are not affected up to ^{99g}Tc/^{99m}Tc ratio of 11.84.

A future goal will be to repeat the experiments with ^{99m}Tc eluates coming from generators with ^{99}Mo calibrated activity higher than 10 GBq, in order to check the possible impact of ^{99g}Tc in higher ^{99m}Tc activities solutions at different ^{99g}Tc/^{99m}Tc ratio.

Another future goal will be to study the impact of accelerated-based ^{99g}Tc and other Tc-isotopes on the image quality and determine the allowed limit for ^{99g}Tc and other Tc-isotopes in the final accelerator-produced Tc.

Conflict of Interests

The authors declare that they have no conflict of interests.

Acknowledgments

References

[1] S. Banerjee, M. R. Ambikalmajan Pillai, and N. Ramamoorthy, "Evolution of Tc-99m in diagnostic radiopharmaceuticals," *Seminars in Nuclear Medicine*, vol. 31, no. 4, pp. 260–277, 2001.

[2] O. P. D. Noronha, A. B. Sewatkar, and R. D. Ganatra, "Fission produced ^{99}Mo-^{99m}Tc generator system for medical use," *Journal of Nuclear Biology and Medicine*, vol. 20, no. 1, pp. 32–36, 1976.

[3] N. Vinberg and K. Kristensen, "Fission Mo-99/Tc-99m generators—a study of their performance and quality," *European Journal of Nuclear Medicine*, vol. 5, no. 5, pp. 435–438, 1980.

[4] J. Vucina, "Technetium-99m production for use in nuclear medicine," *Medicinski Pregled*, vol. 53, no. 11-12, pp. 631–634, 2000.

[5] N. Knight, "Return of the radionuclide shortage," *Journal of Nuclear Medicine*, vol. 50, no. 7, pp. 13N–14N, 2009.

[6] J. Esposito, "Feasibility study report on alternative ^{99}Mo/^{99m}Tc production routes using particle accelerators at LNL, (2001 version)," INFN-LNL-235, 2011.

[7] Report on the 1st Research Coordination Meeting of IAEA CRP Activities (code F22062), "Accelerator-based Alternatives to Non-HEU Production of ^{99}Mo/^{99m}Tc," Vancouver, Canada, April 2012.

[8] J. L. Vucina, "Radionuclide purity of ^{99m}Tc eluate for use in nuclear medicine," *Medicinski Pregled*, vol. 49, no. 1-2, pp. 41–44, 1996.

[9] D. M. Hill, R. K. Barnes, H. K. Y. Wong, and A. W. Zawadzki, "The quantification of technetium in generator-derived pertechnetate using ICP-MS," *Applied Radiation and Isotopes*, vol. 53, no. 3, pp. 415–419, 2000.

[10] J. Bonnyman, "Effect of milking efficiency on ^{99}Tc content of ^{99m}Tc derived from ^{99m}Tc generators," *International Journal of Applied Radiation and Isotopes*, vol. 34, no. 6, pp. 901–906, 1983.

[11] M. Marengo, C. Aprile, C. Bagnara et al., "Quality control of ^{99}Mo/^{99m}Tc generators: results of a survey of the radiopharmacy working group of the Italian Association of Nuclear Medicine (AIMN)," *Nuclear Medicine Communications*, vol. 20, no. 11, pp. 1077–1084, 1999.

[12] M. M. Webber, M. D. Cragin, and W. K. Victery, "Aluminum content in eluents from commercial technetium generators," *Journal of Nuclear Medicine*, vol. 12, no. 10, p. 700, 1971.

[13] A. M. Zimmer and D. G. Pavel, "Rapid miniaturized chromatographic quality-control procedures for Tc-99m radiopharmaceuticals," *Journal of Nuclear Medicine*, vol. 18, no. 12, pp. 1230–1233, 1977.

[14] European Pharmacopoeia, 7th edition, Sodium pertechnetate (^{99m}Tc) injection (fission) (0124).

[15] A. Hammermaier, E. Reich, and W. Bogl, "Chemical, radiochemical, and radionuclide purity of eluates from different commercial fission ^{99}Mo/^{99m}Tc generators," *European Journal of Nuclear Medicine*, vol. 12, no. 1, pp. 41–46, 1986.

[16] P. Nasman and T. Vayrynen, "Impurities of ^{99m}Tc-generators," *European Journal of Nuclear Medicine*, vol. 8, no. 1, pp. 26–29, 1983.

[17] T. Vayrynen, P. Nasman, and K. Kiviniitty, "Residual activity of Tc-generators," *European Journal of Nuclear Medicine*, vol. 6, no. 6, pp. 269–271, 1981.

[18] S. Hoory, D. Bandyopadhyay, J.-C. Vaugeois, and L. M. Levy, "Impurities in generator eluates and radiopharmaceuticals: a computerized quality assurance approach," *Health Physics*, vol. 50, no. 6, pp. 843–848, 1986.

[19] "Radiopharmacy and quality control pharmacists subcommittees of the regional pharmaceutical officers commitee. Quality assurance of radiopharmaceuticals," *Nuclear Medicine Communication*, vol. 15, pp. 886–889, 1994.

[20] E. M. Podolak Jr., "^{134}Cs, ^{86}Rb, and ^{60}Co in ^{99}Mo-^{99m}Tc generator eluate," *Journal of Nuclear Medicine*, vol. 13, no. 6, pp. 388–390, 1972.

[21] I. Zolle, *Technetium-99m Pharmaceuticals: Preparation and Quality Control in Nuclear Medicine*, Springer, Berlin, Germany, 2007.

[22] A. Del Guerra, A. Bartoli, N. Belcari et al., "Performance evaluation of the fully engineered YAP-(S)PET scanner for small animal imaging," *IEEE Transactions on Nuclear Science*, vol. 53, no. 3, pp. 1078–1083, 2006.

Research Article

A Solution-Based Approach for Mo-99 Production: Considerations for Nitrate versus Sulfate Media

Amanda J. Youker, Sergey D. Chemerisov, Michael Kalensky, Peter Tkac, Delbert L. Bowers, and George F. Vandegrift

Chemical Sciences and Engineering Division, Argonne National Laboratory, 9700 S. Cass Avenue, Argonne, IL 60439, USA

Correspondence should be addressed to Amanda J. Youker; youker@anl.gov

Molybdenum-99 is the parent of Technetium-99m, which is used in nearly 80% of all nuclear medicine procedures. The medical community has been plagued by Mo-99 shortages due to aging reactors, such as the NRU (National Research Universal) reactor in Canada. There are currently no US producers of Mo-99, and NRU is scheduled for shutdown in 2016, which means that another Mo-99 shortage is imminent unless a potential domestic Mo-99 producer fills the void. Argonne National Laboratory is assisting two potential domestic suppliers of Mo-99 by examining the effects of a uranyl nitrate versus a uranyl sulfate target solution configuration on Mo-99 production. Uranyl nitrate solutions are easier to prepare and do not generate detectable amounts of peroxide upon irradiation, but a high radiation field can lead to a large increase in pH, which can lead to the precipitation of fission products and uranyl hydroxides. Uranyl sulfate solutions are more difficult to prepare, and enough peroxide is generated during irradiation to cause precipitation of uranyl peroxide, but this can be prevented by adding a catalyst to the solution. A titania sorbent can be used to recover Mo-99 from a highly concentrated uranyl nitrate or uranyl sulfate solution; however, different approaches must be taken to prevent precipitation during Mo-99 production.

1. Introduction

Argonne is assisting two potential domestic suppliers of Molybdenum-99, and both plan to use a fissioning LEU solution as either uranyl nitrate or uranyl sulfate to produce Mo-99. Babcock and Wilcox Technical Services Group (BWTSG) is developing an aqueous homogeneous reactor (AHR) for Mo-99 production, which will utilize an LEU fuel (19.75% U-235) as uranyl nitrate. Their system is referred to as MIPS (Medical Isotope Production System) [1]. SHINE Medical Technologies is developing Subcritical Hybrid Intense Neutron Emitter (SHINE), which is an accelerator-driven process that will use an LEU uranyl sulfate target solution for Mo-99 production [2, 3]. For these systems, Argonne has developed a Mo-recovery process for either the irradiated uranyl sulfate or uranyl nitrate solution using a titania sorbent [4–16].

Solution preparation is much easier for MIPS compared to SHINE [13, 15]. The differences in procedures will be discussed in more detail below.

Uranyl nitrate and uranyl sulfate solutions have been irradiated at the Argonne 3 MeV Van de Graaff accelerator to study the effects of a high radiation field on solution chemistry, specifically related to pH changes, peroxide formation, and molybdenum and iodine redox chemistry. The effect of a high radiation field caused significant pH changes in a uranyl nitrate solution, which resulted from the radiolysis of nitrate to form a variety of reduced nitrogen species from nitrite to NO_x gases and to ammonia [17]. Uranium and fission product precipitation becomes a concern when the pH rises above 3 [1]. As a result, nitric acid will need to be added periodically to the uranyl nitrate MIPS fuel solution during operation to prevent large pH increases that may lead to the precipitation of some fission products and eventually uranium. The pH of a uranyl sulfate solution decreased postirradiation due to water loss from radiolysis [18]. Uranyl peroxide precipitated during irradiation of uranyl sulfate solutions that did not contain catalysts. Ferrous and ferric sulfate, cupric sulfate, potassium iodide, 304 stainless steel turnings, and Zr metal have been

tested as potential catalysts for peroxide destruction during irradiation of uranyl sulfate solutions [19].

Although molybdenum can be recovered from both uranyl nitrate and uranyl sulfate solutions, the task is easier from nitrate media. This is most easily seen by comparing Mo(VI) partitioning between the solutions and the titania sorbent [4, 8, 13–15, 20]. However, plant-scale separation columns have been designed for both MIPS and SHINE systems [8, 9, 12–15]. A general comparison of the two recovery operations will be discussed below. New data to be discussed in this paper are column experiments performed using uranyl sulfate solutions spiked with tracer Mo-99 and stable Mo added as sodium molybdate under a constant radiation dose at the Van de Graaff [21]. Additionally, results from Van de Graaff iodine speciation experiments in nitrate and sulfate media will also be presented [21]. However, the Van de Graaff iodine results do not agree with iodine results obtained using dissolved, irradiated foils added as a spike to a uranyl sulfate solution.

2. Materials and Methods

2.1. Materials. Depleted-uranium metal plates were used to prepare uranyl nitrate and uranyl sulfate solutions. The plates were approximately $2'' \times 2''$ with a width of $1/8''$ and a mass of ~150 g. Concentrated nitric acid and sulfuric acid were obtained from Sigma-Aldrich, and dilutions were made to prepare solutions with different acid concentrations required for the various steps in the uranyl-salt solution-preparation processes. Pure titania sorbents (Sachtopore Normal Phase— 110 and 40 micron particle size) were obtained from Zirchrom Separations, Inc. Sodium molybdate was obtained from Sigma-Aldrich, and Mo-99 was milked from a Lantheus spent Tc-99m generator. 30% hydrogen peroxide was used as received from Sigma-Aldrich. A 3 MeV Van de Graaff (VDG) accelerator was used to generate a radiation field.

2.2. Methods. Uranyl nitrate solutions were prepared by dissolving uranium-metal plates in 8 M nitric acid using a reaction kettle, equipped with a heating mantle, kettle cover, and reflux condenser. The uranyl nitrate solution was brought to dryness several times to drive off excess nitric acid and redissolved in a mixture of nitric acid and water until a final pH of 1.0 was reached at the desired uranium concentration.

Two different avenues have been investigated for the preparation of uranyl sulfate. In the first method of preparation, uranium metal is converted to uranyl nitrate, and heat and sulfuric acid are added to drive off nitrate and form uranyl sulfate. Sulfuric acid (1–18 M) is added directly to the uranyl nitrate solid to prepare uranyl sulfate. A rotary evaporator with a water-cooled condenser kept under constant vacuum is used to facilitate conversion from nitrate to sulfate. An oil bath is used to heat the solution to drive off nitric acid and thus to convert the salt to uranyl sulfate. The second method of preparation involves oxidizing U metal to U_3O_8, forming uranyl peroxide, and redissolving it in dilute sulfuric acid. Uranium metal is oxidized in a furnace at a temperature near

720°C for full conversion and usually takes about 24 h for a single metal plate (~150 g). Approximately 5 mL of 30% H_2O_2 per gram of U_3O_8 and a stoichiometric amount of H_2SO_4 are added to the U_3O_8 with heat. Complete conversion to uranyl peroxide occurs in about 40 minutes for a 50 g-U batch, and the solid product is redissolved in dilute sulfuric acid with heat. Complete dissolution of a 50 g-U batch takes about 1 hour.

Uranium solutions and titania columns were irradiated for 1 hour using the Van de Graaff as a radiation source. Each uranium solution was passed through a titania column over a period of 2 hours, while under a constant radiation dose, uranium solution and titania column were both in the radiation field. Column sizes and experimental parameters are direct downscale designs of the plant-scale designs generated by Versatile Reaction Separation (VERSE) for the SHINE process. The purpose of these experiments was to determine whether a radiation dose of approximately 70 kRad/h caused a change in Mo redox chemistry. After the target solution was loaded onto the column, it was washed with acid and water, and Mo-99 was recovered using 0.1 M NaOH heated to 70°C. Column wash and strip steps were not performed in a radiation field.

Column experiments were performed under a constant radiation dose using a Fluid Metering Inc. (FMI) pump and a stainless steel column at the Van de Graaff. Subsequent wash and Mo elution steps were carried out using an ÄKTA liquid chromatography system. Column and solution temperatures were kept at 80°C except for the Mo strip solution, which was kept at 70°C. Feed solution was loaded in the upflow direction to concentrate Mo at the base of the column and in the case of irradiated solutions, to prevent entrapment of fission gases that may potentially generate channels in the column. The column was washed with acid (0.1–1 M) and then water. Mo was eluted using 0.1 M NaOH heated to 70°C, and a final water wash was performed.

The experimental setup for measuring radiolytic-gas generation and peroxide formation with/without the presence of catalysts was designed with two interconnected systems— the process loop and the sampling manifold. The process loop is a closed loop of stainless steel tubing that consists of a quartz target vessel for the sample, the electron beam, and a peristaltic pump. The target sample is inserted into a holder directly in the accelerator electron-beam path. The holder is attached to a recirculating pump and water bath to provide continuous cooling of the sample. The electron beam impinges on the cooling water and quartz tube in the setup. The 3.0 MeV Van de Graaff accelerator electron beam emits electrons and some X-rays, which interact with the sample. The sample tube has an inlet and outlet valve to recirculate headspace gases throughout the process loop. The sampling manifold is connected to the process loop by a bellows valve. The sampling manifold consists of a capacitance monometer, vacuum pump, and two analytical instruments connected by stainless steel tubing and a series of valves used to either evacuate, measure pressure, or analyze the gaseous constituents in the manifold. The gases are analyzed using a SRI-8610C gas chromatograph with a Thermal Conductivity Detector (TCD) and a Helium Ionization Detector (HID).

Separation is achieved with a 13X molecular sieve column and a Haysep-d column.

A 2 mL test solution is placed in a quartz sample tube. The sample tube is connected to the process loop in the beam path. The system is then evacuated and purged with helium several times to remove atmospheric gases. The process loop is pressurized to 800 torr with Ultra High Purity (UHP) helium.

The 3.0 MeV electron beam is set to 20 μA, and the sample is irradiated for approximately five hours. At 30-minute intervals, a sample of the headspace gas is withdrawn into the evacuated "Sampling Manifold" for analysis. The gas removed is replaced with helium to keep a constant pressure in the system. Prior to these experiments, oxalic-acid dosimetry was performed to determine the approximate dose deposited into the sample [22].

Uranyl sulfate and uranyl nitrate solutions were tested at various concentrations. The pH of the solutions was measured at the end of irradiation. Several known catalysts for the autodestruction of hydrogen peroxide were also tested to determine if each one was a suitable option for peroxide destruction in sulfate solutions.

3. Results and Discussion

3.1. Solution Preparation. Preparation of uranyl nitrate is straightforward because uranium metal can be dissolved directly in nitric acid. Adjustment of pH is relatively easy to do for a uranyl nitrate solution because excess nitrate can be removed by evaporation of nitric acid or by calcining uranyl nitrate to produce oxide. On the other hand, uranium metal cannot be dissolved directly in sulfuric acid without the addition of an oxidizing agent [13, 15, 16, 23, 24]. As a result, additional steps are required for the preparation of uranyl sulfate. Two methods are currently being examined for the preparation of uranyl sulfate: (1) calcine U metal to UO_3/U_3O_8 and dissolve it in a mixture of H_2O_2 and H_2SO_4 with heat, (2) dissolve U metal in HNO_3, use a calcination process to convert uranyl nitrate to UO_3, and dissolve UO_3 in H_2SO_4 [13, 23–27]. Uranyl nitrate is more attractive than uranyl sulfate in terms of solution preparation; however, uranyl sulfate is the better choice in terms of neutron economy and pH stability [1–3, 28–31]. Changes in pH observed upon irradiation at the Van de Graaff for uranyl sulfate, and uranyl nitrate solutions are discussed in more detail in the gas analysis results section.

Because conversion of a uranyl nitrate solution to a uranyl sulfate solution using a rotary evaporator showed that approximately 1–5% nitrate remains in the final uranyl sulfate solution, we recommend thermal oxidation of uranium metal followed by dissolution directly of the uranium oxide in a mixture of hydrogen peroxide and sulfuric acid with heat.

3.2. Mo Recovery: Nitrate versus Sulfate Media. Batch-study results show that Mo adsorbs better on a titania sorbent in a nitrate media than in sulfate media [13, 20]. Sulfate competes more strongly with molybdenum for adsorption sites than nitrate. For example, batch studies were performed in sodium nitrate and sulfate solutions, with anion concentrations representing what would be present in a 150 g-U/L solution of

TABLE 1: Distribution ratios for Mo in the presence of sodium sulfate and sodium nitrate solutions.

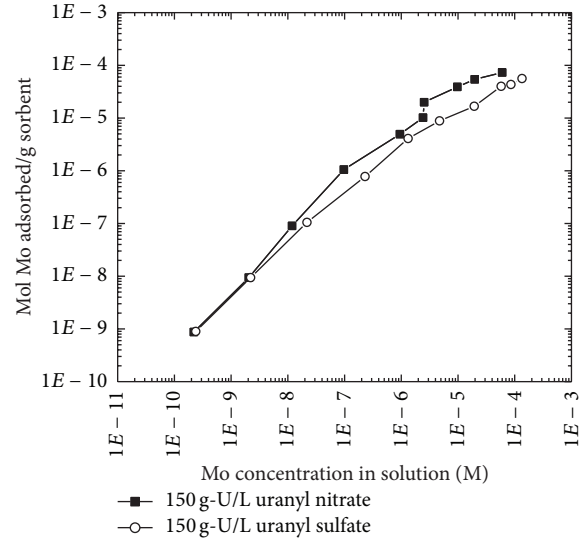| Initial Mo (M)	K_d, Mo (mL/g) 0.63 M Na_2SO_4	K_d, Mo (mL/g) 1.26 M $NaNO_3$
$1E-06$	4900	11000
$1E-05$	3400	7600
$5E-05$	3100	5200

FIGURE 1: Amount of Mo adsorbed per gram of sorbent versus the amount in solution in the presence of solutions containing 150 g-U/L uranyl nitrate and 150 g-U/L uranyl sulfate.

each one. With Mo concentrations in the range expected for MIPS and SHINE (10^{-5}–10^{-6} M), the K_d, which is defined as the ratio of Mo adsorbed on the sorbent (mol/g) to the concentration of Mo in solution (mol/L), values for Mo in the presence of sodium nitrate are 1.7–2.2 times larger than in the presence of sodium sulfate (Table 1). Similar batch studies were performed in the presence of 150 g-U/L uranyl nitrate and uranyl sulfate solutions. Figure 1 shows a direct comparison between the amount of Mo adsorbed per gram of sorbent versus the amount in solution in the presence of uranyl nitrate and uranyl sulfate solutions, and results indicate that more Mo is adsorbed in the presence of a uranyl nitrate solution, especially as the Mo concentration increases.

3.3. Plant-Scale Column Designs. Batch data and small-scale column data for Mo adsorption in the presence of uranyl sulfate and uranyl nitrate solutions using a pure titania sorbent have been collected at Argonne and input into the VERSE simulator, which was developed by Dr. Wang at Purdue University [32]. VERSE takes data obtained in a batch mode and small-scale column setting to design a column for a large-scale separation process. Plant-scale columns have been designed for the MIPS (uranyl nitrate) and SHINE (uranyl sulfate) systems. Based on the batch data shown above, the Mo-recovery column is going to be larger for the SHINE system due to competition from sulfate. Table 2 shows

TABLE 2: Plant-scale column designs for MIPS and SHINE using 110-μm Sachtopore sorbent.

Solution	Inner diameter (cm)	Length (cm)	Column volume (L)
Uranyl nitrate	12	9.7	1.1
Uranyl sulfate	12	13	1.5

the plant-scale column designs for both processes, which assume a uranium concentration between 100 and 150 g-U/L, a feed solution volume of 200–250 L, a Mo concentration near 10^{-5} M, and a 2-hour loading time. The plant-scale column design for SHINE is about 25% larger than for MIPS, which means slightly larger waste volumes.

3.4. Column Experiments and Mo Redox Chemistry. Mo oxidation state is a critical aspect of the separation and recovery process. Separation and recovery of Mo from a uranyl nitrate or uranyl sulfate solution assume that Mo is present as Mo(VI). However, the radiation environment surrounding these solutions is highly reducing and may alter Mo's oxidation state [1, 20, 27]. The likelihood for a change in Mo redox chemistry is much greater in a uranyl sulfate solution because nitrate is an oxidant, and if Mo were reduced, nitrate has the capacity to reoxidize it to Mo(VI). If Mo(VI) was reduced to Mo(V), it can be present as a cationic species, $Mo_2O_4^{2+}$, which will not adsorb on the Mo-recovery column [1, 9, 20, 27, 33, 34]. Because both MIPS and SHINE will be recycling their fuel/target solutions, adding an oxidant is not trivial. The redox potential for Mo(VI)/Mo(V) at pH = 0 is 0.50 V [33], but to what extent, in which system(s), and under what conditions will Mo reduction take place remains uncertain. Column experiments were initiated using the Van de Graaff as a source of constant radiation for uranyl sulfate solutions. Future experiments will use a linac as a constant source of radiation, and fission products will be generated.

Uranyl sulfate solutions were irradiated at the Van de Graaff under a constant radiation dose and passed through a titania column. Previous batch-study results where uranyl nitrate and uranyl sulfate solutions were irradiated at the Van de Graaff showed inconclusive results using sulfate solutions, but there was no observed reduction in Mo adsorption or recovery from nitrate solutions [20]. This is most likely due to the oxidizing behavior of nitrate. As a result, column experiments performed under a constant radiation dose were only performed using uranyl sulfate solutions. The focus of the constant-irradiation-column experiments shifted toward a sulfate media because it is a nonoxidizing environment in the absence of a radiation field. Mo oxidation state is more likely to change in a sulfate system than in a nitrate system. However, at solution dose rates of roughly 700 Gy/h, no changes in Mo redox chemistry were observed. Mo recoveries still ranged from 90 to 100%, and less than 1% Mo was found in the effluent stream, which suggests that Mo(VI) did not reduce to Mo(IV) or Mo(V) when exposed to dose rates in the 700 Gy/h range [21]. Table 3 shows the results from the column experiments performed under constant dose at the Van de Graaff. Errors associated with the gamma counting results for Mo-99 are ±7%, which explains why the total amount of Mo in all solutions does not sum 100%. In experiments where 1 M H_2SO_4 was used to wash the column, 11–15% Mo prematurely eluted during the acid and water washes because at lower pH values, Mo speciation changes from primarily a monoprotonated species, $HMoO_4^-$ [35], at pH 1 to a cationic species that does not adsorb as well on a titania sorbent.

Additional isotopes of concern for both processes were added to the target solutions prior to irradiation to gain a better understanding of their redox chemistry and speciation, which may help deduce where certain isotopes will end up postirradiation and post-Mo-99 recovery. Isotopes that were added to the target solution preirradiation included I-131 and Pu-239. Previous experiments with irradiated solutions showed that iodine contaminates the Mo-99 product prior to entry into the purification process. Iodine contamination in the Mo-99 product partially comes from decay of several Te isotopes, Te adsorbs, and Mo on a titania sorbent [9]. The distribution of isotopes during the separation and recovery processes is important for waste classification purposes. A clearer understanding of which fission products will be recycled to the target solution and which fission products will enter the purification process is needed. Modifications were made to the LEU Modified Cintichem purification process to account for the large amount of iodine, which has been found to coelute with the Mo-99 product [5, 13, 36]. An additional evaporation step using nitric acid was added to promote volatilization and capture of the iodine.

The current steps in the Cintichem process are capable of removing iodine and iodide but not iodate. Iodine speciation experiments at the Van de Graaff performed with uranyl nitrate and uranyl sulfate solutions suggested that all iodine species independent of starting species (iodine, iodide, and iodate were all tested, and isotopic equilibration was initiated with an I-131 spike) were reduced to iodide when exposed to low LET (linear energy transfer) particles [21]. These results are somewhat misleading because it is well known that iodine volatilizes in acidic solution and will most likely appear in multiple places during Mo-99 production, separation, recovery, and purification processes.

Column experiments were performed using a Pu-239 spike (added as Pu(IV)) to understand its behavior in the Mo-recovery process. More than half of the Pu-239 remained adsorbed on the column during the Mo-separation and recovery processes from an irradiated uranyl sulfate solution. Previous batch studies using a uranyl nitrate solution showed that Pu does adsorb on a titania sorbent [15]. Several options are viable for Pu removal from titania, but what, if any options are pursued to remove the Pu, will be dependent on the producer's needs. Results from column experiments performed using uranyl sulfate solutions and batch-contact studies performed using uranyl nitrate solutions suggest that a significant amount of Pu will remain adsorbed on the titania sorbent during the Mo separation and recovery process.

3.5. Gas Analysis Results and pH Changes from Van de Graaff Experiments. Initially, sodium nitrate and sodium sulfate solutions were irradiated using the Van de Graaff as

TABLE 3: Results for Van de Graaff column experiments.

Solution dose rate (Gy/h)	Column dose rate (Gy/h)	% Mo in effluent	% Mo in washes	% Mo in strip	Acid wash (M)
640	160	0.9	0.3	100	0.5
740	180	0.7	15	92	1
680	160	0.6	11	100	1
690	170	0.2	2	95	0.5

a radiation source [18]. Gases produced during irradiation were analyzed, and final pH measurements were taken postirradiation. After sodium salt irradiations were completed, a set of uranyl nitrate and uranyl sulfate solutions were irradiated at the Van de Graaff to measure gases produced and changes in pH. Postirradiated uranium solutions were also examined closely for possible precipitates. Production levels for hydrogen and oxygen gases as a function of radiation dose have been plotted. pH changes are much more significant in nitrate media and can lead to precipitation of fission products and uranium in the absence of a continuous feed of nitric acid. In sulfate media, pH changes are not that significant, but peroxide formation leads to the precipitation of uranyl peroxide if a catalyst to destroy peroxide is not added to the solution prior to irradiation [19].

3.6. Uranyl Nitrate Solutions. Irradiation of sodium nitrate and uranyl nitrate solutions at the Van de Graaff caused significant increases in pH postirradiation. As the nitrate concentration increased, the pH increased more significantly. The pH of a uranyl nitrate solution containing ~80 g-U/L did not change considerably postirradiation; however, as the concentration increased to 128 g-U/L, a final pH reading of 1.84 was measured (initial pH of 1.0). From previous experiments with irradiated uranyl nitrate solutions, fission products began to precipitate at a pH near 1.7 [35]. As the nitrate concentration increased even more (0.74 M and 0.95 M), the pH increased to ~2.2, which becomes a concern for uranium precipitation which occurs around a pH of 3.0 [1]. In similar irradiations with sodium nitrate solutions, the pH reached as high as 10.1 after a dose of $2.3E + 08$ Gy was applied to a solution containing 2.52 M NO_3^- [18].

The total production of hydrogen and oxygen was fairly consistent for uranyl nitrate solutions containing 128–226 g-U/L. A H_2/O_2 ratio between 1.2 and 1.4 was observed for the samples containing higher concentrations of uranyl nitrate, which correlates well with the increases in pH. For the solution containing roughly 80 g-U/L, the H_2 to O_2 ratio is much closer to 2 with a value of 1.75, which agrees with the fact that the pH did not change. Sodium nitrate solutions were also irradiated at the Van de Graaff (data not shown), and results were consistent with what was observed for uranyl nitrate solution irradiations. As the nitrate concentration increases for both sodium and uranyl nitrate solutions, the H_2/O_2 ratio decreases. This is most likely due to ammonia formation, which increases as nitrate increases and can reduce the amount of H_2 produced. These data for uranyl nitrate solutions are shown in Table 4 and Figures 2, 3, and 4.

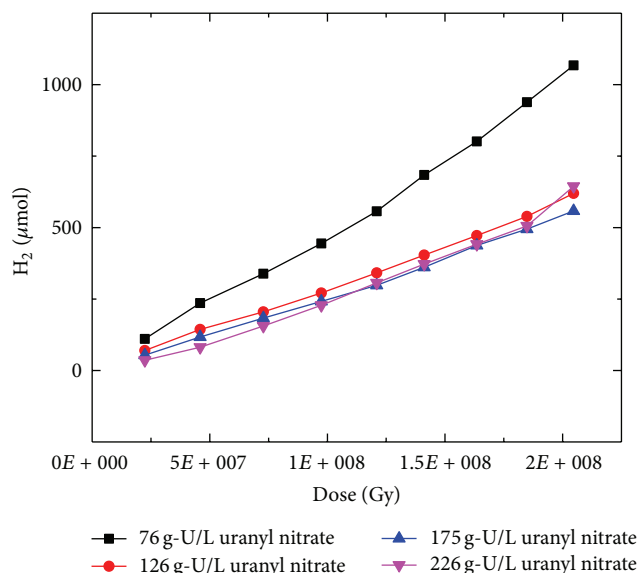Table 5 shows the detection of N_2O and NO during the irradiation of uranyl nitrate solutions at the Van de Graaff. In

FIGURE 2: Hydrogen evolution measured during irradiation of $UO_2(NO_3)_2$ solutions at the Van de Graaff.

Table 5, ND indicates that the analyte was not detected during the experiment. The table shows the number of μmoles detected at each sampling time (t). These data are displayed in this fashion because the concentration of each analyte was below the lowest calibration standard utilized, even though peaks were still detected, and the NO_x compounds are very reactive. NO reacts with oxygen to form NO_2, which is a brown toxic gas. It also can react in the presence of oxygen and water to form nitrous acid, HNO_2. Considering the reactive nature of the NO_x species, it was decided that the best way to report the data are as total μmoles detected at time (t) instead of total accumulated μmoles. N_2O is only detected as a true peak (based on calibration standard) in the samples containing larger amounts of nitrate (175 g-U/L and 226 g-U/L).

3.7. Uranyl Sulfate Solutions. Table 6 shows the experimental data for the irradiation of uranyl sulfate solutions using the Van de Graaff accelerator as a source of radiation. Figures 5 and 6 show the total μmoles of each analyte (either hydrogen or oxygen) versus accumulated dose (Gy) during each five-hour experiment. The H_2/O_2 ratios are presented in Figure 7.
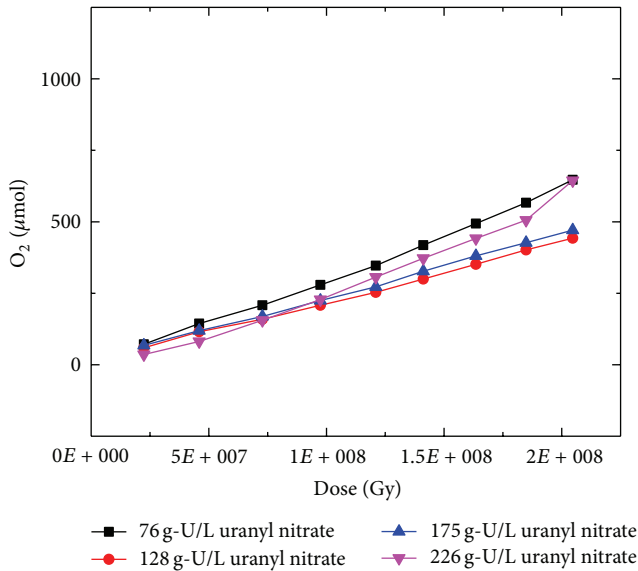
Uranyl peroxide precipitated during irradiation of uranyl sulfate solutions at the Van de Graaff accelerator. Density measurements were performed on the post-irradiated solutions after the precipitate was filtered to determine the

TABLE 4: Experimental data obtained from the irradiation of uranyl nitrate solutions at the Van de Graaff.

Uranium concentration (g-U/L)	Energy deposited (Gy)	Initial pH	Final pH	Total μmoles H$_2$ produced	Total μmoles O$_2$ produced	G value H$_2$ (H$_2$/100 eV)	G value O$_2$ (O$_2$/100 eV)	H$_2$ to O$_2$ ratio
76	$2.32E + 08$	1.0	1.02	1240	710	0.025	0.015	1.75
128	$2.33E + 08$	1.0	1.84	690	490	0.014	0.010	1.41
175	$2.32E + 08$	1.0	2.21	650	520	0.013	0.011	1.24
226	$2.05E + 08$	1.0	2.09	650	550	0.015	0.013	1.17

TABLE 5: N$_2$O and NO in μmoles measured at sampling time for irradiated uranyl nitrate solutions.

Sampling time (min)	76 g-U/L		128 g-U/L		175 g-U/L		226 g-U/L	
	N$_2$O	NO	N$_2$O	NO	N$_2$O	NO	N$_2$O	NO
30	<0.5	<0.5	<0.5	<0.5	<0.5	<0.5	<0.5	<0.5
60	<0.5	<0.5	<0.5	<0.5	<0.5	<0.5	<0.5	<0.5
90	<0.5	<0.5	<0.5	<0.5	<0.5	<0.5	<0.5	<0.5
120	<0.5	<0.5	<0.5	<0.5	<0.5	<0.5	1.52	<0.5
150	<0.5	<0.5	<0.5	<0.5	<0.5	<0.5	3.05	<0.5
180	<0.5	<0.5	<0.5	<0.5	<0.5	<0.5	3.96	<0.5
210	<0.5	<0.5	<0.5	<0.5	1.32	<0.5	4.17	<0.5
240	<0.5	<0.5	<0.5	<0.5	2.84	<0.5	2.64	<0.5
270	<0.5	<0.5	<0.5	<0.5	2.24	<0.5	3.35	<0.5
300	<0.5	<0.5	<0.5	<0.5	2.03	<0.5	N.D.	N.D.

FIGURE 3: Oxygen evolution measured during irradiation of UO$_2$(NO$_3$)$_2$ solutions at the Van de Graaff.

FIGURE 4: Hydrogen to oxygen ratios measured for uranyl nitrate solutions during irradiation tests at the Van de Graaff.

approximate amount of uranium that had precipitated. Uranium concentrations decreased by ~22–36 g-U/L for postirradiated uranyl sulfate solutions. Those data are shown in Table 6. Precipitated uranium can be redissolved by destruction of peroxide at elevated temperatures.

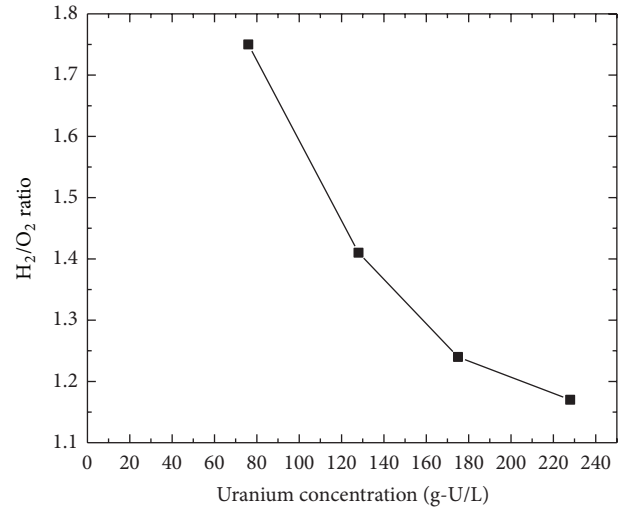The pH values for the postirradiated uranyl sulfate solutions decreased, which is due to the formation of uranyl peroxide and loss of H$_2$O from radiolysis. Sodium sulfate solutions were also irradiated at the Van de Graaff, but no precipitates were observed because sodium peroxide is soluble; however, the pH values of the postirradiated sodium sulfate solutions decreased as well.

The production of hydrogen and oxygen was high for all of the uranyl sulfate irradiation experiments. These data are consistent with results obtained from irradiation of sodium sulfate solutions at the Van de Graaff (data not shown), where H$_2$/O$_2$ ratios increased as the concentration of sulfate increased. The ratio of H$_2$: O$_2$ was at or slightly above 2 : 1,

TABLE 6: Experimental data obtained from the irradiation of uranyl sulfate solutions at the Van de Graaff.

Initial uranium conc. (g-U/L)	Energy deposited (Gy)	Final uranium conc. (g-U/L)	Initial pH	Final pH	Total μmoles H_2 produced	Total μmoles O_2 produced	G value H_2 (H_2/100 eV)	G value O_2 (O_2/100 eV)	H_2 to O_2 ratio
88	$1.71E+08$	63.5	1	0.64	2972	1446	0.082	0.0399	2.05
138	$2.29E+08$	116	1	0.63	1320	634	0.0278	0.0134	2.08
298	$2.03E+08$	262	1	0.58	1092	459	0.0259	0.0109	2.38

TABLE 7: Experimental data obtained from the irradiation of uranyl sulfate solutions in the presence of potential peroxide catalysts at the Van de Graaff.

Catalyst	Uranium concentration (g-U/L)	Energy deposited (Gy)	Did sample precipitate	Total μmoles H_2 produced	Total μmoles O_2 produced	H_2 to O_2 ratio
Cu(II), 62.5 mg-Cu/L	126	$2.20E+08$	No	410	290	1.42
KI, 9.94 mg-I/L	126	$2.28E+08$	No	210	150	1.40
Fe(III), 0.96 mg-Fe/L	126	$2.28E+08$	No	570	370	1.53
304 stainless steel	126	$2.24E+08$	No	260	220	1.17
Zirconium	298	$2.32E+08$	Yes	1110	460	2.42
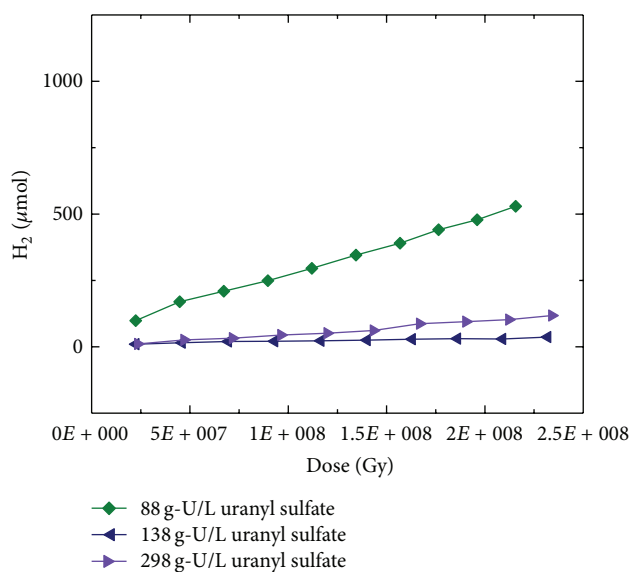
FIGURE 5: Hydrogen evolution measured during irradiation of UO_2SO_4 solutions at the Van de Graaff.
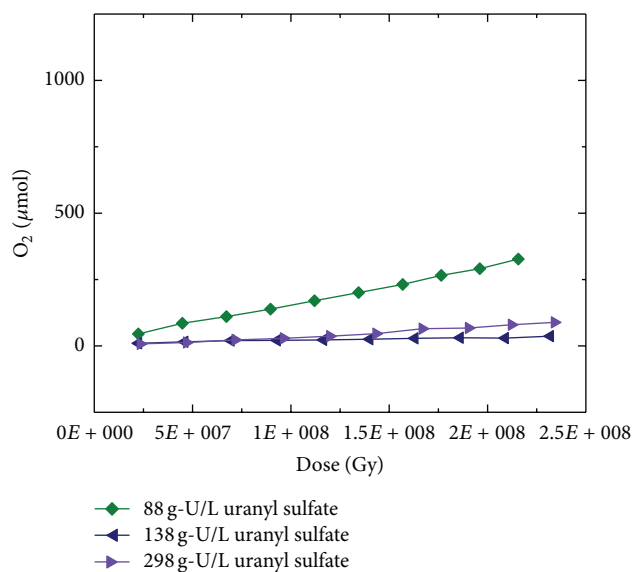
FIGURE 6: Oxygen evolution measured during irradiation of UO_2SO_4 solutions at the Van de Graaff.

favoring production of hydrogen as sulfate increased in sodium and uranyl sulfate solutions. Despite the fact that the H_2/O_2 ratio is close to 2.0 (theoretical value for water) for the 88 g-U/L uranyl sulfate sample, peroxide was still being formed because the pH decreased and a precipitate formed.

3.8. Catalytic Destruction of Peroxide in Uranyl Sulfate Solutions. To prevent precipitation of uranyl peroxide, a catalyst must be added to the uranyl sulfate solution prior to irradiation to decrease the steady-state concentration of radiolytically generated hydrogen peroxide. Fe(II) added as $FeSO_4$ has been shown to accomplish this at concentrations as low as 1 ppm. In order to expand the available options for use in

the SHINE system, other salts were tested because of their known ability to catalyze destruction of H_2O_2. Experiments were performed using aqueous solutions of copper(II) sulfate, potassium iodide, and iron(III) sulfate [37]. Potential target solution vessel materials, 304 stainless steel and zirconium ASME 658, were also tested. The stainless steel and Zr were added as solid turnings to 2 mL of ~130 g-U/L uranyl sulfate solution.

Table 7 and Figures 8–10 show experimental data for the irradiation of uranyl sulfate solutions containing the potential H_2O_2 destruction catalysts discussed above. Each sample contained a different catalyst at the concentration shown. Figures 8 and 9 show the total μmoles of each analyte
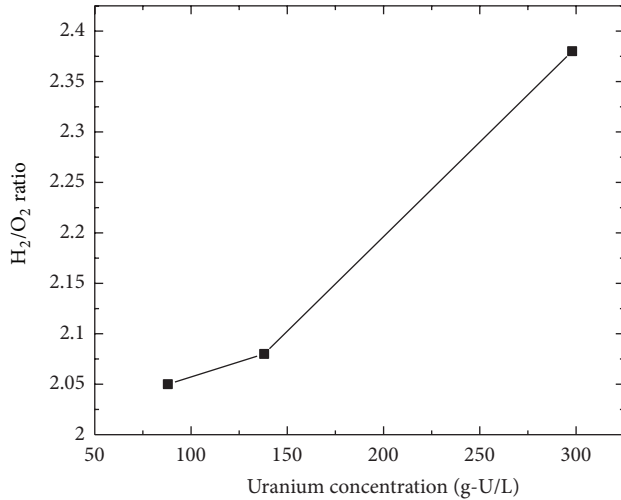
FIGURE 7: Hydrogen to oxygen ratios measured for UO_2SO_4 solutions during irradiation tests at the Van de Graaff.
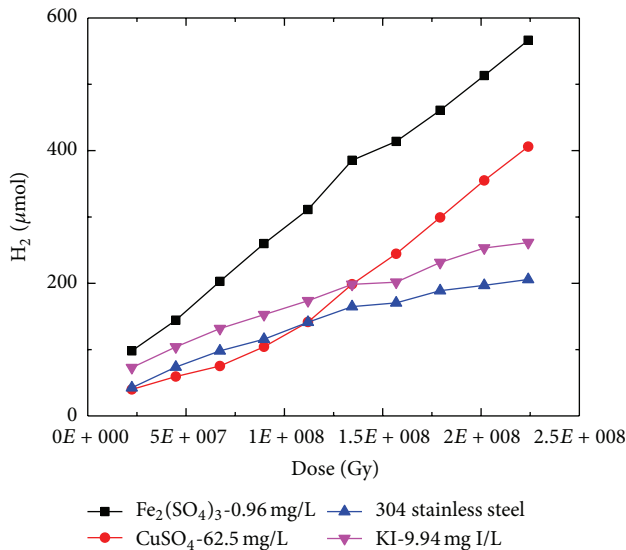

FIGURE 8: Hydrogen evolution measured during irradiation of 126 g-U/L UO_2SO_4 solutions in the presence of potential peroxide catalysts at the Van de Graaff.

FIGURE 9: Oxygen evolution measured during irradiation of 126 g-U/L UO_2SO_4 solutions in the presence of potential peroxide catalysts at the Van de Graaff.

FIGURE 10: Hydrogen to oxygen ratios measured during irradiation of 126 g-U/L UO_2SO_4 solutions in the presence of potential peroxide catalysts at the Van de Graaff.

(either hydrogen or oxygen) versus accumulated dose (Gy) at sampling time during each five-hour experiment. **Figure 10** presents the H_2-to-O_2 ratios versus dose for the data. Comparing Tables 6 and 7, it is evident that the addition of a peroxide catalyst reduces the overall gas production and changes the H_2-to-O_2 ratio from ~2 : 1 to ~1.4 : 1.

Zr metal was not effective at preventing precipitation of uranyl peroxide, so if the target solution vessel for SHINE is made of Zr, an additional catalyst would most likely be required to accelerate peroxide destruction. Irradiated uranyl sulfate solutions containing Zr metal exhibited similar behavior to the irradiated uranyl sulfate solutions where uranyl peroxide precipitated. High volumes of hydrogen and oxygen
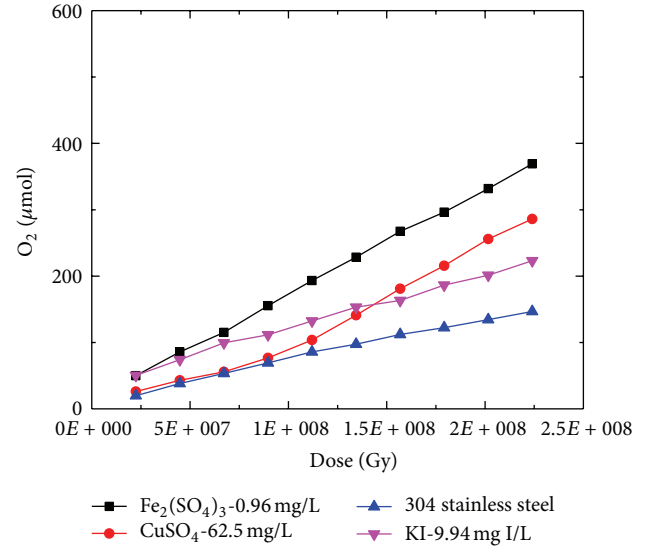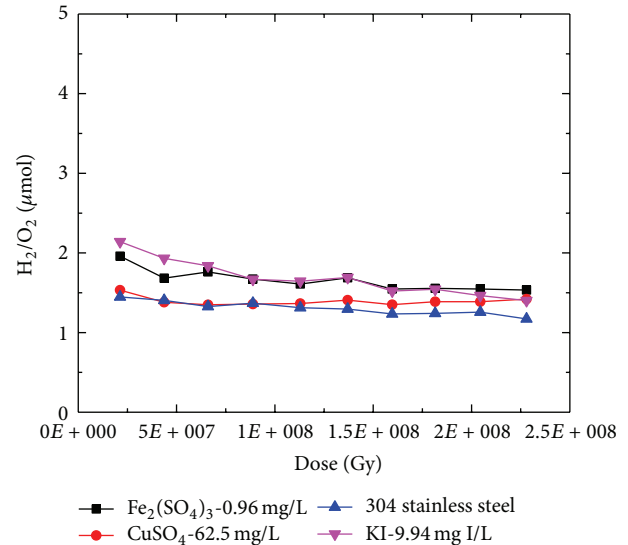
were generated, and H_2-to-O_2 ratios greater than 2 were observed.

The solution containing 304 stainless steel turnings showed no evidence of precipitation, but the exact mechanism of destruction is unknown. It may be a surface effect or through dissolution of reactive ions. The 304 stainless steel test showed low overall gas production and a low $H_2 : O_2$ ratio. The $H_2 : O_2$ ratio was 1.17, which is the lowest ratio observed for any of the uranyl sulfate solutions irradiated with effective catalysts, but the ratio is similar to uranyl nitrate solutions containing higher concentrations of U (175 g-U/L

and 226 g-U/L, see Table 4) that were irradiated at the Van de Graaff.

Irradiations with the metal salt catalysts (copper sulfate, potassium iodide, and ferric sulfate) were also effective at preventing precipitation of uranyl peroxide. All of the salt catalysts reduced the overall gas production and reduced the H_2-to-O_2 ratios to values below 2, but the ratios were still larger than the ratio of 1.17 observed for the uranyl sulfate solution containing the 304 stainless steel turnings.

4. Conclusions

Uranyl nitrate solutions are easier to prepare than uranyl sulfate solutions, but large pH increases are observed upon irradiation. A continuous feed of nitric acid is required to prevent precipitation of uranium and fission products during irradiation. Uranyl sulfate solutions are more difficult to prepare, but large pH increases are not observed upon irradiation. However, a catalyst is required to promote peroxide destruction and prevent precipitation of uranyl peroxide.

Mo recovery is a slightly easier from nitrate media compared to sulfate media. This is due to the fact that sulfate competes more strongly with molybdenum for titania adsorption sites than nitrate. A plant-scale Mo recovery column would be about 25% larger for a uranyl sulfate solution compared to a uranyl nitrate solution. From a neutronics standpoint, uranyl sulfate is preferred due to the fact that nitrogen absorbs thermal neutrons, which creates a loss of neutrons, and decreases the overall reactivity. There are advantages and disadvantages associated with both uranyl salts, but Mo-99 separation and recovery using a titania sorbent followed by Mo-99 purification using the LEU-Modified Cintichem process are feasible using a uranyl sulfate or uranyl nitrate target solution.

Acknowledgment

References

[1] IAEA(International Atomic Energy Association)-TECDOC-1601, *Homogeneous Aqueous Solution Nuclear Reactors for the Production of Mo-99 and Other Short Lived Radioisotopes*, Vienna, Austria, 2008.

[2] G. Piefer, "Mo-99 production using a subcritical assembly," in *Proceedings of the 1st Annual Mo-99 Topical Meeting*, Santa Fe, NM, USA, December 2011.

[3] K. M. Pitas, G. R. Piefer, R. V. Bynum, E. N. Van Abel, and J. Driscoll, "SHINE: technology and progress," in *Proceedings of the Mo-99 Topical Meeting on Molybdenum-99 Technological Development*, Chicago, Ill, USA, April 2013.

[4] A. J. Bakel, S. B. Aase, A. A. Leyva, K. J. Quigley, and G. F. Vandegrift, "Thermoxid sorbents for the separation and purification of [99]Mo," in *Proceedings of the International RERTR Meeting*, Vienna, Austria, November 2004.

[5] A. J. Bakel, D. C. Stepinski, G. F. Vandegrift et al., "Progress in technology development for conversion of [99]Mo production-BATAN'S (INDONESIA) conversion program, progress in the CNEA (Argentina) LEU foil/baseside process, and development of inorganic sorbents for [99]Mo production," in *Proceedings of the International RERTR Meeting*, Boston, Massa, USA, November 2005.

[6] G. F. Vandegrift, A. J. Bakel, and J. W. Thomas, "Overview of 2007 ANL progress for conversion of HEU-based Mo-99 production as part of the U.S. Global Threat Reduction—Conversion Program," in *Proceedings of the International RERTR Meeting*, Prague, Czech Republic, September 2007.

[7] G. F. Vandegrift, J. Fortner, A. J. Bakel et al., "Overview of argonne progress related to implementation of Mo-99 production by use of a homogeneous reactor," in *Proceedings of the International RERTR Meeting*, Washington, DC, USA, October 2008.

[8] A. J. Ziegler, D. C. Stepinski, J. F. Krebs, S. D. Chemerisov, A. J. Bakel, and G. F. Vandegrift, "Mo-99 recovery from aqueous-homogeneous-reactor fuel—behavior of termoxid sorbents," in *Proceedings of the International RERTR Meeting*, Washington, DC, USA, October 2008.

[9] D. Stepinski, A. Ziegler, J. Jerden et al., "Sorbent selection progress report," ANL/CSE-13/16, Argonne National Laboratory, 2009.

[10] G. F. Vandegrift, D. C. Stepinski, A. J. Ziegler et al., "Overview of argonne progress in developing LEU-based processes for the production of Mo-99," in *Proceedings of the International RERTR Conference*, Beijing, China, November 2009.

[11] E. O. Krahn, A. S. Hebden, G. F. Vandegrift, P.-L. Chung, and L. Wang, "Mechanical stability study," ANL/CSE-13/3, Argonne National Laboratory, 2010.

[12] A. J. Youker, P.-L. Chung, E. O. Krahn, D. C. Stepinski, A. V. Gelis, and G. F. Vandegrift, "Mo-99 stripping results and column designs for Mini-Medical Isotope Production System (MIPS)," ANL/CSE-13/15, Argonne National Laboratory, 2011.

[13] A. J. Youker, P.-L. Chung, P. Tkac et al., "Separation, purification, and clean-up developments for MIPS and SHINE," in *Proceedings of the 1st Annual Mo-99 Topical Meeting*, Santa Fe, NM, USA, December 2011.

[14] A. J. Youker, P.-L. Chung, E. O. Krahn, and G. F. Vandegrift, "Column optimization studies," ANL/CSE-13/2, Argonne National Laboratory, 2012.

[15] A. J. Youker, D. C. Stepinski, L. Ling, and G. F. Vandegrift, "Mo recovery updates and physical properties of Uranyl sulfate solutions," ANL/CSE-13/20, Argonne National Laboratory, 2012.

[16] A. J. Youker, D. C. Stepinski, M. Kalensky et al., "Progress Related to Mo-99 Separation, Precipitation Prevention, and Clean-Up for SHINE System," in *Proceedings of the Topical Meeting on Molybdenum-99 Technological Development*, Chicago, Ill, USA, April 2013.

[17] C. Milhano and D. Pletcher, "The electrochemistry and electrochemical technology of Nitrate," *Modern Aspects of Electrochemistry*, vol. 45, pp. 1–61, 2009.

[18] M. Kalensky, S. Chemerisov, A. Youker et al., "Radiolysis of nitrate and sulfate solutions," ANL/CSE-13/23, Argonne National Laboratory, 2012.

[19] M. Kalensky, S. Chemerisov, A. Youker et al., "Means to eliminate uranyl peroxide in SHINE target solution," ANL/CSE-13/21, Argonne National Laboratory, 2013.

[20] A. Gelis, S. Chemerisov, A. Bakel, and G. Vandegrift, "Radiolysis effects on molybdenum oxidation state and recovery

from aqueous-homogeneous-reactor fuel," in *Proceedings of the International RERTR Meeting*, Washington, DC, USA, October 2008.

[21] A. Youker, J. Krebs, A. Hebden, K. Quigley, D. Stepinski, and G. Vandegrift, "Van de graaff experiments: Mo redox chemistry and iodine speciation," ANL/CSE-13/17, Argonne National Laboratory, 2012.

[22] I. Draganic', "Oxalic Acid: the only aqueous dosimeter for In-Pile use," *Nucleonics*, vol. 21, pp. 33–35, 1963.

[23] C. A. Laue, D. Gates-Anderson, and T. E. Fitch, "Dissolution of metallic uranium and its alloys. Part I. Review of analytical and process-scale metallic uranium dissolution," *Journal of Radio-analytical and Nuclear Chemistry*, vol. 261, no. 3, pp. 709–717, 2004.

[24] J. A. Lane, "Properties of aqueous fuel solutions," in *Aqueous Homogeneous Reactors*, chapter 3, pp. 85–123, Oak Ridge National Laboratory, 1958.

[25] G. F. Vandegrift, "Transformation of urex effluents to solid oxides by concentration, denitration, and calcination," Tech. Rep. ANL-00/25, Argonne National Laboratory, 2000.

[26] A. J. Bakel and G. F. Vandegrift, "Equipment and method choices for concentration and denitration of the uranium product from UREX," ANL/CSE-13/1, Argonne National Laboratory, 2013.

[27] G. E. Dale, D. A. Dalmas, M. J. Gallegos et al., "^{99}Mo separation from high-concentration irradiated Uranium Nitrate and Uranium sulfate solutions," *Industrial and Engineering Chemistry Research*, vol. 51, pp. 13319–13322, 2012.

[28] H. L. Anderson, "High power water boiler," LA-394, Los Alamos National Laboratory, 1945.

[29] H. M. Busey, "Composition and decontamination of residual water-boiler off-gas," LA-1521, Los Alamos National Laboratory, 1953.

[30] P. R. Kasten, *Reactor Dynamics of the Los Alamos Water Boiler*, vol. 50 of *C.E.P. Symposium*, Nuclear Engineering, 1954.

[31] S. Klein, "Effects of solution chemistry on aqueous reactor (AHR) reactivity," LA-UR 10-04317, Los Alamos National Laboratory, 2010.

[32] J. A. Berninger, R. D. Whitley, X. Zhang, and N.-H. L. Wang, "A versatile model for simulation of reaction and nonequilibrium dynamics in multicomponent fixed-bed adsorption processes," *Computers and Chemical Engineering*, vol. 15, no. 11, pp. 749–768, 1991.

[33] Olleman-Wiberg, *Inorganic Chemistry*, Academic Press, 1995.

[34] Spinks and Woods, *Introduction to Radiation Chemistry*, John Wiley & Sons, 1990.

[35] J. Jerden, J. Kropf, A. Bakel, and G. Vandegrift, "Speciation and concentration of metals in a homogeneous reactor fuel solution," ANL/CSE-13/7, Argonne National Laboratory, 2009.

[36] A. Bakel, A. Leyva, T. Wiencek et al., "Overview of progress related to implementation of the LEU-Modified cintichem process," in *Proceedings of the International RERTR Meeting*, Washington, DC, USA, October 2008.

[37] J. H. Baxendale, "Decomposition of hydrogen peroxide by catalysts in homogeneous aqueous solution," *Advances in Catalysis*, vol. 4, no. C, pp. 31–86, 1952.